

# Identification of wind energy systems



Gijs van der Veen

# Identification of wind energy systems

PROEFSCHRIFT

ter verkrijging van de graad van doctor  
aan de Technische Universiteit Delft,  
op gezag van de Rector Magnificus prof.ir. K.C.A.M. Luyben,  
voorzitter van het College voor Promoties,  
in het openbaar te verdedigen op  
dinsdag 16 april 2013 om 12:30 uur

door

**Gijsbrecht Jan VAN DER VEEN**

ingenieur in de luchtvaart en ruimtevaart  
geboren te Vianen



Dit proefschrift is goedgekeurd door de promotor:  
prof.dr.ir. M. Verhaegen

Copromotor:  
dr.ir. J.W. van Wingerden

Samenstelling promotiecommissie:

Rector Magnificus,	voorzitter
prof.dr.ir. M. Verhaegen,	Technische Universiteit Delft, promotor
dr.ir. J.W. van Wingerden,	Technische Universiteit Delft, copromotor
prof.dr. D.T. Westwick,	University of Calgary, Canada
prof.dr.ir. J.A. Mulder,	Technische Universiteit Delft
prof.dr.ir. G.A.M. van Kuik,	Technische Universiteit Delft
prof.dr. M. Lovera,	Politecnico di Milano, Italië
dr.ir. H.F. Veldkamp,	Vestas Wind Systems, Denemarken



This dissertation has been completed in partial fulfilment of the requirements of the Dutch Institute of Systems and Control (DISC) for graduate studies.



The work presented in this thesis was supported by Vestas Wind Systems A/S, Denmark.

ISBN/EAN: 978-94-6191-665-5

Copyright © 2013 by G.J. van der Veen.

All rights reserved. No part of the material protected by this copyright notice may be reproduced or utilized in any form or by any means, electronic or mechanical, including photocopying, recording or by any information storage and retrieval system, without written permission from the copyright owner.

Printed by Ipskamp Drukkers in The Netherlands.

Cover: Vestas V52-850 kW turbines at Mehuken, Norway. Image courtesy of Vestas Wind Systems A/S.

# Contents

<b>1</b>	<b>Introduction</b>	<b>1</b>
1.1	Wind power in Europe . . . . .	1
1.2	The cost of wind energy . . . . .	1
1.3	Modelling and control of wind turbines . . . . .	4
1.3.1	Wind turbine modelling . . . . .	7
1.3.2	The role of data-driven modelling in wind turbine control design . . . . .	9
1.3.3	Prediction error methods and subspace methods . . . . .	11
1.4	Key challenges and contributions . . . . .	12
1.4.1	Closed-loop operation . . . . .	12
1.4.2	Periodic loads . . . . .	13
1.4.3	Nonlinear system . . . . .	13
1.4.4	Poor signal-to-noise ratio . . . . .	14
1.4.5	Cost . . . . .	14
1.5	Publications . . . . .	16
<b>2</b>	<b>Closed-loop subspace identification of LTI systems</b>	<b>17</b>
2.1	Introduction . . . . .	17
2.2	Discrete-time identification framework . . . . .	20
2.2.1	Preliminaries and notation . . . . .	21
2.2.2	Data equations . . . . .	22
2.2.3	Relation to the ARX model structure . . . . .	23
2.2.4	Closed-loop identification issues . . . . .	23
2.2.5	Estimating the predictor Markov parameters . . . . .	24
2.2.6	Statistical properties and stochastic least-squares . . . . .	25
2.2.7	Least-squares sensitivity . . . . .	26
2.2.8	Relation to subspace predictive control . . . . .	27
2.3	Obtaining a state-space realisation . . . . .	27
2.3.1	Direct parameterisation . . . . .	27
2.3.2	A realisation algorithm . . . . .	27
2.3.3	Predictor-based subspace identification (PBSID <sub>opt</sub> ) . . . . .	30
2.3.4	Closed-loop MOESP . . . . .	31
2.3.5	Closed-loop MOESP relying solely on <i>R</i> -factors . . . . .	33
2.3.6	User choices and other issues . . . . .	34
2.3.7	Notes on continuous-time identification . . . . .	35
2.4	Evaluation . . . . .	36
2.4.1	Numerical example: simple closed-loop configurations . . . . .	36
2.4.2	Numerical example: behaviour with poor excitation . . . . .	37
2.4.3	Experimental example: “smart” beam dynamics . . . . .	38
2.5	Concluding remarks . . . . .	45
<b>3</b>	<b>LTI identification of wind energy systems: practical aspects</b>	<b>49</b>
3.1	Introduction . . . . .	49
3.2	Periodic disturbances . . . . .	49
3.2.1	Sources of periodic loads . . . . .	50
3.2.2	Effects of periodic loads on system identification . . . . .	50
3.2.3	Example: data from an experimental “smart” rotor . . . . .	53
3.2.4	Conclusions . . . . .	54

3.3	Active suppression of control surface flutter . . . . .	55
3.3.1	Identification experiments and control design . . . . .	58
3.3.2	Experimental evaluation and load alleviation . . . . .	61
3.3.3	Conclusions . . . . .	62
3.4	Rapid evaluation of controller performance on an experimental turbine . . . . .	62
3.4.1	Control design procedure . . . . .	63
3.4.2	Identification of closed-loop wind turbine behaviour . . . . .	64
3.4.3	Identification from field test data . . . . .	66
3.4.4	Conclusions . . . . .	67
3.5	Conclusions . . . . .	69
<b>4</b>	<b>Subspace predictive control of aeroelastic systems</b>	<b>71</b>
4.1	Introduction . . . . .	71
4.2	Identification framework . . . . .	72
4.2.1	Recursive solution of the parameter estimation problem . . . . .	73
4.2.2	Square-root covariance RLS with directional forgetting . . . . .	74
4.2.3	Example 1 - Parameter estimation . . . . .	78
4.2.4	Example 2 - Parameter tracking . . . . .	79
4.3	Deriving the subspace predictor . . . . .	81
4.4	Setting up the predictive control problem . . . . .	82
4.4.1	Algorithm summary . . . . .	83
4.4.2	Implementation . . . . .	83
4.4.3	Parameter selection . . . . .	83
4.5	Experimental evaluation: active damping of a “smart” beam . . . . .	84
4.5.1	Experimental setup . . . . .	84
4.5.2	Control design . . . . .	85
4.5.3	Results . . . . .	85
4.6	Experimental evaluation: speed control of a wind turbine scale model . . . . .	86
4.6.1	Experimental setup . . . . .	86
4.6.2	Identification and controller design . . . . .	88
4.6.3	Results . . . . .	90
4.7	Conclusions . . . . .	92
<b>5</b>	<b>Closed-loop subspace identification of Hammerstein systems</b>	<b>95</b>
5.1	Introduction . . . . .	95
5.2	Identification of MIMO Hammerstein systems . . . . .	97
5.2.1	Nonlinear static modelling using multivariate simplex splines . . . . .	97
5.2.2	Hammerstein identification . . . . .	100
5.3	Recovering the low-rank structure of the overparameterised model . . . . .	100
5.3.1	SVD truncation . . . . .	101
5.3.2	Separable least-squares regression . . . . .	101
5.3.3	Obtaining local linear models . . . . .	103
5.4	Examples . . . . .	103
5.4.1	A theoretical example . . . . .	103
5.4.2	Global identification of a wind turbine . . . . .	104
5.5	Discussion . . . . .	108
<b>6</b>	<b>Nonlinear data-driven modelling of wind turbines</b>	<b>111</b>
6.1	Introduction . . . . .	111
6.2	Basic wind turbine mechanics . . . . .	114
6.2.1	Rotor . . . . .	115
6.2.2	drive train . . . . .	115
6.2.3	Tower . . . . .	115
6.2.4	Controls . . . . .	116
6.3	Global system identification of wind turbines . . . . .	117
6.3.1	Structure of the problem . . . . .	117
6.3.2	Modelling the aerodynamic coefficients using splines . . . . .	119
6.3.3	Identification of a wind turbine . . . . .	119
6.3.4	Further aspects related to system identification . . . . .	120
6.4	Experimental results . . . . .	122

- 6.4.1 Time-domain validation in closed-loop . . . . . 123
- 6.4.2 Comparison of local linear models . . . . . 128
- 6.5 Concluding remarks . . . . . 134
- 7 Conclusions and recommendations . . . . . 137**
  - 7.1 Conclusions . . . . . 137
  - 7.2 Recommendations . . . . . 139
- A Parameterizing an orthogonal matrix . . . . . 141**
- B Floating wind turbines and fundamental limitations . . . . . 143**
  - B.1 Introduction . . . . . 143
  - B.2 Dynamics . . . . . 144
  - B.3 Control objectives . . . . . 145
    - B.3.1 Regions of operation . . . . . 145
    - B.3.2 Control in above rated conditions . . . . . 146
  - B.4 Control of tilt oscillations . . . . . 148
    - B.4.1 Passive solutions . . . . . 148
    - B.4.2 Active solutions . . . . . 148
  - B.5 Future turbines . . . . . 151
  - B.6 Conclusions . . . . . 153
- Bibliography . . . . . 155**
- List of abbreviations . . . . . 167**
- Summary . . . . . 169**
- Samenvatting . . . . . 171**
- Acknowledgements . . . . . 173**
- Curriculum Vitae . . . . . 175**



# Introduction

In the next decades it is expected that wind energy will secure a firm share of the total energy production capacity in many countries. To increase competitiveness of wind power with other power sources lowering the cost of wind energy is critical. Given the design of a turbine, this objective can be attained in several ways: by increasing the energy production of a wind turbine, by lowering loads on the wind turbine in order to reduce maintenance costs and by mass production. Research performed in recent years has shown that *advanced control* plays an important role in the first two aspects. Refined control design can increase power production, for instance by using feedforward information about the wind field provided by modern (distributed) sensors. At the same time, control can reduce wear of the turbine by mitigating fatigue and extreme loads, also using feedforward and feedback information from multiple sensors in combination with novel actuator concepts. For the design process of new and advanced control concepts which meet these objectives, detailed models are essential. Data-driven modelling can provide such models and help to understand differences between the theoretical and practical worlds of wind turbine modelling.

## 1.1 Wind power in Europe

Over the last decade, wind power has established itself as a significant provider of electrical power in Europe. Even though the concept of wind energy raises controversy in some quarters, the irrefutable fact is that the wind power production capacity of many European countries has grown significantly and accounts for at least 5% of production capacity in the majority of countries and approaches in excess of 20% of the capacity in 5 countries (Table 1.1). Table 1.1 also shows the predicted capacities one and two decades from now, indicating that this trend is likely to continue. The numbers mentioned thus far specify the share of wind power in terms of *total generation capacity*. It is interesting to note that at times when the demand of a certain country is below its total generation capacity, wind power may account for a much large share of the *actual generated power*. For instance, in Spain the share of wind power regularly exceeds 35% (Red Eléctrica de España, 2012). In a recent report, the European Wind Energy Association (EWEA) has developed a number of scenarios for the next two decades (Zervos and Kjaer, 2008). The European Union currently imports almost 60% of its energy and this figure is growing. This power is imported “*from unstable regions, in ever-fiercer competition with the rest of the world and at staggering environmental cost*” (Zervos and Kjaer, 2008). Hence, it is crucial for Europe to secure its own (renewable) energy resources and meet the energy demand of tomorrow in a sustainable and reliable way. In addition, EWEA identifies this challenge as an opportunity for Europe to lead this development and emerge as a winner from this challenge.

## 1.2 The cost of wind energy

While the increasing costs associated with scarce fossil fuels will in the long run increase the competitiveness of wind power, it is important to go to great lengths to decrease the current cost of wind power, for instance in terms of €/kWh. The reason is to increase

	% of total capacity					
	1980	1990	2000	2010	2020	2030
Denmark	0.0	4.2	19.5	28.3	38.6	47.4
Portugal	0.0	0.0	0.8	20.8	25.8	29.9
Spain	0.0	0.1	4.2	20.0	28.7	35.5
Ireland			2.5	18.1	37.9	46.9
Germany	0.0	0.1	5.0	16.3	24.4	29.7
Netherlands		0.4	2.2	8.4	13.8	25.9
Bulgaria	0.0	0.0	0.0	7.9	16.8	19.6
Greece	0.0	0.0	1.9	7.8	28.7	
Cyprus	0.0	0.0	0.0	7.6		
United Kingdom	0.0	0.0	0.5	6.6	23.1	28.0
Estonia			0.0	6.1	22.2	
Sweden	0.0	0.0	0.8	6.1	14.3	23.2
Italy	0.0	0.0	0.5	4.8		
Austria			0.4	4.7	5.8	7.3
France	0.0	0.0	0.0	4.7	12.8	20.2
Lithuania	0.0	0.0	0.0	4.5	7.7	13.8
Poland	0.0	0.0	0.0	3.8	15.4	15.1
Belgium	0.0	0.0	0.1	3.0	7.8	15.1
Luxemburg	0.0	0.0	1.3	2.9	3.0	3.4
Hungary	0.0	0.0	0.0	2.7	7.1	7.6
Romania	0.0	0.0	0.0	2.4	14.6	18.7
Finland	0.0	0.0	0.2	1.4	12.3	16.1
Latvia	0.0	0.0	0.1	1.2	9.9	14.8
Czech Republic	0.0	0.0	0.0	1.1	3.0	4.6
Slovakia	0.0	0.0	0.0	0.6	0.7	
Slovenia	0.0	0.0	0.0	0.0	0.0	
Norway	0.0	0.0	0.0		7.6	11.6

**Table 1.1** – Past, current and projected wind energy production capacity in European countries as a percentage of total electricity generation capacity (EURELECTRIC, 2011).

the competitiveness of wind power not only with fossil fuels, but also with alternative energy sources such as nuclear power and solar energy. While this thesis does not set out to give an opinion on the potential for alternative energy sources other than wind or a preference for one form or the other, it is clear that a lower cost of wind energy is relevant in allowing wind energy to secure a firm share in the European energy mix. In this context it is important to note, however, that the scope of “cost of energy” is often defined with a far too narrow scope. For instance, taking into account the social costs related to particulate matter emissions, carbon dioxide emissions, acidification and treatment of waste products it is often the case that wind energy is at a *significant advantage* (*Wind Energy Factsheets 2010*).

The cost of wind energy in relation to a single turbine is essentially dominated by two driving factors: its effective production capacity, usually in terms of the *annual energy production* (AEP), and its cost:

- **Annual energy production.** To increase capacity and spurred by technological advances, the last two decades have seen a tremendous increase of rotor sizes from the typical 30 m diameter turbines around 1990 to the 160 m diameter turbines to appear soon. This is by far the most effective way of increasing capacity, harnessing the fact that the rotor area grows with the square of its diameter and so does the potential extracted power. Hence, tomorrow’s rotors will provide a near 25-fold

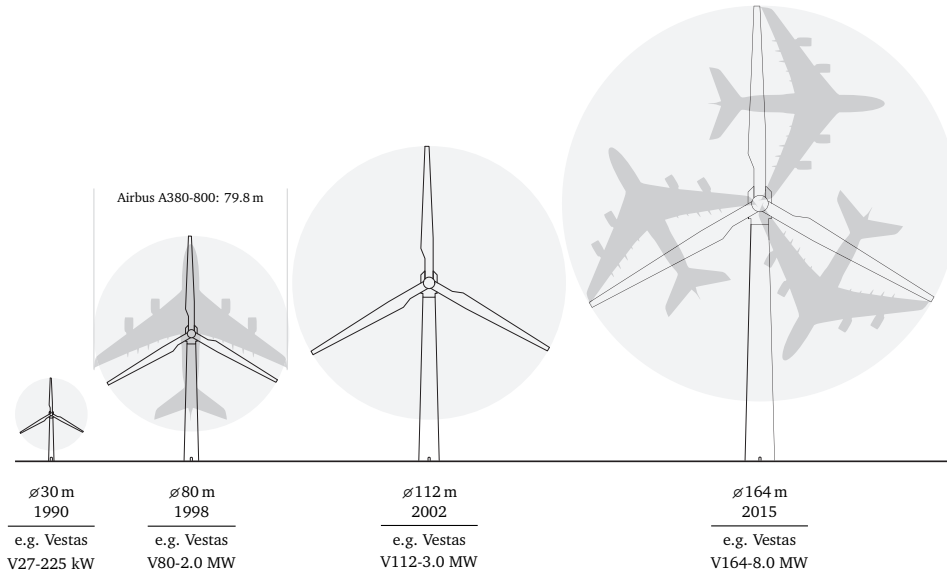


**Figure 1.1** – Development of wind turbine sizes between 1990 and 2015. Also indicated are representative turbines marketed by Vestas in these size classes<sup>1</sup>.

increase of power production potential compared to those of 20 years ago! In addition, compared to having numerous small turbines, mounting a larger rotor on a single nacelle and tower structure brings the advantage of having only once the (albeit larger) construction costs and needing to maintain only the single turbine.

- **Cost.** The fact that failures of large turbines lead to more severe production losses is a first indicator that high reliability is crucial for larger turbines and also brings us to the second driver of cost of energy: capital cost. The service life of a turbine is related to component reliability and durability and obviously a longer service life and reduced maintenance requirements will decrease depreciation costs and hence lower the cost of energy.

Finally, it is worth noting that we have only so far considered the cost of energy related to a single turbine. When considering wind farms, multiple wind farms and wind farms in relation to the grid, additional drivers of the cost of energy emerge, such as the capability to optimally regulate and forecast wind farm output and to maintain grid stability and reliability as the share of wind power on a power grid increases.

Figure 1.1 shows the development of wind turbine rotor diameters over the last two decades. The figure also presents a comparison to the dimensions of one of the largest currently operating passenger jets. Even though this comparison is in itself not very valuable from a technical point of view, it illustrates that the technological challenges involved with designing and constructing such large rotors rival those in the construction of large aircraft in some aspects. Furthermore, the fact that turbines are often designed for a service life of 25 years introduces cyclic *fatigue* loads with cycle counts several orders of magnitude larger than seen during the life of an aircraft (Sutherland, Veers and Ashwill, 1993; Nijssen, 2006). Finally, the fact that a wind turbine operates in the lowermost atmosphere in turbulent and continuously varying wind conditions introduces significant loads on such a large structure.

In recent years wind turbine manufactures and power companies have started to consider and exploit *offshore* locations for wind turbines. Such locations provide vast areas

<sup>1</sup>The illustration of the A380 by Clem Tillier is used under the creative commons share alike license: [http://commons.wikimedia.org/wiki/File:Giant\\_planes\\_comparison.svg](http://commons.wikimedia.org/wiki/File:Giant_planes_comparison.svg)

of wind resource and wind resources at sea are usually of a more sustained level and less turbulent due to the smooth surface (Nielsen, Hanson and Skaare, 2006). Offshore locations are typically less susceptible to raising social and environmental issues. On-shore turbines, in particular large ones, often face problems related to visual impact, noise production and limited availability of real estate (Burton, Sharpe, Jenkins et al., 2001). Despite initial scepticism, offshore wind energy is gradually becoming more accepted and with many offshore wind farms currently in operation the required technology is in the process of becoming more mature. One of the issues in constructing offshore turbines is the cost of the foundation, which makes construction of offshore turbines only feasible at locations with limited depths of the sea bed (typically less than 25–50 m (Jonkman, 2007)). To circumvent this problem, several floating wind turbine concepts have now been tested by a number of syndicates of wind turbine manufacturers with other involved industries (Renewable Energy Focus, 2009; Roddier, Cermelli, Aubault et al., 2010). For offshore turbines efficient and reliable operation is even more crucial. Construction costs are often higher, in particular due to the foundations and distant grid connection. Also, the opportunities for maintenance and repair are more restricted and expensive. Floating wind turbines also present additional control challenges, see (Larsen and Hanson, 2007; Jonkman, 2008; Lackner, 2009; van der Veen, Couchman and Bowyer, 2012) and Appendix B.

### 1.3 Modelling and control of wind turbines

In the previous section we have touched upon some of the challenges of wind turbine engineering, mainly in terms of the high loads and large scale structures involved.

A wind turbine left on its own is an unstable system. Depending on the blade pitch angles, the rotor speed and the wind speed, the rotor will develop a torque. This torque acts on the main shaft of the turbine and, depending on the counter-torque exerted by the generator, the drive train will accelerate. This mode is essentially a *rigid-body mode* and hence if the torque balance is constant, the drive train will continue to accelerate or decelerate. Traditionally, several active or passive operating modes have been used to regulate power production, e.g.:

- fixed-speed, fixed-pitch machines;
- fixed-speed, variable-pitch machines;
- variable-speed, fixed-pitch machines;
- variable-speed, variable-pitch machines.

In Burton, Sharpe, Jenkins et al. (2001) and Bianchi, De Battista and Mantz (2007) these modes and how they lead to power regulation are described in some detail, which is outside the scope of this thesis. Since practically all current multi-MegaWatt turbines fall in the last category, we will focus our discussion on this class. A variable-speed, variable-pitch turbine has the most essential control degrees-of-freedom to enable optimal<sup>2</sup> power production over a wide range of wind speeds. At a certain designed *cut-in* wind speed the power production on the turbine is initiated. This wind speed forms the threshold of so-called *region I*. In this region, the control system aims at maximising the efficiency with which the turbine extracts power from the wind. The aerodynamic power generated by a rotor is typically expressed as:

$$P_a = \frac{1}{2} \rho \pi R^2 C_P(\lambda, \beta) V^3,$$

where  $\rho$  is the air density,  $R$  is the rotor radius,  $V$  is the undisturbed wind speed and  $C_P(\lambda, \beta)$  is a dimensionless *power coefficient*, the value of which depends on the current collective pitch angle of the blades  $\beta$  and the tip-speed ratio  $\lambda$ , defined as:

$$\lambda \triangleq \frac{\Omega R}{V}. \quad (1.1)$$

---

<sup>2</sup>The term *optimal* is used loosely here and in the sense that the turbine operates close to its true optimal operating point.

A typical power coefficient surface is shown in Figure 1.2. This figure clearly shows that there is a pair  $(\lambda_{\text{opt}}, \beta_{\text{opt}})$  that results in maximum power capture by attaining  $C_{P,\text{opt}}(\lambda_{\text{opt}}, \beta_{\text{opt}})$ . Given the definition of the tip-speed ratio this implies that the rotor speed

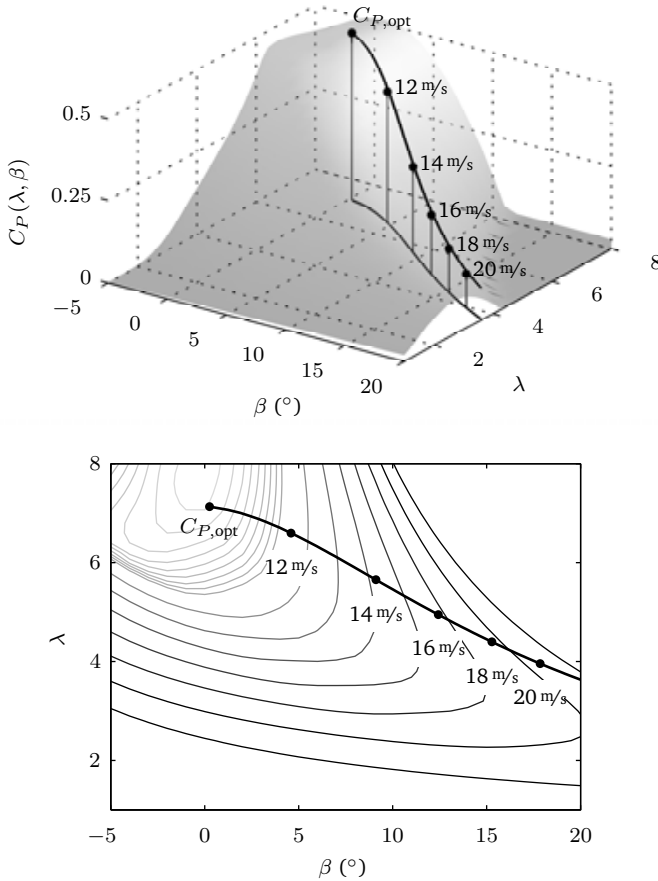


**Figure 1.2** – The power coefficient surface and a representation of the above-rated (region II) operating strategy required to maintain rated power. The character of the power coefficient surface shown here is typical for most utility-scale wind turbines.

$\Omega$  should vary in proportion to the wind speed: as wind speed increases, so should the rotor speed:

$$\Omega_{\text{opt}} = \frac{\lambda_{\text{opt}}}{R} V. \quad (1.2)$$

In this region the generator torque  $T_g$  is controlled so that the rotor speed tracks this tip-speed ratio for optimal efficiency. At a certain point, the *rated power* of the generator is reached and the turbine enters *region II*, in which the objective is to maintain the generated power at its rated value. This implies that, with the increasing wind speed, the conversion efficiency of the rotor should be decreased. This is often achieved by pitching the blades into the wind (*pitch-to-feather*) by means of which the local lift forces on the blade are reduced and hence the aerodynamic torque (Bossanyi, 2000; van der Hooft, Schaak and van Engelen, 2003). Again, in Figure 1.2 an example is shown of how increasing the pitch angle can be used to reduce the power coefficient as the wind speed increases, with the objective of maintaining rated power.

On many turbines, regions I and II are divided by certain other regions. For instance, prior to the generator reaching its rated power, the rotor may reach its maximum allowed rotational speed. The acoustic noise emission of a turbine is linked to the tip speed of the blades and therefore this maximum rotor speed is often constrained by limitations on acoustic noise emissions. In other cases, the generator torque may first reach its limit, in which case the rotor is sped up after reaching maximum torque. This implies that the tip-speed ratio departs from its optimal value before reaching rated power.

Also note that Figure 1.2 provides a first demonstration of the nonlinearity of wind turbines. This can be seen as follows: depending on the current operating point, specified by a pair  $(\lambda, \beta)$ , a small change in pitch angle  $\beta$  causes a change in the power coefficient. This change in power coefficient depends on the local gradient of the power coefficient surface and this gradient clearly varies with the operating point. Hence, one could state that the control effectiveness of the pitch input varies with the current operating point.

At this point we have only considered the static equilibrium behaviour of the turbine. In practice the wind speed varies continuously and hence the controller should continuously adjust the generator torque (in region I) or the pitch angles (in region II). This variation also induces an elastic response of the turbine structure. The combined behaviour is determined by the structural response, the aerodynamic response and the response of the control system to these effects, commonly termed *aeroservoelasticity*. The speed with which the controller adjusts the control parameters is the consequence of an important trade-off: a slow adjustment results in poor tracking of the optimal tip-speed ratio (leading to loss of produced power in region I) or regular exceedance of rated power (in region II). In contrast, very fast adjustment introduces high loads on the structure, drive train and pitch systems. This *multi-objective* character of the control system (Skogestad and Postlethwaite, 1996) has become increasingly important in recent years. One reason is that a key to extending the service life of a turbine and thus lowering the cost of energy is to reduce cyclic and extreme loads. Another reason is that the increase in turbine sizes has led to larger, more flexible blades and larger towers, causing the structural frequencies to enter the control bandwidth of most turbines. In this context designing a “stiff” turbine is not feasible for obvious weight and cost reasons and lowering the control bandwidth is equally undesirable. Consequences of a smaller control bandwidth are a less stable power output and require that larger margins be imposed on generator speeds, torque and power limits, ultimately leading to a more conservative operating strategy. Both solutions are not satisfactory from a cost-of-energy viewpoint and hence more sophisticated multi-objective control is the true answer.

In its simplest form, an objective of the control system is often to provide identical step responses (e.g., in terms of rotor speed error) in all operational wind speeds. Given the fact that a wind turbine’s pitch sensitivity is operating point dependent, a fact which we have indicated before, this leads to a simple form of *gain scheduling* on the pitch signal which is very common in current wind turbines (Bossanyi, 2000). In a refined sense, it is often argued that the trade-off between power regulation and load reduction objectives should also be time-varying (Leith and Leithead, 1996; Bianchi, De Battista and Mantz, 2007; Østergaard, Stoustrup and Brath, 2009). For instance, in a certain wind speed range, typically in the transition from region I to region II, the rotor (stochastic) loading is high, and hence emphasis could shift towards tower load reduction in this regime. In other regimes, where loads are lower, emphasis could shift towards optimal power production.

As discussed before, the *static* operating strategy typically requires exclusively torque actuation in region I and exclusively pitch actuation in region II. Considering a multi-objective design where power and loads are simultaneously dynamically controlled, it is logical to consider using simultaneous pitch and torque actuation for load control in both region I and II, such that both degrees of freedom are exploited. The (collective) pitch degree of freedom allows effective control of fore-aft oscillations whereas the torque degree of freedom allows effective control of side-side and drive train oscillations. Modern *individual pitch* degrees-of-freedom offer the additional benefit of allowing individual blade loads to be controlled and reduced (Bossanyi, 2003a, 2005; Larsen, Madsen and Thomsen, 2005; van Engelen, 2006; Selvam, Kanev, van Wingerden et al., 2009; Bossanyi, Fleming and Wright, 2012). The same can be said for local lift control devices such as trailing edge

flaps, which typically allow higher control bandwidths (Basualdo, 2005; Marrant and van Holten, 2006; Buhl, Bak, Gaunaa et al., 2007; van Wingerden, Hulskamp, Barlas, Marrant et al., 2008; Barlas and van Kuik, 2010; van Wingerden, Hulskamp, Barlas, Houtzager et al., 2011).

Finally, an active area of research is the use of LIDAR (light detection and ranging) technology for feedforward control of wind turbines (Schlipf, Trabucchi, Bischoff et al., 2010; Schlipf, Schlipf and Kühn, 2012; Wang, Johnson and Wright, 2012). Such devices provide preview information on the wind field upstream of a turbine. A difficulty is that the wind field evolves before reaching the rotor. Hence, it remains to be shown that measured information on higher frequency turbulent structures upstream is of use for load control. It has been shown, however, that the look ahead information (mainly at low frequencies) can be used to lower the pitch activity of a turbine (Bossanyi, 2012), which is in itself a significant advantage.

### 1.3.1 Wind turbine modelling

From the previous discussion it is clear that future wind turbines increasingly rely on refined multiobjective control design, where power and load regulation are achieved in a balanced manner. To enable such designs it is crucial to have accurate models describing the aeroelastic behaviour of the turbine. In the design stage it is common practice to develop a detailed model on the basis of first principles. Such models typically comprise the following elements (Molenaar, 2003):

- A **rotor aerodynamic model**: Typically, a *blade element momentum* code is employed to describe the rotor aerodynamics, extended with a number of corrections to address its limitations. Corrections usually applied are for blade tip and root effects, dynamic inflow, 3D effects and wake dynamics;
- A **mechanical model** to describe the structural response. Often, this model is based on a superposition of structural modes (*modal formulation*) or a formulation in terms of multibody elements. A direct finite element formulation is rarely used in wind turbine simulation, but often used for separate static or dynamic analyses and to derive mode shapes for the modal formulation mentioned earlier;
- A **generator model**. In many cases the generator is effectively described in terms of a static relation, possibly with a small time delay and certain electrical losses. This is based on the fact that power electronics employed in modern turbines are typically orders of magnitude faster than the other wind turbine modes;
- A **wind model**. Since the wind is such an important factor in determining the stochastic (fatigue) loading a turbine experiences, describing a wind field accurately and realistically is crucial in wind turbine simulation models. The wind field is a 3D structure and its direction and wind speed vary spatially and with time. Required specifications on generated wind fields are laid down in, amongst others, the IEC standard (*Wind turbines – Design requirements 2005*);
- A **wave model**. In the design of offshore turbines a significant share of the loads on a turbine may be due to wave loads, in particular since wave frequencies are often near structural frequencies.

It is interesting to note that while much more advanced and detailed methods exist to address some of these aspects, these methods are often not feasible from a practical and engineering point of view. The rotor aerodynamics and the wind field, for instance, could be described and simulated in great detail by solving the Navier-Stokes equations in a *direct numerical simulation* (DNS). This approach, however, is to date far from feasible due to its prohibitive computational cost.

While the modelling and simulation framework described thus far is very useful for predicting a turbine's dynamic behaviour in response to external loading it is not suited to systematic and multiobjective control design. The majority of control design techniques – from the industry-standard and in fact state-of-the-art frequency-domain loop shaping and P/I/D approaches (Ogata, 1997) to the “modern” model-based control design methods

(Franklin, Powell and Emani-Naeini, 1994; Skogestad and Postlethwaite, 1996) – rely on *linear time invariant* (LTI) models. Such models can often be obtained from the detailed first principles models by linearising them around an operating point.

Recent efforts in modelling and control of *linear, parameter-varying* (LPV) systems have been aimed at developing specific LPV control methodologies for wind turbines. By considering wind turbines as LPV systems, the nonlinear behaviour is explicitly accounted for and the control design framework can deliver a scheduled LPV controller. In references such as Bianchi, Mantz and Christiansen (2004); Ohtsubo and Kajiwara (2004); Bianchi, Mantz and Christiansen (2005); Lescher, Zhao and Martinez (2006); Bianchi, De Battista and Mantz (2007); Østergaard (2008); Østergaard, Stoustrup and Brath (2008, 2009); Bianchi, De Battista and Mantz (2010) progress was made on a) linking LPV model structures to the nonlinear first principles models and b) developing control design methodologies for these LPV systems. It is important to realise that these LPV models usually have the wind speed as one of their *scheduling parameters*. This wind speed is hard to measure on a turbine and is often estimated using one of the various techniques discussed in Bossanyi (2000); van der Hooft and van Engelen (2003); van der Hooft, Schaak and van Engelen (2003); van der Hooft and van Engelen (2004); Johnson, Fingersh, Balas et al. (2004); Østergaard, Brath and Stoustrup (2007); Knudsen, Bak and Soltani (2011).

A third control framework that has drawn a lot of attention in wind energy research is the model predictive control (MPC) framework (Henriksen, 2008; Kumar and Stol, 2009; Soliman, Malik and Westwick, 2011; Soltani, Wisniewski, Brath et al., 2011; Barlas, van der Veen and van Kuik, 2012). MPC relies on models to predict the behaviour of a turbine over a certain prediction horizon. On the basis of these predictions control actions are designed by minimising an objective function in each time step. While most MPC formulations are readily extended<sup>3</sup> to time-varying or parameter-varying systems it is noteworthy that nearly all cited references exclusively consider examples constrained to a single operating point, exceptions being Kumar and Stol (2009); Soliman, Malik and Westwick (2011).

Finally, adaptive control methodologies have been considered for the control of wind turbines (Johnson, Pao, Balas et al., 2006; Johnson and Fingersh, 2008; Frost, Balas and Wright, 2009; Stotsky and Egardt, 2012). Adaptive control has a long history in the field of control theory and many formulations apply directly to nonlinear systems specified in the form of coupled ordinary differential equations on the basis of Lyapunov techniques. Depending on the framework chosen, there may be challenges associated with the control of nonminimum phase systems, with guaranteeing persistence of excitation and with avoiding parameter drift instability (Åström and Wittenmark, 1994). The power of adaptive control lies in its capability to adapt to certain classes of unknown, unmodelled or slowly time-varying dynamics, either by estimating parameters or by adapting the control law. Furthermore, adaptive control laws are often derived in such a way, by constructing a candidate Lyapunov function, that stability and convergence conditions follow more or less directly.

As a first step towards unifying the stages of modelling and control design, subspace predictive control has been conceived as one way to deal with unknown but slowly-varying dynamics. Subspace predictive control uses adaptively estimated system parameters in a model predictive control law (Favoreel and De Moor, 1998; Favoreel, De Moor, Van Overschee et al., 1999; Woodley, 2001; Dong, Verhaegen and Holweg, 2008; Hallouzi, 2008). Hence, this framework may also be seen as an adaptive control framework and offers a layer of robustness to faults.

Having mentioned a number of control frameworks it is important to stress that control paradigms beyond the classical P/I/D and SISO loop shaping techniques are not widely used (if at all) in industry. Most wind energy systems are controlled by P/I speed controllers, possibly augmented with SISO compensator or filter networks for load control

---

<sup>3</sup>Readily only in the case that, for time-varying systems, the time-varying behaviour is known over the prediction horizon or, for LPV systems, the scheduling parameter is extrinsic and assumed to be known over the prediction horizon.

(e.g., drive train and tower dampers) or more refined speed/power control (Bossanyi, 2000). Since a few years, some manufacturers are exploring the potential of (multivariable) robust control or, predictive control (typically in the role of a supervisory control system). A main motivation for manufacturers to study these methodologies is that they allow including load reduction objectives from the outset. One example is controller design for floating wind turbines (van der Veen, Couchman and Bowyer, 2012). For floating turbines a significant control challenge is to regulate the speed of the turbine and simultaneously limit the fore-aft (and side-side) oscillations. Since these effects are directly coupled, the potential of SISO control design, e.g. by successive loop closure, as opposed to a direct MIMO design is limited (van der Veen, Couchman and Bowyer, 2012) (see Appendix B).

One of the reasons for the reluctance in adopting “advanced” control frameworks is that simplicity is highly favourable in new designs of complex systems (cf. the Philips company motto: “Sense and simplicity”). SISO control loops are intuitive and readily designed for systems with limited coupling or frequency-separated coupling between distinct input-output pairs. Thus, SISO control loops may work quite well and it is often hard to demonstrate significant benefits of using advanced control solutions in terms of power production and/or load reduction, which are required to justify research into such new paradigms. In addition, more complex control frameworks often require expert knowledge and present many design and tuning parameters. A third and very significant factor is that the control system contains a large body of knowledge which has been acquired over the years by the manufacturer. In fact, this knowledge embedded in the control system may make or break the competitive position of a turbine for a manufacturer and part of this knowledge might have to be discarded when transitioning to a new control framework. Finally, a reason used to be that high order controllers and model predictive control presented computational challenges, but these have now largely been overcome with the advent of cheap and high capacity computing power. Obviously, the previous statements only apply to systems where linear time invariant control is potentially feasible. There are many systems, for example in robotics, where linear control laws cannot stabilise the system, let alone provide any level of performance. In such cases nonlinear control techniques, which may be seen as “advanced” by default must necessarily be considered.

### 1.3.2 The role of data-driven modelling in wind turbine control design

The first principles aeroelastic models described above have a few drawbacks. While aeroelastic models are vital in the design stage of wind turbines to predict fatigue and extreme loads, power production and evaluate possible control systems, it is inevitable that many factors contribute to uncertainty or errors in the prediction of dynamic modes and time constants. Among those are: differences between expected and actual material properties; differences in manufacturing; differences in soil or foundation characteristics; modelling assumptions and simplifications and unmodelled sensor characteristics. System identification may aid in understanding the true underlying dynamics and as a consequence may be a *key enabler* for improvements to the design of multi-objective controllers for power production and load reduction. In the control engineering community, system identification has proved to be a powerful tool for the analysis of dynamic systems. The capability to derive models from operational data allows engineers to gain insight into the dynamics of systems which have been modelled with certain coarse or restrictive assumptions or errors, or systems of which only simplified models are available. An additional motivation for system identification is that it automatically delivers a model that describes the phenomena which manifest themselves in the data. In physical first-principles modelling, the model complexity is primarily a choice made by the user, who may opt for over-modelling to ensure that any possibly relevant dynamics are incorporated. In practice, not all modes that can be described by a model may be relevant in the ultimate manifested behaviour.

As early as in 1994, the late Peter Bongers argued in his thesis (Bongers, 1994):

“... direct validation of models describing wind energy conversion systems by a direct comparison with measured data is of very limited use. One of the few possible solutions to this problem is the application of system identification techniques.”

This argument is based on the fact that control design relies on accurate knowledge of the behaviour from (actuator) inputs to (sensor) outputs – in terms of gains and phases for LTI systems. Updating a complicated nonlinear aeroservoelastic model on the basis of comparisons with measured data, which are subject to significant variations due to large stochastic contributions resulting from turbulence, is a time consuming method to obtain accurate input-output models and is not guaranteed to be successful.

The most established identification techniques for dynamic systems are those designed for linear time invariant (LTI) systems. The system-theoretic framework of LTI systems is extremely powerful, with a wealth of theoretical and practical results. The practical value of this framework is, in part, due to the fact that all smooth nonlinear systems permit a locally linear description of their dynamics around some constant operating point (Ljung, 1999; Khalil, 2002; Verhaegen and Verdult, 2007). This is also the case for wind turbines and indeed first results on the estimation of LTI models of wind turbines were seen in the early 1990s and since then several scientific articles have appeared on this topic (van Baars, Mosterd and Bongers, 1993; James III, Carne and Lauffer, 1993; van Baars and Bongers, 1994; Knudsen, Andersen and Toffner-Clausen, 1997; Marrant and van Holten, 2004; Hansen, Thomsen, Fuglsang et al., 2006; Iribas-Latour and Landau, 2009; Houtzager, Kulcsár, van Wingerden et al., 2010; van der Veen, van Wingerden and Verhaegen, 2010c; Iribas-Latour and Landau, 2012).

Currently, system identification is almost not used in the wind energy industry, but in recent years several major manufacturers have performed studies to determine the potential for system identification in their control design approaches. In part, this could be attributed to the fact that thus far industry has been satisfied with the performance of controllers (van Wingerden, 2008). To date these have been aimed predominantly at power regulation and it is to be expected that once multi-variable and multi-objective control design becomes commonplace the need for accurate and refined models will increase.

It was argued before that wind turbines are nonlinear systems when we considered the variable gain of the pitch input. One way to capture this nonlinearity is to identify models in several operating points, that is at several mean wind speeds (Jelavic, Peric and Petrovic, 2006; Iribas-Latour and Landau, 2012). However, since wind turbines operate in a continuously changing wind field it can be particularly difficult to maintain a reasonably steady operating point. This makes it hard, if not impossible, to obtain suitable data records for LTI identification, since large wind speed variations cause the linearity assumptions to be violated. The consequence is that one can only identify a “mean” model which describes the experimental data in the best way.

If one could explicitly model the dominant nonlinear effects, one could use an arbitrary sequence of data obtained from the turbine, in which the wind speed varies. One family of methodologies is provided by the tools aimed at the identification of LPV systems. Identification of LPV systems has seen major developments during the last decade (Lee and Poolla, 1999; Verdult, 2002; van Wingerden, 2008; Tóth, 2010). While these developments are significant steps forwards, it is hard to apply these methods to certain real systems such as wind turbines. There are a few aspects which contribute to these difficulties:

- LPV models are specified in terms of a *scheduling parameter* which determines the instantaneous dynamics. From first principles it is often possible to motivate a certain choice of scheduling parameter for the dynamics in continuous-time, but this is far from the case for the equivalent discrete-time models (Tóth, 2010);
- LPV identification methods often require either solving non-convex parameter estimation problems (for prediction-error methods) or solving very high-dimensional least-squares problems. The latter problem was partly addressed in van Wingerden (2008), but it remains a challenging aspect since the solution comes with an increased variance on the estimated models.

In Figure 1.3 we show some common model classes considered in system identification. Proceeding from LTI models on the left to full non-linear models on the right the figure is meant to give a qualitative indication that an increase in model fidelity comes with an increase in complexity, in terms of number of parameters, the complexity of the dynamic behaviour and the complexity of identification and control algorithms. We have previously

argued that LPV techniques are not yet sufficiently mature to be applied to real wind turbines and hence our focus will be on making developments in the highlighted area.

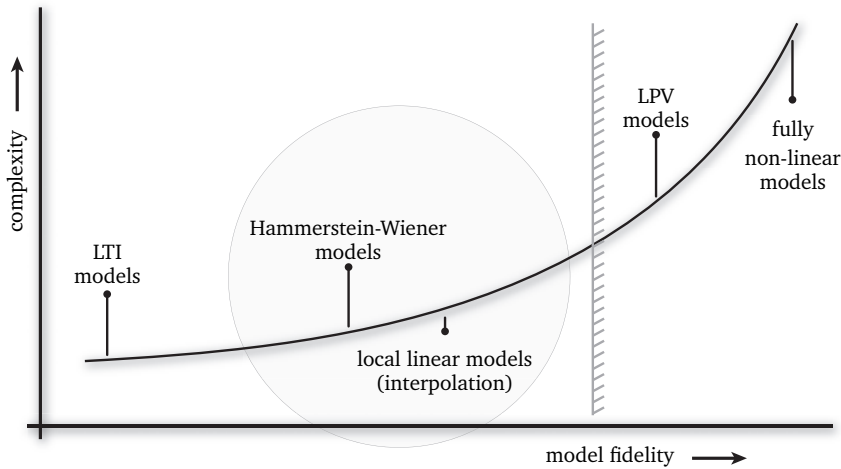


**Figure 1.3** – Qualitative indication of fidelity versus computational complexity of different modelling frameworks in system identification. From a practical point of view, LPV and generic nonlinear methods are often still out of reach.

### System identification and industrial practice

Given the state of the art of control system design for wind turbines it is most likely that system identification methods will first fulfil a role in the development of new wind turbine designs. The main role will then be to provide models of the turbine which allow the engineers to investigate differences between the first principles models and the real (test) turbine. Also, the controller design could subsequently be based on the identified model.

As system identification technology advances, identification could be performed for each installed turbine, e.g. as a built-in functionality, in order to account for manufacturing differences and local foundation characteristics. This seems to be useful only if the model can be used directly in an (adaptive) model-based controller, or by defining a few instrumental parameters such as natural frequencies which are to be tuned in the commissioning phase. System identification could then also be regularly performed to account for changing aerodynamics due to accumulation of dirt on the blades and due to seasonal air density variations, insofar these effects are significant.

### 1.3.3 Prediction error methods and subspace methods

Concerning the history of the identification of LTI systems two major identification frameworks have emerged over the years: the *prediction error*<sup>4</sup> (PE) framework and the *subspace identification* framework. In the present context we will consider as methods belonging to the PE framework all those which require the specification of a *model structure* explicitly in terms of parameters, where these parameters are subsequently estimated by minimising an identification error criterion (Ljung, 1999) or maximising a certain likelihood function. In contrast, we will call subspace methods those which rely on constructing data matrices from input-output data and seek matrices containing system

<sup>4</sup>Informally, we will also classify output error methods under this framework.

parameters in (intersections of) subspaces of these data matrices (Van Overschee and De Moor, 1996; Verhaegen and Verdult, 2007).

Since we are predominantly dealing with multiple-input-multiple-output (MIMO) systems of a fairly high order (typically 20 or higher), the choice for subspace identification methods is a natural one for the following reasons:

- Considering high-dimensional aeroelastic systems, it is most likely that these are described by a set of coupled nonlinear differential equations. Linearising such a model naturally leads to a high order state-space structure. It is not feasible to write such a model explicitly in terms of physical parameters (not least because of the inherent non-injectivity of such a description (Verhaegen and Verdult, 2007)). Besides, it is hard to prescribe a specific structure for the disturbances, other than modelling these as originating from filtered white noise. These two aspects lead to a generic state-space structure which is the natural underlying structure in subspace methods;
- It is difficult to estimate a priori which modes of a first principles model will in the end contribute to the measured output data, i.e., which modes manifest themselves in the data. The order detection mechanism of subspace methods allows the order of the identified model to be selected in a systematic way and does not require it to be fixed a priori as is the case for PE methods;
- Subspace methods do not require solving a nonlinear least-squares optimisation problem to estimate the parameters of the state-space model. Parameterised high-order MIMO state-space models in particular almost inevitably lead to error criteria which have many local minima (Ljung, 1999; Haverkamp, 2001; Verdult, Bergboer and Verhaegen, 2003). In such cases subspace methods are more likely to give repeatable results (Haverkamp, 2001; Verhaegen and Verdult, 2007). PE methods can always be applied in a subsequent step, where the parameters of the subspace model are used as initial condition for the nonlinear optimisation process.

Before presenting ideas to on the one hand overcome the limitations of LTI modelling and, on the other hand avoid the significant challenges of LPV and generic nonlinear modelling we will devote some attention to the challenges associated with system identification of wind turbines.

## 1.4 Key challenges and contributions

Wind turbines present a number of specific challenges when it comes to applying system identification. These challenges motivate research into identification techniques tailored to wind turbines and related systems. The result of this tailoring should be that each of these challenges is addressed so that the resulting new identification techniques become valuable to the wind energy industry. This motivation also leads us to the main contributions of this thesis.

### 1.4.1 Closed-loop operation

A wind turbine must typically operate in closed-loop with a controller<sup>5</sup>. Maintaining the rotor speed requires that the torque balance is dynamically regulated. A consequence of this requirement is that the stochastic disturbances acting on the turbine – e.g., rotor speed variations due to turbulence – are rejected by the control system and hence the input signals to the turbine will be correlated with these disturbances. In system identification it is often assumed that input signals are uncorrelated with stochastic disturbances in order to achieve consistent models and this has traditionally hampered subspace identification methods in particular. Over the last decade, methods have appeared which do not rely on such assumptions.

---

<sup>5</sup>Except stall-controlled fixed-speed-fixed-pitch turbines which can be seen as “self-regulating”.

We have developed a closed-loop subspace identification method which extends the classical multivariable output-error state-space (MOESP) algorithm for open-loop situations. We have further placed most of the advances in closed-loop subspace identification methods of the last fifteen years in a common framework, showing how the different methods relate to each other.

– see **Chapter 2** and (van der Veen, van Wingerden and Verhaegen, 2010a; van der Veen, van Wingerden, Bergamasco et al., 2012)

We have also shown how the application of closed-loop subspace identification methods can form a valuable step in the process of controller design for aeroelastic systems: in the first place to serve as a basis for model-based control design and in the second place to serve as a rapid diagnostic tool to evaluate closed-loop performance of the designed control system.

– see **Chapter 3** and (Barlas, van der Veen and van Kuik, 2012; Bernhammer, De Breuker, Karpel et al., 2012; Fleming, van Wingerden, Scholbrock et al., 2013)

The closed-loop identification framework provides an interesting extension to control. As a means to address slowly time-varying nonlinear behaviour we have considered the *subspace predictive control* (SPC) framework. In this framework system parameters are recursively estimated, which are used to construct an output predictor. This output predictor is then used in a predictive control setting. To recursively identify parameters in a robust way we present a directional forgetting least-squares method in square root form. We also demonstrate the application of SPC to two real experimental systems.

– see **Chapter 4**

#### 1.4.2 Periodic loads

Many components of a turbine are subject to very significant periodic loads. These loads arise from (Burton, Sharpe, Jenkins et al., 2001; Bianchi, De Battista and Mantz, 2007):

- the rotor blades passing through the tower velocity deficit during each revolution;
- the rotor moving through a skewed wind field as a consequence of wind shear, yaw misalignment and rotor tilt;
- the rotor rotating through a slowly (in a relative sense) moving turbulent wind field, thereby periodically sampling the wind field;
- the cyclic effect of gravity as the rotor blades complete a revolution;
- rotor imbalance due to mass and stiffness non-uniformities.

These periodic loads are directly related to the rotor azimuth and hence present frequency content at the instantaneous rotor frequency and higher harmonics. In system identification it is standard practice to model disturbances as filtered white noise sources. These (almost) periodic and hence very narrowband disturbance cannot be adequately represented as filtered white noise.

We have extended closed-loop subspace identification methods to deal with the very dominant (quasi)periodic signals found in certain wind turbine measurements. We have shown on several realistic experimental data sets that by embedding periodic basis functions, parameterised by the rotor azimuth signal, in the set of input signals we can achieve improved identification results.

– see **Chapter 3** and (van der Veen, van Wingerden and Verhaegen, 2010a,c)

#### 1.4.3 Nonlinear system

As mentioned several times before wind turbines are nonlinear systems. When performing LTI system identification it is necessary to ensure that the turbine operates close to a fixed operating point during measurement. This is a challenge in a turbulent wind field and makes it hard to obtain long data records. Identification techniques for LPV and generic nonlinear systems are not mature enough for application to wind turbines. This aspect

motivates research into methods which extend LTI techniques in a structured way to deal with the specific nonlinear behaviour of wind turbines.

We have extended methods for closed-loop subspace identification of multivariable linear time invariant systems to identification of Hammerstein systems by exploiting a recent least-squares framework for multivariate splines. We have shown how separable least-squares regression can be used in a classical overparameterisation approach to achieve a desired low-rank solution. The algorithm has been demonstrated on a detailed wind turbine simulation example.

– see Chapter 5 and (van der Veen, van Wingerden and Verhaegen, 2011, 2012)

Since wind turbines operate in a continuously changing wind field, a challenge is to develop identification methods which are feasible in a practical context. As argued before, sophisticated identification techniques such as LPV techniques are not sufficiently mature to address this issue. Hence, a goal will be to develop methods which seek a balance between the ability to describe the time-varying dynamics of wind turbines and practical feasibility. Motivated by this desire to bring closed-loop identification methods closer to practical applicability we have tailored Hammerstein system identification methods to the identification of wind turbines. This makes it possible to capture the essential nonlinearities without resorting to LPV or nonlinear black-box identification techniques which are still limited in their practical applicability. The potential of this method has been demonstrated and validated on the basis of experimental data obtained from a real wind turbine.

– see Chapter 6 and (van der Veen, van Wingerden and Verhaegen, 2011; van der Veen, van Wingerden, Fleming et al., 2013)

#### 1.4.4 Poor signal-to-noise ratio

The local loads on a turbine rotor and the rotor torque and thrust arising from these local loads are determined by a complex 3-dimensional wind field impinging upon the rotor. This turbulent wind field is a complicated structure with spatially and temporally varying wind speeds, both in terms of direction and magnitude. Since there are no or very limited means of measuring these local wind speeds it is necessary to consider a large portion of these variations, say the deviations from the mean freestream wind speed, as stochastic excitation. This makes system identification a challenging task and calls for robust methods which can deal with large amounts of data and operate in a numerically reliable way.

The subspace identification methods developed and applied throughout this thesis are numerically reliable and efficient. Furthermore, these methods, with the exception of the Hammerstein identification method presented in Chapter 5, do not rely on nonlinear least-squares optimisation. As a consequence, they can be seen as robust methods in the sense that they are numerically reliable and are unlikely to give very different results for two different experiments as a consequence of ending up in local minima of the prediction error objective function. In this sense, the aspect of signal-to-noise ratio is a central theme throughout this thesis.

#### 1.4.5 Cost

For processes such as system identification or controller development and commissioning it is necessary to perturb the regular operation of the wind turbine by exciting the system. Typically, this consists of exciting the pitch system and the torque degrees-of-freedom in the case of system identification, or running and monitoring the turbine's performance over extended periods of time in the case of controller commissioning. Usually, scheduled time is limited a priori, since during such experimental procedures the turbine is not available for actual power production. These aspects call for efficient use of allocated time.

In this thesis we show an example where system identification is used to rapidly evaluate the closed-loop performance of a wind turbine with a new or redesigned controller. In this example 10 minutes of data are sufficient to demonstrate that the controller performance was not satisfactory for one of the controllers. In this case, other methods such as rainflow counting methods would, on the one hand, require data acquired over extended

periods of time and, on the other hand, give only an indirect indication of poor controller performance, i.e., not a possible cause. In this context, system identification tools offer the benefit of judging controller performance in a shorter time frame and hence at a lower cost compared to traditional tools.

– see Section 3.4 in Chapter 3 and (Fleming, van Wingerden, Scholbrock et al., 2013)

It should also be noted that in certain disciplines where system identification is starting to become quite common, e.g., in mechatronic applications, it is often feasible to perform many repeated measurements with random inputs. Such systems are often fast and data records only span a few seconds. In those applications spectral analysis with averaging techniques is useful to obtain high quality nonparametric estimates (Pintelon and Schoukens, 2012). In the field of wind turbines much longer sequences are required – consider for instance the 0.01 Hz oscillation mode of a floating turbine – and it is not feasible to perform many repeated experiments. In a few upcoming examples we demonstrate how identification using one identification and validation data set has led to successful controller design in one go.

– see Section 3.3 in Chapter 3 and (Barlas, van der Veen and van Kuik, 2012; Bernhammer, De Breuker, Karpel et al., 2012)

## 1.5 Publications

The lists below summarise the publications that resulted from the work presented in this thesis.

### Peer-reviewed journal articles

- I – G. J. van der Veen, J. W. van Wingerden and M. Verhaegen (2012). ‘Global identification of wind turbines using a Hammerstein identification method’. In: *IEEE Transactions on Control Systems Technology*
- II – G. van der Veen, J. van Wingerden, P. Fleming, A. Scholbrock, M. Verhaegen (2013). ‘Global data-driven modeling of wind turbines in the presence of turbulence’. In: *Control Engineering Practice* 21.4, pp. 441–454
- III – G. J. van der Veen, J. W. van Wingerden, M. Bergamasco, M. Lovera, M. Verhaegen (2012). ‘Closed-loop subspace identification methods: an overview’. In: *IET Control Theory and Applications (submitted)* —, pages
- IV – L. O. Bernhammer, R. De Breuker, M. Karpel, G. J. van der Veen (2012). ‘Aeroelastic control using distributed floating flaps activated by piezoelectric tabs’. In: *AIAA Journal of Aircraft*. in press
- V – T. K. Barlas, G. J. van der Veen and G. A. M. van Kuik (2012). ‘Model predictive control for wind turbines with distributed active flaps: incorporating inflow signals and actuator constraints’. In: *Wind Energy* 15.5, pp. 757–771

### Peer-reviewed conference proceedings

- VI – G. J. van der Veen, J. W. van Wingerden and M. Verhaegen (2010c). ‘Closed-loop system identification of wind turbines in the presence of periodic effects’. In: *Proc. of the 3<sup>rd</sup> conference, The Science of Making Torque from Wind, Heraklion, Crete, Greece*
- VII – G. J. van der Veen, J. W. van Wingerden and M. Verhaegen (Dec. 2010a). ‘Closed-loop MOESP subspace model identification with parametrisable disturbances’. In: *Proc. of the 49<sup>th</sup> IEEE Control Conference on Decision and Control*. Atlanta
- VIII – G. J. van der Veen, J. W. van Wingerden and M. Verhaegen (July 2011). ‘Data-driven modelling of wind turbines’. In: *Proc. of the American Control Conference (ACC), 2011*. San Francisco, pp. 72–77
- IX – P. M. O. Gebraad, J. W. van Wingerden, G. J. van der Veen, M. Verhaegen (July 2011). ‘LPV subspace identification using a novel nuclear norm regularization method’. In: *Proc. of the American Control Conference*, pp. 165–170
- X – G. J. van der Veen, I. A. Couchman and R. O. Bowyer (2012). ‘Control of floating wind turbines’. In: *Proceedings of the 2012 American Control Conference, Montreal, QC, Canada*
- XI – P. A. Fleming, J. W. van Wingerden, A. K. Scholbrock, G. J. van der Veen, A. D. Wright (2013). ‘Field testing of a wind turbine drivetrain/tower damper using advanced design and validation techniques’. In: *Accepted for the American Control Conference, Washington, DC*
- XII – L. O. Bernhammer, S. P. W. Teeuwen, R. D. Breuker, G. J. van der Veen, E. van Solingen (2012). ‘Performance optimization and gust load alleviation of a UAV wing using variable camber’. In: *ICAST2012: 23<sup>rd</sup> International Conference on Adaptive Structures and Technologies, Nanjing, China*

# Closed-loop subspace identification of LTI systems

Motivated by the fact that many dynamical systems operate in closed-loop and that traditional subspace identification algorithms may give biased estimates in such cases, a significant number of closed-loop subspace identification methods have been developed over the last fifteen years. In this chapter we present one such method, the closed-loop MOESP algorithm. Furthermore, we present a framework based on autoregressive modelling which will turn out to be at the heart of almost all closed-loop subspace identification methods. We view many of the algorithms found in the literature as variants of the algorithms discussed here. In this chapter our aim is to give a clear overview of some of the more successful methods presented throughout the last decade. Furthermore, we retrace these methods to a common origin and show how they differ. We compare the methods both on the basis of simulation examples and real data.

## 2.1 Introduction

In the previous chapter we have stressed the role of system identification as a complement to first principles modelling. The system identification methods presented in this thesis all rely on a common framework that will be introduced and discussed in this chapter. Referring to the challenges set out in Section 1.4 of Chapter 1, we address the problem of closed-loop identification. Closed-loop subspace identification of linear systems is of great practical interest for a number of reasons. Linear models are often required for (model-based) control design and, by directly using measured data, system identification overcomes some of the limitations of first principles modelling. Often, simplifying assumptions are made and limited knowledge of physical parameters is available. Since system identification circumvents these modelling assumptions and the use of incomplete knowledge and instead directly considers phenomena present in the data, it may provide more accurate estimates of natural frequencies and input-output gains and hence may also complement modelling on the basis of first principles. In particular, the advantage of subspace methods compared to prediction error methods (Ljung, 1999) has long been recognized in the context of multivariable systems. For these systems, the parameterization of a prediction-error model structure often leads to an error criterion that is not convex in the parameters. In contrast, the successful closed-loop subspace identification methods developed in recent years consist of a sequence of linear least-squares problems and a model reduction step. In fact, these methods combine prediction-error identification – the estimation of a high-order ARX (Autoregressive with external inputs) model – as an initial step with typical subspace-related subsequent steps (Qin and Ljung, 2003b; Chiuso, 2007b; Di Ruscio, 2009b; van der Veen, van Wingerden and Verhaegen, 2010a). Furthermore, regarding the closed-loop nature of such methods, one may observe that in many practical cases feedback is indeed present. On the one hand this may be necessary due to instability of the open-loop plant, tight process tolerances, limited access to internal signals of the system or the requirement to stay close to an equilibrium around which one can consider the behaviour of the plant linear. On the other hand, in the literature on identification for control (Gevers, 2005) it has often been pointed out that it is desirable to identify a system under circumstances that are close to the real application – i.e., in closed-loop – since

this results in improved estimation of the dynamics, in particular around the cross-over frequency.

In a closed-loop setting the input signal to the system is typically correlated with the process and measurement noise sources. The presence of correlation due to feedback of stochastic signals (e.g., the feedback of process and/or measurement noise) has traditionally hampered subspace identification (and other open-loop system identification techniques) in achieving consistent estimates. First efforts to develop subspace methods for data obtained under closed-loop conditions were made in the mid-nineties, soon after the development of the main open-loop subspace methods, see for instance Verhaegen (1993a); Ljung and McKelvey (1996); Chou and Verhaegen (1997); Van Overschee and De Moor (1997). The method developed in Verhaegen (1993a) shows similarities to the *joint input-output method* well-known in closed-loop prediction-error identification (Ng, Goodwin and Anderson, 1977; Van den Hof and de Callafon, 1996; Van den Hof, 1998), by combining identification of the closed-loop system with knowledge about the controller. In Chou and Verhaegen (1997) closed-loop subspace identification of a restricted class of closed-loop systems is considered by means of instrumental variables (IV). In Van Overschee and De Moor (1997) the N4SID (Numerical algorithm for subspace state space identification) class of open-loop methods is extended to closed-loop systems, but certain knowledge about the controller is required.

One could state that the ideas presented in Ljung and McKelvey (1996) have been pivotal to reaching the current state of the art. In that article high-order ARX modelling was first proposed as a means to deal with correlation issues due to operation in closed-loop, and it is now a feature of the state-of-the-art algorithms. In the year 2003 several articles appeared which again considered the problem of identification in feedback (Chiuso and Picci, 2003a,b; Jansson, 2003; Qin and Ljung, 2003b). The article by Qin and Ljung (Qin and Ljung, 2003b) described the first “innovation estimation” algorithm, in which the first step is to estimate the innovations process. In the article by Jansson (Jansson, 2003) the construction of a state predictor as it is currently used in the closed-loop state estimation algorithms, such as PBSID (Predictor-based subspace identification), was first considered. The articles by Chiuso and Picci in that same year (Chiuso and Picci, 2003a,b) provided much of the theoretical insight behind these methods, discussing how to deal with feedback models.

While, as we mentioned, (Jansson, 2003) already considered the construction of a state predictor, it was not until 2007 (Chiuso, 2007b) that these developments were combined with the estimation of an ARX model as was proposed earlier in (Ljung and McKelvey, 1996). This resulted in the efficient PBSID (Predictor-based subspace identification) algorithm (Chiuso, 2007b), which is currently one of the most promising solutions in closed-loop subspace identification. The innovation estimation algorithm by Qin and Ljung has also seen several further developments over the last decade, resulting in simpler and more efficient implementations (Qin, Lin and Ljung, 2005; Di Ruscio, 2009b; van der Veen, van Wingerden and Verhaegen, 2010a).

It is interesting to note that all these methods have in common that they rely on estimating a high-order ARX structure to start with. As pointed out by Chiuso (Chiuso, 2006b), the developments in these two broad classes of subspace methods (the state estimation and innovation estimation algorithms) can be seen as a significant step forward towards a satisfactory solution for closed-loop subspace identification problems.

Several other modifications to the existing subspace algorithms, to deal with the closed loop identification problem, have been proposed in parallel, see for instance Oku and Fujii (2004); Katayama, Kawauchi and Picci (2005); Gilson and Mercère (2006). In Oku and Fujii (2004) a method is presented that is analogous to the indirect *two-stage method* in prediction error identification (Van den Hof, 1998). In Katayama, Kawauchi and Picci (2005) a joint input-output method is presented similar to Verhaegen (1993a), which focusses on the deterministic subsystems. Finally, in Gilson and Mercère (2006) an IV approach was developed which requires an estimate of the noise model which is not available a priori (see Gilson, Garnier, Young et al. (2011) for a recent overview of these IV methods for prediction error identification.). Hence an iterative procedure is proposed to estimate the model.

In prediction-error identification the available approaches can typically be classified as *direct*, *indirect* and *joint input-output* approaches (Van den Hof, 1998). In this paper we focus on closed-loop subspace methods which we would like to classify as direct methods (Qin, Lin and Ljung, 2005; Chiuso, 2007b; Di Ruscio, 2009b; van der Veen, van Wingerden and Verhaegen, 2010a). Although these methods consist of several steps, they operate directly on the available input-output data. These “direct” subspace methods have the advantage that they place the fewest restrictions on the feedback mechanism. The main drawbacks of the indirect and joint input-output methods (Verhaegen, 1993a; Van Overschee and De Moor, 1997; Oku and Fujii, 2004; Katayama, Kawauchi and Picci, 2005; Gilson and Mercère, 2006) are that linearity of the closed-loop system (not just the plant) must be assumed and that care must be taken with pole-zero cancellations between the plant and the controller.

Based on the foregoing discussion it can be concluded that the field of closed-loop subspace identification has been very active. So active in fact, that a first-time survey of algorithms and methodologies may be daunting to readers who are new to the field. The aim of this paper is to give an overview of some of the more successful methods presented throughout the last decade. Furthermore, we retrace these methods to a common origin and show how they differ. A natural question to be asked is which method is the best for a particular purpose. This is a hard question, since indeed it depends on the purpose of the identified model (Gevers, 2005), the type of the underlying system (Chiuso and Picci, 2005) – particularly using finite sequences – and experimental conditions. Many authors have addressed this issue from a theoretical perspective, regarding asymptotic consistency and variance (Paternell, Scherrer and Deistler, 1996; Jansson and Wahlberg, 1998; Knudsen, 2001; Chiuso and Picci, 2005). When dealing with practical conditions, that is, finite-length sequences and systems of unknown order (or distributed-parameter systems), the various methods discussed here may perform rather differently.

While most of the research in system identification focuses on discrete-time models, in many situations of practical interest (such as, e.g., aircraft and rotorcraft identification, see for example Klein and Morelli (2006); Tischler and Remple (2006); Bergamasco and Lovera (2011a)) the direct estimation of the parameters of a continuous-time model from sampled input-output data is desirable, so that dedicated methods and tools are needed. In addition, there exist special cases in which identifying discrete-time models can be critical, such as the identification of stiff systems or the use of non-equidistantly sampled data, which make it necessary to develop special algorithms that can deal with these cases. The development of identification methods for continuous-time models is a challenge of its own, and has been studied extensively (see, e.g., the recent book by Garnier and Wang (2008) and the references therein). The problem of closed-loop subspace identification in continuous-time has been first considered in the literature in Mohd-Moktar and Wang (2008), where the application of the errors-in-variables approach of Chou and Verhaegen (1997) is proposed to deal with correlation in a continuous-time setting. More recently, see Bergamasco and Lovera (2010a,b, 2011b), novel continuous-time SMI schemes, based on the derivation of PBSID-like algorithms within the all-pass domains proposed in Haverkamp (2001) and Ohta and Kawai (2004) and relying, respectively, on Laguerre filtering and Laguerre projections of the sampled input-output data have been proposed. For an overview of recent techniques in continuous-time closed-loop subspace identification the reader is referred to the aforementioned papers as well as our overview paper (van der Veen, van Wingerden, Bergamasco et al., 2012).

This chapter is organised as follows: first, in Section 2.2 we present the predictor framework that is common to all the methods discussed in this chapter. In Section 2.3 it is shown how the results from Section 2.2 can be used in several ways to arrive at a state-space realisation. This leads us to the essential features of many of the different methods considered in the literature. Finally, in Section 2.4 we describe the results of some experimental studies performed using the presented algorithms in order to highlight some of the differences.

While this chapter mainly deals with the closed-loop identification framework and the performance of the various methods on some test cases, the next chapter will focus exclusively on aspects related to applying these methods in practice, in particular in the

domain of wind energy.

## 2.2 Discrete-time identification framework

In this section we present the framework for closed-loop identification of discrete-time systems that is common to the methods described in this chapter. It is assumed throughout that the system to be identified is a finite-dimensional, linear time invariant system, subject to measurement and/or process noise. A state-space representation of such a system is given by:

$$\mathcal{S} : \begin{cases} x_{k+1} = Ax_k + Bu_k + w_k, \\ y_k = Cx_k + Du_k + v_k, \end{cases}$$

with  $A \in \mathbb{R}^{n \times n}$ ,  $B \in \mathbb{R}^{n \times n_u}$ ,  $C \in \mathbb{R}^{n_y \times n}$  and  $D \in \mathbb{R}^{n_y \times n_u}$ . The vectors  $x_k \in \mathbb{R}^n$ ,  $u_k \in \mathbb{R}^{n_u}$ ,  $y_k \in \mathbb{R}^{n_y}$  are the state vector, input signal and output signal, respectively. The signals  $w_k \in \mathbb{R}^n$  and  $v_k \in \mathbb{R}^{n_y}$  describe the process noise and measurement noise, respectively, with joint covariance matrix:

$$\mathbb{E} \left\{ \begin{pmatrix} w_j \\ v_j \end{pmatrix} \begin{pmatrix} w_k \\ v_k \end{pmatrix}^T \right\} = \begin{bmatrix} Q & S \\ S^T & R \end{bmatrix} \delta_{jk}. \quad (2.2)$$

Furthermore, it is assumed that  $R \succ 0$ .

It is well-known that such systems admit a so-called innovation state-space representation given by:

$$\mathcal{P} : \begin{cases} x_{k+1} = Ax_k + Bu_k + Ke_k, \\ y_k = Cx_k + Du_k + e_k, \end{cases} \quad (2.3a)$$

$$(2.3b)$$

with a Kalman gain  $K \in \mathbb{R}^{n \times n_y}$  and the (unique) ergodic, zero-mean white noise innovation sequence  $e_k \in \mathbb{R}^{n_y}$  with covariance matrix  $\mathbb{E}\{e_j e_k^T\} = W \delta_{jk}$ , with  $W \succ 0$ .

It is important to note that the model (2.3) incorporates both the dynamics of the system to be identified as well as the dynamics of the process and measurement noise. This is possible if it is assumed that all noise sources can be modelled as being filtered white noise processes. This, in turn, holds for arbitrarily coloured process and measurement noise sequences when those noise sequences have nonsingular and rational spectra.

It is assumed that the eigenvalues of  $A - KC$  are strictly inside the unit circle, which is equivalent to the natural assumption that the model to be identified is reachable and observable. More precisely, it is assumed that the pair  $(A, C)$  is observable and the pair  $(A, [B \quad KW^{\frac{1}{2}}])$  is reachable.

In representation (2.3),  $e_k$  may be eliminated from the first equation to yield a system description in one-step-ahead predictor form:

$$x_{k+1} = \tilde{A}x_k + \tilde{B}u_k + Ky_k, \quad (2.4a)$$

$$y_k = Cx_k + Du_k + e_k, \quad (2.4b)$$

where  $\tilde{A} \equiv A - KC$  and  $\tilde{B} \equiv B - KD$  have been introduced for brevity. We will use the notation  $\tilde{\cdot}$  whenever a parameter refers to the predictor model (2.4). This representation forms the basis for the predictor-based subspace identification (PBSID) framework (Chiuso, 2007a).

The goal of the following subsections will be to deliver a unified presentation of the closed-loop subspace identification methods, showing that they have a common origin. Our aim is to provide the reader with a good understanding of key steps in the algorithms, both for implementation and analysis purposes.

For reference purposes we define the identification problem below in Problem 2.1. It is assumed that the plant  $\mathcal{P}$  operates in closed-loop with a, not necessarily linear, controller  $C$  as shown in Figure 2.1. In this figure, it is already assumed that the noise effects are

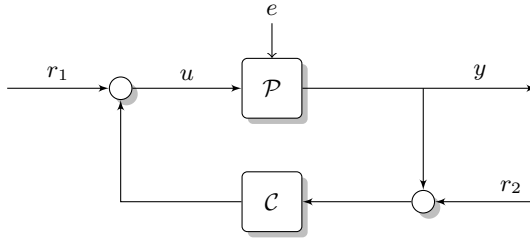


**Figure 2.1** – The closed-loop configuration  $\Sigma$  considered in Problem 2.1.

modelled as if originating from a filtered innovation sequence. For convenience we define a combined reference signal (without assuming that the controller is LTI):

$$r_k = r_{1,k} + \mathcal{C}(r_{2,k}).$$

Note that recent research has demonstrated that care must be taken when identifying an LTI system controlled by a nonlinear feedback mechanism. In Enqvist (2012) it is demonstrated that problems may occur if the controller is nonlinear and if the true noise model is not stably invertible, e.g., if it is nonminimum phase.

We assume that the feedback system is well-posed, implying that the output is uniquely determined by the states. The feedback system is well-posed if the controller or the plant or both have no direct feedthrough component. If the system and the controller are both LTI, the condition for well-posedness is satisfied if  $I_{n_y} + DD_c$  is nonsingular, where  $D_c$  is the feedthrough matrix of the controller (Van Overschee and De Moor, 1997; Katayama, 2005). Hence, without any means of constraining the structure of  $D$ , we can either choose to include it or not in the identification procedure, depending on the feedback system having direct feedthrough or not. Note that a correct choice is necessary to obtain consistent estimates of the Markov parameters, see Section 2.2.5.

It is further assumed that the reference signal  $r_k$  is such that  $u_k$  and  $y_k$  are jointly persistently exciting of sufficiently high order (see Section 2.2.5 for more details).

**Problem 2.1. Discrete-time subspace identification problem** Based on a finite set of input and output data  $\{u_k, y_k\}_{k=0}^{N-1}$  obtained from a system  $\Sigma$ , estimate the order  $n$  of the discrete-time system  $\mathcal{P}_d$  and the associated system matrices  $(A, B, C, D, K)$  up to a similarity transformation.

### 2.2.1 Preliminaries and notation

Before deriving the data equations for subspace identification, we will introduce some notation. We introduce a stacked sample of input and output data  $z_k$  according to:

$$z_k = \begin{bmatrix} u_k \\ y_k \end{bmatrix}.$$

The stacked vector  $z_k^{(p)}$  is defined as

$$z_k^{(p)} = [ z_{k-p}^T, z_{k-p+1}^T, \dots, z_{k-1}^T ]^T,$$

where  $p$  denotes the *past window* size. We also define a reversed extended controllability matrix  $\tilde{\mathcal{K}}^{(p)}$ :

$$\tilde{\mathcal{K}}^{(p)} = [ \tilde{A}^{p-1}\tilde{B}, \tilde{A}^{p-2}\tilde{B}, \dots, \tilde{B} ], \quad (2.5)$$

where we have defined  $\bar{B} = [\tilde{B}, K]$  for brevity. We emphasise that this matrix contains parameters pertaining to the *predictor* representation (2.4). We will further denote block Hankel matrices constructed from data sequences according to:

$$Y_{i,s,N} = \begin{bmatrix} y_i & y_{i+1} & \cdots & y_{i+N-1} \\ y_{i+1} & y_{i+2} & \cdots & y_{i+N} \\ \vdots & \vdots & \ddots & \vdots \\ y_{i+s-1} & y_{i+s} & \cdots & y_{i+N+s-2} \end{bmatrix},$$

such that  $Y_{i,s,N}$  has  $y_i$  as its first element and possesses  $s$  block rows and  $N$  columns. We will sometimes consider block-row matrices, i.e., with  $s = 1$ , which we shall denote by  $Y_{i,N}$ . Finally, we define the block-Toeplitz matrix  $H^{(f)}(B, D)$  pertaining to the innovation model (2.3), which is to be used later when the MOESP algorithm is outlined:

$$H^{(f)}(B, D) = \begin{bmatrix} D & 0 & 0 & \cdots & 0 \\ CB & D & 0 & \cdots & 0 \\ \vdots & \ddots & \ddots & \ddots & \\ CA^{f-2}B & CA^{f-3}B & \cdots & CB & D \end{bmatrix}. \quad (2.6)$$

Likewise, we define the matrix  $H^{(f)}(K, I)$ , and the versions with a tilde ( $\tilde{H}^{(f)}(B, D)$  and  $\tilde{H}^{(f)}(K, 0)$ ) containing parameters of the predictor form (2.4) instead of the innovation form.

## 2.2.2 Data equations

In this section we derive the data equation that is common to many of the closed-loop subspace algorithms. Starting from some initial state  $x_k$ , the state equation (2.4a) can be propagated forward in time, resulting in the expression:

$$x_{k+p} = \tilde{A}^p x_k + \tilde{K}^{(p)} z_{k+p}^{(p)}. \quad (2.7)$$

Based on (2.7) and the output equation (2.4b), the output at time  $k+p$  can then be written as:

$$y_{k+p} = C\tilde{A}^p x_k + C\tilde{K}^{(p)} z_{k+p}^{(p)} + Du_{k+p} + e_{k+p}. \quad (2.8)$$

By the assumption that  $\tilde{A}$  has all its eigenvalues inside the open unit disc, the term  $\tilde{A}^p$  can be made arbitrarily small, i.e.,  $\|\tilde{A}^p\|_2 \approx 0$ , by choosing  $p$  sufficiently large<sup>1</sup>. For that reason, the first term on the right hand sides of (2.7) and (2.8) will be neglected. Since all further algorithms are based on this assumption, we introduce it formally.

**Assumption 2.1** (Negligible bias). *It is assumed that the choice of the past window size  $p$  results in  $\tilde{A}^p = 0$ .*

Depending on the number of samples available and based on Assumption 2.1, (2.8) can be repeated to obtain expressions for  $y_p$  up to  $y_{N-1}$ , resulting in:

$$Y_{p,N_p} = C\tilde{K}^{(p)} Z_{0,p,N_p} + DU_{p,N_p} + E_{p,N_p}. \quad (2.9)$$

Here we have defined  $N_p = N - p$  for brevity. In the remainder of this article the equality in (2.9) is understood to hold under Assumption 2.1. As noted before, the feedthrough term  $D$  should only be included when the feedback loop contains at least a one-sample delay (i.e. has no direct feedthrough) to retain consistency of the identification problem. From (2.9) it is clear that if the controller has direct feedthrough,  $U_{p,N_p}$  is correlated with  $E_{p,N_p}$  and the Markov parameters can no longer be estimated consistently.

<sup>1</sup>See also section 2.3.6 further on regarding this issue in relation to finite data lengths.

*Remark 2.1.* If one leaves out the input terms in the assumed model structure (2.3), it is possible to identify a stochastic model (spectral factor) of a process driven by white noise on the basis of output measurements only. In these cases, however, there is no need to apply a closed-loop identification method. See, e.g., Van Overschee and De Moor (1996, Chapter 3), Goethals, Van Gestel, Suykens et al. (2003); Katayama (2005).

### 2.2.3 Relation to the ARX model structure

Taking a closer look at the data equation (2.8), neglecting the first term on the right hand side, it is seen to have a vector-ARX (VARX) structure. Usually, an ARX model structure prescribes a severely restrictive noise model because it forces the system and noise model to have a common set of poles as seen from the following equation:

$$A(z)y_k = B(z)u_k + e_k, \quad (2.10)$$

with  $z^{-1}$  the unit backshift operator and:

$$\begin{aligned} A(z) &= I - a_1 z^{-1} - \dots - a_p z^{-p}, \\ B(z) &= b_0 + b_1 z^{-1} + \dots + b_p z^{-p}. \end{aligned}$$

In this context, based on the assumption that  $p$  is chosen sufficiently large and working with the predictor form (2.4), it follows that the high order VARX model is fully equivalent to the predictor model. The fact that a high order ARX model can approximate a predictor model with arbitrary accuracy is well-known in prediction error identification, cf. Verhaegen and Verdult (2007, example 10.11).

Regarding the ARX model structure defined in (2.10), the parameters  $a_i$  and  $b_i$  can explicitly be given as the Markov parameters of the predictor form (2.4):

$$a_i = C\tilde{A}^{i-1}K, \quad \text{for } i = 1 \dots p, \quad (2.11a)$$

$$b_i = C\tilde{A}^{i-1}\tilde{B}, \quad \text{for } i = 1 \dots p, \quad (2.11b)$$

$$b_0 = D. \quad (2.11c)$$

This follows by a direct comparison of (2.10) with (2.8) after neglecting the contribution of the initial state.

### 2.2.4 Closed-loop identification issues

Traditional formulations of subspace identification methods often require the plant to operate under open-loop conditions. If such methods are applied to data obtained under closed-loop conditions, the fact that the input signal to the system is correlated with the noise processes is disregarded or neglected. The implicit assumption in such methods is that the input signal  $u_k$  is uncorrelated with the past noise process  $e_k$ . In a closed-loop situation, however, it is clearly seen that this condition is violated:

$$\mathbb{E}\{u_k e_j^T\} \neq 0 \quad \text{for } j < k.$$

Over the last two decades, several strategies have been introduced to deal with this issue, of which we mention a few:

1. Use an open-loop subspace identification method and either accept the bias on the system estimate or use it as an initial model in a prediction-error method (Ljung, 1999). Many prediction error methods are available to deal with closed-loop situations (Van den Hof and Schrama, 1995; Van den Hof, 1998). It is nevertheless of interest to use a subspace method that is better suited to closed-loop data to obtain a better initial estimate for prediction-error methods which rely on solving a non-convex optimization problem;

2. Use a particularly chosen reference signal  $r_k$  as, e.g., discussed in Chou and Verhaegen (1997) to retain certain consistency properties of the identification algorithm. In Di Ruscio (2003) it is argued that, if the feedback is still an open choice, correlation issues due to feedback can also be remedied by a particular choice of the feedback mechanism, e.g., if state feedback based on a Kalman filter is applied. The states estimated by a Kalman filter are (in an ideal setting) uncorrelated with the innovations. Hence, the feedback signal contains no feedback of the noise process(es). Obviously, this approach only lends itself to certain design cases;
3. Use knowledge of the controller, which is then often assumed to be LTI, to achieve consistent estimates (Verhaegen, 1993a; Van Overschee and De Moor, 1997; Katayama, Kawauchi and Picci, 2005);
4. Modify the subspace identification algorithms so as to achieve identification methods that are directly suited to closed-loop data (Ljung and McKelvey, 1996; Jansson, 2003; Qin and Ljung, 2003b; Oku and Fujii, 2004; Qin, Lin and Ljung, 2005; Gilson and Mercère, 2006; Chiuso, 2007b; Katayama and Tanaka, 2007; Di Ruscio, 2009b; van der Veen, van Wingerden and Verhaegen, 2010a). In this chapter we treat the most dominant developments in closed-loop subspace identification, given by the methods which perform high-order ARX modelling followed by a second step which includes model reduction (Ljung and McKelvey, 1996; Jansson, 2003; Qin and Ljung, 2003b; Qin, Lin and Ljung, 2005; Chiuso, 2007b; Di Ruscio, 2009b; van der Veen, van Wingerden and Verhaegen, 2010a). In prediction-error identification the available approaches can typically be classified as *direct*, *indirect* and *joint input-output* approaches (Van den Hof, 1998). In this chapter we focus on closed-loop subspace methods which we would like to classify as direct methods (Ljung and McKelvey, 1996; Jansson, 2003; Qin and Ljung, 2003b; Qin, Lin and Ljung, 2005; Chiuso, 2007b; Di Ruscio, 2009b; van der Veen, van Wingerden and Verhaegen, 2010a). Although these methods consist of several steps, they operate directly on the available input-output data and have the advantage that they place the fewest restrictions on the feedback mechanism.

In the PBSID framework, resulting in (VARX) data equations of the form (2.9), the estimation is not affected by such correlation issues by segregating the data into collections of “past” and “future” samples. Thus, asymptotically in the number of samples  $N$  and the past window size  $p$ , the parameters can be consistently estimated.

## 2.2.5 Estimating the predictor Markov parameters

Based on the assumption that  $e_k$  is the zero-mean white noise innovation sequence and on Assumption 2.1, the predictor Markov parameters in (2.9) can be consistently estimated in a least-squares sense:

$$\arg \min_{[C\tilde{K}^{(p)} D]} \left\| \begin{bmatrix} Y_{p,N_p} \\ U_{p,N_p} \end{bmatrix} - \begin{bmatrix} C\tilde{K}^{(p)} \\ D \end{bmatrix} \begin{bmatrix} Z_{0,p,N_p} \\ U_{p,N_p} \end{bmatrix} \right\|_F^2. \quad (2.12)$$

For a full-rank data matrix  $[Z_{0,p,N_p}^T, U_{p,N_p}^T]^T$ , the least-squares solution can be found from an RQ decomposition (Golub and Van Loan, 1996) of the data. Performing an RQ factorisation of the stacked data matrices one obtains:

$$\begin{bmatrix} \begin{bmatrix} Z_{0,p,N_p} \\ U_{p,N_p} \\ Y_{p,N_p} \end{bmatrix} \end{bmatrix} = \begin{bmatrix} R_{11} & 0 \\ R_{21} & R_{22} \end{bmatrix} \begin{bmatrix} Q_1 \\ Q_2 \end{bmatrix}, \quad (2.13)$$

from which it can be derived that the parameters can be found by solving:

$$R_{21} = \widehat{[C\tilde{K}^{(p)} D]} R_{11},$$

e.g., using back-substitution. Additionally, using the orthogonality of the rows of  $Q$ , we may obtain an estimate of  $E_{p,N_p}$ , according to:

$$\widehat{E}_{p,N_p} = R_{22}Q_2. \quad (2.14)$$

This matrix contains an estimate of the innovation sequence of the innovation state-space model (2.3). Note that the innovation sequence is obtained without explicitly solving the least-squares problem.

We also note that the feedthrough term  $D$ , which has been included so far, should only be included when the loop transfer function of the feedback loop contains at least a one-sample delay to retain well-posedness of the identification problem. If  $D$  is included, it has now been estimated and thus its estimation will not be considered further on.

Based on the least-squares solution, we now have estimates of the predictor Markov parameters (2.11) and the innovation sequence  $\{e_k\}_{k=p}^{N-1}$ .

It is obvious that uniqueness of the parameter estimate requires  $\bar{Z} = [Z_{0,p,N_p}^T, U_{p,N_p}^T]^T$  to be of full rank. The information matrix  $\mathcal{I} = \bar{Z}\bar{Z}^T$  related to the least-squares solution will then be positive definite. This requirement in turn depends on the experimental data, and thus on the true system, reference excitation and the nature of the feedback mechanism (Bazanella, Gevers and Mišković, 2009). For interesting accounts regarding model identifiability and experiment requirements see, e.g., Bazanella, Gevers and Mišković (2009); Gevers, Bazanella, Bombois et al. (2009). We emphasise that in practice, purely from an identification point of view it is usually advantageous to make the reference perturbations as large as possible within the limitations of the system and the requirement to stay close to an operating point around which the system behaves linearly. In many cases it may be necessary to be more judicious in the choice of perturbations: this leads to the topic of least costly identification (Gevers, 2005; Bombois, Scorletti, Gevers et al., 2006).

### 2.2.6 Statistical properties and stochastic least-squares

We will briefly analyse the statistical properties of the LS solution (2.12). To maintain a compact notation, let us for the moment denote the data equation (2.9) concisely as:

$$Y = \Theta Z + E,$$

with obvious definitions of the (matrix) terms.

It is important to realise that we are considering a matrix least-squares problem. This is in fact a multiple linear regression problem, which could be treated by solving several vector-valued least-squares problems. In this case, each output of the system can be considered in turn to estimate subsequent rows of  $\Theta$ . In terms of the normal equations, the LS solution to finding the parameters  $\Theta$  is given by:

$$\widehat{\Theta} = YZ^T (ZZ^T)^{-1}.$$

Assuming that the data is actually generated by the data equation (2.9) with the true parameters  $\Theta$ , we can compute the expected value of the parameters:

$$\begin{aligned} \mathbb{E}\{\widehat{\Theta}\} &= \mathbb{E}\{(\Theta Z + E)Z^T (ZZ^T)^{-1}\} \\ &= \Theta + \mathbb{E}\{EZ^T (ZZ^T)^{-1}\} \\ &= \Theta. \end{aligned}$$

This leads to the conclusion that the least-squares estimate is unbiased. Next, we consider the parameter error covariance. Since the parameters are contained in a matrix ( $\Theta$ ), and we are considering the error variance of its elements, we vectorise the parameter matrix

and study the covariance:

$$\begin{aligned}
& \mathbb{E} \left\{ \text{vec} \left( \widehat{\Theta} - \Theta \right) \text{vec} \left( \widehat{\Theta} - \Theta \right)^T \right\} \\
&= \mathbb{E} \left\{ \text{vec} \left( E Z^T \left( Z Z^T \right)^{-1} \right) \text{vec} \left( E Z^T \left( Z Z^T \right)^{-1} \right)^T \right\} \\
&= \left( \left( Z Z^T \right)^{-1} Z \otimes I \right) \mathbb{E} \left\{ \text{vec}(E) \text{vec}(E)^T \right\} \left( \left( Z Z^T \right)^{-1} Z \otimes I \right)^T \\
&= \left( \left( Z Z^T \right)^{-1} Z \otimes I \right) (I \otimes W) \left( \left( Z Z^T \right)^{-1} Z \otimes I \right)^T \\
&= \left( Z Z^T \right)^{-1} \otimes W.
\end{aligned}$$

Note that we have not used any information on the covariance of the innovation signal. Had we known the value of the innovation signal covariance  $W$ , we might be prompted to compute the *weighted least-squares estimate* to this stochastic least-squares problem. This solution however, will turn out to be the same as the ordinary least-squares solution given before. The reason is that we are performing multiple linear regression, in which each row of the parameter matrix  $\Theta$  could have been solved for independently of the other rows. Therefore, the fact that the innovation signal might have a different variance in each output channel does not affect the estimate. We can conclude that the LS estimate (2.12) is the *best linear unbiased estimator* of  $\Theta$ , if a model of the form (2.9) underlies the data.

## 2.2.7 Least-squares sensitivity

It is interesting to note that using the estimate  $\widehat{E}_{p,N_p}$  instead of the Markov parameters may be advantageous in certain cases where the data matrix  $\bar{Z} = [z_{0,p,N_p}^T, u_{p,N_p}^T]^T$  is poorly conditioned. This may occur when the joint input-output data is not rich enough, e.g., due to the nature of the experiment, poor excitation of reference signals or a low-complexity feedback path (Bazanella, Gevers and Mišković, 2009). In fact, it can be shown that the estimate of the least-squares residual of (2.12) is less sensitive to ill-conditioning than the estimate of the parameters themselves. The worst-case sensitivities of the two estimates are related to the condition number  $\varrho$  of the data matrix as follows (Golub and Van Loan, 1996):

$$\begin{aligned}
& \frac{\left\| \Delta \left[ C \widehat{\mathcal{K}}^{(p)}, D \right] \right\|_2}{\left\| \left[ C \tilde{\mathcal{K}}^{(p)}, D \right] \right\|_2} \propto \varrho(\bar{Z})^2, \\
& \frac{\left\| \Delta \widehat{E}_{p,N_p} \right\|_2}{\left\| Y_{p,N_p} \right\|_2} \propto \varrho(\bar{Z}),
\end{aligned}$$

where  $\varrho(\cdot)$  denotes the condition number. This shows that the estimate of the parameters may be far more sensitive to ill-conditioning than the estimate of the residual.

It is hard to draw further general conclusions from these facts, in particular since one of the estimates is used in state reconstruction algorithms (e.g., PBSID<sub>opt</sub>, section 2.3.3), whereas the other is used in algorithms which estimate the observability matrix (e.g., CLMOESP, section 2.3.4). It is expected, however, that in cases where the data matrix is severely ill-conditioned, the estimate of the innovation sequence may be more reliable than that of the Markov parameters, in particular for the subsequent step of estimating the observability matrix and hence the eigenvalues. Section 2.4.2 discusses an example which illustrates this possible effect.

### 2.2.8 Relation to subspace predictive control

An adaptive control paradigm that was first introduced by Favoreel and De Moor (Favoreel and De Moor, 1998; Favoreel, De Moor, Van Overschee et al., 1999) combines the predictor estimated in Section 2.2.5 with a predictive control law to result in a multivariable adaptive controller. These original formulations considered a predictor that was closely related to the data equations in the open-loop N4SID class of subspace algorithms. Since the inherent goal of these estimated predictors is to use them in a feedback control system, it is clear that the assumption of a system operating in open-loop conditions is violated. The VARX framework described in this section allows for consistent estimation of predictors in closed-loop operation and this was exploited by Hallouzi (2008) and Dong, Verhaegen and Holweg (2008); Dong (2009). For a derivation of this algorithm the reader is referred to Chapter 4.

## 2.3 Obtaining a state-space realisation

In the previous section estimates were obtained for the Markov parameters and the innovation signal pertaining to the predictor model (2.4). In the following subsections we consider four different methods to arrive at a solution to the identification problem (Problem 2.1) based on these estimates. Figure 2.2 schematically depicts the different routes from input-output data to an identified model with references to the appropriate subsections.

### 2.3.1 Direct parameterisation

It is possible to directly obtain a non-minimal state-space model, by casting the estimated ARX model parameters into a state-space parameterisation of order  $(n_y + n_u)p$  (2.15).

$$z_{k+1} = \begin{bmatrix} 0 & I & & \\ & \ddots & \ddots & \\ & & 0 & I \\ \hline 0 & \cdots & \cdots & 0 \\ \hline & \widehat{C\tilde{K}^{(p)}} & & \end{bmatrix} z_k + \begin{bmatrix} 0 \\ \vdots \\ 0 \\ I \\ D \end{bmatrix} u_k + \begin{bmatrix} 0 \\ \vdots \\ 0 \\ I \end{bmatrix} e_k \quad (2.15a)$$

$$y_k = \widehat{C\tilde{K}^{(p)}} z_k + D u_k + e_k. \quad (2.15b)$$

Since the VARX parameters are directly placed in the state-space matrices, we shall refer to this parameterisation as the *direct parameterisation*. The order of this model could subsequently be reduced using a model reduction algorithm. A notable advantage of the direct parameterisation is that the state is measurable, since it is given by delayed samples of input/output data. Furthermore, the variance on the elements of the state-space matrices is directly provided by the least-squares estimate (2.12). These interesting features were exploited in Kulcsár and Verhaegen (2010) for purposes of robust state feedback compensator design. Direct use is also made of the predictor Markov parameters in closed-loop subspace predictive control SPC (Dong, Verhaegen and Holweg, 2008). A drawback of the direct parameterisation is that it is nonminimal and typically has a large state dimension when  $p$  is moderate to large. This may be a problem for subsequent control design. Standard model reduction techniques can be applied to reduce the order of this model.

### 2.3.2 A realisation algorithm

Realisation methods, initiated with the development of the Ho-Kalman realisation algorithm (Ho and Kalman, 1966; Kung, 1978; Juang and Pappa, 1985), are the oldest methods that could be classified under the subspace methods. Whereas earlier approaches depart from a set of Markov parameters or impulse response parameters, later approaches typically start with estimating predictor Markov parameters, or, equivalently, the predictor impulse

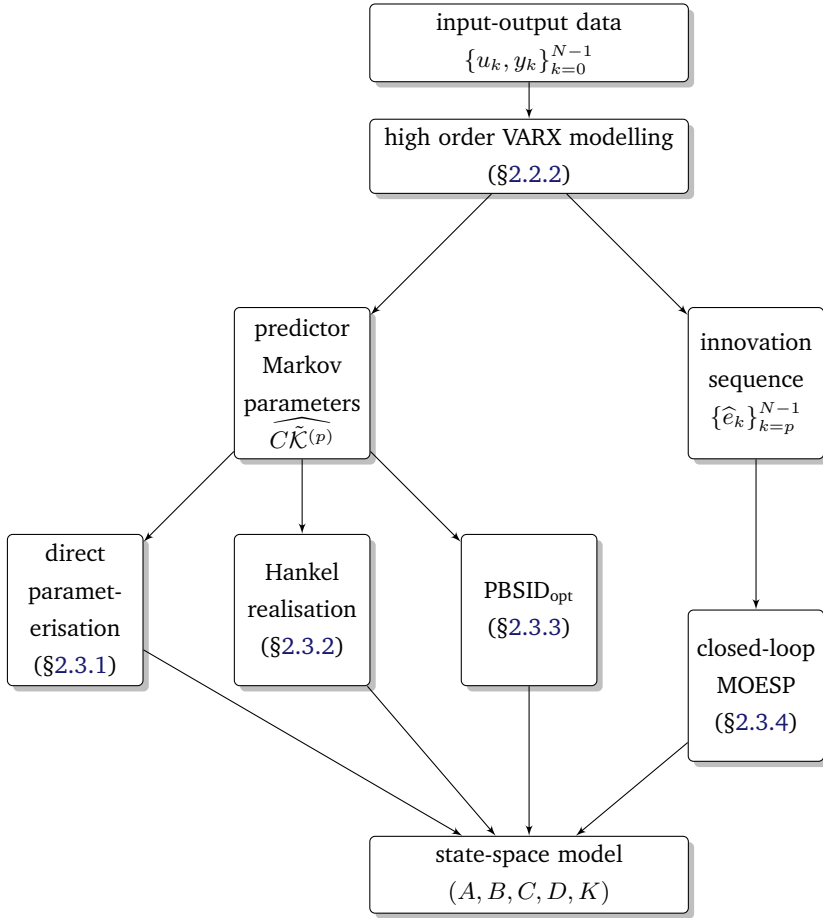


**Figure 2.2** – Schematic representation of the relation between the different closed-loop subspace algorithms.

response, very similar to the VARX step described in Section 2.2.5. In fact, the approach of estimating predictor Markov parameters followed by a realisation step was already presented as early as in 1993 Phan, Horta, Juang et al. (1993). The approach outlined here is a variation on the Observer/Kalman Filter Identification (OKID) method (Phan, Horta, Juang et al., 1995). In this approach, contrary to the Ho-Kalman approach, first an estimate is obtained of the predictor impulse response, using the fact that this response tends to zero after  $p$  steps.

The realisation method relies on forming an *extended observability-times-controllability* matrix. Let us first introduce the extended observability matrix of the predictor and innovation models:

$$\tilde{\Gamma}^{(f)} = \begin{bmatrix} C \\ C\tilde{A} \\ \vdots \\ C\tilde{A}^{f-1} \end{bmatrix}, \quad \Gamma^{(f)} = \begin{bmatrix} C \\ CA \\ \vdots \\ CA^{f-1} \end{bmatrix}.$$

Given a “future” window  $f > n$ , the extended observability-times-controllability matrix

$\tilde{\Gamma}^{(f)} \tilde{\mathcal{K}}^{(p)}$  can be constructed, which has the following structure:

$$\tilde{\Gamma}^{(f)} \tilde{\mathcal{K}}^{(p)} = \begin{bmatrix} C\tilde{A}^{p-1}\tilde{B} & C\tilde{A}^{p-2}\tilde{B} & \dots & C\tilde{B} \\ C\tilde{A}^p\tilde{B} & C\tilde{A}^{p-1}\tilde{B} & \dots & C\tilde{A}\tilde{B} \\ \vdots & \vdots & \ddots & \vdots \\ C\tilde{A}^{p+f-2}\tilde{B} & C\tilde{A}^{p+f-3}\tilde{B} & \dots & C\tilde{A}^{f-1}\tilde{B} \end{bmatrix}. \quad (2.16)$$

Based on the earlier assumption that  $\|\tilde{A}^p\|_2 \approx 0$ , the same approximation can be introduced here, resulting in:

$$\tilde{\Gamma}^{(f)} \tilde{\mathcal{K}}^{(p)} \approx \begin{bmatrix} C\tilde{A}^{p-1}\tilde{B} & C\tilde{A}^{p-2}\tilde{B} & \dots & C\tilde{B} \\ 0 & C\tilde{A}^{p-1}\tilde{B} & \dots & C\tilde{A}\tilde{B} \\ \vdots & \ddots & \ddots & \vdots \\ 0 & & & C\tilde{A}^{f-1}\tilde{B} \end{bmatrix} \equiv \begin{bmatrix} \Xi_0 \\ \Xi_1 \\ \vdots \end{bmatrix}. \quad (2.17)$$

Having estimated the predictor Markov parameters  $C\tilde{\mathcal{K}}^{(p)}$ , it is straightforward to construct this matrix, by noticing that each block-row  $\Xi_i$  is obtained from the previous by shifting it and padding it with zeroes. The first block-row  $\Xi_0$  consists of all predictor Markov parameters, i.e.,  $\Xi_0 \equiv C\tilde{\mathcal{K}}^{(p)}$ .

Using the former definition of  $\tilde{\mathcal{K}}^{(p)}$  (2.5), it is possible to derive a recursive expression which provides the approximate block-rows of the following extended observability-times-controllability matrix:

$$\Gamma^{(f)} \tilde{\mathcal{K}}^{(p)} \equiv \begin{bmatrix} \mathcal{H}_0 \\ \mathcal{H}_1 \\ \vdots \\ \mathcal{H}_{f-1} \end{bmatrix}, \quad (2.18)$$

where the recursive expression is given by (Phan, Horta, Juang et al., 1993; Dong, Verhaegen and Holweg, 2008):

$$\mathcal{H}_j = \Xi_j + \sum_{\tau=0}^{j-1} (C\tilde{A}^{j-\tau-1}K)\mathcal{H}_\tau, \quad \mathcal{H}_0 = \Xi_0.$$

Based on the assumption of minimality, which holds for both the innovation and predictor representations, it immediately follows that  $\text{rank}(\Gamma^{(f)} \tilde{\mathcal{K}}^{(p)}) = n$ . In practice the number of nonzero singular values is not  $n$ , due to the fact that we construct the matrix (2.17) using estimated parameters. Then, an SVD of  $\Gamma^{(f)} \tilde{\mathcal{K}}^{(p)}$  can be used to find approximations of  $\Gamma^{(f)}$  and  $\tilde{\mathcal{K}}^{(p)}$  and the order  $n$ :

$$\Gamma^{(f)} \tilde{\mathcal{K}}^{(p)} \approx \mathcal{U}_n \Sigma_n \mathcal{V}_n^T,$$

so that we may take:

$$\Gamma^{(f)} = \mathcal{U}_n, \quad \tilde{\mathcal{K}}^{(p)} = \Sigma_n \mathcal{V}_n^T.$$

Estimates of the system matrices can then be obtained as follows:  $C$ ,  $B$  and  $K$  are simply read off from the appropriate matrices:

$$C = \Gamma^{(f)}(1:n_y, :), \\ [B - KD, K] = \tilde{\mathcal{K}}^{(p)}(:, (p-1)(n_u + n_y) + 1:p(n_u + n_y)),$$

whereas  $A$  is found as the solution to the overdetermined problem:

$$\Gamma^{(f)}(1:(s-1)n_y, :)A = \Gamma^{(f)}(n_y + 1:sn_y, :), \quad (2.19)$$

(using MATLAB notation).

### 2.3.3 Predictor-based subspace identification (PBSID<sub>opt</sub>)

In predictor-based subspace identification, a predictor for the state sequence is constructed. If an estimate of the state sequence is known, the system matrices can be found directly from two least-squares problems, similar to what is done in the open-loop N4SID class of algorithms, based on the following identities:

$$X_{p+1, N_p-1} = [A \quad B \quad K] \begin{bmatrix} X_{p, N_p-1} \\ U_{p, N_p-1} \\ E_{p, N_p-1} \end{bmatrix}, \quad (2.20)$$

$$Y_{p, N_p} = [C \quad D] \begin{bmatrix} X_{p, N_p} \\ U_{p, N_p} \end{bmatrix} + E_{p, N_p}. \quad (2.21)$$

On the basis of (2.7) it can be concluded that, neglecting the first term, the product  $\tilde{\mathcal{K}}^{(p)} Z_{0,p,N_p}$  represents the state sequence  $X_{p,N_p}$ . Unfortunately, this product cannot be estimated directly. What is available is an estimate of the parameters  $C\tilde{\mathcal{K}}^{(p)}$ . As in the OKID algorithm in Section 2.3.2 we can construct the matrix in (2.17) using these parameters. This matrix is used in the PBSID<sub>opt</sub> algorithm, whereas the standard PBSID algorithm makes use of the full matrix in (2.16).

*Remark 2.2.* Following the estimation of the Markov parameters (2.12) we only have available the Markov parameters required to construct the matrix in (2.17). It is also possible, however, to construct the full matrix in (2.16), by solving a sequence of  $f$  shifted versions of (2.12) of increasing order  $p$ . This is detailed in, e.g., Chiuso (2007b). In Chiuso (2007a,b) it was shown that the “optimised” version described here results in a lower variance than the standard PBSID algorithm.

Thus, having constructed the matrix  $\tilde{\Gamma}^{(f)}\tilde{\mathcal{K}}^{(p)}$ , the product  $\tilde{\Gamma}^{(f)}\tilde{\mathcal{K}}^{(p)}Z_{0,p,N_p}$  can be calculated. This product corresponds, by definition, to the extended observability matrix times the state sequence:  $\tilde{\Gamma}^{(f)}X_{p,N_p}$ . Using an SVD, the order of the system and the state sequence can then be estimated:

$$\tilde{\Gamma}^{(f)}X_{p,N_p} = \tilde{\Gamma}^{(f)}\tilde{\mathcal{K}}^{(p)}Z_{0,p,N_p} = \mathcal{U}_n \Sigma_n \mathcal{V}_n^T. \quad (2.22)$$

The state sequence is recovered (up to a similarity transformation) as:

$$\hat{X}_{p,N_p} = \Sigma_n \mathcal{V}_n^T. \quad (2.23)$$

In practice, the matrix  $\tilde{\Gamma}^{(f)}\tilde{\mathcal{K}}^{(p)}$  is constructed using estimated parameters. Hence, the SVD in (2.22) will not exactly contain  $n$  nonzero singular values and we will only obtain an estimate of the true state sequence  $\hat{X}_{p,N_p}$ .

Subsequently, (2.20) and (2.21) are solved in a least-squares sense. First, (2.21) is solved and subsequently its residual  $\hat{E}_{p,N_p}$  is used in the solution of (2.20).

#### Variants

Several variants of the PBSID<sub>opt</sub> algorithm can be found in the literature, some of which have already been mentioned. The PBSID<sub>opt</sub> is asymptotically equivalent (Chiuso, 2006a) to the SSARX algorithm proposed by Jansson (Jansson, 2003). Several other modifications are discussed in Di Ruscio (2009a).

#### Recursive implementation

The PBSID<sub>opt</sub> can be also employed for on-line applications, by working out recursive implementations. The problem has been studied in the literature by a number of authors and a template for recursive closed-loop subspace identification can be outlined as follows, along the lines of the general ideas proposed in Chiuso, Muradore and Marchetti (2010) and of the algorithm in Houtzager, van Wingerden and Verhaegen (2009a):

- Recursive update of the solution of the least squares problem (2.12), using a conventional RLS scheme.
- Update of the estimate of the state sequence, i.e., of the state estimate given by (2.23). In this respect, note that this is the most critical step in the implementation, as one has to ensure that the recursive state estimates are expressed in a consistent state space basis. One way of guaranteeing this is given by, e.g., the scheme proposed in Houtzager, van Wingerden and Verhaegen (2009a), which is based on the so-called propagator method for the recursive update of the state sequence (see also Mercère, Lecœuche and Lovera (2004) for details).
- Recursive estimate of the state space matrices of the system, i.e., update of the solution of the least squares problem (2.20), again by means of RLS.

### 2.3.4 Closed-loop MOESP

In Section 2.2.5 it was shown that besides the Markov parameters, an estimate of the innovation sequence can be obtained. If we revisit the innovation model (2.3) an estimate,  $\{\hat{e}_k\}_{k=p}^{N-1}$ , of the innovation sequence  $\{e_k\}_{k=p}^{N-1}$  is now available (although not over the full data horizon  $k = 0 \dots N - 1$ ). First obtaining an estimate of the innovation sequence results in a class of *innovation estimation* methods, first introduced by Qin and Ljung and leading to their PARSIM method (Qin and Ljung, 2003a). Having knowledge of the innovation sequence, we are effectively left with a deterministic identification problem to which solutions are well-known. The deterministic MOESP (Multivariable Output-Error State-sPace) algorithm is one such algorithm. The method described here, CLMOESP, was presented in de Korte (2009); van der Veen, van Wingerden and Verhaegen (2010a,b) and is inspired by and in many respects similar to (Qin and Ljung, 2003b; Di Ruscio, 2009b).

Estimating the extended observability matrix  $\Gamma^{(f)}$

Referring to Verhaegen and Verdult (2007) for a detailed derivation, we consider the following data equation in the MOESP algorithm.

$$Y_{p,f,N_f} = \Gamma^{(f)} X_{p,N_f} + H^{(f)}(B, D)U_{p,f,N_f} + H^{(f)}(K, I)E_{p,f,N_f},$$

with  $N_f = N - f - p + 1$ . This is also the data equation considered in the deterministic MOESP setting, since the signals constituting  $U_{p,f,N_f}$  and  $E_{p,f,N_f}$  are both at our disposal and no further stochastic disturbances are present. The influences of the input and the innovation can be eliminated using orthogonal subspace projection. For this purpose we construct the orthogonal projection matrix:

$$\Pi_{\mathcal{Z}_{p,f,N_f}}^\perp = I - \mathcal{Z}_{p,f,N_f}^\dagger \mathcal{Z}_{p,f,N_f},$$

where the definition  $\mathcal{Z}_{p,f,N_f} = \begin{bmatrix} U_{p,f,N_f} \\ E_{p,f,N_f} \end{bmatrix}$  is used. Applying this projection results in:

$$Y_{p,f,N_f} \Pi_{\mathcal{Z}_{p,f,N_f}}^\perp = \Gamma^{(f)} X_{p,N_f} \Pi_{\mathcal{Z}_{p,s,N_f}}^\perp.$$

In practice, this projection may be obtained by performing an RQ factorisation of the input and output data, which is numerically much more efficient and stable than evaluating the large projection matrix:

$$\begin{bmatrix} \mathcal{Z}_{p,f,N_f} \\ Y_{p,f,N_f} \end{bmatrix} = \begin{bmatrix} R_{11} & 0 \\ R_{21} & R_{22} \end{bmatrix} \begin{bmatrix} Q_1 \\ Q_2 \end{bmatrix}.$$

Using the properties of the RQ factorisation we can then equivalently write:

$$Y_{p,f,N_f} \Pi_{\mathcal{Z}_{p,f,N_f}}^\perp = \Gamma^{(f)} X_{p,N_f} \Pi_{\mathcal{Z}_{p,f,N_f}}^\perp = R_{22} Q_2.$$

If the input and noise sequences are persistently exciting of at least order  $fn_u$  and  $fn_y$  respectively for the input and innovation signals (Verhaegen and Verdult, 2007), the following holds, since then the column space of the observability matrix is preserved in  $Y_{p,f,N_f} \Pi_{\bar{Z}_{p,f,N_f}}^\perp$  after projection:

$$\begin{aligned} \text{range}(\Gamma^{(f)}) &= \text{range} \left( \lim_{N \rightarrow \infty} \frac{1}{\sqrt{N-p}} Y_{p,f,N_f} \Pi_{\bar{Z}_{p,f,N_f}}^\perp \right) \\ &= \text{range} \left( \lim_{N \rightarrow \infty} \frac{1}{\sqrt{N-p}} R_{22} \right). \end{aligned}$$

Thus, because  $Q_2$  has full row rank, the column-space of  $R_{22}$  serves as a basis for the column space of the extended observability matrix  $\mathcal{O}_f$ . Performing an SVD of  $R_{22}$  gives:

$$R_{22} = U_n \Sigma_n V_n^T, \quad (2.24)$$

where  $n$  is the number of dominant singular values and also the order of the underlying innovation system. The columns of  $U_n$  provide a basis for  $\Gamma^{(f)}$ . A gap between successive singular values will often indicate the order of the system (see Verhaegen (1993b) for more details).

Estimating the  $A$  and  $C$  matrices

Estimates of the  $A$  and  $C$  matrices can subsequently be obtained from  $U_n$ . Given the structure of  $\Gamma^{(f)}$ , the  $C$  matrix is found as the first  $n_y$  rows of  $U_n$ .  $A$  can be found as the solution to the overdetermined problem:

$$U_n(1:(f-1)n_y, :)A = U_n(n_y+1:fn_y, :), \quad (2.25)$$

(using MATLAB notation). The matrices  $B$ ,  $D$  and  $K$  can be computed in a second step by solving a least-squares problem as shown in the next subsection.

Estimating  $B$ ,  $D$ ,  $K$  and the initial state

Based on the system description (2.3), the output at time  $k$  can be written as:

$$y_k = CA^k x_0 + \sum_{\tau=0}^{k-1} CA^{k-\tau-1} (Bu_\tau + Ke_\tau) + Du_k + e_k.$$

Applying the vectorisation operator and exploiting a property of the Kronecker product (Brewer, 1978), this can be rewritten as:

$$y_k = \underbrace{\begin{bmatrix} \Phi_k^{x_0} & \Phi_k^B & \Phi_k^K & \Phi_k^D \end{bmatrix}}_{\Phi_k} \underbrace{\begin{bmatrix} x_0 \\ \text{vec}(B) \\ \text{vec}(K) \\ \text{vec}(D) \end{bmatrix}}_{\Theta} + e_k, \quad (2.26)$$

where we have defined:

$$\begin{aligned} \Phi_k^{x_0} &= CA^{k-1}, & \Phi_k^B &= \sum_{\tau=0}^{k-1} u_\tau^T \otimes CA^{k-\tau-1}, \\ \Phi_k^K &= \sum_{\tau=0}^{k-1} e_\tau^T \otimes CA^{k-\tau-1}, & \Phi_k^D &= u_k^T \otimes I_{n_y}. \end{aligned}$$

Equation (2.26) is a linear expression in the unknown elements of  $x_0$ ,  $B$ ,  $D$  and  $K$ , which can be solved for the parameters in a least-squares sense with the available data

set  $\{u_k, y_k, e_k\}_{k=p}^{N-1}$ . For this purpose, define  $\Phi_k$  and  $\Theta$  as in (2.26). Then the least squares problem can be stated as:

$$\hat{\Theta} = \arg \min_{\Theta} \sum_{k=p}^{N-1} \|y_k - \Phi_k \Theta\|_2^2 = \arg \min_{\Theta} \|Y - \Phi \Theta\|_2^2, \quad (2.27)$$

which can be solved efficiently using a QR factorisation (Golub and Van Loan, 1996). It must be noted that, although the described way to find  $B$ ,  $D$ ,  $K$  and the initial state is conceptually simple, it is computationally prohibitive due to the Kronecker products involved. Much more efficient procedures exist to find the matrix  $\Phi$  which avoid evaluation of Kronecker products for each  $k$ . Such procedures are detailed in Verhaegen and Varga (1994); Haverkamp (2001). The approach presented here must be modified slightly in case the system is open-loop unstable, see Chou and Verhaegen (1997).

#### Variants

Here we have considered one possible ‘‘innovation estimation’’ algorithm, which we have chosen for its simplicity. One variant is the first innovation estimation algorithm: the PARSIM method presented in Qin and Ljung (2003b), where the innovation and Markov parameters are estimated in a recursive fashion. Subsequently, the DSR.e algorithm was presented in Di Ruscio (2004), Nilsen (2005, Chapter 6.2) and Di Ruscio (2009b). In fact, the latter algorithm seems to be very similar to solving for the innovation sequence followed by the deterministic MOESP projection (Verhaegen and Verdult, 2007; de Korte, 2009), even though this is not mentioned.

*Remark 2.3.* In the four previous sections, estimates have been obtained for the matrix  $K$  using least-squares techniques. Although these estimates minimise the appropriate least-squares criteria, they do not automatically satisfy the requirement of having a stable predictor and thus are not proper Kalman gains. If the identified models are to be used in the context of observing or prediction, this is a crucial property. An alternative way to obtain  $K$  is by solving a discrete algebraic Riccati equation (DARE). Such approaches are described in Van Overschee and De Moor (1997); Katayama (2005); Verhaegen and Verdult (2007).

### 2.3.5 Closed-loop MOESP relying solely on $R$ -factors

A potential disadvantage of the innovation estimation methods is that, considering the RQ factorisation (2.13), the computation of the innovation sequence according to (2.14) requires that the entire matrix  $Q$  be stored (or, at least, the Householder reflectors constituting it). In this section it will be shown that it is possible to work with just the triangular factor  $R$  in order to compute the column space of the extended observability matrix  $\Gamma^{(f)}$ . Consider the following data equation:

$$Y_{p,f,N} = \Gamma^{(f)} \tilde{\mathcal{K}}_p Z_{0,p,N} + H^{(f)}(B, D) U_{p,f,N} + H^{(f)}(K, I) E_{p,f,N}. \quad (2.28)$$

We can only solve a single row of this data equation ( $f = 1$ ) for the parameters ( $C \tilde{\mathcal{K}}_p, D$ ) due to correlation between samples  $u_k$  and past samples of  $e_k$ . Alternatively, we can write:

$$Y_{p,f,N} = \tilde{\Gamma}^{(f)} \tilde{\mathcal{K}}_p Z_{0,p,N} + \tilde{H}^{(f)}(B, D) U_{p,f,N} + \tilde{H}^{(f)}(K, 0) Y_{p,f,N} + E_{p,f,N}. \quad (2.29)$$

Using this data equation we can solve for the parameters in a row-wise manner. This can be performed using a single RQ factorisation, after organising the rows of the future Hankel matrices in a staggered fashion:

$$\begin{bmatrix} Z_{0,p,N} \\ U_{p,N} \\ Y_{p,N} \\ U_{p+1,N} \\ Y_{p+1,N} \\ \vdots \end{bmatrix} = \begin{bmatrix} R_{11} & & & & & \\ R_{21} & R_{22} & & & & \\ R_{31} & R_{32} & R_{33} & & & \\ R_{41} & R_{42} & R_{43} & R_{44} & & \\ R_{51} & R_{52} & R_{53} & R_{54} & R_{55} & \\ \vdots & & & & & \end{bmatrix} \begin{bmatrix} Q_1 \\ Q_2 \\ Q_3 \\ Q_4 \\ Q_5 \\ \vdots \end{bmatrix}. \quad (2.30)$$

We emphasise that the (typically large) orthogonal matrices  $Q_i$  don't need to be stored. On the basis of this factorisation we obtain estimates of the noise sequences:

$$E_{p,N} = R_{33}Q_3 \quad (2.31)$$

$$E_{p+1,N} = R_{55}Q_5 \quad (2.32)$$

$$\text{etc...} \quad (2.33)$$

Reorganising, we can form the data equation required for analysis of the ordinary MOESP data equation:

$$Y_{p,f,N} = \Gamma^{(f)}X_{p,N} + H^{(f)}(B, D)U_{p,f,N} + H^{(f)}(K, I)E_{p,f,N}. \quad (2.34)$$

Since  $U_{p,f,N}$  is known and we have an estimate of the block-rows of  $E_{p,f,N}$ , we can perform the MOESP projection using the following stacked data matrices:

$$\begin{bmatrix} U_{p,f,N} \\ E_{p,f,N} \\ Y_{p,f,N} \end{bmatrix} = \begin{bmatrix} R_{21} & R_{22} & & & \\ R_{41} & R_{42} & R_{43} & R_{44} & \\ \vdots & & & & \\ \hline 0 & 0 & R_{33} & & \\ 0 & 0 & 0 & 0 & R_{55} \\ \vdots & & & & \\ \hline R_{31} & R_{32} & R_{33} & & \\ R_{51} & R_{52} & R_{53} & R_{54} & R_{55} \\ \vdots & & & & \end{bmatrix} \begin{bmatrix} Q_1 \\ Q_2 \\ Q_3 \\ Q_4 \\ Q_5 \\ \vdots \end{bmatrix}. \quad (2.35)$$

Performing a second RQ factorisation of this new data matrix, we obtain:

$$\begin{bmatrix} U_{p,f,N} \\ E_{p,f,N} \\ Y_{p,f,N} \end{bmatrix} = \begin{bmatrix} R'_{11} & & \\ R'_{21} & R'_{22} & \\ R'_{31} & R'_{32} & R'_{33} \end{bmatrix} \begin{bmatrix} Q'_1 \\ Q'_2 \\ Q'_3 \end{bmatrix}. \quad (2.36)$$

(Once again, the matrices  $Q'_i$  do not need to be stored.) We can then recover the column space of the extended observability matrix  $\Gamma^{(f)}$  from the column space of  $R'_{33}$ :

$$\text{range} \left( \lim_{N \rightarrow \infty} \frac{1}{\sqrt{N}} R'_{33} \right) = \text{range} \left( \Gamma^{(f)} \right). \quad (2.37)$$

### 2.3.6 User choices and other issues

Having paid attention to the main algorithmic issues in the previous sections, this section focuses on some of the important user choices and related issues in the closed-loop subspace algorithms. Many of these choices and issues have been studied in the literature and it remains an area of active research with several open problems.

Past window

Algorithmically, the main effect of the past window size  $p$  is to ensure that the neglected term  $\tilde{A}^p$  in equation (2.8) is so small that it can be neglected. One should keep in mind, however, that the number of parameters estimated in the least-squares problem (2.12) is  $pn_y(n_u + n_y) + n_y n_u$  and hence grows linearly with  $p$ , which is the order of the VARX model (2.10). Thus, when using finite length data sequences the variance will grow and there is a risk of over-fitting. Order selection tools such as the Akaike Information Criterion (Ljung, 1999) could be used to avoid such issues in selecting the order of the VARX model (2.10). Cross-validation between data sets is also an option.

It may also be advantageous to employ regularization in the least-squares regression problem, e.g., using Tikhonov regularization which was pioneered in Chiuso, Pillonetto

and De Nicolao (2008) and has been implemented in Houtzager, Wingerden and Verhaegen (2010), or  $\ell_1$ -regularized regression. The bias due to a finite  $p$  can be remedied by using a Vector ARMAX structure, as was proposed in Houtzager, van Wingerden and Verhaegen (2009b). This approach was shown to work well when the order of the identified system corresponds exactly to the order of the “true” system.

Asymptotic consistency results, e.g., for  $p \rightarrow \infty$ , can be found in Bauer and Ljung (2002); Chiuso and Picci (2005); Kuersteiner (2005); Chiuso (2007b), while the effect of choosing a finite  $p$  remains hard to quantify for general situations. First results on the statistical behaviour of subspace algorithms as a function of the window size  $p$  were reported in Bauer and Ljung (2002) where the authors study the effect of  $p$  on the variance of the estimated system’s invariants for white inputs. Reference Chiuso (2007b) also discusses the effect of  $p$  in the context of the recent closed-loop subspace methods (PBSID). It is shown that  $p$  must be chosen in relation to the number of available samples  $N$  to result in the statistically optimal choice. Finally, Kuersteiner (2005) focusses on how the infinite order ARX model which consistently describes the underlying system (i.e., (2.8) when letting  $p \rightarrow \infty$ ) can be approximated by an ARX model of finite order and how  $p$  must be chosen to achieve certain statistical properties.

#### Future window

The choice of the future window in the PBSID<sub>opt</sub> algorithm in section 2.3.3, constrained by  $f \geq n$ , affects the variance of the invariants associated with the identified system (e.g., the elements of the system matrices in a certain fixed basis, pole locations, or the transfer function). In particular, it can be shown for certain classes of inputs that the variance on these invariants is a nonincreasing function of the future window. These issues are extensively discussed in Chiuso (2010). Tools to compute the asymptotic variance on the system matrices estimated with the PBSID<sub>opt</sub> method are discussed in van Wingerden (2012). For the choice of the subspace dimension parameters in the CLMOESP algorithm we refer to results for the classical subspace algorithms (Deistler, Peternell and Scherrer, 1995; Bauer and Jansson, 2000; Bauer and Ljung, 2002).

#### Incorporating prior knowledge

In recent years the possibility of incorporating certain prior knowledge on the system to be identified has regularly received attention. For instance, it is possible to enforce stability or positive realness of the identified models. In Van Gestel, Suykens, Van Dooren et al. (2001); Goethals, Van Gestel, Suykens et al. (2003), it is shown how the least-squares regressions (cf. equations (2.19), (2.20), (2.25)) can be modified in a simple way by adding a regularization term. The amount of regularization required to achieve a specific spectral radius of  $A$ , or positive realness of the system can be determined by solving a generalized eigenvalue problem. The former has been implemented in the PBSID toolbox (Houtzager, Wingerden and Verhaegen, 2010). In Miller and de Callafon (2013) it is shown how linear matrix inequalities can be formulated to constrain the eigenvalues of the identified system to lie in certain convex regions. Finally, in Lyzell, Enqvist and Ljung (2009) some steps are made towards prescribing a certain model structure (e.g., OE, ARMAX, ...) in subspace methods. Constraints can also be added to incorporate certain prior information on the input-output behaviour, such as the steady-state gain, as discussed in Trnka and Havlena (2009); Alenany, Shang, Soliman et al. (2011). In a similar vein, research has been directed towards allowing more accurate estimation of finite-order models in cases where this is not trivial, for instance using nuclear norm regularization (Liu and Vandenberghe, 2009; Hansson, Liu and Vandenberghe, 2012).

### 2.3.7 Notes on continuous-time identification

As mentioned in the introduction to this chapter, there are cases of practical interest where direct identification of continuous-time models from sampled input-output data is desirable. The objective of this thesis has not been to develop or improve continuous-time subspace identification methods. The problem of closed-loop subspace identification

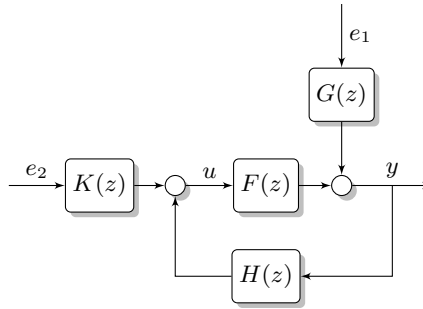


Figure 2.3 – The closed-loop identification setting from Chiuso and Picci (2005).

in continuous-time has been considered by several authors (Mohd-Moktar and Wang, 2008; Bergamasco and Lovera, 2010a,b, 2011b). For an overview of recent techniques in continuous-time closed-loop subspace identification the reader is referred to those papers as well as our overview paper (van der Veen, van Wingerden, Bergamasco et al., 2012).

## 2.4 Evaluation

In this section the closed-loop subspace identification methods discussed in the previous sections are applied to a number of examples. First, we consider two numerical examples. The first example deals with a number of simple closed-loop systems with different characteristics and the second example discusses the differences between PBSID<sub>opt</sub> and CLMOESP in the case of ill-conditioned data caused by poor excitation. Then, we consider two experimental examples. In the first example we evaluate the performance of the main discrete-time algorithms on datasets obtained from a flexible beam and in the second example we identify continuous-time models of this same system.

### 2.4.1 Numerical example: simple closed-loop configurations

In this example we apply the different methods to a series of closed-loop identification problems taken from Chiuso and Picci (2005). The closed-loop system shown in Figure 2.3 is simulated with the transfer functions from Table 2.1.  $e_1$  and  $e_2$  are unit variance zero-mean white signals. For this example, past and future window sizes of 10 are chosen and 2<sup>nd</sup> order models are identified using 1000 samples. The system is identified for 1000 Monte Carlo simulations using the four different methods. The distributions of the identified pole locations, transfer functions and variance-accounted for (VAF) on validation data were studied for the combinations in Table 2.1. The variance-accounted-for is defined as (Verhaegen and Verdult, 2007):

$$\text{VAF} = \max \left\{ 0, \left( 1 - \frac{\text{var}(y - \hat{y})}{\text{var}(y)} \right) \times 100\% \right\}, \quad (2.38)$$

and equals the coefficient of determination ( $R^2$ ) frequently used in statistics. It is important to note that these systems are first order, single-input-single-output systems. Therefore, they may not highlight some of the aspects that distinguish the different methods when they are applied to MIMO systems with an order that is not clearly defined.

Figures 2.4 through 2.7 show the results of the Monte Carlo experiments in terms of the identified transfer functions  $\hat{G}(z)$  and their variance. In addition to these results, Figures 2.8 show the errors in the identified pole locations the identified model  $\hat{G}(z)$ . The error between an estimated pole  $\hat{\lambda}$  and a true pole  $\lambda$  is expressed as error =  $|\hat{\lambda} - \lambda|$ . We have also included Table 2.2 showing the mean and standard deviations of the VAF obtained with validation data. The identified models were simulated in the same closed-loop configuration as the true system.

Of the closed-loop methods,  $\text{PBSID}_{\text{opt}}$  displays the smallest variance and bias overall in the identified transfer functions. This is also reflected in the standard deviation of the VAF values and is consistent with the conclusions in Chiuso (2007a). The results for the innovation estimation method CLMOESP show a slightly larger variance overall. This may be caused by ill-conditioned projections and poor scaling related to the observability matrix of unstable systems Chiuso and Picci, 2005. Note, in this context, that systems 2-3 are indeed highly unstable with a pole far outside the unit disc; a situation which may not likely arise in practice. It is interesting to note that in example 3,  $\text{PBSID}_{\text{opt}}$  shows a small bias which is not seen with the other methods. In example 3, one of the closed-loop system poles is very close to the unit circle. The variance, on the other hand, is still the smallest among all methods. In example 3, the innovation estimation method CLMOESP experiences some difficulties in terms of a large variance in the VAF on validation data.

It is interesting to note that in these four examples the OKID and direct parameterization methods work quite reliably. This is in contrast to what will be observed in section 2.4.3 where a high-order MIMO system is identified. It appears that differences between the identifications methods become far more pronounced when we are dealing with higher order multivariable systems with an undefined system order. For low order systems these differences are minor.

### 2.4.2 Numerical example: behaviour with poor excitation

In this example we consider closed-loop identification of a simple 4<sup>th</sup> order system with 2 inputs and 2 outputs. The system is controlled using a static output feedback matrix. Figure 2.9 shows a comparison of poles estimated using the CLMOESP and  $\text{PBSID}_{\text{opt}}$  methods and Figure 2.10 shows the identified transfer functions. In this example each reference channel was supplied with a single sinusoid near  $\frac{\pi}{2}$  rad/s. Additive white noise with a variance of  $10^{-12}$  was supplied. Due to the poor excitation, the condition number of the VARX data matrix (cf. Eq. 2.12) was on the order of  $\rho = 10^7$ . In the figures, the better

Ex.	$F(z)$	$H(z)$	$G(z)$	$K(z)$
1	$\frac{0.3}{z-0.7}$	-1	$\frac{z+0.5}{z}$	1
2	$\frac{2.5}{z-3}$	-1	$\frac{z+0.5}{z}$	1
3	$\frac{2.5}{z-3}$	-1	$\frac{z+0.999}{z}$	$\frac{0.2(z+0.999)}{z-0.99}$
4	$\frac{2.5}{z-3}$	-1	$\frac{z+0.999}{z}$	1

**Table 2.1** – Systems defined in Chiuso and Picci (2005).

Ex.		Direct	CLMOESP	$\text{PBSID}_{\text{opt}}$	OKID
1	mean	89%	97%	97%	97%
	std.dev.	5.3%	2.6%	2.2%	2.6%
2	mean	98%	100%	100%	100%
	std.dev.	0.9%	0.6%	0.5%	0.7%
3	mean	100%	94%	100%	96%
	std.dev.	0.1%	18%	0.1%	5.8%
4	mean	97%	99%	98%	99%
	std.dev.	1.6%	1.2%	2.9%	1.1%

**Table 2.2** – Mean and standard deviation of the VAF on validation data for the four examples and four methods over 1000 experiments.

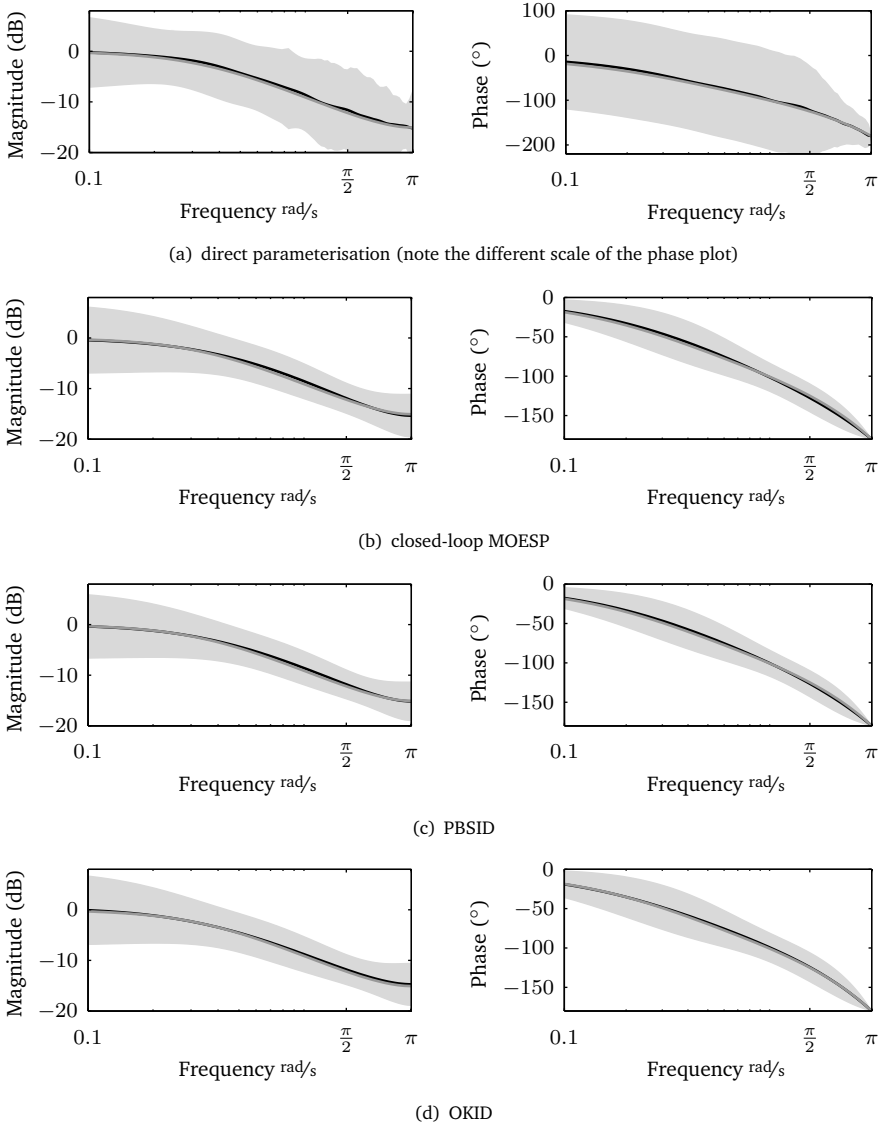


**Figure 2.4** – Mean and variance ( $\pm 3\sigma$  confidence bounds) of identified transfer functions for example 1 compared to the true transfer function (dark gray line).

numerical behaviour of the innovation estimation-type algorithm, in this case CLMOESP, is evident (cf. §2.2.7).

### 2.4.3 Experimental example: “smart” beam dynamics

In this example we consider the closed-loop identification of a “smart” beam setup. This system is of interest since it is of a distributed-parameter nature and hence of potentially infinite order. Furthermore, within the considered bandwidth there are many resonances at frequencies an order of magnitude apart, such that this system could be considered to be a “stiff” system.

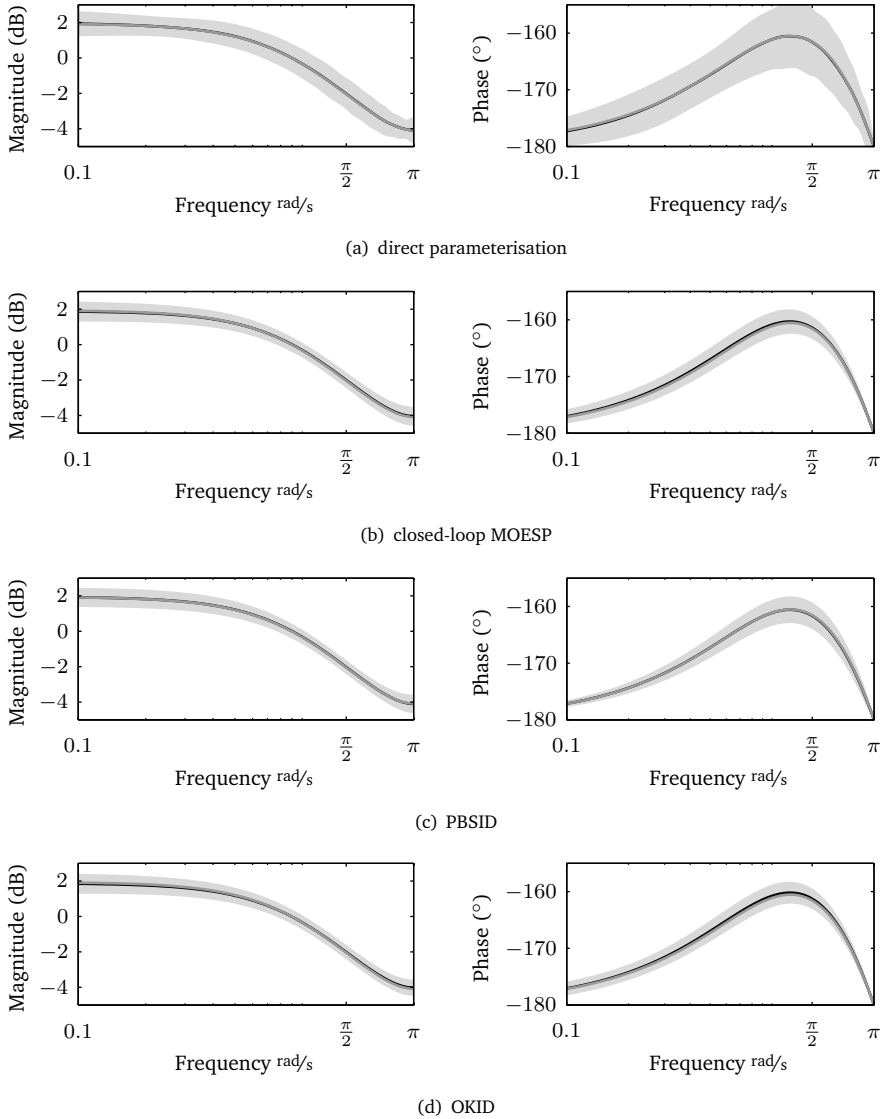


**Figure 2.5** – Mean and variance ( $\pm 3\sigma$  confidence bounds) of identified transfer functions for example 2 compared to the true transfer function (dark gray line).

Figure 2.11 shows the setup that was used for experimental testing. The beam is approximately 1 m long and clamped at one end. It is equipped with six piezoelectric transducers (type M8528, from Smart Material Corp.), of which two are used for sensing, two for control and the two at the tip for introducing a disturbance which is to be rejected. The beam is controlled with an  $\mathcal{H}_\infty$  controller which attempts to reject the disturbances injected at the tip.

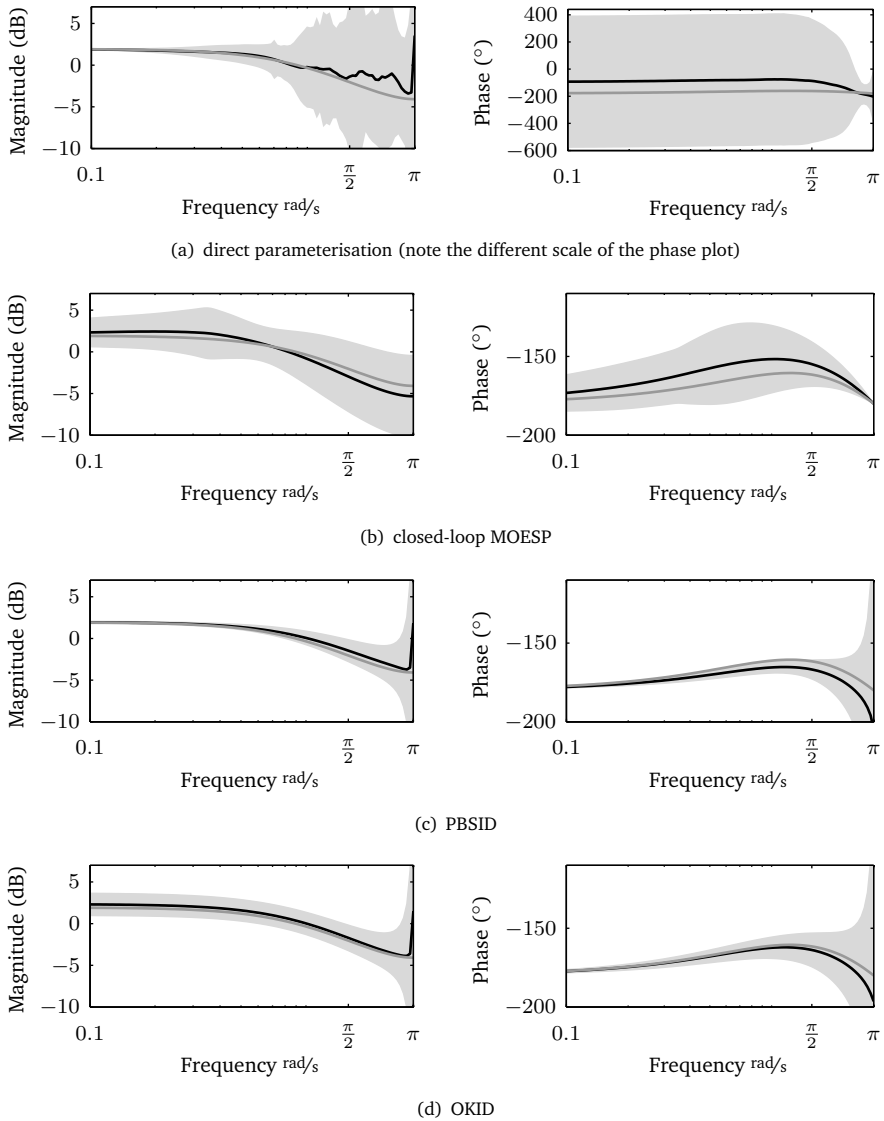


**Figure 2.6** – Mean and variance ( $\pm 3\sigma$  confidence bounds) of identified transfer functions for example 3 compared to the true transfer function (dark gray line).

### Excitation and noise

To be able to identify a model of the system in closed-loop, it is beneficial to inject a perturbation into the reference channels<sup>2</sup>. In principle we may choose either  $r_1$  or  $r_2$  or both to inject this perturbation (see Figure 2.1). In the present example we inject a pseudorandom binary signal with an amplitude of 40 V into each of the two references. The switching probability was chosen so as to obtain a white perturbation for frequencies up to 200 Hz. Similar signals were generated to act as noise on the actuators at the tip. Here,

<sup>2</sup>Although it may not be necessary, see e.g., Bazanella, Gevers and Mišković (2009), a higher signal to noise ratio results in a smaller variance of the identified model.

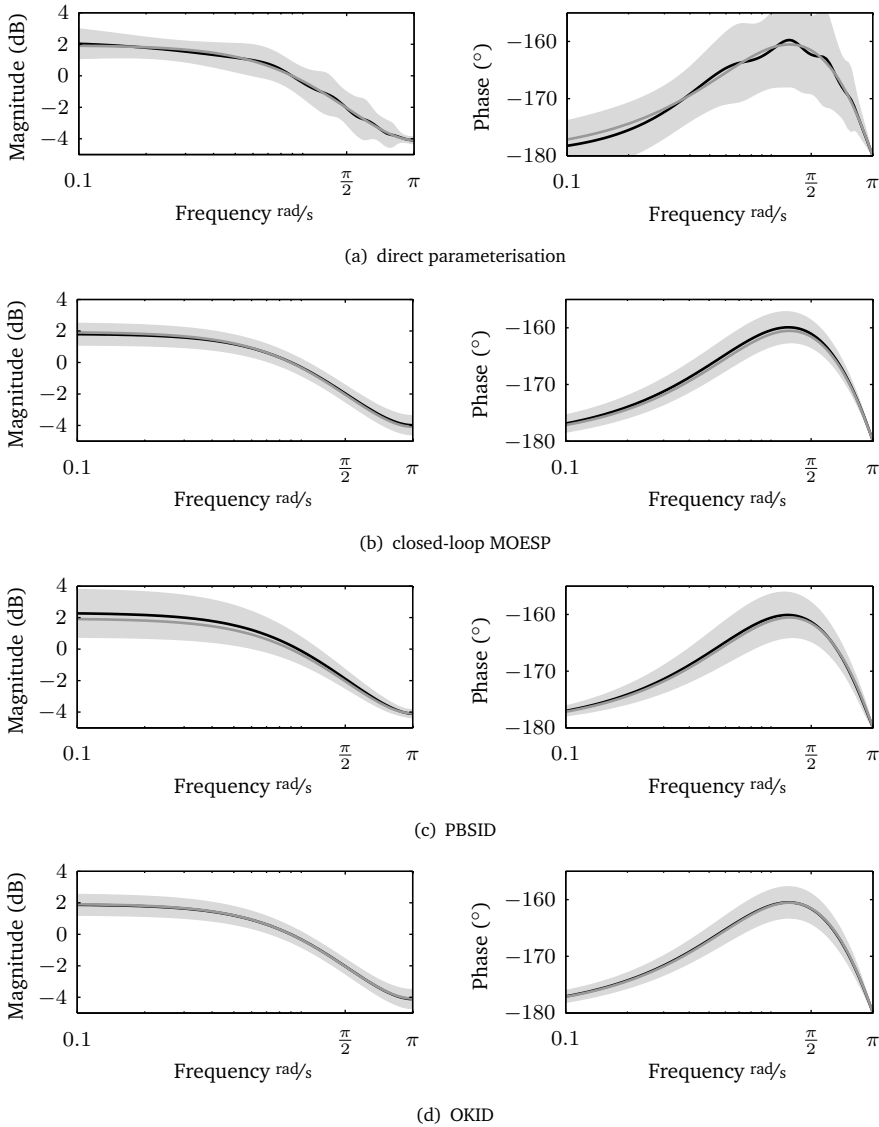


**Figure 2.7** – Mean and variance ( $\pm 3\sigma$  confidence bounds) of identified transfer functions for example 4 compared to the true transfer function (dark gray line).

an amplitude of 20V was used. Signals were sampled at a rate of 1 kHz and  $N = 4000$  and  $N = 16666$  samples were used for identification and validation respectively. 65 of such experiments were performed, each with independent realisations of the perturbation and disturbance signals, allowing statistical properties of the estimates to be inferred. We remark that the data length for identification causes the data set to contain less than 15 cycles of the lowest natural frequency (3.7 Hz).

#### Reference model

As a reference model we consider a non-parametric spectral estimate based on a long experiment ( $N = 50000$  samples) performed under the same conditions as the other

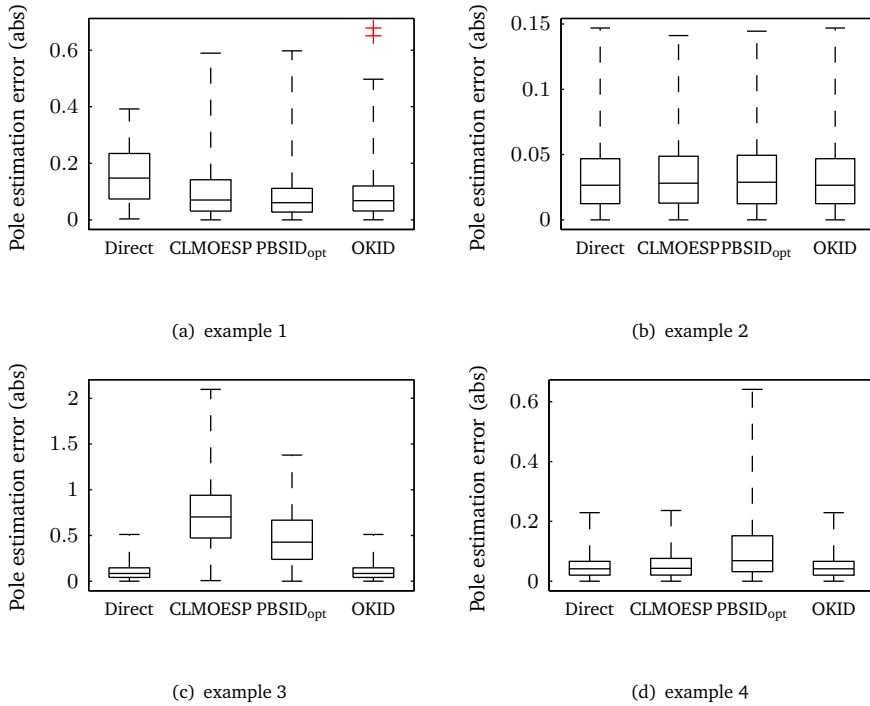


**Figure 2.8** – Box plots of errors (absolute Euclidean distance in the  $z$ -plane) in the estimated pole locations.

experiments. This estimate was subsequently averaged further over the 65 independent experiments so as to obtain an even smoother estimate. The estimate is obtained following the method in Akaike (1967); Pintelon, Schoukens, Vandersteen et al. (2010):

$$\hat{G}(e^{j\omega}) = \hat{\Phi}_{yr} \hat{\Phi}_{ur}^{-1}, \quad (2.39)$$

where  $\hat{\Phi}_{yr}$  is the estimated cross spectrum between  $y_k$  and  $r_k$  and  $\hat{\Phi}_{ur}$  is the estimated cross spectrum between  $u_k$  and  $r_k$ . This estimate can be shown to yield an asymptotically unbiased estimate provided the reference is persistently exciting and uncorrelated with the noise signal. Obviously, the estimator will only give good estimates in the frequency range where  $r_k$  excites the system. We have computed this estimate using the recent *local polynomial* method for nonparametric frequency response estimation (Pintelon, Schoukens, Vandersteen et al., 2010). This is a reliable method which significantly reduces the adverse effects of spectral leakage. Typically, a comparison with a closed-loop spectral estimate is one powerful means of validating identified state-space models.

## Results

The most critical tuning parameter common to the subspace algorithms is the choice of the past window size  $p$  (equivalently, the VARX model order). Well-known tools in prediction-error identification can be used to choose the value of  $p$  (Peternell, Scherrer and Deistler, 1996; Ljung, 1999; Chiuso and Picci, 2005; Kuersteiner, 2005; Chiuso, 2007b). One such tool is the Akaike information criterion (AIC) (Ljung, 1999). For the VARX regression step we have shown the average AIC over 10 experiments in Fig. 2.12 as a function of  $p$ . The AIC clearly suggests an order in the vicinity of  $p = 100$ . To investigate the effect of the parameter  $p$  and the validity of the value  $p = 100$  suggested by the AIC, identification was performed for  $p = \{60, 100, 200\}$ . It is clear that the asymptotic variance of the VARX

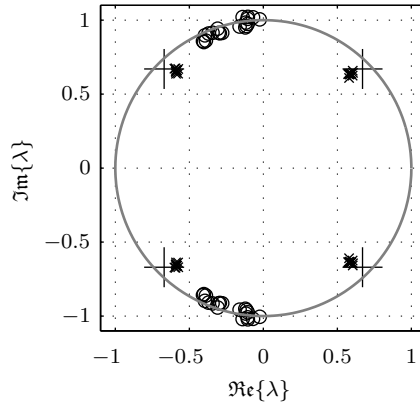


Figure 2.9 – Comparison of estimated poles using the CLMOESP (×) and PBSID<sub>opt</sub> (○) methods.

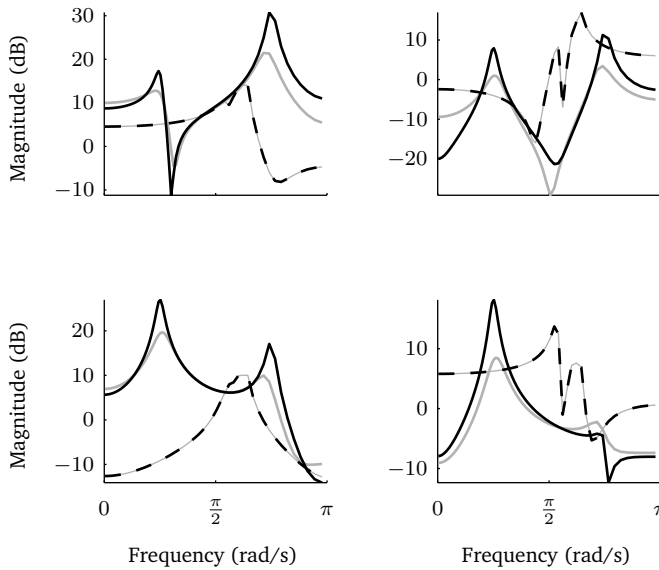
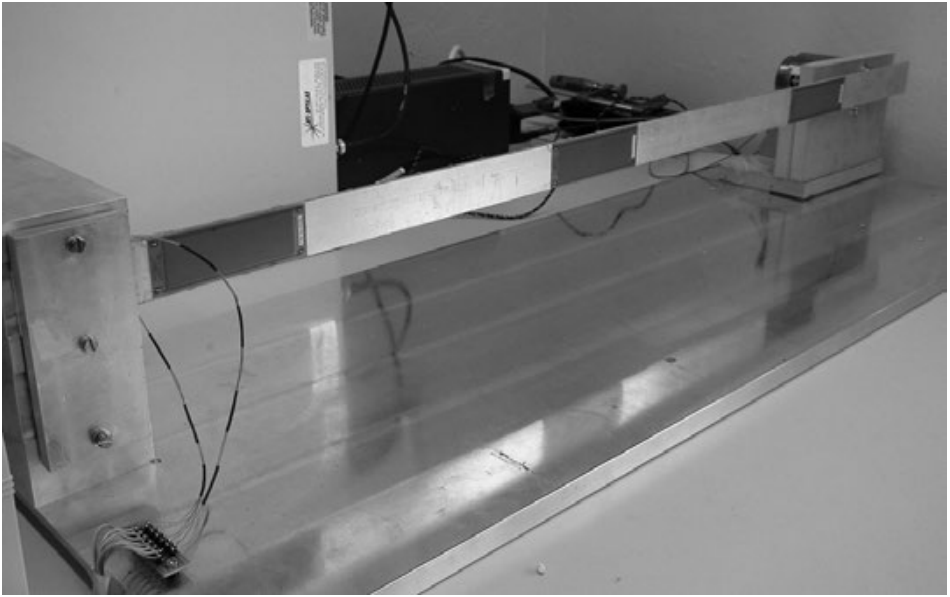


Figure 2.10 – Comparison of estimated models using the CLMOESP (solid gray) and PBSID<sub>opt</sub> (dashed) methods. The true system is indicated with the black line.



**Figure 2.11** – The “smart” beam setup. A clamped beam is equipped with six piezoelectric transducers capable of either producing or sensing strain.

method	% stable models		
	$p = 60$	$p = 100$	$p = 200$
PBSID <sub>opt</sub>	100%	98%	91%
Direct	100%	91%	72%
OKID	40%	10%	5%
CLMOESP	100%	97%	86%

**Table 2.3** – Typical success rates of identifying a stable model (65 experiments). (Instability always occurred due to poles marginally outside the unit disc.)

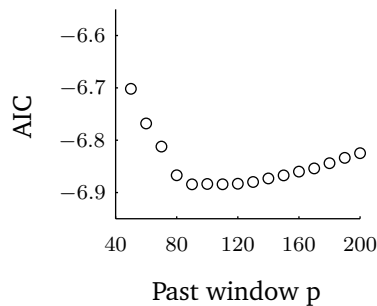


**Figure 2.12** – The Akaike information criterion (AIC) as a function of chosen past window size in the VARX step (§2.2.5).

parameters will grow when the least-squares information matrix becomes ill-conditioned. This strongly depends on the amount of samples available and the richness of the signal  $z_k$ , as discussed in Section 2.2.5.

A choice of  $p \geq 60$  turned out to give a fairly “white” innovation estimate. For simplicity, the future window  $f$  in the PBSID<sub>opt</sub>, OKID and CLMOESP methods was taken equal to  $p$ , but note that the choice of  $f$  also affects the variance of the estimates, as discussed in Section 2.3.3 and in Chiuso, 2010, in particular when the input spectrum exhibits zeros near the unit circle.

Using the order detection mechanisms (SVD) of the PBSID<sub>opt</sub> and CLMOESP methods a model order of  $n = 29$  was found to give good prediction capability on a validation dataset. This order was also selected for the SVD truncation in the OKID method, since order detection in that method itself was rather unclear. Figures 2.13 and 2.14 show the estimated confidence bounds resulting from the nonparametric estimate and the four key discrete-time methods (PBSID<sub>opt</sub>, Direct parameterization, OKID and CLMOESP) applied to 65 independent datasets for  $p = \{60, 200\}$ . Although the beam system is a 2-input-2-output MIMO system, only the responses from input 1 to output 1 are shown.

Fig. 2.15 shows how well the estimated models predict the system’s output on a validation dataset in terms of the variance-accounted-for<sup>3</sup> Verhaegen and Verdult, 2007 (VAF). The figures show that

- i) the prediction accuracy increases with past window  $p$  for the PBSID<sub>opt</sub> method in particular;
- ii) the OKID method delivers unreliable estimates overall, where the other methods provide good models. A large choice of  $p$  is required to obtain a reasonable model. This is related to the direct decomposition of the matrix in (2.18);
- iii) the VARX direct parameterization method exhibits more outliers and a larger variance than the methods PBSID<sub>opt</sub> and CLMOESP, probably due to the lack of a model reduction step;
- iv) the spectral estimation method cannot capture the first resonance mode, probably due to the short duration (4 s) of the data records;
- v) a large value of  $p$  helps to capture the first resonance mode. This may also be related to increasing the value of  $f$  (note that we have chosen  $f = p$ ).

The results show that for  $p = 100$  all resonances are captured and that the VAF improves when moving from  $p = 60$  to  $p = 100$  (much less when going from  $p = 100$  to  $p = 200$ ). This underlines the usefulness of the AIC as an order selection tool in the VARX modelling step. Although a choice of  $p = 100$  was suggested by the AIC, it can be seen in Figures 2.13 and 2.14 that the variance of the VARX model increases marginally for larger  $p$ ; this trend was found to hold up to a past window of approx.  $p = 700$ , at which point the information matrix quickly became ill-conditioned. Of course, this highly depends on the character of  $z_k$  and the amount of samples.

## 2.5 Concluding remarks

Besides presenting the closed-loop MOESP algorithm, the goal of this chapter was to organise the wide range of closed-loop subspace methods that has appeared over the last fifteen years. Most of the algorithms can be derived from a few fundamental steps, which in turn can be traced back to autoregressive (VARX) modelling. Based on experimental data obtained in repeated measurements several characteristics of the methods that are highly relevant in a practical context have been demonstrated. It turns out that the PBSID<sub>opt</sub> method (Chiuso, 2007b) is a reliable method. The innovation estimation methods (Qin and Ljung, 2003b), among which CLMOESP (van der Veen, van Wingerden and Verhaegen,

<sup>3</sup>VAF =  $\max \left\{ 0, \left( 1 - \frac{\text{var}(y - \hat{y})}{\text{var}(y)} \right) \times 100\% \right\}$

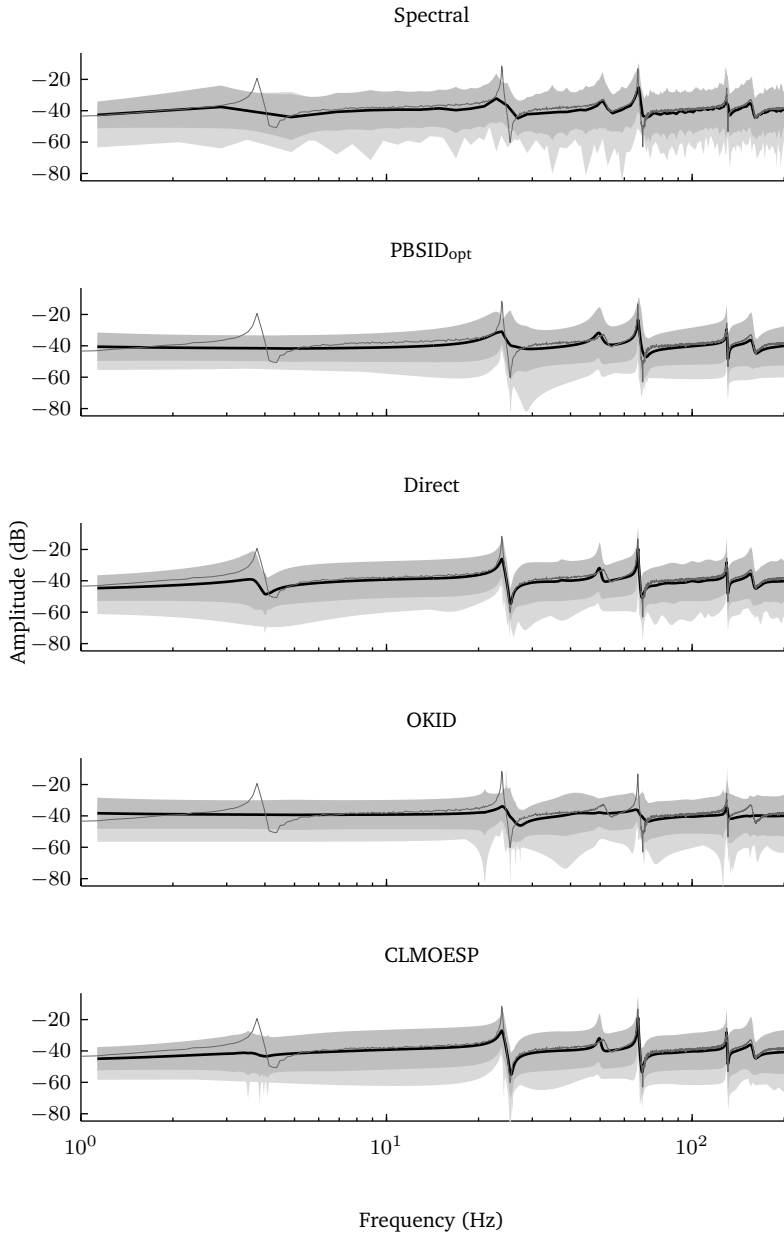


**Figure 2.13** – Frequency response and confidence bounds; mean model (black solid), mean  $\pm 2\sigma$  (gray shaded), extreme models (light gray shaded) and reference model (gray solid) –  $p = 60$ .

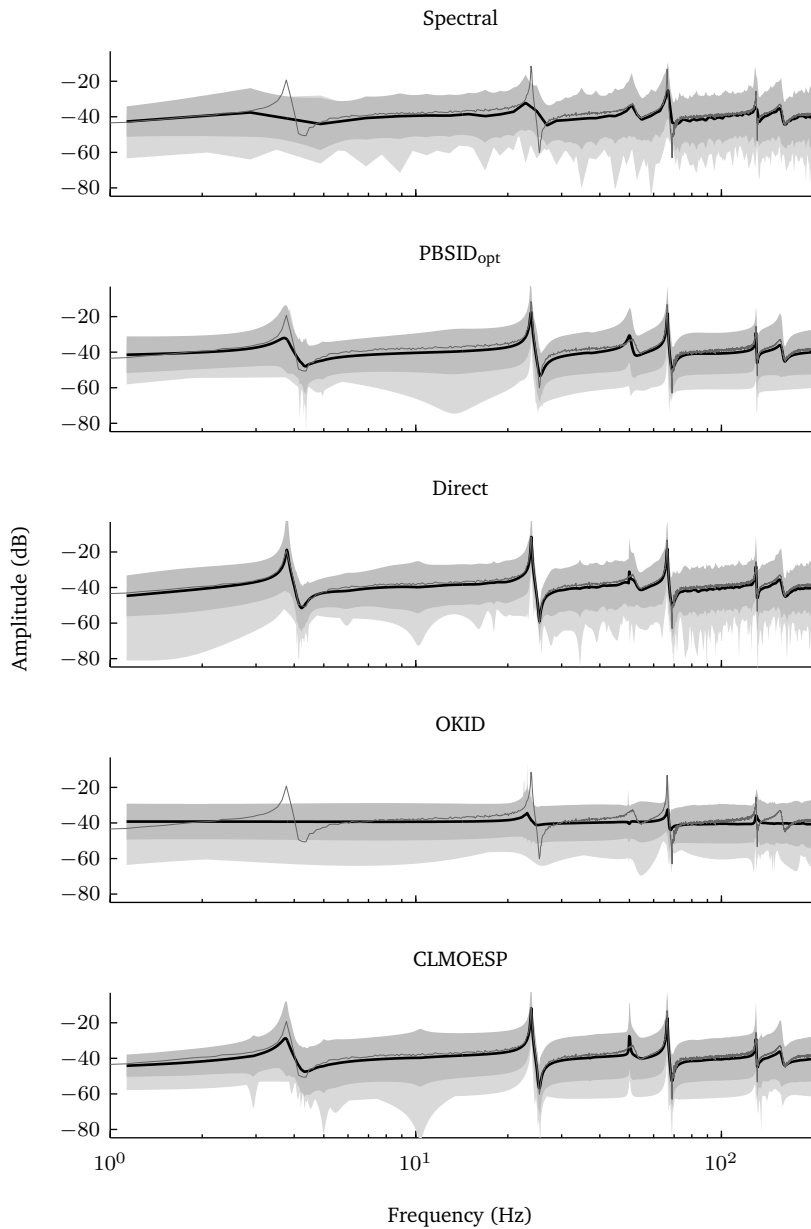


**Figure 2.14** – Frequency response and confidence bounds; mean model (black solid), mean  $\pm 2\sigma$  (gray shaded), extreme models (light gray shaded) and reference model (gray solid) –  $p = 200$ .

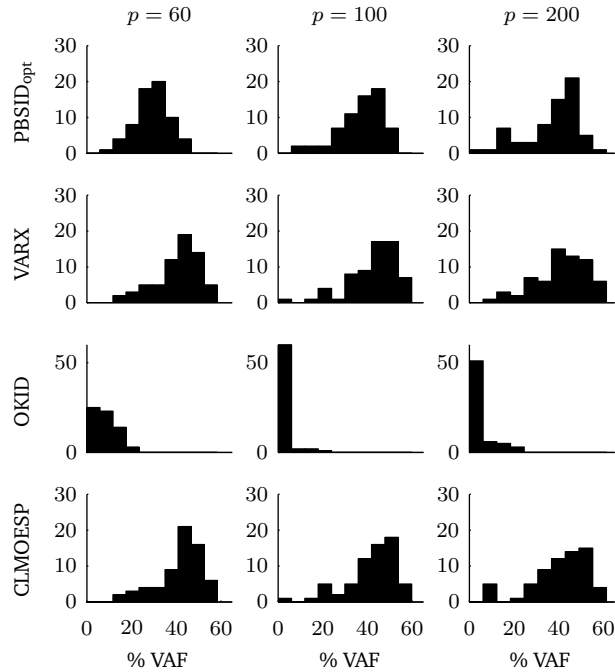


**Figure 2.15** – Histograms of model quality in terms of output prediction: histogram of attained VAFs.

2010a), are of interest due to better numerical conditioning in the case of poorly exciting signals and their accurate order indication. The realisation-based approaches can only be used reliably if sufficiently large Hankel matrices can be constructed and may regularly incorrectly estimate the stability of resonant systems. Direct parameterisation of the VARX parameters has its own value in the sense that uncertainty on the parameters is readily characterised, but the models are not minimal and exhibit larger variance due to lack of a model reduction step.

Finally, it is worth mentioning that all the methods in this chapter have been described in their most basic forms. For instance, regularisation techniques are available to solve the least-squares problem for the Markov parameters when it is ill-conditioned. None of these techniques have been employed and, as such, the methods could each perform differently with regularisation. This makes it hard to compare identification results found in the literature.

# LTI identification of wind energy systems: practical aspects

While system identification typically refers to a suite of generic techniques to obtain dynamic models from measured data it turns out that specific domain knowledge is essential to the success of applying such techniques. Treating systems to be identified as “black boxes” and directly applying “black box” techniques is rarely a successful enterprise to embark on. This chapter focusses on some practical examples, demonstrating how specific system knowledge is of practical value for linear system identification.

First, we pay attention to periodic disturbances that appear in wind turbine measurements and present a way to account for these disturbances. Next we discuss two examples in which the tools of the previous chapter have been used successfully to identify dynamic models.

## 3.1 Introduction

In the previous chapter we have treated the identification of LTI models from input-output data under closed-loop conditions. The methods presented there can be viewed as “black box” methods in the sense that they directly produce a generic state-space model from input-output data. The subspace techniques do not require the user to specify a parameterisation and the only decision parameters are the subspace dimensions and the system order, of which the algorithm itself gives an indication.

In this chapter we discuss some specific practical aspects related to identification of models of aeroelastic systems, in particular wind turbines. First, it turns out that incorporating domain knowledge into the identification procedure is beneficial, allowing more accurate models to be obtained. Second, we demonstrate on the basis of examples that the subspace techniques are reliable and efficient, allowing controller design in a “one-shot” approach. By stressing these aspects, we aim to support the claims made in the introduction, that the identification methods described in this thesis contribute to achieving a lower cost of identification experiments by making the best use of available time.

First, in Section 3.2, we discuss the effect of periodic disturbances on input-output data acquired from wind turbines. We will show how these disturbances adversely affect identification results and how the adverse effects can be remedied in a simple way. Then, in Section 3.3 we demonstrate application of the techniques of Chapter 2 to the identification and control of a flutter wing. Finally, in Section 3.4 we describe how the subspace identification framework can be applied as a tool supporting controller design, by using it for rapid diagnosis of the performance of a new controller.

## 3.2 Periodic disturbances

Since wind turbines can to a large extent be classified as “rotating machinery”, it is likely that periodic effects play an important role. Indeed, many loads are induced during wind turbine operation which are periodic in nature. These loads typically propagate through the structure and find their ways into blade root loads, tower loads, accelerations and any other

structural measurements. Since most of these periodic loads originate from the (typically 2 or 3<sup>1</sup>) blades which rotate about the main shaft, the combined effects can be quite different when measured in the “fixed”<sup>2</sup> frame of reference (Johnson, 1994; Hansen, 2007).

### 3.2.1 Sources of periodic loads

Main sources of periodic loads are gravity, tower shadow, wind shear, yawed inflow, rotor tilt, and imbalance. Most of the loads originate from the blades, which experience a significant once-per-revolution (1P) component along with higher harmonics (2P, 3P, . . .) of this frequency. The nature of these periodic loads is complicated by that fact that while most loads originate locally on the rotor blades, their combined effect on the hub and turbine structure can be different (Hansen, 2003, 2007; Bir, 2008). An important characteristic of these loads is that they are imposed on the blades with an exact 120° phase difference. For instance, 1P *out-of-plane* loads on the individual blades combine at the hub into a loading approximately consisting of a constant (i.e., 0P, or zero-frequency) thrust force, a constant vertical tilt moment on the hub and a constant horizontal yawing moment on the hub<sup>3</sup>. This forms the basis for cyclic pitch or tilt-yaw control (Bossanyi, 2003b; Selvam, Kanev, van Wingerden et al., 2009). Similarly, 1P *in-plane* blade loads result in constant vertical and lateral hub loads and a constant torque. For these periodic disturbances it holds that,  $N$ P periodic loads on the blades result in  $(N - 1)$ P periodic loads on the hub. One could also call these loads the *rotor* loads since they express the combined effects of the three blades.

In cases where two measurement frames of reference are involved and one of these is fixed and the other rotating, for instance when controlling the individual pitch angles of the blades and measuring loads in the hub frame of reference, these frames are inextricably linked to each other by a time varying transformation (Hansen, 2003; Bir, 2008). As a consequence, the model describing the dynamics between these signals in these cases is also a time varying model. Frequent use has been made of the Coleman transformation to transform these dynamics to time invariant (non)linear models (Hansen, 2003; Bossanyi, 2005; Bir, 2008; Skjoldan and Hansen, 2009). In this thesis we are only concerned with inputs and outputs defined in the fixed frame of reference. Hence, we can treat the dynamics as time invariant (but possibly nonlinear). The periodic loads, however, will still affect these measurements and we will treat those loads as disturbances with the character of periodic signals. Figure 3.1 shows a typical example of the dominance of periodic loads in measured signals.

Finally, we note that we have only so far considered the effect of loads affecting the blades such that these effects are 120° out of phase. A different situation occurs when the natural modes of the blades are considered. The blade natural modes, say at a frequency  $\omega_n$  can occur with distinct phase differences. The consequence of this is that the natural modes of the rotor caused by the combined blade modes occur at  $\omega_n \pm \Omega$ , where  $\Omega$  is the rotor speed. Thus, in the fixed frame of reference such modes appear as two new modes, shifted by  $\Omega$ . This implies that the rotor modes are dependent upon the operating condition via the current rotational speed. Considering the work in this thesis, however, these rotor modes play a small role in the spectral energy content of the measured signals (see Figure 3.1) and hence these effects are disregarded.

### 3.2.2 Effects of periodic loads on system identification

The LTI system identification framework introduced in Chapter 2 is very general in the sense that it captures linear time invariant systems subject to coloured process and measurement noise. The crucial assumption made in this framework was that these noise sources have

<sup>1</sup>Note that in this thesis only results for three-bladed turbines are discussed.

<sup>2</sup>The term fixed is relative here; while the hub is fixed in the sense that it is mounted to the tower, it can of course rotate and translate as the tower bends.

<sup>3</sup>The loads only combine into constant hub loads under particular conditions, e.g., a constant wind speed, no turbulence, identical blades.

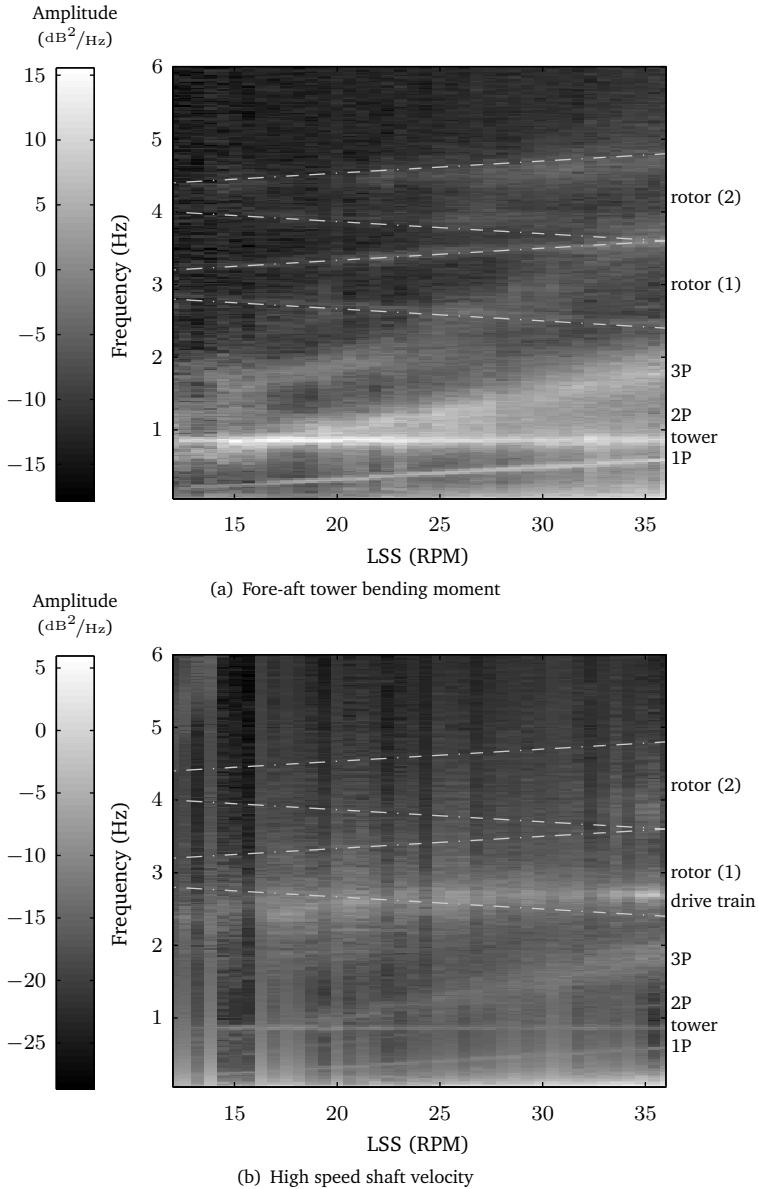


**Figure 3.1** – Waterfall plots showing the spectral content of the fore-aft tower bending moment and the high speed shaft velocity as a function of rotor speed (based on almost 2.5 hours of data from the CART 3 turbine). The periodic effects and the tower and drive train resonances are clearly visible. Also visible are two rotor-related modes, each with a forward and backward component. These modes are far less dominant.

smooth, rational spectra. In the previous subsection it was shown that many loads on wind turbines have very dominant periodic components. These components violate the assumptions on the standard disturbance models; for all practical purposes the disturbances have discrete or near-discrete spectra, possibly with components at 1P, 2P, etc... As will be demonstrated in an example below, these disturbances may lead to identified models with erroneous dynamics. In van Baars, Mosterd and Bongers (1993); van Baars and Bongers

(1994); van der Veen, van Wingerden and Verhaegen (2010c) ideas were presented to incorporate these periodic disturbances into standard system identification frameworks. The idea is very simple: Since the periodic disturbances are exactly related to the current azimuth of the rotor, one can construct additional input signals representing the effect of the periodic disturbances. The identification algorithm can then correlate the measured signals to these constructed signals to account for the presence of the periodic effects.

#### Constant rotor speed

Consider first the case of a constant rotor speed  $\bar{\Omega}$  (rad/s). Any discrete-time, zero-mean periodic disturbance  $d(k)$  with a frequency  $\bar{\Omega}$  can then be described in terms of a Fourier series:

$$d(k) = \sum_{n=1}^{\infty} a_n \cos(n\bar{\Omega}k\Delta t) + b_n \sin(n\bar{\Omega}k\Delta t), \quad (3.1)$$

where  $\Delta t$  is the sampling interval and  $k\Delta t$  is the current time instant. Since the wind turbine is a mechanical system it has a low-pass character and the harmonics present in the measured signals are typically at most the first few. Thus, one conceivable way of modelling the disturbances is to examine the spectra of the measured signals, check for the dominant presence of 1P, 2P, . . . , NP disturbances and add sine and cosine basis functions at these harmonics to the input vector.

#### Varying rotor speed

One way of dealing with a moderately varying rotor speed is to map all signals to an azimuth domain as suggested in van Baars, Mosterd and Bongers (1993). However, due to the complications arising when describing dynamics in a domain different from a time or frequency domain, in particular when the rotor speed varies significantly, we will not pursue this approach. If we assume that the shape of the disturbance does not vary with rotor speed and only its fundamental period changes, we can simply use the same Fourier series as before (3.1) with the same coefficients, but with the current rotor speed  $\Omega$ . Note further that in the constant-speed case the term  $\bar{\Omega}k\Delta t$  represents in fact the current rotor azimuth, to which effectively all periodic effects can be related. In the case of a varying rotor speed, the term  $\Omega k\Delta t$  represents a similar term, but the phase information (or, in fact, the absolute position reference) is missing. This can be solved simply by using the actual rotor azimuth  $\Psi(k)$  (rad), resulting in:

$$d(k) = \sum_{n=1}^{\infty} a_n \cos(n\Psi(k)) + b_n \sin(n\Psi(k)).$$

A measurement of the rotor azimuth<sup>4</sup> can hence be exploited to predict the periodic disturbances. If  $\Psi$  is known, we can generate (vector) signals:

$$\psi_n(k) = \begin{pmatrix} \cos(n\Psi(k)) \\ \sin(n\Psi(k)) \end{pmatrix}, \quad n = 1, 2, 3, \dots, \quad (3.2)$$

where  $n$  indicates which periodic component, e.g., 1P, 2P, etc., we wish to represent. Subsequently, we can add these signals as virtual inputs to the identification problem. Note that for most cases of practical interest, the rotor speed is not constant and as a consequence these signals are not truly periodic. This is beneficial for identification algorithms since this causes the signals to be persistently exciting to some extent as opposed to signals with spectra which are only non-zero at a few discrete frequencies.

A few remarks are in order regarding the approach here:

<sup>4</sup>Although the rotor speed and azimuth are not always measured on commercial turbines, they can be estimated from the generator speed and azimuth and the gearbox ratio (if present), noting that these are one-to-one related at low frequencies, i.e., below any drive train natural frequencies.



**Figure 3.2** – “Smart” rotor scale model in the Open Jet facility (van Wingerden, Hulskamp, Barlas, Houtzager et al., 2011).

- In some cases the Fourier basis functions may not be the most efficient ones. Consider a case where blade dynamics are identified and tower shadow is a significant disturbance. In this case it is likely that many harmonics are necessary, while the same could be achieved with a suitably shaped periodic function. As argued in van Baars, Mosterd and Bongers (1993), one could use a signal with a sequence of steps representing the tower shadow acting on the blade during the brief instant it passes the tower. In the cases we have studied, however, most disturbances can be represented well by a few sinusoidal basis functions;
- A major assumption is that the profile of the disturbance and its effect on the output remains the same regardless of the current rotor speed or wind speed. Regarding the profile of the disturbance, consider the case of tower shadow, for example. The typical potential flow model (Burton, Sharpe, Jenkins et al., 2001) for tower shadow shows that the velocity deficit profile can be quite different at different wind speeds. Regarding the effect on the output, periodic disturbances may propagate through the structure in different ways depending on the current rotor speed caused by varying degrees of structural coupling (Hansen, 2007).

### 3.2.3 Example: data from an experimental “smart” rotor

In the framework of the European UpWind project (UPWIND, 2012) experiments were carried out recently to determine the potential of “smart” rotors for wind turbine fatigue load alleviation (van Wingerden, Hulskamp, Barlas, Houtzager et al., 2011). “Smart” rotors are rotors where each of the blades is equipped with one or more flow control devices, in this case piezoelectric trailing edge flaps. The flaps modify the local coefficient of lift of the blade profile and as such offer a high-bandwidth (compared to the blade pitch system) opportunity to regulate loads on the blade root and the the wind turbine structure. The experimental turbine comprised a two-bladed configuration, where each blade was equipped with two piezoelectric flaps (used in unison for this study) and a strain sensor at the blade root.

In an effort to reduce the fatigue loads related to the flap-wise root bending moment, the control objective was formulated as: minimise the variance of the strains measured at

the blade roots. In order to obtain suitable (MIMO, LTI, state-space) models for control design, system identification was chosen for its capacity to directly model dynamic input-output relations. Although extensive aeroelastic modelling was performed, the stacking of uncertainties related to material properties, unsteady aerodynamics with complicated unsteady and rotational flows near the roots and tips, unknown actuator/sensor behaviour, would likely imply that models can only be computed with limited accuracy.

Figure 3.3 shows the power spectra for one of the strain measurements. With no excitation we clearly see multiple periodic disturbances, mainly at 1P through 4P. If we excite the trailing edge flaps using their full actuation capability we see that we can achieve a good signal-to-noise ratio, except at the 1P and 3P frequencies. Based on this

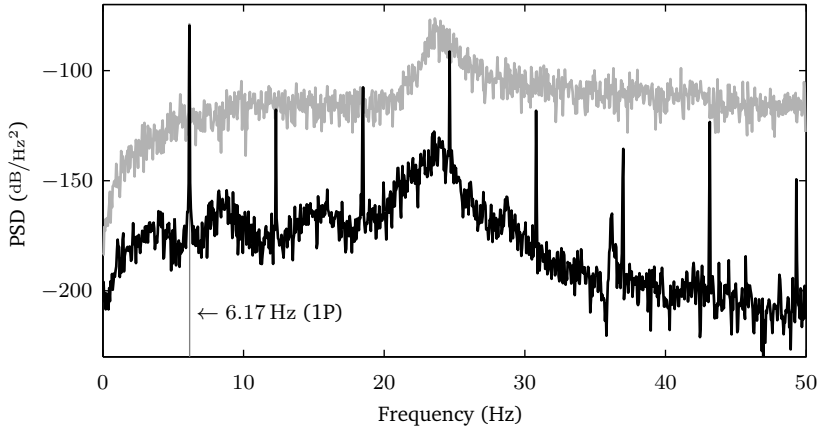


**Figure 3.3** – Power spectra of measured strain gage signals for two cases: without trailing edge flap excitation (black) and with trailing edge flap excitation (gray). The figure clearly shows the dominance of the 1P periodic load. (Results valid for  $V = 7 \text{ m/s}$  and  $\Omega = 370 \text{ rpm}$ .)

insight identification was performed using the closed-loop MOESP algorithm and adding signals  $\psi_1(k)$  and  $\psi_3(k)$  (3.2) as inputs. Figure 3.4 shows the identified 2-by-2 system in terms of Bode magnitude plots. Clearly, when the periodic signals are not accounted for, spurious resonances are identified at the 1P and 3P frequencies. This is also reflected in the phases, shown in Figure 3.5, where these spurious dynamics lead to large phase shifts. The identified models were successfully used for subsequent feedforward-feedback control design (van Wingerden, Hulskamp, Barlas, Houtzager et al., 2011).

### 3.2.4 Conclusions

In this section we have shown how periodic components in measurement data obtained from rotating systems such as wind turbines can be accounted for in a straightforward way. The example demonstrated the importance of doing this in order to obtain consistent and reliable estimates. This means that one of the challenges mentioned in the introduction (see Section 1.4), namely dealing with periodic disturbances, has been partly addressed, specifically for the case of a constant rotor speed and constant wind speed. The results in chapters 6 will show that these results extend to the case of varying rotor speed under turbulent conditions. Finally, it is relevant to mention that this was possible by using specific domain knowledge about the behaviour of wind turbines to understand where the periodic signals originate. This knowledge could then be embedded in the otherwise “black-box” system identification framework.

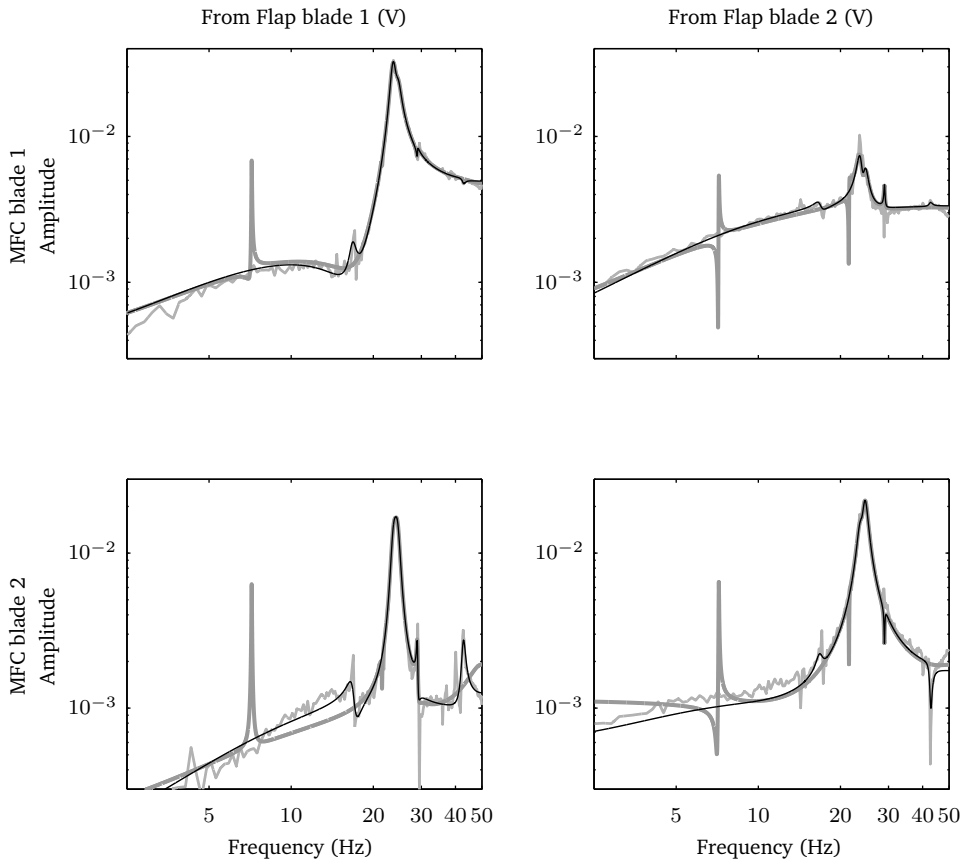


**Figure 3.4** – Amplitude responses of the identified transfer functions from the two piezoelectric flaps to the two strain measurements. Shown are the identified models without compensation for periodic disturbances (solid gray), with compensation for periodic disturbances (solid black) and spectral estimate (thin gray line). (Results valid for  $V = 7 \text{ m/s}$  and  $\Omega = 370 \text{ rpm}$ .)

### 3.3 Active suppression of control surface flutter

It is well-known that coupling between aerodynamics and structural mechanics can lead to flutter (Bisplinghoff, Ashley and Halfman, 1996), a phenomenon extensively studied in the field of aerospace engineering. One particular type of flutter is control surface flutter. In its initial year in service, control surface flutter occurred on the rudder surfaces of the Airbus A310, which was later attributed to changes in mass distribution due to accumulation of moisture (*Aviation Investigation Report – Loss of Rudder in Flight 2005*). Other structural changes leading to control surface flutter could be wear of the control system, e.g., free play in hinges and linkages, or changes in actuator stiffness and control surface torsional stiffness. Typically, structural modifications such as mass balancing are made to avoid control surface flutter inside the operating envelope of the aircraft. Flutter can lead to premature wear of structural components and in the worst case to loss of entire airframe components.

In a recent research project, carried out jointly between the Faculty of Aerospace

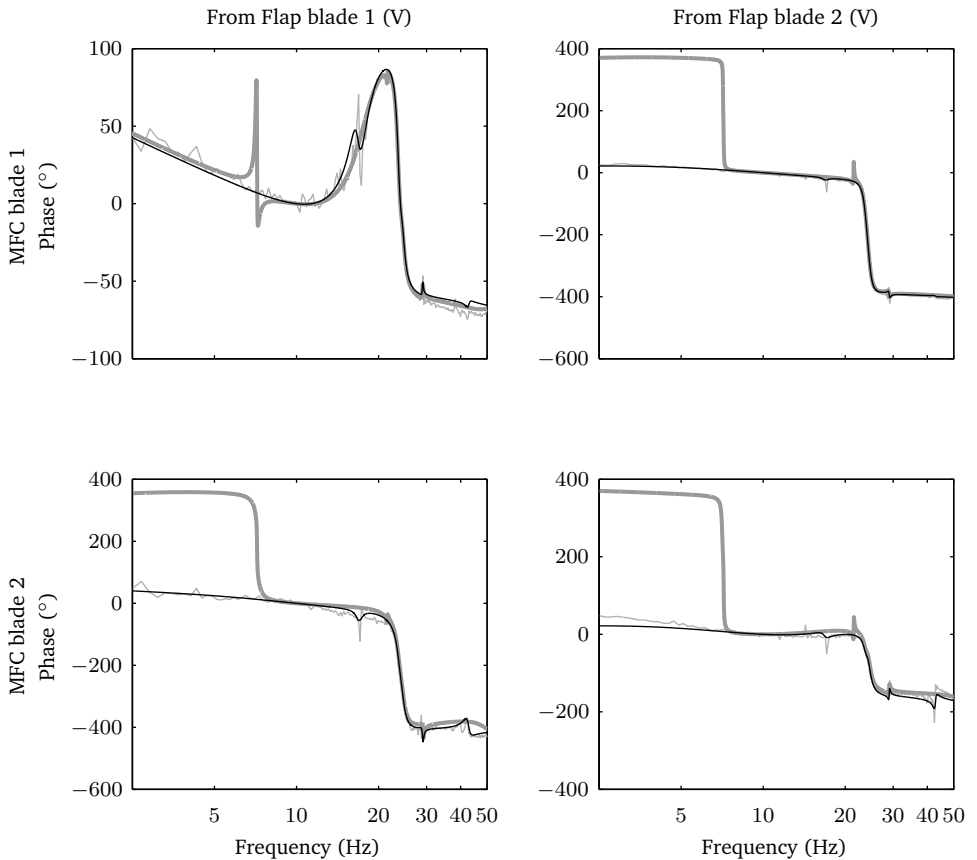


**Figure 3.5** – Phase responses of the identified transfer functions from the two piezoelectric flaps to the two strain measurements. Shown are the identified models without compensation for periodic disturbances (solid gray), with compensation for periodic disturbances (solid black) and spectral estimate (thin gray line). (Results valid for  $V = 7$  m/s and  $\Omega = 370$  rpm.)

Engineering, Delft University of Technology and Technion, Haifa, Israel, a feasibility study was performed to investigate the use of an active flutter suppression and load alleviation system. One such concept, which has a limited impact on mass and structural complexity, is to use free-floating flaps with small piezoelectrically-driven trailing edge tabs. Figure 3.6 shows an illustration of this concept. The main idea is that the small tab, being located at the trailing edge, has a leverage advantage. A small deflection of the tab causes the rudder surface to rotate in the opposite direction, which in turn generates the desired control surface effect. This is similar to the use of *servo tabs* on many current aircraft. Important experimental work on this concept was carried out by Heinze and Karpel (2006) and besides the potential for aeroelastic (flutter) control, the concept is also a candidate for wind turbine load alleviation by controlling local blade loads (Barlas and van Kuik, 2007; van Wingerden, Hulskamp, Barlas, Marrant et al., 2008).

A scale model of a vertical tailplane, depicted in Figure 3.7, with two such free-floating flaps equipped with piezoelectric tabs was built in order to perform a technology demonstration. The experimental tailplane – with all piezoelectrics self-contained within

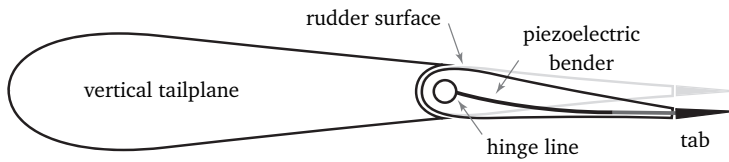


**Figure 3.6** – Schematic representation of the vertical tailplane with free-floating rudder control surface and the piezoelectric tab at the trailing edge. As the tab deflects, the free-floating rudder moves in the opposite direction.

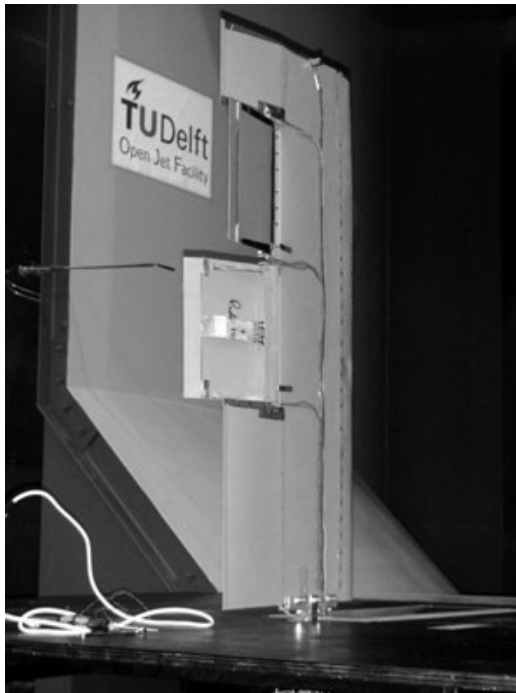


**Figure 3.7** – The experimental vertical tailplane in the Open Jet Facility at Delft University of Technology. The two free-floating flaps are shown deflected in opposite directions.

the freely hinged rudder control surfaces – was such that the configuration exhibited low-speed flutter, predominantly due to the fact that the flaps are under-balanced (Bernhammer, De Breuker, Karpel et al., 2012). Since the active flutter suppression system relies on feedback, it is crucial to obtain an accurate model describing the dynamic input-output behaviour of the system in terms of the gain and phase behaviour. In this case the inputs are the control voltages to the two piezoelectric trailing edge tabs. The controlled output is the acceleration measured by an accelerometer mounted at the tip of the vertical tailplane, which is assumed to be representative for any vibrations of the structure. In Bernhammer, De Breuker, Karpel et al. (2012) the aeroservoelastic modelling procedure is described that was used to model the dynamic behaviour of the entire vertical tailplane. The dynamic behaviour was predicted using numerical analysis and for several reasons it cannot be expected that, for example, the predicted eigenmodes are equal to the modes of the true experimental structure:

- Mass, stiffness and damping properties of the structure are different than predicted. This is mainly due to differences in the geometry and construction. Furthermore, a situation of perfect clamping was assumed in the numerical analysis which did not correspond to the true clamping conditions which were more flexible;
- Simplified unsteady aerodynamics were assumed in the numerical analysis, consisting of the harmonic solution of a potential flow model. This simplified model and assumed lift characteristics may differ from the actual behaviour;
- Actuator dynamics were not incorporated in the analysis and a simplified model of the piezoelectric bender was applied;
- Because of the experimental nature, production inaccuracies were large and the behaviour of the two piezoelectric tabs was not entirely equal.

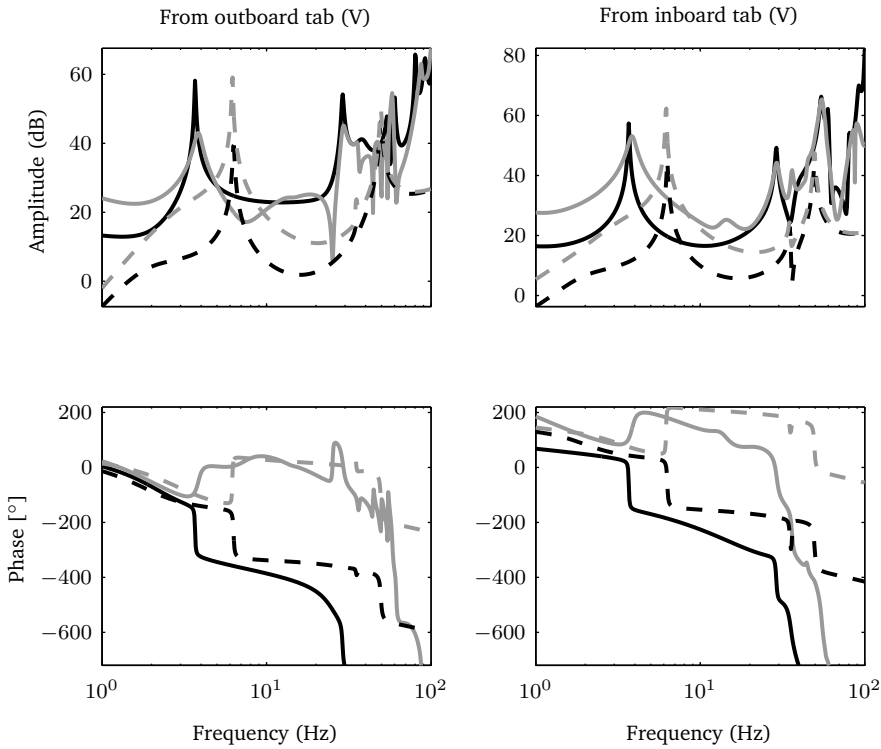
One way to deal with the differences between predicted and actual behaviour of the vertical tail plane is to iteratively tune the numerical model until a sufficient level of agreement is reached. For the purpose of control system design, however, it is not given that such a procedure will result in an accurate model describing the dynamics from actuators to sensors. The interconnection of different subsystem models, each with a certain amount of inaccuracies makes tuning of the compound model a challenging task. In these cases, system identification can complement first principles modelling.

### 3.3.1 Identification experiments and control design

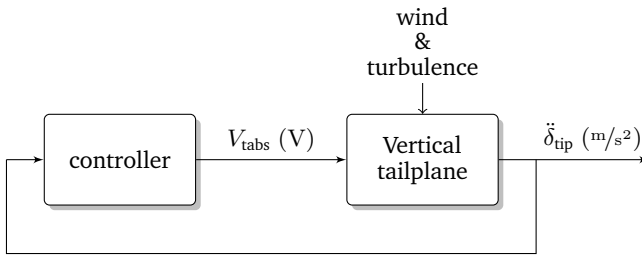
In initial wind tunnel measurements, the flutter point was determined by gradually increasing the wind speed while perturbing the tip of the vertical tailplane with small impulses. Once the flutter point had been determined, identification experiments were performed at several wind speeds by injecting random signals into the actuator control channels. To achieve the best possible signal-to-noise ratio, pseudo-random binary sequences with amplitudes of  $\pm 100$  V (equal to the hardware limits) were used. These signals were then filtered with a low-pass filter with cutoff frequency of 50 Hz to avoid excitation of high-frequency modes outside the bandwidth of interest. Signals were sampled during 90 s at a rate of 2 kHz and subsequently filtered and downsampled to 200 Hz. The closed-loop MOESP algorithm was used to identify models of the rudder. In this application the PBSID<sub>opt</sub> and CLMOESP methods are likely to yield similar results, but CLMOESP was favoured because of the clearer order indication.

Figure 3.8 shows the identified transfer functions at two different wind speeds: 10 m/s which is below the flutter speed and 16 m/s which is well into the flutter regime. The first bending mode is identified at 3.7 Hz and the first torsion mode at 29 Hz. These frequencies are much lower than those predicted by the first principles model and, while the amplitude and phase behaviour are similar to the behaviour predicted by the numerical model, the differences between the identified and predicted modes are likely to imply that a controller designed for the first principles model will not stabilise the system. To make it work, the designed controller would have to be excessively robust, resulting in a conservative design.

Models were first identified below the flutter speed, since in those conditions experiments could be performed without a controller active. On the basis of one of these identified



**Figure 3.8** – Bode diagrams of the predicted (dashed) and identified (solid) transfer functions from microtab voltages to accelerometer output. Results are shown for 10 m/s (black line) and for 16 m/s (gray line).



**Figure 3.9** – Diagram of the flutter control and load alleviation system.

models, specifically just below the flutter speed at 10 m/s, a controller was designed based on manual frequency domain loop-shaping techniques. A schematic representation of the control system is shown in Figure 3.9. For reasons of simplicity and since the goal was to control only the first bending mode of the tailplane, it was decided to control both flaps in unison. This controller is composed of several elements:

- Low-pass filters to attenuate any high-frequency content beyond 10 Hz related to the nature of acceleration measurements;
- A notch filter to further attenuate the structural torsion mode at 35 Hz;
- A lead compensator adding phase lead to result in a loop phase close to zero degrees

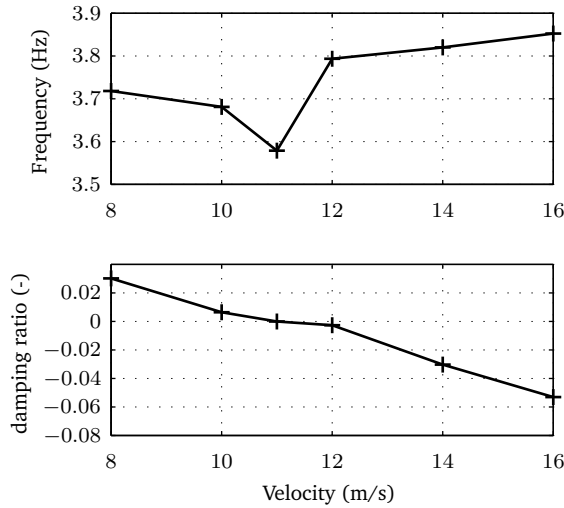


**Figure 3.10** – Identified frequencies and damping ratios as a function of wind speed corresponding to the dynamic mode related to flutter.

at the first bending mode (3.7 Hz) and sufficient gain and phase margins of 10 dB and  $45^\circ$ , respectively, at the crossover frequencies.

Once this controller was designed for a speed of  $10 \text{ m/s}$ , the wind speed was increased beyond the original flutter speed up to the new flutter speed determined by the closed-loop dynamics. This procedure allowed us to identify models under closed-loop conditions at wind speeds higher than the original flutter speed; a powerful capability of closed-loop subspace identification methods. Table 3.1 shows values of the variance-accounted-for (cf. (2.38) on page 36) for the identified models. Figure 3.10 shows how the dominant structural mode, namely the first bending mode, varies with wind speed and changes from a lightly damped mode into a flutter mode at  $11 \text{ m/s}$ .

It was found that the designed control system was able to move the flutter point from the previous value of  $11 \text{ m/s}$  to a new flutter speed just beyond  $16 \text{ m/s}$ , beyond which speed the tailplane would become unstable. Hence, a model identified at this speed of  $16 \text{ m/s}$  was used to redesign a controller. A Nyquist plot of the loop gain is shown in Figure 3.11 for a wind speed of  $14 \text{ m/s}$ , indicating stability and robustness of the compensator design. With the updated controller, the flutter speed could be increased beyond  $21 \text{ m/s}$ . No further iterations were performed, since at these wind speeds the control signals were frequently well beyond their saturation limit. Hence, extending the flutter boundary even further would require using control surfaces with more authority. It is important to note that in this study no attempts were made to optimise switching between the two controllers. Both controllers were permanently active, with the output of one of them directed to the tabs; the switching was performed manually near a wind speed of  $16 \text{ m/s}$ .

**Table 3.1** – The variance-accounted-for for the identified models at different wind speeds.

wind speed (m/s)	8	10	11	12	14	16
stable (y/n)	y	y	n	n	n	n
VAF (open-loop)	85.5%	86.4%	–	–	–	–
VAF (one-step-ahead predictor)	89.6%	95.4%	99.6%	93.5%	88.5%	86.7%

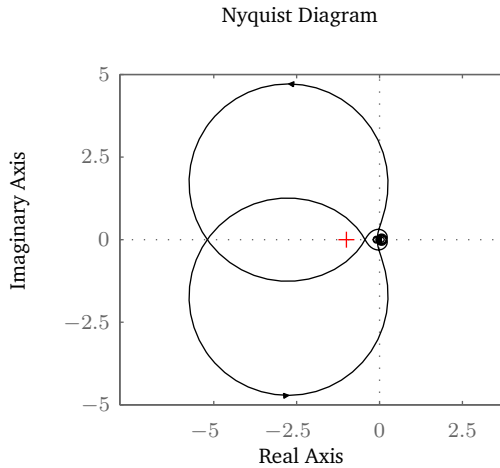


**Figure 3.11** – Nyquist plot of the loop gain at  $14 \text{ m/s}$ . The plot clearly shows that the encirclement criterion is met (2 counterclockwise encirclements of  $s = -1$ , corresponding to the unstable complex conjugate pole pair) and that the phase and gain margins are sufficient – the trajectories steer clear of the critical point  $s = -1$ .

At the start of this chapter we stated that system identification techniques can only be applied successfully by combining them with specific domain knowledge. At first it might appear that in this example the methods from Chapter 2 have been applied as “black-box” techniques. This is not true, however. To be able to obtain accurate and reliable models efficiently, i.e., in a short span of time, we have used knowledge of the predicted behaviour of the wing to determine important aspects such as:

- **Perturbation signals.** We have used the predicted modes and input-output behaviour to determine appropriate excitation signal bandwidths and levels. These did not need to be adjusted afterwards.
- **Bandwidth.** Based on prior analysis we knew which modes to expect and which modes would be targeted by the controller. Based on this information an appropriate sample frequency, experiment length and identification bandwidth were chosen.

### 3.3.2 Experimental evaluation and load alleviation

Flutter tests were performed to evaluate the performance of the closed-loop system. For a wind speed below flutter at  $10 \text{ m/s}$ , a model was identified and a controller designed. Then, with the system under closed-loop control, the wind speed was steadily increased to determine the new flutter point. At a wind speed just before this extended flutter point at  $16 \text{ m/s}$ , a new model was identified in closed-loop for which a new controller was designed. It turned out to be sufficient to lower the gain of the updated controller at this higher wind speed. With these two design iterations, the flutter point could be extended from  $11 \text{ m/s}$  to beyond  $21 \text{ m/s}$ .

Besides demonstrating the flutter control potential of the microtab control system, it was also shown that at wind speeds near the flutter point dynamic loads which excite the first bending mode could be attenuated using the same controller by as much as 40% in terms of the root bending moment (Bernhammer, De Breuker, Karpel et al., 2012). Interestingly, in all tested cases the tailplane could be successfully stabilised, despite applying large impulse excitations which caused the control signal to saturate, cf. Figure 3.12. Apparently, a bang-bang type control law works well in this case: the rudder motion is in opposite phase to the bending, thereby removing energy from the system (Bernhammer, De Breuker, Karpel et al., 2012).

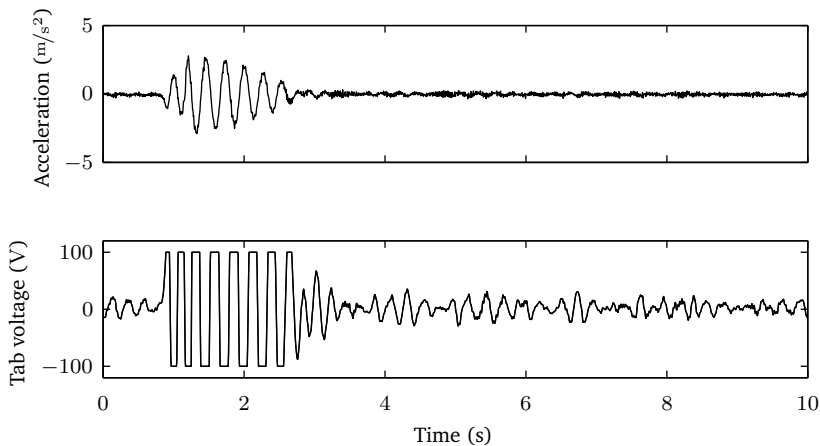


**Figure 3.12** – Response to a large impulse excitation. Even though the control signal saturates, the tailplane bending motion is rapidly damped and the system retains its stability.

### 3.3.3 Conclusions

In this example we have shown the potential of the closed-loop subspace identification methods described in Chapter 2 from a practical point of view. We have shown how a controller was successfully designed in one go on the basis of an identified model, while the first principles model would require many iterations of model updating to result in similar dynamic behaviour. We have further shown how the stabilised system could be re-identified under closed-loop conditions to perform an iteration of the controller design which resulted in a refined controller for the changed dynamics at higher wind speeds.

While updating of the first principles model could potentially be very time consuming, all these experiments, including model identification, control design and evaluation were performed in less than two days. Of course, it is important from a design point of view to refine first principles models. Still, in this case identification experiments can be useful since the resulting models immediately point out the differences in behaviour between the actual system and the first principles model. This may guide engineers to where the models need refinement.

At the start of this chapter we stated that “black-box” system identification techniques can only be applied successfully by combining them with specific domain knowledge. In this section we have stressed how using this knowledge to design the perturbation signals and the excitation bandwidth was relevant to the success of identification and control design in this example.

## 3.4 Rapid evaluation of controller performance on an experimental turbine

In an ongoing effort to investigate and evaluate new control strategies for wind turbines experiments were recently performed at the National Renewable Energy Laboratory (NREL) in the US in collaboration with Delft University of Technology. Increasingly, turbines are equipped with a control system which does not only regulate the power output of the turbine, but also regulates loads. In this instance, it was investigated how the existing speed controller, measuring generator speed and controlling generator torque, could be extended with a load reduction controller. The goal of adding this capability was to add damping to the very lightly damped drive train resonance and the lightly damped tower side-side motion. The available actuation signal would remain generator torque, but to

add information on the tower motion, a side-side accelerometer signal was incorporated in the design. To be able to provide results which are repeatable we followed a systematic procedure and hence (industry-) standard techniques were adhered to as much as possible in the designs.

In this section we show how system identification can be applied to rapidly and efficiently judge the performance of the closed-loop system. For that purpose we will first describe how several controllers were designed. Next, we describe how the closed-loop behaviour was identified and how perturbation signals were designed. Finally, we will show some results of applying these ideas to the CART 3 research turbine in field tests.

### 3.4.1 Control design procedure

We start by briefly discussing the control design procedure which led to three designs to be evaluated. The reader is referred to Fleming, van Wingerden, Scholbrock et al. (2013) for details on these procedures. Controllers were designed on the basis of LTI models governing the dynamics from torque demand to generator speed and side-side acceleration. The models were derived from the nonlinear model of the CART 3 in the aeroelastic code FAST (Jonkman, 2012). Some effort was made recently to tune this model on the basis of modal tests (Osgood, Bir, Mutha et al., 2011).

The most important degrees of freedom included in these linearised models are the generator speed, drive train torsion and tower side-side bending. Furthermore, these models include dynamics of the torque roll-off filter and time delays. The goal of the controllers closing the loops from generator speed to torque demand and side-side acceleration to torque demand is to augment the baseline controller with active damping of the drive train torsion mode and the tower side-side bending mode. The design of the damping controllers led to three designs to be evaluated, which are listed here:

1. **The baseline design.** This design consists of the existing single-loop speed controller which ensures that the generator speed setpoint is maintained. The design process followed industry-standard techniques (Bossanyi, 2000);
2. **A multi SISO (mSISO) design.** In the mSISO design a classical “successive loop closure” approach, widespread in industry, was applied to extend the baseline controller. The two loops closed successively are:
  - a) A feedback loop to enhance damping of the drive train resonance. This loop was designed using loop-shaping and root locus techniques. The tower frequency was notched out, followed by a lead filter and a gain, to result in (mainly) feedback of the drive train resonance;
  - b) A feedback loop to enhance damping of the tower side-side bending mode. This loop was designed around the intermediate closed-loop system using similar techniques. The accelerometer signal was first filtered and then integrated in order to obtain a measure of tower velocity. From this signal the drive train resonance frequency was notched out, followed by a lead-lag compensator to result in tower velocity feedback.

Both control signals were passed through a filter cascade to attenuate feedback of known (high frequency) noise and to avoid interference with the baseline speed controller;

3. **An  $H_\infty$  design.** In the  $H_\infty$  design the single-input-multi-output plant was considered and used in a mixed sensitivity  $H_\infty$  synthesis procedure (Skogestad and Postlethwaite, 1996). Weights were imposed on the actuator signals and output signals expressing the desired loop shapes. These weights were chosen very similar to the ones in the mSISO design:
  - a) The actuator penalty weights comprised a bandpass filter to penalise low and high frequency control actions and inverted notches to penalise control of resonances which are not of interest;
  - b) The output penalty consisted of inverted notches on the drive train frequency and the side-side bending frequency respectively for the generator speed and accelerometer outputs respectively, in order to penalise these resonances.

During a period of several months, starting in April 2012, the controllers were run under various conditions and sensor data was acquired. In total about 20 hours' worth of baseline data was acquired, 1.5 hours' worth of mSISO operation and 5.25 hours' worth of  $H_\infty$  operation. In Fleming, van Wingerden, Scholbrock et al. (2013) an extensive analysis was performed to determine the performance of each of the controllers in terms of reducing fatigue-critical damage equivalent loads due to cyclic loading (Hayman, 2012). This analysis led to the following conclusions:

1. The  $H_\infty$  controller successfully damped the drive train resonance whereas the mSISO controller merely shifted the resonance frequency;
2. Both controllers damped the side-side motions equally well;
3. Both controllers resulted in an increase in torque activity, with the mSISO design causing slightly more torque activity;
4. Both controllers achieved tower bending fatigue load reduction, but only the  $H_\infty$  controller achieved drive train torsion fatigue load reduction.

Regarding these field test results it is important to note that in the design stage both controllers worked equally well, both in linear and in nonlinear simulations. Apparently there are differences between the LTI models and the true behaviour (Fleming, Wright, Fingersh et al., 2011).

The foregoing analysis resulted in the conclusions that the  $H_\infty$  controller performed well since it was robust to differences between modelled and true dynamics, whereas the mSISO controller failed as a consequence of these differences. These conclusions were based on analysing significant amounts of data gathered over the course of months. Nevertheless, the amount of data was not sufficient to draw definitive conclusions (Fleming, van Wingerden, Scholbrock et al., 2013). In the next sections we will show the value of system identification in this context and we will investigate how system identification might be able to accelerate this process.

### 3.4.2 Identification of closed-loop wind turbine behaviour

To identify the closed loop LTI behaviour of a controlled system a few important aspects must be considered. These are first discussed.

#### Selection of identification signals

Although many signal configurations can be considered, the basic differences are indicated in Figure 3.13, which shows a highly simplified schematic of the CART 3 control system. Considering the system boundary labelled as "open-loop", the (partly controlled) signals entering the turbine are the pitch angle  $\beta$  and the generator torque  $T_g$ . The wind speed may be considered a disturbance in the context of LTI identification. Using these input signals for identification will result in the open-loop dynamics of the wind turbine. Using the control framework presented in Chapter 2, no restrictions are placed on how these signals are generated, i.e., what the character of the controller is, and no knowledge of the controllers is required.

If we now consider the boundary labelled as "closed-loop", we have as signals entering the system perturbations on the pitch angle, perturbations on the generator torque and perturbations on the generator speed reference. If we use one or more of these signals for identification, it is clear that we identify the closed-loop behaviour of the turbine. When doing so in an effort to model the closed-loop as an LTI system, it is important to ensure not only that the turbine operates in a fairly narrow operating range, but also that the controllers act as LTI systems. If the controllers act in a nonlinear way, e.g., by switching continuously between full-load and partial-load strategies in the transition region, identification is unlikely to be successful since the closed-loop system is then nonlinear.

One such effect was found in preliminary data analysis of measured CART 3 data. Since in this section the goal is to estimate the closed-loop dynamics, specifically those of the

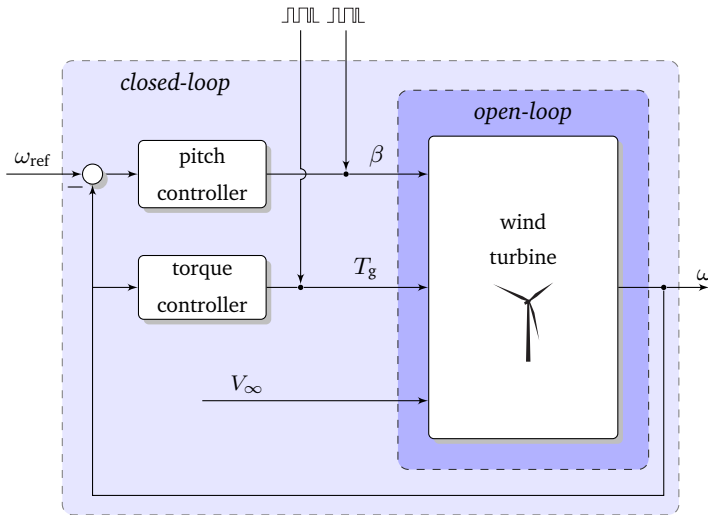


**Figure 3.13** – Schematic representation of the CART 3 control system. The dashed areas indicate the system boundaries used when considering the closed-loop dynamics and the open-loop dynamics respectively.

drive train, we considered the perturbations on the generator torque as inputs, with the “closed-loop” boundary in Figure 3.13. In data batches where the rotor speed crossed the tower natural frequency, significant impact of the supervisory control system was found. In order to prevent the 3P frequency (i.e., three times the rotor speed) from corresponding with the tower side-side natural frequency, a tower resonance avoidance strategy has been implemented in the supervisory controls of CART 3. This strategy rapidly ramps up or down the generator torque if the 3P frequency approaches the tower frequency from above or below, so that the turbine quickly accelerates or decelerates past this critical frequency, see Figure 3.14. This additional torque contribution presents a nonlinear control action, which violates the assumption of LTI behaviour. This means that data sets where this happens are not suitable for identification of closed-loop dynamics. One straightforward solution to bypass this problem would be to model the torque contribution by the supervisory control system as an additional (measured) external input signal (or add it onto the perturbation signals). The point we wish to make here, however, is that care must always be taken. It is important to know the paths that (perturbation) signals follow before reaching the actual controlled system. If this is not done, it is clear that this may lead to unexpected results.

#### Design of perturbation signals for wind turbines

In system identification it is often necessary to apply perturbation signals. This is done to excite all relevant modes of a system and to achieve a good signal-to-noise ratio between the output signal content due to the excitations and due to disturbances and noise. While from an identification point of view it may appear beneficial to make these perturbation signals as large as possible, this is not the case in practice:

- Large perturbations may cause the system to operate in a wide range, causing the assumption of LTI dynamics to be violated;
- Large perturbations are costly. Just as is the case for many industrial systems, perturbations cause the system to operate suboptimally. In the case of wind turbines, torque perturbations appear in the output power and may excite lightly damped drive train and side-side modes leading to fatigue damage. Pitch perturbations cause the rotor speed to vary, may excite fore-aft tower motions and cause wear of the pitch system. Both perturbations may induce large loads by exciting modes of the turbine.

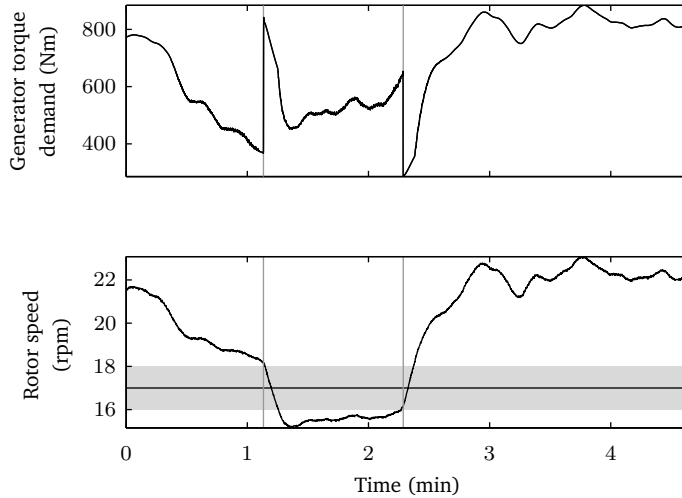


**Figure 3.14** – The tower resonance avoidance strategy on CART 3: the generator torque is modified in order to prevent the rotor speed from dwelling near 17 rpm which would cause the 3P frequency to line up with the tower natural frequency.

- Pitch and torque perturbations must satisfy actuator (rate) limits. Hence it is necessary to design these signals and verify satisfaction of these constraints.

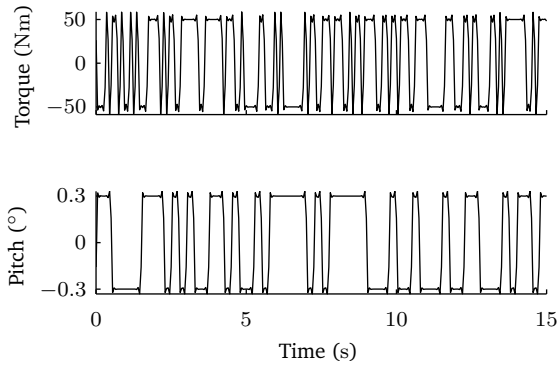
Typically, the wear and fatigue related aspects are less pronounced in this context, since system identification is not a continuous process. This does not hold however for the continuous system identification performed in subspace predictive control in Chapter 4, where perturbation signal design is a key issue.

Figure 3.15 shows the pitch and torque perturbation signals designed for the CART 3 turbine. Initial excitation signal designs were performed with the aid of a *Bladed* (*Bladed 2011*) simulation model of the turbine. The turbine was simulated at constant mean wind speeds and perturbation signals were applied. The turbulence was gradually increased up to the level of the turbulence which CART 3 typically experiences ( $I_{\text{ref}} = \pm 20\%$ ). Attempts were made to identify models for different excitation levels. By an iterative process suitable values were determined. These values were further adjusted on the basis of earlier field testing and identification results. Figure 3.15 shows the designed signals, with a pseudo-random binary signal of  $\pm 50 \text{ Nm}$  for the torque perturbation and a pseudo-random binary signal of  $\pm 0.3^\circ$  for the pitch perturbation.

### 3.4.3 Identification from field test data

In our experience, controller design typically requires several iterations. Initially, a controller is designed on the basis of linearised first principles models and simulations in aeroelastic codes such as FAST (*Jonkman, 2012*). Subsequently, this controller is evaluated in field tests. In the case of more refined controllers, mismatch between modelled and true dynamics can cause the controller to under-perform, in particular when considering resonance frequencies which may differ between the aeroelastic code and the true wind turbine. Obviously, system identification can be applied to identify models of the turbine which may then serve to support controller design. Even if this step is skipped, we will show that system identification can quickly reveal the behaviour of the closed-loop system.

During the experiments mentioned before, in which each of the controllers was activated in turn, system identification experiments were also performed. In these experiments the



**Figure 3.15** – Example time traces of perturbations applied to the pitch and torque reference signals.

generator torque was perturbed with a pseudo-random binary signal of  $\pm 50$  Nm in order to excite all the relevant modes – in particular the modes targeted for damping enhancement. In this case only the generator torque was perturbed, since only the dynamics in response to the torque input are considered. Then, on the basis of the signals measured during periods of approximately 10 minutes, models of the closed-loop dynamics from torque input to generator speed were identified using the closed-loop MOESP subspace identification technique discussed in Chapter 2.

Figure 3.16 shows the identified closed-loop dynamics of the turbine in terms of the magnitude response. The results near the drive train resonance frequency clearly indicate that the  $H_\infty$  design seems to perform rather satisfactorily, while the mSISO controller seems to merely shift the drive train frequency as opposed to add damping. This prompts further investigation into the design and possibly the effects of model mismatch. This quick diagnostic may therefore significantly expedite controller design. Figure 3.18 confirms these results by showing the power spectral densities of three relevant measurements. These PSDs have been computed using all available measurement data. The PSD of the generator speed shows that the  $H_\infty$  controller completely damps out the drive train resonance and both controllers add some damping to the side-side motion of the tower. Figure 3.17 shows how the identified (open-loop) dynamics near the drive train resonance differ from those described by the linearised first principles model, obtained from the FAST aeroelastic code. Note that the resonance is in reality much more damped than predicted and furthermore that the frequency is slightly different. This may indicate that the poor damping observed with the mSISO controller can be attributed to model mismatch. Furthermore, the phase response is quite different due to the presence of nonminimum phase zeros in the identified model. The presence of these nonminimum phase zeros suggests a fundamental bandwidth limit in the above-rated speed control loop. This limit would imply a bandwidth limit of about 0.4 Hz to be safe. Nonminimum phase zeros associated with the tower natural frequency and occurring in the loop from pitch angle to generator speed are well-known to exist under certain conditions and have been studied, for instance in Leithead and Dominguez (2006); Larsen and Hanson (2007); van der Veen, Couchman and Bowyer (2012) and in Appendix B. One should keep in mind that there is some uncertainty in the identified model, requiring further (identification) experiments to be performed to determine the exact character of these zeros.

#### 3.4.4 Conclusions

In this section we have described how the controller design process for a wind turbine can be supported with system identification. Typically, extensive field tests are required to judge the performance and effects on fatigue loads. While these field tests are still necessary to obtain statistically significant results, the testing process can be streamlined. With only a

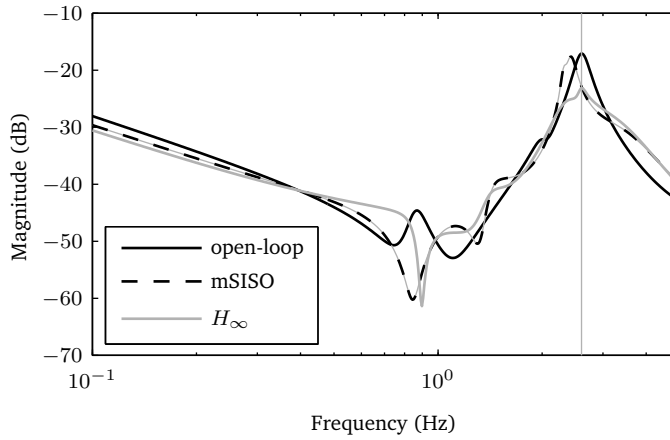


**Figure 3.16** – Identified dynamics from generator torque to generator speed for the baseline turbine, the turbine augmented with an mSISO controller and the turbine augmented with an  $H_\infty$  controller.

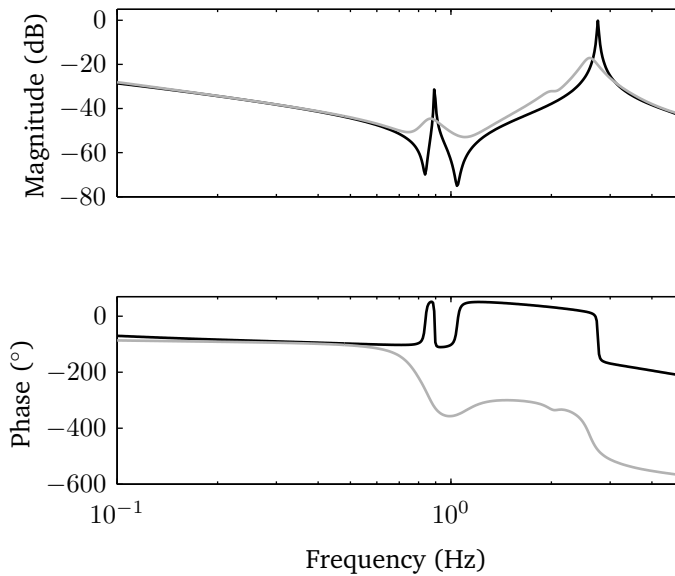


**Figure 3.17** – Predicted (black) and identified (gray) dynamics from generator torque to generator speed.

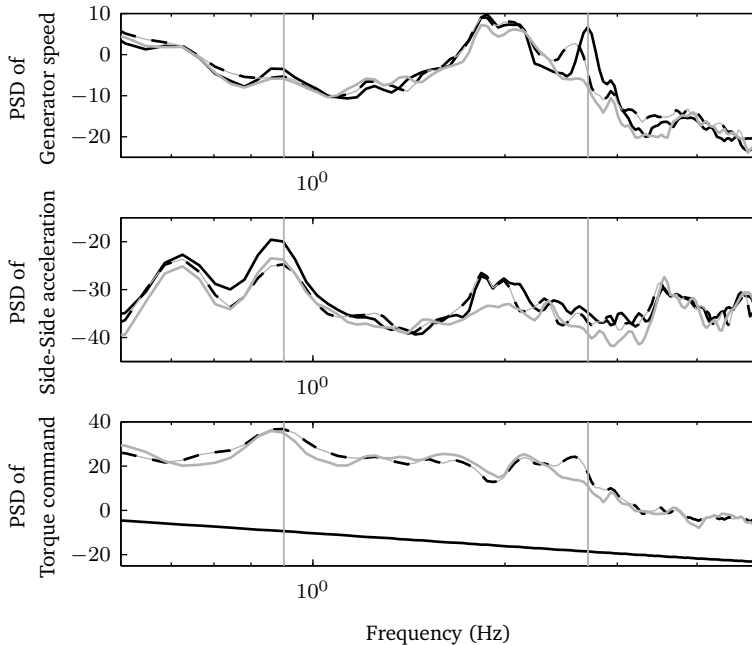


**Figure 3.18** – Power spectral densities of input and output signals for the baseline controller (black), the mSISO controller (dashed) and the  $H_\infty$  controller (gray).

few short data sets, system identification can give an indication of closed-loop performance, prompting a redesign if necessary.

### 3.5 Conclusions

We started this chapter by stressing the importance of combining “black-box” identification techniques with specific domain knowledge about the problem at hand. Over the course of this chapter we have collected a number of important aspects related to domain knowledge about the identification problem. Using this knowledge resulted in identification of accurate and reliable models.

Summarising, we arrive at the following important aspects:

- **Periodic disturbances.** Knowledge of the wind turbine mechanics explains the mechanisms by which periodic signals appear in certain measurements taken from wind turbines. This enabled us to extend the identification framework of Chapter 2 to consistently and reliably identify models despite the presence of these periodic disturbances.
- **Perturbation signals.** Knowledge of the dynamics, for instance from an aeroelastic code, can be used to determine appropriate excitation signal bandwidths and levels. This can speed up the identification experiments and prevents significant redesigns from being necessary.
- **Bandwidth.** Based on prior analysis one knows which modes to expect and which modes should be targeted by the controller. Based on this information, in fact consisting of the control objectives, an appropriate sample frequency, experiment length and identification bandwidth can be chosen.
- **Nonminimum phase behaviour.** Detailed knowledge about the potential nonminimum phase behaviour of wind turbines and floating wind turbines in particular

and the mechanisms by which these occur is useful in determining where (at which frequencies) identified models should be put under close scrutiny to determine the actual presence of nonminimum phase behaviour. Further experiments may be necessary to establish the full character.

- **Signal paths.** In Section 3.4.2 we have shown that knowing exactly where input signals are measured is of fundamental importance. This may mean the difference between identifying open or closed-loop dynamics. Also, it determines whether or not actuator dynamics and/or filters are included and whether a supervisory control system could influence signals “downstream” of where they have been measured.

# Subspace predictive control of aeroelastic systems

This chapter considers direct data-driven control of systems whose dynamics can be described locally by LTI models. The control algorithm is based on the predictor-based subspace identification framework. In a linear least-squares problem, the observer Markov parameters of the system are recursively estimated. Those parameters are used to construct an output predictor which is used to solve a predictive control problem subject to constraints. In this chapter we also present a square root estimation scheme with directional forgetting of past information.

The feasibility of the approach is highlighted by applying it to two experimental setups using an efficient implementation. First, we consider control of vibrations in a flexible structure equipped with piezoelectric transducers. This serves to demonstrate that computations can be performed in realtime for a realistic system and we show how the scheme rapidly adapts when a sudden significant change in structural dynamics is introduced by changing one of the structural parameters. Second, we consider speed regulation of an experimental wind turbine subject to wind speed and setpoint changes.

## 4.1 Introduction

In this chapter we consider subspace predictive control (SPC) as a first step towards unifying the fields of identification and control design. The SPC framework offers a way to combine the advantages of a model predictive control law (MPC) with the capability to deal with unknown and slowly time-varying dynamics. Obvious advantages of MPC are the ability to deal with constraints and the intuitive tuning which is not dissimilar to tuning of a linear quadratic regulator. The adaptivity is useful for systems which can be considered locally linear, but have dynamics which vary mildly with the operating condition. SPC has been presented primarily as a framework for fault-tolerant control design (Dong, Verhaegen and Holweg, 2008; Hallouzi, 2008), as the recursive estimation scheme will automatically detect events such as actuator failures. This is the main strength of the SPC framework.

Subspace predictive control was first presented in Favoreel and De Moor (1998); Favoreel, De Moor, Van Overschee et al. (1999) and later in Woodley (2001) for data-driven  $H_\infty$  control. The identification framework used in these versions was the framework of open-loop subspace identification. Since in SPC the identification will by definition take place under closed-loop conditions, modified versions were presented in Dong, Verhaegen and Holweg (2008); Hallouzi (2008) using the predictor-based subspace identification framework of Chiuso (2007a) and discussed in Chapter 2. Compared to the original algorithms, the predictor-based version is asymptotically unbiased in closed-loop operation.

SPC comes with a number of challenges, which are still largely open problems. First, estimation is performed recursively and to be able to identify the dynamics consistently, all modes must be excited continuously. The challenge is to add the minimal amount of perturbations to maintain a sufficient signal-to-noise ratio and persistence of excitation, since perturbations will adversely affect the process. This problem has been considered in Dong (2009). A partial remedy to this requirement of persistent excitation is to update parameters only when new information is available using a directional forgetting scheme.

Such a strategy is considered in this chapter. A further challenge is the stability of the control scheme. Efforts have been made to take into account the uncertainty on the estimated parameters to result in cautious  $H_2$  control (Dong and Verhaegen, 2009; Kulcsár and Verhaegen, 2010). Similar techniques could be applied to take the uncertainty on the Markov parameters into account in a stochastic robust MPC scheme (Bemporad and Morari, 1999), possibly using the framework developed in Evans, Cannon and Kouvaritakis (2012).

Despite these challenges, SPC is an attractive framework due to its conceptual simplicity. In the literature it has been applied primarily to numerical examples, exceptions being Woodley (2001); Kadali, Huang and Rossiter (2003); Dong, Verhaegen and Holweg (2008), where only the latter considered the closed-loop identification framework. Important aspects of ordinary MPC, such as offset-free control and feedforward control are readily implemented in SPC as shown in Kadali, Huang and Rossiter (2003); Soliman, Malik and Westwick (2012). The main focus of this chapter is to show the successful application of SPC to two real examples. As a by-product, we derive an efficient and reliable square-root recursive least-squares scheme with directional forgetting. This directional forgetting scheme is based on the ideas in Bittanti, Bolzern and Campi (1990); Cao and Schwartz (2000) and exhibits guaranteed boundedness of the covariance matrix even if there is no excitation.

In the first example we consider vibration control of a flexible beam. Vibration control of flexible structures continues to be an area of active research. In particular, there is interest in “smart” structures equipped with electrically deformable materials. Recent overviews of control design techniques for such structures are given in e.g., Preumont and Seto (2008) and Moheimani and Fleming (2006). It is frequently the case in practice that the characteristics of flexible structures change, e.g., due to variable loading or changing boundary conditions. Adaptive control methodologies for resonant structures have been proposed in Niederberger, Fleming, Moheimani et al. (2004). Alternatively, robust control techniques can be applied to synthesise controllers that take uncertainty into account, but dealing with shifting resonance frequencies in such a framework is challenging, and may require resorting to LPV or IQC techniques. Recently, the feasibility of model predictive control (MPC) for vibration control has been demonstrated, e.g., in Wills, Bates, Fleming et al. (2008). Hence, we will show the application of SPC to such a system.

In the second example we consider SPC to track a generator speed setpoint on an experimental wind turbine. Two cases are considered. In the first, tracking of a varying reference is performed. In the second, the task is to maintain a constant setpoint in the presence of a varying wind speed. In both cases the varying operating conditions may cause the local dynamics to be different. In the second example the recursive estimation scheme also estimates the dynamics from a wind speed change ahead of the turbine to the rotor speed, making use of a pitot-static tube measurement. This disturbance model helps to anticipate these wind speed variations.

The contributions of this chapter are threefold. We first present an attractive directional forgetting recursive least-squares scheme in square root form. Second, we demonstrate the potential of SPC as an adaptive control methodology in dealing with time-varying system dynamics. Third, we present the application of the algorithm to realistic examples, as opposed to most implementations of SPC thus far, posing some additional challenges.

## 4.2 Identification framework

The underlying model and identification framework used in the subspace predictive control scheme are identical to those presented in Section 2.2 of Chapter 2. For that reason we will not repeat them here. Instead, we will only present elements of the derivations which are specific to subspace predictive control (more details can be found in Dong, Verhaegen and Holweg (2008); Hallouzi (2008)). It is assumed that the system operates in the vicinity of a steady operating point during some time and any variations in the operating point or the system dynamics occur slowly. To make this more precise, it is assumed that there is a clear separation between the time constants of the system dynamics and the much slower time constants of parameter variations.

### 4.2.1 Recursive solution of the parameter estimation problem

In this section we discuss the procedure of recursively estimating the parameters in an online setting using recursive least squares (RLS). The starting point for our derivations is the least-squares estimation of the predictor Markov parameters (2.12), which has been repeated here for convenience:

$$\arg \min_{[C\tilde{\mathcal{K}}^{(p)} D]} \left\| \begin{bmatrix} Y_{p,N_p} \\ Z_{0,p,N_p} \\ U_{p,N_p} \end{bmatrix} - \begin{bmatrix} C\tilde{\mathcal{K}}^{(p)} \\ D \end{bmatrix} \begin{bmatrix} Z_{0,p,N_p} \\ U_{p,N_p} \end{bmatrix} \right\|_F^2. \quad (4.1)$$

This formulation considers the offline case of identification using a batch of input-output data. We reformulate this estimation problem to deal with new samples of input-output data arriving at each sample interval.

To maintain a compact notation, the least-squares problem (2.12) will be concisely written in the standard form:

$$\hat{\Theta}_k = \arg \min_{\Theta} \|Y_k - \Phi_k \Theta\|_F^2, \quad (4.2)$$

where the subscript  $k$  signifies that data up to time instant  $k$  is available and used. Hence, the involved matrices are defined as (cf. (4.1)):

$$Y_k \triangleq \begin{bmatrix} y_{p+1}^T \\ y_{p+2}^T \\ \dots \\ y_k^T \end{bmatrix}, \quad \Phi_k \triangleq \begin{bmatrix} \varphi_{p+1}^T \\ \varphi_{p+2}^T \\ \dots \\ \varphi_k^T \end{bmatrix}, \quad \Theta \triangleq [C\tilde{\mathcal{K}}^{(p)} D]^T,$$

with:

$$\varphi_k \triangleq \begin{bmatrix} z_k^{(p)} \\ u_k \end{bmatrix}.$$

Furthermore, let  $n_{\Theta} = \dim_{\mathbb{R}} \text{vec}(\Theta)$  denote the number of parameters to be estimated.

Obviously, the data matrices one time instant later, i.e.,  $Y_{k+1}$  and  $\Phi_{k+1}$  contain the new samples  $u_{k+1}$  and  $y_{k+1}$  and these matrices therefore grow in time. Explicitly, these matrices become:

$$Y_{k+1} \triangleq \begin{bmatrix} y_{p+1}^T \\ y_{p+2}^T \\ \dots \\ y_k^T \\ \hline y_{k+1}^T \end{bmatrix}, \quad \Phi_{k+1} \triangleq \begin{bmatrix} \varphi_{p+1}^T \\ \varphi_{p+2}^T \\ \dots \\ \varphi_k^T \\ \hline \varphi_{k+1}^T \end{bmatrix}.$$

The full-rank least-squares solution of (4.2) can now be written as:

$$\hat{\Theta}_k = (\Phi_k^T \Phi_k)^{-1} \Phi_k^T Y_k. \quad (4.3)$$

Suppose a new sample, described by  $(y_{k+1}, \varphi_{k+1})$  becomes available. It is straightforward to show that the new least-squares solution satisfies:

$$\hat{\Theta}_{k+1} = \underbrace{(\Phi_k^T \Phi_k + \varphi_{k+1} \varphi_{k+1}^T)^{-1}}_{=P_{k+1}=\mathcal{I}_{k+1}^{-1}} (\Phi_k^T Y_k + \varphi_{k+1} y_{k+1}).$$

We now define the *information matrix*  $\mathcal{I}_k$  and the *covariance matrix*  $P_k$  as:

$$\mathcal{I}_k = \Phi_k^T \Phi_k, \quad P_k = (\Phi_k^T \Phi_k)^{-1}.$$

Making use of this definition, the underbraced term can be simplified using the matrix inversion lemma, in order to avoid inverting a large matrix in each time step:

$$\begin{aligned}
 \mathcal{I}_{k+1}^{-1} &= (\mathcal{I}_k + \varphi_{k+1}\varphi_{k+1}^T)^{-1} \\
 &= \mathcal{I}_k^{-1} - \mathcal{I}_k^{-1}\varphi_{k+1} \left( I_{n_y} + \varphi_{k+1}^T \mathcal{I}_k^{-1} \varphi_{k+1} \right)^{-1} \varphi_{k+1}^T \mathcal{I}_k^{-1} \\
 &= P_k - P_k \varphi_{k+1} \left( I_{n_y} + \varphi_{k+1}^T P_k \varphi_{k+1} \right)^{-1} \varphi_{k+1}^T P_k. \tag{4.4}
 \end{aligned}$$

Note that this expression merely requires the inversion of an  $n_y$ -by- $n_y$  matrix. The parameter update can now be written as:

$$\begin{aligned}
 \widehat{\Theta}_{k+1} &= (I - P_k \varphi_{k+1} (I + \varphi_{k+1}^T P_k \varphi_{k+1})^{-1} \varphi_{k+1}^T) \widehat{\Theta}_k + P_{k+1} \varphi_{k+1} y_{k+1} \\
 &= \widehat{\Theta}_k - \underbrace{P_k \varphi_{k+1} (I + \varphi_{k+1}^T P_k \varphi_{k+1})^{-1} \varphi_{k+1}^T}_{\text{underbraced}} \widehat{\Theta}_k + P_{k+1} \varphi_{k+1} y_{k+1}
 \end{aligned}$$

For the underbraced term in the previous equation we can derive the following identity:

$$\begin{aligned}
 P_k \varphi_{k+1} (I + \varphi_{k+1}^T P_k \varphi_{k+1})^{-1} \\
 &= P_k \varphi_{k+1} (I + \varphi_{k+1}^T P_k \varphi_{k+1})^{-1} (I + \varphi_{k+1}^T P_k \varphi_{k+1} - \varphi_{k+1}^T P_k \varphi_{k+1}) \\
 &= (P_k - P_k \varphi_{k+1} (I + \varphi_{k+1}^T P_k \varphi_{k+1})^{-1} \varphi_{k+1}^T P_k) \varphi_{k+1} \\
 &= P_{k+1} \varphi_{k+1}
 \end{aligned}$$

which allows the parameter update to be rewritten concisely as:

$$\widehat{\Theta}_{k+1} = \widehat{\Theta}_k - P_{k+1} \varphi_{k+1} (y_{k+1} - \varphi_{k+1}^T \widehat{\Theta}_k). \tag{4.5}$$

In practice a forgetting factor  $\lambda < 1$  is introduced to maintain a finite memory in the least-squares problem as opposed to an infinite memory. This ensures that the parameters remain adaptive; furthermore this is required to maintain a finite (nonzero) covariance matrix. Exponential forgetting is introduced by adding the following update step to the algorithm:

$$\bar{\mathcal{I}}_k = \lambda \mathcal{I}_k,$$

so that accumulated information is uniformly discounted over time. The matrix  $\bar{\mathcal{I}}_k$  is then used instead of  $\mathcal{I}_k$  to perform the information update in (4.4). Applying this sequence of operations it is straightforward to show that the standard RLS algorithm with exponential forgetting satisfies the following update relations (Åström and Wittenmark, 1994):

$$P_k = \frac{1}{\lambda} \left( P_{k-1} - P_{k-1} \varphi_k \left( \lambda I_{n_y} + \varphi_k^T P_{k-1} \varphi_k \right)^{-1} \varphi_k^T P_{k-1} \right) \tag{4.6}$$

$$\widehat{\Theta}_k = \widehat{\Theta}_{k-1} - P_k \varphi_k (y_k - \varphi_k^T \widehat{\Theta}_{k-1}) \tag{4.7}$$

For  $n_y = 1$  these equations simplify to their more well-known forms. It is finally noted that in propagating the covariance matrix  $P_k = (\Phi_k \Phi_k^T)^{-1}$  in finite precision arithmetic the RLS algorithm is not guaranteed to retain a positive definite covariance matrix due to accumulation of round-off errors. This effect becomes more pronounced as the condition number of  $P_k$  grows. In the next subsection we discuss an implementation that does not suffer from these problems.

#### 4.2.2 Square-root covariance RLS with directional forgetting

For the reasons mentioned, the simple RLS scheme above is rarely used and instead a square-root algorithm is used (Verhaegen, 1989; Sayed, 2003). Such algorithms propagate the Cholesky factor of the covariance matrix (or the information matrix) by executing a

sequence of orthogonal transformations in each time step. Such square root algorithms are numerically superior to their counterpart described above. The computational complexity of the standard RLS as well as the square root algorithms is  $\mathcal{O}(n_\Theta^2)$  per iteration ( $n_\Theta = p(n_u + n_y) + n_u n_y$  is the number of parameters in the LS problem for the Markov parameters (2.12)). i.e., quadratic in the number of parameters.

We will now derive this square-root version of the update equations, in which the Cholesky factor of the covariance is updated. This algorithm is sometimes also called the *inverse QR* RLS algorithm (Sayed, 2003). For a comprehensive overview of (square-root) recursive least-squares algorithms consult e.g., Pan and Plemmons (1989); Sayed (2003). In Verhaegen (1989), the round-off error propagation characteristics of several RLS algorithms are analysed. The results of the analysis show that the square-root covariance RLS method has some attractive properties with regard to round-off error propagation and maintaining a symmetric positive definite covariance matrix. A standard reference regarding the update of several factorisations applied here is Gill, Golub, Murray et al. (1974).

Let  $P_k = R_k R_k^T$ , where  $R_k$  is a lower-triangular Cholesky factor of the covariance matrix, then the covariance update (4.6) is given by:

$$R_k R_k^T = \frac{1}{\lambda} R_{k-1} R_{k-1}^T - \frac{1}{\lambda} R_{k-1} R_{k-1}^T \varphi_k \left( \lambda I_{n_y} + \varphi_k^T P_{k-1} \varphi_k \right)^{-1} \varphi_k^T R_{k-1} R_{k-1}^T \quad (4.8)$$

This equation can be factored as follows:

$$\underbrace{\begin{bmatrix} \sqrt{\lambda} I_{n_y} & \varphi_k^T R_{k-1} \\ 0 & \frac{1}{\sqrt{\lambda}} R_{k-1} \end{bmatrix}}_{\text{pre-array}} Q = \underbrace{\begin{bmatrix} a & 0 \\ G_k & R_k \end{bmatrix}}_{\text{post-array}}, \quad (4.9)$$

where:

$$G_k = \left( \frac{1}{\lambda} R_{k-1} R_{k-1}^T \varphi_k \left( \lambda I_{n_y} + \varphi_k^T P_{k-1} \varphi_k \right)^{-1} \varphi_k^T R_{k-1} R_{k-1}^T \right)^{\frac{1}{2}}$$

$$a = \left( \lambda I_{n_y} + \varphi_k^T R_{k-1} R_{k-1}^T \varphi_k \right)^{\frac{1}{2}}.$$

Multiplying both sides of this equation by their respective transposes will show that (4.8) is indeed satisfied. This array representation shows that by first forming the pre-array in (4.9) and subsequently performing a sequence of orthogonal transformations  $Q$  in order to lower-triangularise the post-array, we can obtain the updated Cholesky factor  $R_k$ . This Cholesky factor is read off from the post-array. The parameter update is then given by:

$$\hat{\Theta}_k = \hat{\Theta}_{k-1} + \sqrt{\lambda} G_k a^{-1} (y_k - \varphi_k^T \hat{\Theta}_{k-1}) \quad (4.10)$$

In a typical least-squares formulation, we consider the information matrix  $\mathcal{I}$ , which is an accumulation of rank-one updates. As was shown before, the information matrix is typically updated according to:

$$\mathcal{I}_k = \lambda \mathcal{I}_{k-1} + \varphi_k \varphi_k^T.$$

For convenience further on, we will explicitly split the steps of forgetting and updating according to:

$$\tilde{\mathcal{I}}_{k-1} = \lambda \mathcal{I}_{k-1},$$

$$\mathcal{I}_k = \tilde{\mathcal{I}}_{k-1} + \varphi_k \varphi_k^T.$$

In this relation,  $\lambda$  is the forgetting factor, usually close to one, used to discount old information in an exponential way (i.e., observation  $k - j$  is weighted with  $\lambda^j$  in the least-squares criterion). A common expression for the effective window length. is given by (Sayed, 2003):

$$N = \frac{1}{1 - \lambda}.$$

A drawback of this scheme is that all information is forgotten uniformly. As a consequence, the matrix  $\mathcal{I}$  may become singular over the course of time if the observations  $\varphi_k$  do not excite all directions. Suppose the information matrix is an  $n$ -by- $n$  square matrix  $\mathcal{I} \in \mathbb{R}^n$ , then over time  $\varphi_k \in \mathbb{R}^n$  should uniformly “visit” all directions in the space  $\mathbb{R}^n$ . This effect is coupled to the notion of persistent excitation (Johnstone, Johnson, Bitmead et al., 1982).

In Cao and Schwartz (2000) a directional forgetting algorithm is proposed that uses a decomposition of the information matrix. At each time instant, the information matrix is decomposed according to:

$$\mathcal{I}_k = \mathcal{I}_k^{(1)} + \mathcal{I}_k^{(2)}.$$

The decomposition is such that  $\mathcal{I}_k^{(1)}\varphi_k = 0$ . This implies that the update  $\varphi_k$  is orthogonal to the columns of  $\mathcal{I}_k^{(1)}$ . This does not define  $\mathcal{I}_k^{(2)}$  uniquely. Since the updates are rank-one modifications to  $\mathcal{I}_k$ , one can make the restriction that  $\mathcal{I}_k^{(2)}$  is a rank-one matrix. Furthermore, it should hold that  $\mathcal{I}_k^{(2)}\varphi_k = \mathcal{I}_k\varphi_k$ . In Cao and Schwartz (2000) it was shown that a unique decomposition can then be found.

*Remark 4.1.* Here, we treat the derivations for the case  $n_y = 1$  for clarity of presentation. Note that in case  $n_y > 1$ , updating the covariance matrix can proceed sequentially, i.e. by performing the update steps for each column of  $\varphi_k$  in turn. The end result is the same.

We now consider an alternative derivation of these results. Based on the new regressor vector  $\varphi_k$ , we can define orthogonal projection matrices:

$$\begin{aligned}\Pi_{\varphi_k} &= \frac{\varphi_k \varphi_k^T}{\varphi_k^T \varphi_k}, \\ \Pi_{\varphi_k}^\perp &= I - \Pi_{\varphi_k} = I - \frac{\varphi_k \varphi_k^T}{\varphi_k^T \varphi_k},\end{aligned}$$

such that for an arbitrary vector  $\xi$  we have

$$\Pi_{\varphi_k} \xi \parallel \varphi_k \quad \text{and} \quad \Pi_{\varphi_k}^\perp \xi \perp \varphi_k.$$

Thus  $\Pi_{\varphi_k}$  projects a vector (matrix) onto  $\varphi_k$  and  $\Pi_{\varphi_k}^\perp$  projects a vector (matrix) onto the orthogonal complement of  $\varphi_k$ . One decomposition of the information matrix  $\mathcal{I}$  is:

$$\mathcal{I}_k = \underbrace{\mathcal{I}_k \Pi_{\varphi_k}^\perp}_{\perp \varphi_k} + \underbrace{\mathcal{I}_k \Pi_{\varphi_k}}_{\parallel \varphi_k}. \quad (4.11)$$

The main idea is then that forgetting can be applied only along the direction of the new data, that is, according to:

$$\bar{\mathcal{I}}_k = \mathcal{I}_k \Pi_{\varphi_k}^\perp + \lambda \mathcal{I}_k \Pi_{\varphi_k}, \quad (4.12)$$

where  $\bar{\mathcal{I}}$  denotes the information matrix with discounted old information. The decomposition (4.11) clearly satisfies the requirements imposed on the decomposition before. A third requirement, however, is not satisfied automatically. The decomposition must be symmetric in the sense that  $\mathcal{I}_k^{(1)}$  and  $\mathcal{I}_k^{(2)}$  must both be symmetric matrices or else the forgetting proposed in (4.12) will result in a loss of symmetry. In general, the matrices  $\mathcal{I}_k \Pi_{\varphi_k}^\perp$  and  $\mathcal{I}_k \Pi_{\varphi_k}$  are not symmetric (although all individual matrices are symmetric), since the information matrix and the projection matrices do not share the same eigenspace. To solve this, we must modify the projections to:

$$\begin{aligned}\Pi_{\varphi_k} &= \frac{\varphi_k \varphi_k^T \mathcal{I}_k}{\varphi_k^T \mathcal{I}_k \varphi_k}, \\ \Pi_{\varphi_k}^\perp &= I - \Pi_{\varphi_k} = I - \frac{\varphi_k \varphi_k^T \mathcal{I}_k}{\varphi_k^T \mathcal{I}_k \varphi_k}.\end{aligned}$$

These projections ensure that the range of  $\Pi_{\varphi_k}$  is still  $\varphi_k$  (which is necessary to ensure  $\Pi_{\varphi_k} \varphi_k = \varphi_k$ ), while the orthogonal complement of its null space (i.e., that set of directions which are annihilated by the projection) is given by  $\mathcal{I}_k \varphi_k$ , so  $\varphi_k$  transformed into the range of  $\mathcal{I}_k$  (which is necessary to ensure that  $\Pi_{\varphi_k}$  does not modify the eigenspace of  $\mathcal{I}_k$ ). Using these projections, we still have the decomposition (4.11), where the two components are now each symmetric. Using the expressions for the projections, (4.12) can be written explicitly as:

$$\bar{\mathcal{I}}_k = \mathcal{I}_k F = \mathcal{I}_k \left( I + (\lambda - 1) \frac{\varphi_k \varphi_k^T \mathcal{I}_k}{\varphi_k^T \mathcal{I}_k \varphi_k} \right). \quad (4.13)$$

In a recursive least-squares scheme, usually the covariance matrix  $P_k = \mathcal{I}_k^{-1}$  is updated, to avoid inversion in each time step. Using the Woodbury matrix identity we obtain:

$$\bar{P}_k = F^{-1} P_k = \left( I + \frac{1 - \lambda}{\lambda} \frac{\varphi_k \varphi_k^T \mathcal{I}_k}{\varphi_k^T \mathcal{I}_k \varphi_k} \right) P_k.$$

Note that some care must be taken to ensure that the rank-one downdate in (4.13) does not cause  $F$  to become singular (Seeger, 2004). Further simplification results in:

$$\bar{P}_k = P_k + \frac{1 - \lambda}{\lambda} \frac{\varphi_k \varphi_k^T}{\varphi_k^T \mathcal{I}_k \varphi_k} = P_k + \alpha_k \varphi_k \varphi_k^T, \quad (4.14)$$

with the scalar  $\alpha_k$  given by:

$$\alpha_k = \frac{1 - \lambda}{\lambda} \frac{1}{\varphi_k^T \mathcal{I}_k \varphi_k} \geq 0, \quad (4.15)$$

which shows that the directional forgetting procedure is equivalent to a symmetric positive rank-one update to  $P_k$ .

*Note that a significant drawback of this directional forgetting algorithm is that the matrix  $\mathcal{I}_k$  must be available to compute (4.15). This was not mentioned in Cao and Schwartz (2000), but implies that one should either update both the information and covariance matrices in each time step, or that one should invert the covariance matrix in each time step. An attractive alternative results from a square root formulation of this problem, which we shall now describe.*

In the square-root RLS filter, we work with the Cholesky factor  $R_k$  of the covariance matrix, such that  $P_k = R_k R_k^T$ . Substituting this factorisation into the update law (4.14) yields:

$$\bar{R}_k \bar{R}_k^T = R_k R_k^T + \alpha_k \varphi_k \varphi_k^T. \quad (4.16)$$

From this equation it is straightforward to derive an array representation:

$$\underbrace{\begin{bmatrix} \sqrt{\alpha_k} \varphi_k & R_k \end{bmatrix}}_{\text{pre-array}} Q = \underbrace{\begin{bmatrix} 0 & \bar{R}_k \end{bmatrix}}_{\text{post-array}}, \quad (4.17)$$

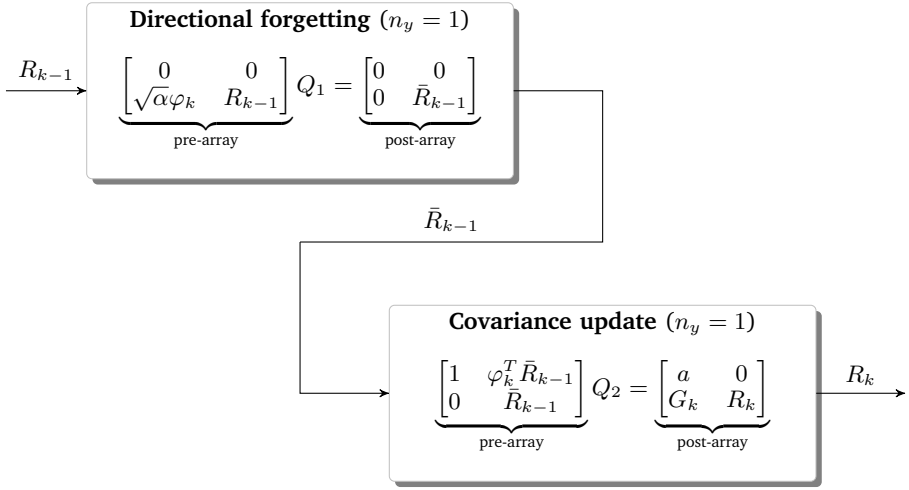
with:

$$\alpha_k = \frac{1 - \lambda}{\lambda} \frac{1}{\|R_k^{-1} \varphi_k\|_2^2}, \quad (4.18)$$

and where  $Q$  is an arbitrary orthogonal transformation used to zero the elements in the first columns of the pre-array, e.g., by means of a sequence of Givens rotations.

*Note that in the square root formulation we find an alternative expression to compute  $\alpha_k$  (4.15), given by (4.18). Since we have at our disposal the Cholesky factor  $R_k$  and this Cholesky factor is lower triangular, the term  $R_k^{-1} \varphi_k$  is readily computed by means of forward substitution as opposed to computing the inverse explicitly!*

*Remark 4.2.* Comparing (4.17) with the RLS update in (4.9) it is clear that, in terms of allocated space, the same pre-array can be used for the directional forgetting and the covariance update steps. This is shown more explicitly below:



Furthermore, both orthogonal factorisations require the same number of floating point operations<sup>1</sup>.

The preceding analysis shows that it is a simple matter to incorporate directional forgetting into an RLS scheme that is based on updating the square root of the covariance matrix: before updating the Cholesky factor of the covariance matrix with new data (cf. (4.9)), first (4.17) is used to apply forgetting only in the direction of the new data.

A significant advantage of the directional forgetting scheme is that old information is only discounted if it can be replaced with new information, thus relaxing persistency of excitation requirements. Further, as suggested in Cao and Schwartz (2000), a deadzone can be introduced so that the forgetting is only applied if the norm of  $\varphi_k$  exceeds some threshold, determined, for instance, by the noise level:

$$\alpha_k = 0 \text{ if } \|\varphi_k\|_2 \leq \epsilon. \quad (4.19)$$

Since each new data vector appended to the least-squares problem in (4.2) is in fact just a shifted version of its predecessor with a new sample appended, this knowledge can be exploited to reduce the computational complexity of the algorithm (Sayed, 2003; Houtzager, van Wingerden and Verhaegen, 2009a). This is used in the derivation of so-called fast-array RLS algorithms whose complexity is  $\mathcal{O}(n_\Theta)$ , thus linear in the number of parameters. These formulations, however, do not typically possess the robust numerical properties of the standard square root solutions (Sayed, 2003) and shall hence not be considered in this work.

### 4.2.3 Example 1 – Parameter estimation

We simulate  $N = 1000$  samples of the following model:

$$y_k = \frac{bz^2}{z^2 + a_1z + a_2} u_k + v_k,$$

<sup>1</sup>In a naive implementation, that is. The structure (zeros) of the directional forgetting pre-array could be exploited using Givens rotations to lower the number of operations.

with

$$\Theta \triangleq \begin{pmatrix} b \\ a_1 \\ a_2 \end{pmatrix} = \begin{cases} \begin{pmatrix} 0.5 & 0.3 & 0.4 \end{pmatrix}^T, & 0 \leq k \leq 500, \\ \begin{pmatrix} -0.5 & 0.9 & 0.9 \end{pmatrix}^T, & 500 < k \leq 1000 \end{cases}$$

where  $u_k$  and  $v_k$  are zero-mean white noise sequences with variances of 1 and 0.01 respectively. We simulate the traditional RLS algorithm with exponential forgetting and the directional forgetting algorithm, both with a forgetting factor  $\lambda = 0.95$ . The directional forgetting deadzone tolerance (4.19) is set to 0.4.

#### Case I: Loss of excitation

In case I, we simulate a loss of excitation. Between samples  $k = 200$  and  $k = 400$  we do not excite the system,  $u_k = 0$  so that the output is dominated by noise.

Figure 4.1(a) shows the results. It is clear that during the period with no excitation, the covariance matrix of the exponential forgetting algorithm grows exponentially, whereas the covariance matrix of the directional forgetting algorithm stays bounded. As a consequence, the parameter estimates themselves stay closer to the true values. It is also interesting to observe that the directional forgetting algorithm exhibits a slower convergence. Possibly this has to do with the deadzone tolerance: the value is chosen such that during no excitation no forgetting is performed if the norms of the regressor vectors are below 0.4, based on the noise level. It could be the case, however, that even during excitation the norm of  $\varphi_k$  is sometimes less than 0.4, so that the directional forgetting algorithm is slightly conservative in these events.

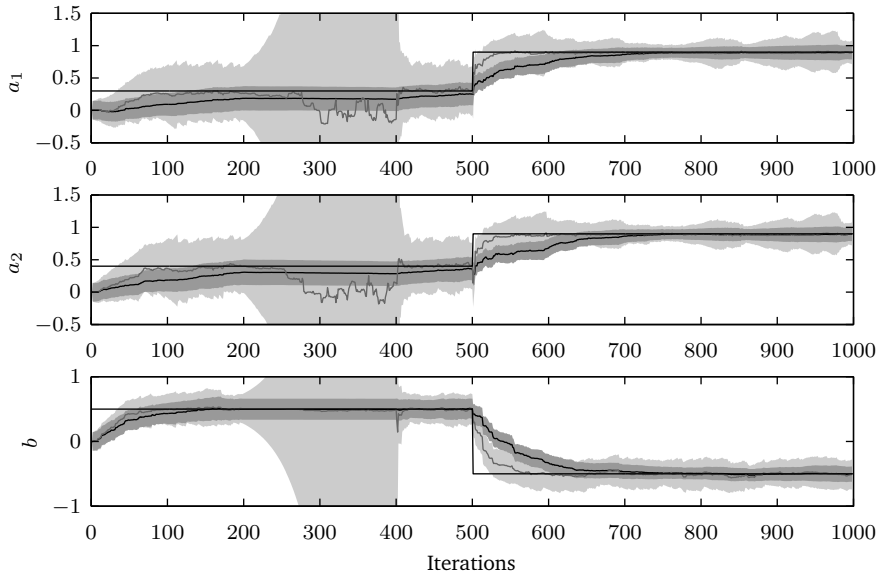
#### Case II: Special excitation

In case II we modify the regressor vectors  $\varphi_k$ . Between samples  $k = 700$  and  $k = 900$  we project the regressor vectors onto the vector  $[1 \ 0 \ 1]^T$ . This causes the regressor vectors to be non-informative on parameter  $a_1$ .

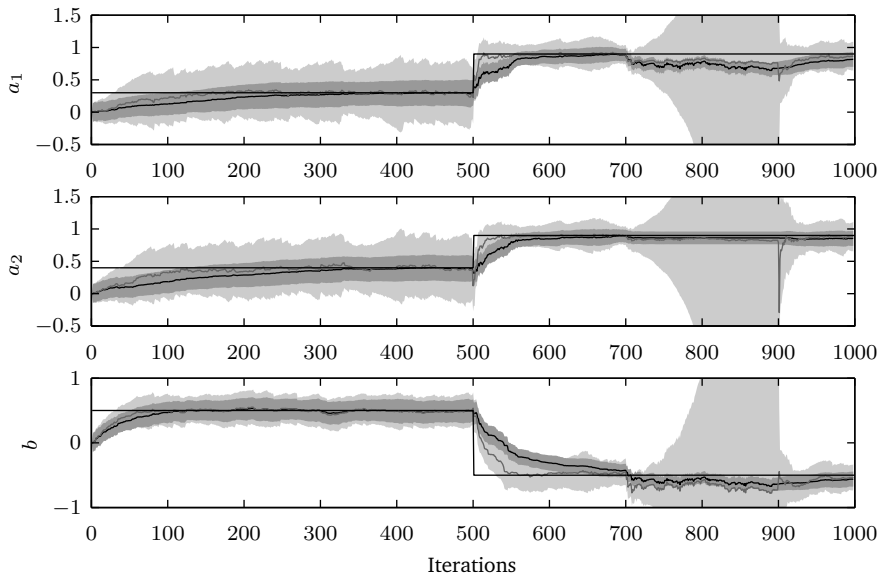
Figure 4.1(b) shows the results. The results are very similar to the ones shown in case I. The main consequence of the projection is that the exponential forgetting algorithm will diverge. The directional forgetting algorithm on the other hand will keep operating properly, simply maintaining the information related to parameter  $a_1$  at a constant level as long as no new information comes in.

### 4.2.4 Example 2 – Parameter tracking

As discussed in Bittanti, Bolzern and Campi (1990); Cao and Schwartz (2000), the first directional forgetting modifications to the exponential forgetting RLS scheme were presented in Hägglund (1983); Kulhavý and Kárný (1984); Hägglund (1985); Kulhavý (1987). In Bittanti, Bolzern and Campi (1990) the convergence properties of these proposed algorithms are studied and it is shown by a deterministic counterexample (a parameter tracking problem) that these directional forgetting algorithms do not converge for this counterexample. The article also proposes a modification to these original directional forgetting algorithms by means of adding a regularisation term to the covariance update in order to retain adaptivity. Figure 4.2 compares the results of the original directional forgetting algorithm with the modified directional forgetting algorithm and the square-root directional forgetting algorithm presented in this section. It turns out that our method exhibits very similar convergence properties to the modified algorithm suggested in Bittanti, Bolzern and Campi (1990). The parameter estimates generated by the latter two approaches are barely distinguishable in Figure 4.2.



(a) Case I



(b) Case II

**Figure 4.1** – Progression of the parameter estimates and their covariances for the exponential RLS algorithm (gray line and light gray shading) and the directional forgetting RLS algorithm (black line and dark gray shading). The true parameters are indicated by the horizontal black lines.

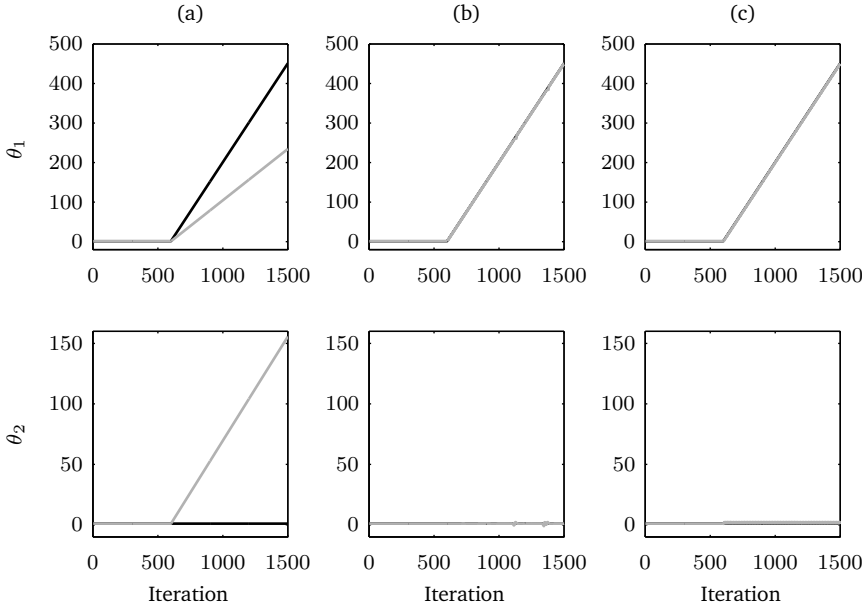


**Figure 4.2** – Progression of the parameter estimates for the counterexample from Bittanti, Bolzern and Campi (1990) for the standard directional forgetting RLS algorithm (a), the modified directional forgetting RLS algorithm proposed in Bittanti, Bolzern and Campi (1990) (b) and the directional forgetting RLS algorithm proposed in Cao and Schwartz (2000) and described in this chapter (c). The true parameters follow the black line.

### 4.3 Deriving the subspace predictor

Having estimated the predictor Markov parameters from least-squares problem (2.12), which were explicitly given in (2.11), the next step is to construct an output predictor for a sequence of future outputs. As a starting point (2.8) is revisited:

$$y_{k+p} = \widehat{C}\widehat{\mathcal{K}}z_k^{(p)} + \widehat{D}u_{k+p},$$

where the term  $e_{k+p}$  has been omitted since for purposes of prediction we have  $\mathbb{E}\{e_{k+p}\} = 0$ .

At time instant  $k$ , we consider the outputs at time instant  $k + 1$  up to  $k + N$ , where the arbitrary length of the prediction interval is denoted by  $N \in [1, \infty)^2$ . Define by  $y_k^{(N)}$  a stacked sequence of outputs according to:

$$y_k^{(N)} = [y_{k+1}^T, \dots, y_{k+N}^T]^T.$$

A stacked sequence  $u_k^{(N)}$  is defined analogously. Then it is straightforward to derive that:

$$y_k^{(N)} = \tilde{\Gamma}^{(N)}\tilde{\mathcal{K}}^{(p)}z_k^{(p)} + \tilde{H}^{(N)}(B, D)u_k^{(N)} + \tilde{H}^{(N)}(K, 0)y_k^{(N)}, \quad (4.20)$$

where  $\tilde{H}^{(N)}(B, D)$  and  $\tilde{H}^{(N)}(K, 0)$  have been defined in (2.6) in Section 2.2 and where  $\tilde{\Gamma}^{(N)}\tilde{\mathcal{K}}^{(p)}$  has been defined in (2.16) in Section 2.3.

These matrices can be constructed directly from the estimated predictor Markov parameters  $\widehat{C}\widehat{\mathcal{K}}^{(p)}$ ,  $\widehat{D}$ . Note that since the predictor parameters are used, the output

<sup>2</sup>It is remarked here that the prediction horizon  $N$  is not limited by the past window dimension  $p$ .

prediction  $y_k^{(N)}$  appears on both sides of the equation. To obtain the open-loop subspace predictor, the data equation is pre-multiplied with  $(I - \tilde{H}^{(N)}(K, 0))^{-1}$  to obtain the open-loop predictor:

$$y_k^{(N)} = \Gamma^{(N)} \tilde{\mathcal{K}}^{(p)} z_k^{(p)} + H^{(N)}(B, D) u_k^{(N)}. \quad (4.21)$$

There are at least two efficient ways to obtain the open-loop output predictor. First, one can simply perform the pre-multiplication with  $(I - \tilde{H}^{(N)}(K, 0))^{-1}$ . For that purpose it is highly advantageous to note that the matrix  $(I - \tilde{H}^{(N)}(K, 0))$  is lower unit-triangular, allowing an efficient forward-substitution to be used. An alternative method, derived in Dong (2009), uses a recursive formulation of the forward-substitution procedure to immediately build the predictor matrices, without explicitly forming  $(I - \tilde{H}^{(N)}(K, 0))$ . This procedure thus requires less storage, but a higher amount of looped operations, so the preferred method is implementation-dependent. In both cases it is possible to show, by carrying out the pre-multiplication, that the open-loop predictor contains the Markov parameters of the *innovation model* (2.3) as opposed to those of the *predictor model* (2.4).

#### 4.4 Setting up the predictive control problem

In this section we consider the derivation of the predictive control problem, based on the predictor (4.21) derived in the previous section. We consider a typical model predictive control performance index with output weighting. In this context, the goal is to, at each time instant, minimise the value of the following objective function:

$$J_k = \sum_{i=1}^N (y_{k+i} - r_{k+i})^T Q_y (y_{k+i} - r_{k+i}) + u_{k+i}^T R_u u_{k+i} + \Delta u_{k+i}^T R_{\Delta u} \Delta u_{k+i},$$

subject to:

$$\begin{aligned} u_{\min} \leq u_{k+i} \leq u_{\max}, & \quad i = 1 \dots N, \\ \Delta u_{\min} \leq \Delta u_{k+i} \leq \Delta u_{\max}, & \quad i = 1 \dots N. \end{aligned}$$

This objective expresses that the output should track a reference signal  $r_{k+i}$ , while minimising the control effort  $u_{k+i}$  and control rate  $\Delta u_{k+i}$ <sup>3,4</sup>. Using the notation introduced before, the objective can be reduced to:

$$J_k = \|y_k^{(N)} - r_k^{(N)}\|_{\tilde{Q}_y} + \|u_k^{(N)}\|_{\tilde{R}_u} + \|\Delta u_k^{(N)}\|_{\tilde{R}_{\Delta u}}, \quad (4.22)$$

after defining block-diagonal matrices  $\tilde{Q}_y$ ,  $\tilde{R}_u$  and  $\tilde{R}_{\Delta u}$  appropriately. In this equation,  $\|x\|_Q \triangleq x^T Q x$  denotes the weighted Euclidean norm.

To obtain the control rate  $\Delta u$ , the following matrices are defined:

$$S_{\Delta} = \begin{bmatrix} I_m & & & & \\ -I_m & I_m & & & \\ & & \ddots & & \\ & & & \ddots & \\ & & & & -I_m & I_m \end{bmatrix}, \quad S_0 = \begin{bmatrix} 0 & \cdots & I_m & 0 \\ \vdots & & & \\ 0 & \cdots & 0 & 0 \end{bmatrix}$$

so that:

$$\Delta u_k^{(N)} = S_0 z_k^{(p)} + S_{\Delta} u_k^{(N)}. \quad (4.23)$$

<sup>3</sup>  $\Delta u_k$  can be related to physical rate limits using the approximation  $(\Delta u_k)_{\max} \approx \left(\frac{du}{dt}\right)_{\max} \cdot T_s$ , with  $T_s$  the sample time and  $\left(\frac{du}{dt}\right)_{\max}$  the actual rate limit.

<sup>4</sup> Note that due to this formulation of the objective, perfect steady-state nonzero reference tracking can never be achieved when  $u_{ss} \neq 0$  if the second cost term is included, except when  $R_u = 0$  is chosen.



- The past window dimension  $p$ . The value of  $p$  determines the number of system parameters that are estimated and the order of the underlying ARX model (2.10). In off-line identification, this parameter is usually taken quite large, e.g., several times the maximum expected model order. In the recursive formulation (4.1), however, this choice directly affects the computational complexity of the update. Furthermore, estimating a larger number of parameters reduces the convergence rate of the recursive least-squares scheme. In an off-line analysis, a suitable value of  $p$  can be obtained, for instance, by validating the hypothesis that the least-squares residual resembles a zero-mean white noise sequence and whether the predictor Markov parameters indeed tend to zero at  $p$ .
- The forgetting factor  $\lambda$ . The value of  $\lambda$  should always be strictly less than 1 to avoid overflow issues when updating the covariance matrix with new observations (that is, for  $\lambda = 1$  the information matrix will grow unbounded, cf. (4.4)). This is also necessary to retain adaptivity of the parameters by forgetting, in an exponential sense, older data. The effective window length is usually expressed as  $N \approx 1/(1 - \lambda)$ . Depending on the characteristics of new observations, if the effective window is too short, information will be discarded too rapidly and the covariance matrix will become ill-conditioned. This choice of  $\lambda$  is essentially a trade-off between the ability to track parameter changes and the mean square errors of the estimated parameters. Again, in off-line analysis a value for  $\lambda$  can be chosen that suits the process at hand. Sometimes,  $\lambda$  itself may be an adaptive value, which is chosen as a function of the regressors and excitation levels (Kulhavý, 1987).
- The directional forgetting tolerance  $\epsilon$  (4.19). The value of  $\epsilon$  determines when directional forgetting is applied. In some instances where there is little excitation, the regressor  $\varphi_k$  may be small and dominated by noise. In these cases  $\epsilon$  can be used to restrict directional forgetting from being applied in such instances. Also, a large initial covariance is often chosen to expedite learning in the early stages of the estimation.
- The prediction horizon  $N_p$  is typically chosen such that the prediction interval contains the crucial dynamics of the process; its value can be based on the system's step response.
- The control horizon  $N_c$  determines the number of future inputs that is free. A small  $N_c$  reduces the complexity of the QP and further has a smoothing effect on the control signal, which is important for stability.
- The GPC weights,  $Q_y$ ,  $R_u$  and  $R_{\Delta u}$ , determine the trade-off between control authority (disturbance rejection) and actuator use. In the finite-horizon predictive control problem, these parameters also to a large extent affect the stability of the closed-loop system. These parameters are usually tuned so as to ensure that the control signals stay within their saturation and rate limits during regular operation.

## 4.5 Experimental evaluation: active damping of a “smart” beam

The SPC algorithm derived in the previous sections was derived before in the literature (Dong, Verhaegen and Holweg, 2008; Hallouzi, 2008), but it has rarely been applied to real systems (Woodley, 2001; Dong, Verhaegen and Holweg, 2008). In this section and the next one we consider two experiments in which we have tested the SPC algorithm on real systems.

### 4.5.1 Experimental setup

The subspace predictive control formulation derived in the previous sections is applied to a vibration control problem on a beam equipped with piezoelectric transducers, see Figure 4.3. This is the same setup as was used in Section 2.4.3. Two of these transducers are configured as actuators and two are configured as sensors. A schematic representation of the beam is given in Figure 4.4. The beam is an aluminium strip of 95 cm length. At locations 1 and 2, two (almost) collocated sensor-actuator pairs are situated. The actuators are flexible Macro Fiber Composite (MFC) devices, type M8528, from Smart Material Corp.

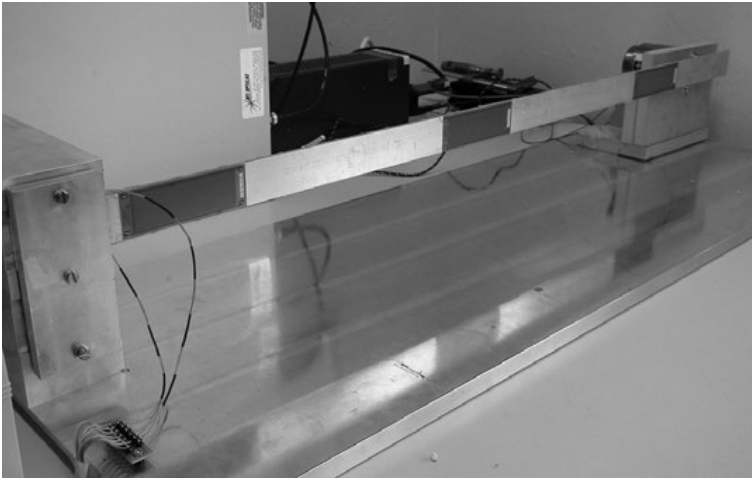


**Figure 4.3** – Photograph of the laboratory setup. The magnetic holding device is visible towards the far end.

The sensors are connected to high-impedance buffers and the actuators are driven by high-voltage amplifiers. As shown in Figure 4.3, the beam is clamped at the near end. At the far end either of two boundary conditions can be activated by means of an electromagnetic holding device. If the holding device is inactive, configuration (a), the beam is free at the far end, resulting in clamped-free boundary conditions, see Figure 4.4(a). If the holding device is active, configuration (b), the beam is effectively pinned at the far end, resulting in clamped-pinned boundary conditions, see Figure 4.4(b). These two different configurations result in two radically different dynamic behaviours, as can be seen from the expected vibration modes in Figure 4.4. The beam has a potentially infinite number of vibration modes, the lowest of which have very low intrinsic damping. For the given beam, the first two modes of configuration (a) are located at  $f_1^{(a)} = 3.7$  Hz and  $f_2^{(a)} = 23.7$  Hz, respectively. The first mode of configuration (b) is located at  $f_1^{(b)} = 18.6$  Hz.

#### 4.5.2 Control design

The objective of the control algorithm will be to augment damping of the first two vibration modes of configuration (a) and the first mode of configuration (b). During operating, the configuration can switch and the algorithm should track the associated changes in the dynamic behaviour.

To allow the digital control algorithm to operate at a rate of 200 Hz, data was sampled at 2 kHz, then filtered using a second order Butterworth anti-aliasing filter with a corner frequency at 60 Hz and then downsampled to 200 Hz. The control signal was upsampled to 2 kHz and then low-pass filtered at 250 Hz to eliminate the high frequency content introduced by the zero-order hold reconstruction.

In the current experiment the following parameter values were chosen: a past window dimension of  $p = 25$ ; a forgetting factor of  $\lambda = 0.99995$ , a prediction horizon of  $N_p = 50$  ( $=0.25$  s) and a control horizon of  $N_c = 10$ .

#### 4.5.3 Results

An experiment was performed in which the beam was subjected to random excitations on both actuators. At  $t = 10$  s the controller is switched on. Then, at  $t = 50$  s, an electromagnetic actuator clamps the tip of the beam. This momentarily introduces an

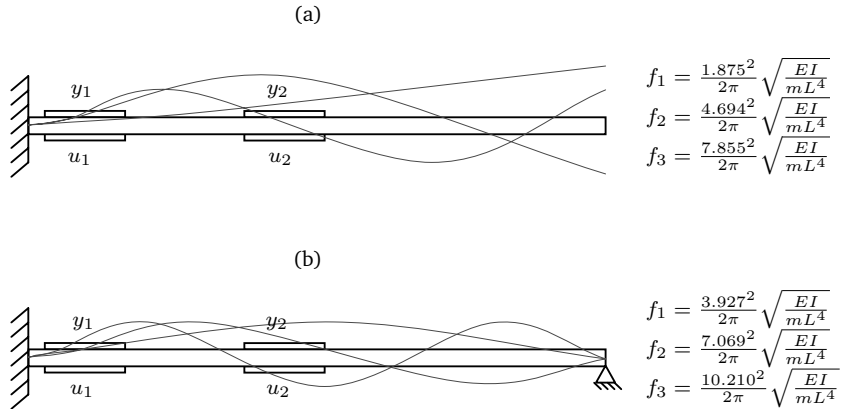


**Figure 4.4** – Schematic view of the two beam configurations and the associated natural vibration modes (Inman, 2001): (a) clamped, (b) clamped-pinned.

impulse disturbance (shock) and results in permanently changed characteristics. During this switching, the controller is kept switched on. From Figure 4.5 (the size of the moving window, 10 s, somewhat skews the temporal view of the results) one can see that almost immediately after switching on the controller the second mode is almost completely eliminated. Furthermore, after the change in dynamics, the controller adapts to the new configuration in seconds, after which the first mode of configuration (b) is also almost eliminated. In Figure 4.6 we compare the results of identifying the open and closed-loop systems for the first input-output pair. These responses clearly show that the modes at  $f_2^{(a)} = 23.7$  Hz and  $f_1^{(b)} = 18.6$  Hz, respectively for the two configuration, are attenuated by approximately 20 dB. The first mode at  $f_1^{(a)} = 3.7$  Hz in configuration (a) is attenuated by about 10 dB.

## 4.6 Experimental evaluation: speed control of a wind turbine scale model

In this experiment we have applied SPC to regulate the rotational speed of a small wind turbine. In the context of a master thesis project we have studied the potential of using look-ahead information on upcoming wind speed changes. Often, feedback control is used to regulate a wind turbine's rotor speed. This feedback control measures the current rotor speed, determines the error between this speed and the setpoint and gives proportional and integral feedback. The considerable inertia of the rotating system implies that there is a large time constant between changes in aerodynamic torque and actual speed changes. As a consequence, the potential of feedback control is hampered by a large phase disadvantage. In that master thesis project we have considered how disturbance rejection improves when a feedforward signal is used and when predictive control is used. We have taken this opportunity to also perform experiments using the SPC algorithm presented in this chapter.

### 4.6.1 Experimental setup

The scale model, shown in Figure 4.7, is a modified Extractor wind turbine produced by Alternate Power Technologies Inc. The rotor diameter is 1.5 m and the rated power is approximately 300 W. The rotor speed is limited by a passive pitch mechanism which actively stalls the blades when a rotational speed of  $\pm 750$  RPM is approached. Since this pitch regulation mechanism results in slow limit cycle oscillations of the rotor speed when it

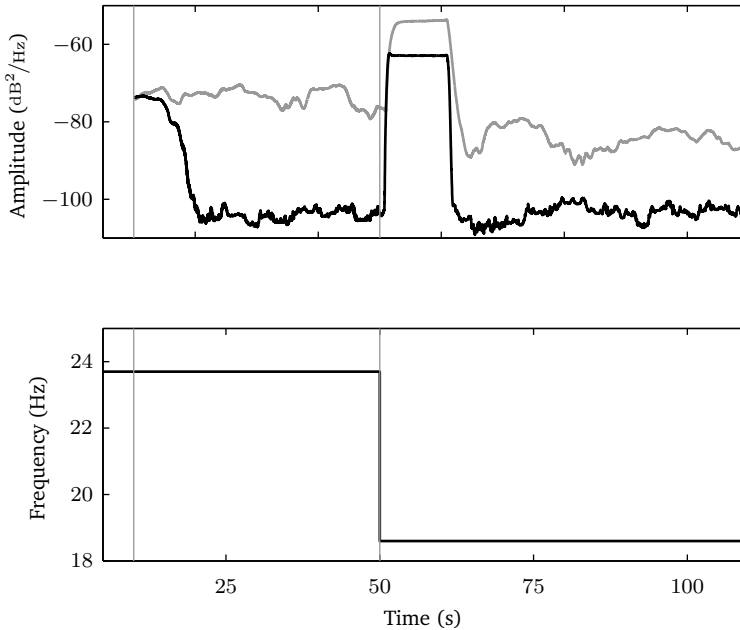


**Figure 4.5** – Plot showing the spectral amplitude (estimated) and frequency of the controlled mode.

This is the second bending mode of configuration (a) in Figure 4.4 and the first bending mode of configuration (b) in Figure 4.4, measured at sensor 1 ( $y_1$ ) as a function of time: (gray) open-loop, (black) closed-loop. The vertical lines indicate switching on of the controller ( $t = 10$  s) and the instant at which the beam is clamped ( $t = 50$  s).

is active, we have only considered operation in below-rated conditions to avoid interaction of the two control systems. Electrical power is generated by a three-phase permanent magnet alternator with a built-in rectifier to result in an (almost) direct current output. The electrical torque is regulated by means of a variable resistive load. The schematic of this load is shown in Figure 4.8. The load is varied by activating or deactivating one resistor in a series network of two resistors by means of pulse width modulation (PWM). Using the 20 kHz PWM signal the resistance can be varied (linearly as a function of the duty cycle) between  $4.8 \Omega$  (at 0% duty cycle) and  $0.1 \Omega$  (at 100% duty cycle). Hence, increasing the duty cycle implies a lower resistance, allowing a larger current  $I$  to flow through the generator, thereby increasing the generator torque and slowing down the rotor.

The experiments took place at the Open Jet Facility of the Faculty of Aerospace Engineering at Delft University of Technology. This wind tunnel has a large test section and a jet opening with a diameter of 3 m allowing fairly large rotating models to be tested. Figure 4.9 shows the measured steady-state rotor speed and electrical power for a range of wind speeds and duty cycles. Based on these results we have chosen a wind speed of  $7 \text{ m/s}$  and a rotor speed of 380 RPM as the central operating point for the experiments. At these conditions the corresponding duty cycle is near 50%, giving a good control range of  $\pm 50\%$  in both directions.

To be able to evaluate the feedforward control strategies a pitot-static tube was placed at the opening of the jet. The model was placed about 6 metres downwind. Theoretically, at a wind speed of  $7 \text{ m/s}$  and disregarding the effects of induction, this would give almost

<sup>4</sup>Photograph courtesy of Nick Verwaal.

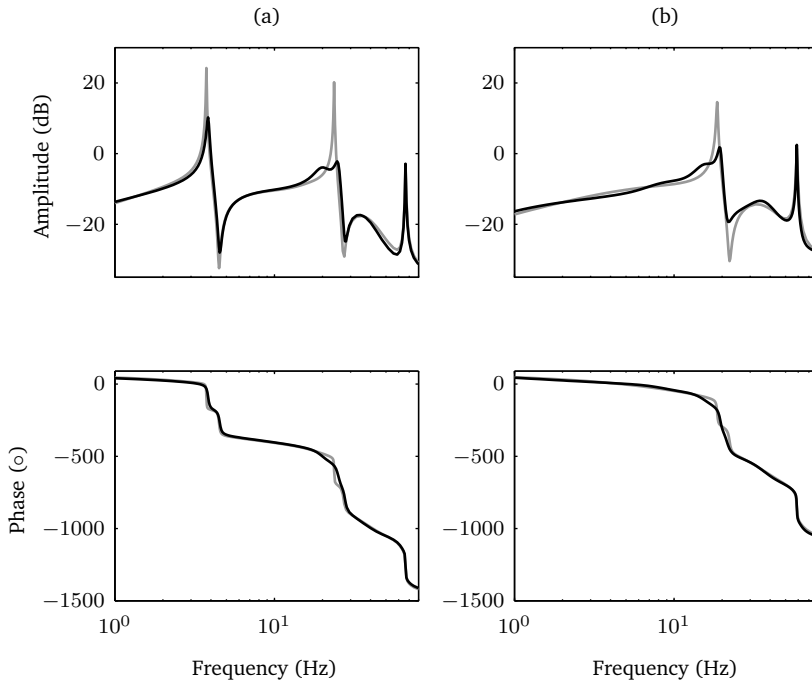


**Figure 4.6** – Identified frequency responses of the open-loop (gray) and closed-loop (black) system under SPC control from disturbance  $u_1$  to output  $y_1$  for the clamped configuration (a) and the clamped-pinned configuration (b).

1 second of look-ahead time. Although the wind speed measurement was taken inside the tunnel opening, before the flow had been able to expand and slow down to its actual velocity, the changes in dynamic pressure are still proportional to those in the test section.

All signals were sampled at 2 kHz and filtered with 1<sup>st</sup> order Butterworth low-pass filters with a cutoff frequency of 200 Hz. Since the wind speed measurement turned out to be very noisy, it was filtered with a cutoff frequency of 1 Hz. The PI and feedforward controllers were run at 2 kHz, whereas SPC was run at 20 Hz.

#### 4.6.2 Identification and controller design

To identify the dynamics of the turbine relevant to these experiments two measurements were performed. In the first, the turbine was run in the chosen operating point (7 m/s, 380 RPM) and the duty cycle was perturbed around its steady-state value using a pseudorandom binary signal of  $\pm 10\%$ . We have only focussed on the time constant related to the rotor inertia. The measured data was used to identify the dynamics from the duty cycle input to the rotor speed response. Using the MOESP method a first order model was identified.

In the second experiment, the same conditions were used but now the wind speed was changed. The measured data was used to identify the dynamics from the wind speed measured at the pitot tube to the rotor speed response. Using the MOESP method a first order model was identified.

The models have time constants of 7 seconds and 9 seconds, respectively, and have different DC gains. Based on the transfer function from duty cycle to rotor speed a PI controller was designed to regulate the rotor speed to its setpoint.

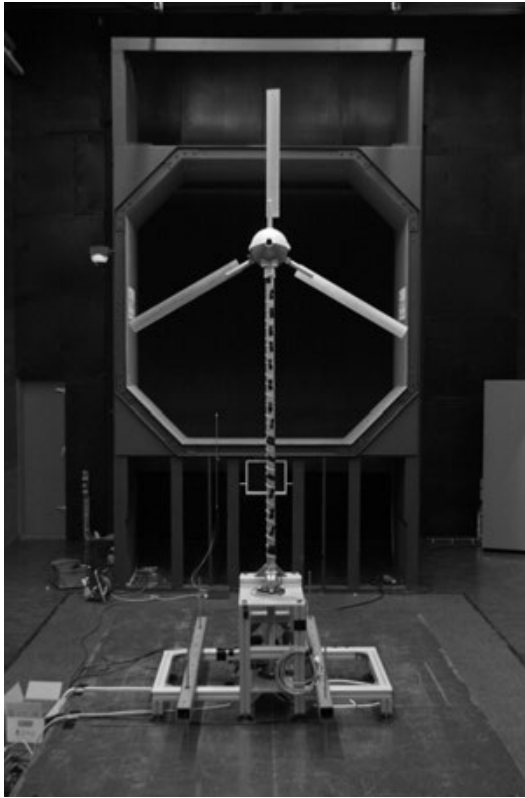


**Figure 4.7** – Photograph of the experimental wind turbine in the Open Jet Facility<sup>5</sup>. The pitot-static tube can be seen protruding into the tunnel mouth.

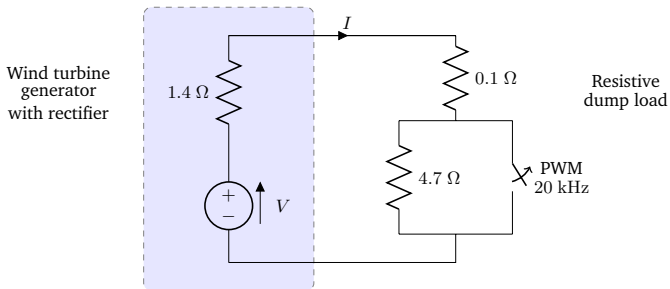


**Figure 4.8** – The variable dump load configuration attached to the wind turbine scale model. The duty cycle of the switch determines the effective resistance of the resistive load.

To avoid some of the complications arising from the fact that we are tracking a nonzero reference and hence adding an integral component to the model would be necessary, we have first subtracted the operating equilibrium from the input and output signals, so that the controller truly operates around the chosen operating point. For a more elegant and flexible solution the techniques discussed in Kadali, Huang and Rossiter (2003); Soliman, Malik and Westwick (2012) could be employed.

In each experiment, the first 40 seconds of the simulation were used to initialise the

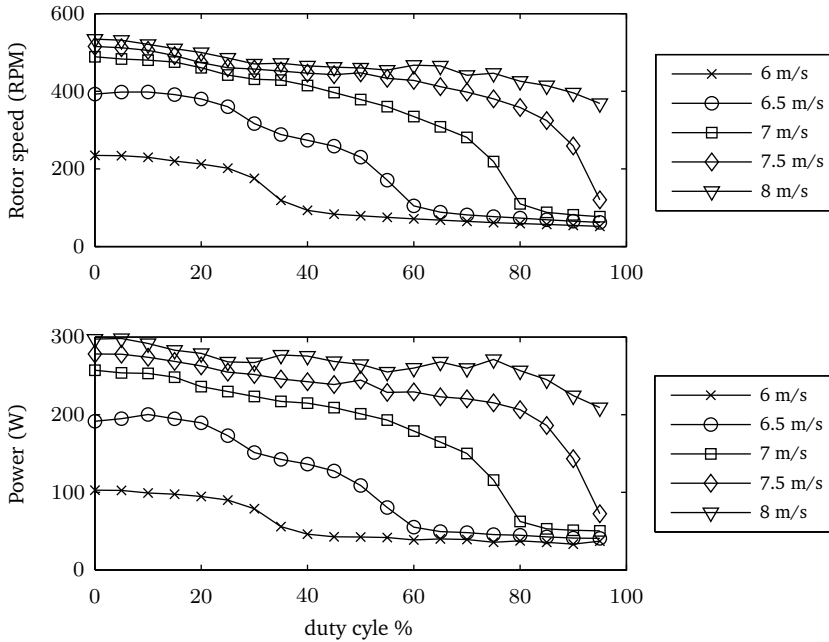


**Figure 4.9** – Steady-state rotor speed and electrical power for a range of wind speeds and duty cycles.

estimation of the system Markov parameters and during this time the PI controller was used to track the reference. Over a number of trials the SPC parameters were tuned. We started with a small weight on the tracking error, which was gradually increased to result in good tracking and disturbance rejection while satisfying the constraints. Ultimately, the following parameters were used: an ARX order of  $p = 50$ , a forgetting factor of  $\lambda = 1 - 2 \cdot 10^{-7}$ , a prediction horizon of  $N = 50$  and a control horizon of  $N_c = 20$ . Note that this forgetting factor is so close to one that there is effectively no forgetting. No weights were imposed on the control rate and the weight on the control input was kept equal to 1. A weight of  $Q_y = 8000$  was imposed on the reference tracking error.

### 4.6.3 Results

First, a repetitive sequence of setpoint changes was applied. In the first 40 seconds of the simulation the PI controller was used and during this time the system Markov parameters were estimated by the RLS algorithm. After these 40 seconds, control was handed over to the SPC controller. Figure 4.10 shows the results. It is interesting to see that the first set of setpoint changes is not tracked very well (e.g. at  $t = 60$  s), but in the second sequence (at 140 s) the changes are tracked much better.

Note also that the wind speed signal in Figure 4.10 is very noisy. This is not due to turbulence in the wind tunnel, but rather due to poor quality of the pressure transducer. It remains to be investigated whether this noise level negatively affects the feedforward performance of the SPC controller.

In the second experiment repetitive wind speed changes were created by controlling the wind tunnel. Again, the first 40 seconds were used to initialise the RLS algorithm after which control was handed over to SPC. Figure 4.11 shows the results. After the initial transient at the switching instant, the SPC controller immediately starts rejecting the wind speed disturbances. Furthermore, the control signal appears to become smoother as time

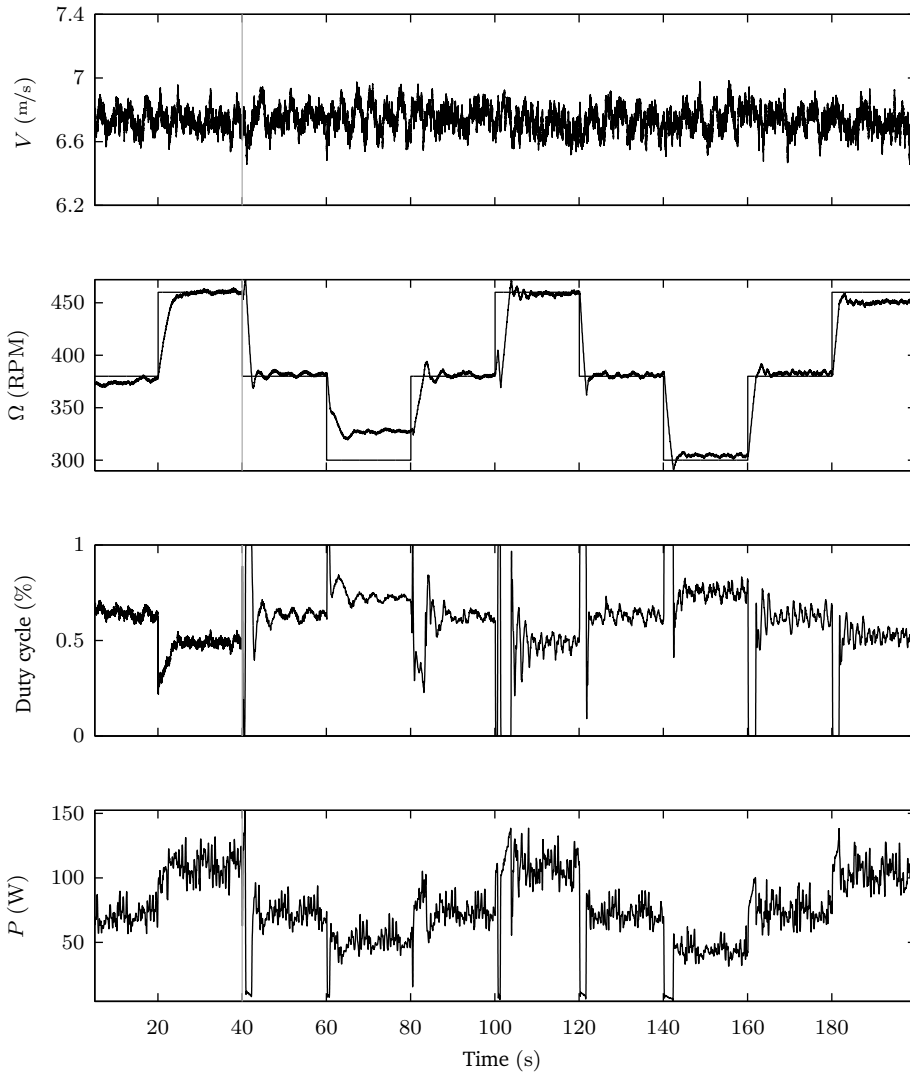


**Figure 4.10** – Result of applying SPC to track rotor speed setpoint variations indicated by the thin line in the rotor speed plot. At  $t = 40$  s, indicated by the vertical line, the control is handed over from the PI controller to the SPC controller.

progresses. It is important to mention that, compared to the first experiment, wind speed is taken as a measured input. The wind speed measurement was very noisy and this noise presents itself in the control signal.

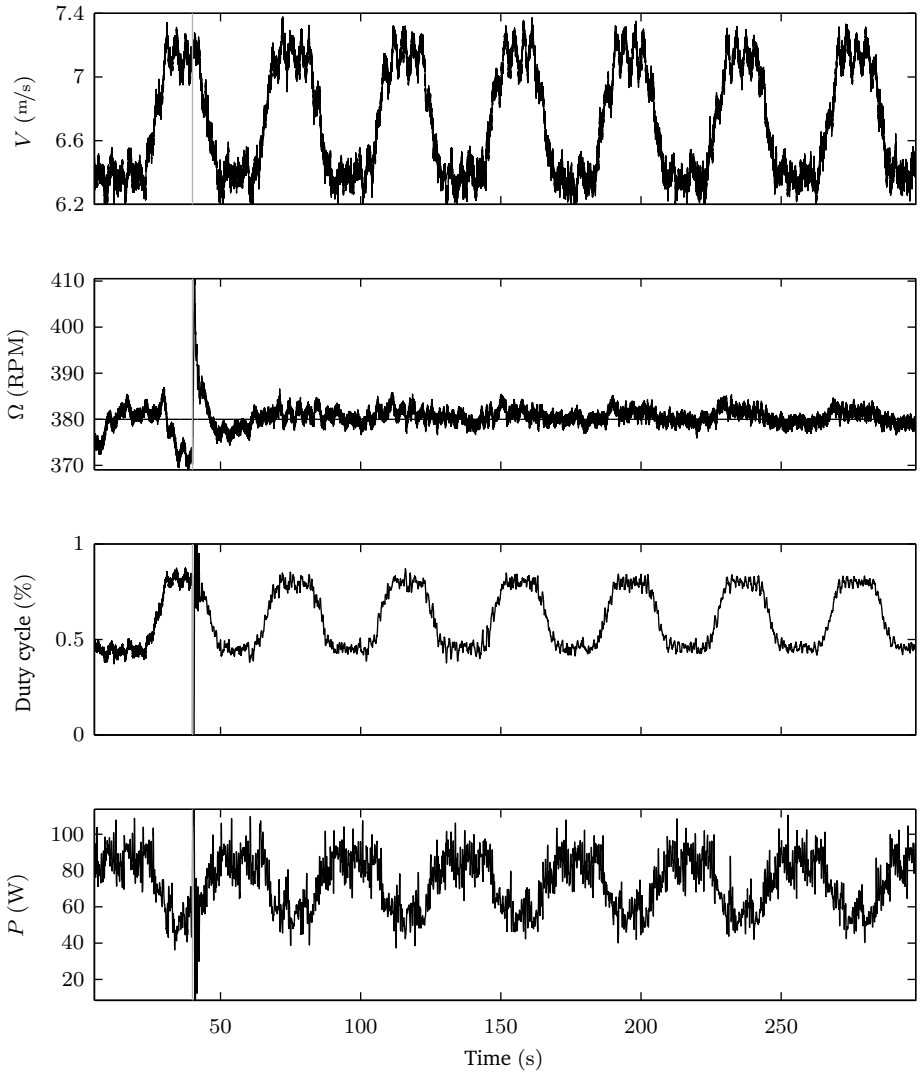


**Figure 4.11** – Result of applying SPC to maintain the rotor speed setpoint of 380 RPM. At  $t = 40$  s, indicated by the vertical line, the control is handed over from the PI controller to the SPC controller. After an initial transient, SPC successfully maintains the speed setpoint by rejecting the effects of wind speed variations.

## 4.7 Conclusions

In this chapter we have applied subspace predictive control to two illustrative examples. We have shown that subspace predictive control can be derived as a direct extension of the predictor-based identification framework in Chapter 2. In that sense it forms a

first step towards the fusion of identification and control into data-driven control. The ultimate goal of such an approach is that overall controller design and tuning becomes more straightforward by directly exploiting system information embedded in measured data.

We have demonstrated how subspace predictive control can be applied to vibration control problems in flexible structures and we have shown that damping can be achieved when the dynamics change considerably. We have also shown the application to reference tracking on an experimental wind turbine. Key advantages are the adaptation to changes in dynamics and the limited set of tuning parameters. Although the scheme may be computationally complex, it can easily be run on present-day processors by exploiting structure in the algorithm.

To maintain proper conditioning of the covariance matrix in a forgetting RLS scheme it is necessary that conventional persistence of excitation conditions are satisfied. This can be achieved by applying an appropriate reference perturbation that is as small as possible (to avoid loss of performance). Guaranteeing a sufficient level of excitation during operation is an active area of further research. In this chapter we have presented a directional forgetting RLS scheme which ensures that the covariance matrix remains bounded during periods of no excitation, or when the excitation does not cover the full parameter space.



# Closed-loop subspace identification of Hammerstein systems

Many nonlinear systems, including wind turbines, can be accurately described by linear time invariant models when operating close to a constant operating equilibrium. For control, however, it can be desirable to have a globally valid description as opposed to models in discrete operating points. Furthermore, in particular in the case of wind turbines, it is nearly impossible to maintain a constant operating point during the process of data acquisition for system identification. Instead of resorting to available black box nonlinear identification techniques, which are often hard to apply in practical contexts, we investigate in this chapter a new method for identifying simple nonlinear systems consisting of static nonlinearities in series with linear time invariant dynamics – so-called Hammerstein systems.

In this chapter we present a novel methodology to identify such systems from closed-loop data. The dynamic subsystem is identified using one of the closed-loop subspace methods presented in Chapter 2. The nonlinearity is described using a recently developed linear regression framework for multivariate simplex splines. We further propose a separable least-squares regression framework for recovery of the low-rank structure between the nonlinearity and the LTI system.

As a relevant example application we consider the identification of a wind turbine. We have previously shown that the elementary dynamics of wind turbines can be represented in the form of a multivariable closed-loop Hammerstein structure, where the nonlinear mappings consist of the torque and thrust coefficients. Similar structures, with nonlinearities in the form of aerodynamic coefficients (or lookup tables), are further found throughout the field of aerospace vehicle dynamics.

## 5.1 Introduction

One of the challenges mentioned in the introduction to this thesis is that wind turbines are nonlinear systems. In practical situations with continuously varying operating conditions this makes the potential for LTI system identification limited. In this chapter, we present an extension to the well-established LTI techniques that extends the model class to Hammerstein systems, i.e., systems consisting of a static nonlinearity in series with an LTI dynamic part, cf. Figure 5.1. Identification techniques for Hammerstein systems have a fairly long history (Narendra and Gallman, 1966; Chang and Luus, 1971; Verhaegen and Westwick, 1996; Bai, 1998; Goethals, Pelckmans, Suykens et al., 2005). Main classes of methods are nonparametric approaches (Vandersteen, Rolain and Schoukens, 1997), subspace approaches (Verhaegen and Westwick, 1996; Goethals, Pelckmans, Suykens et al., 2005) and parametric prediction-error approaches (Chang and Luus, 1971; Bai, 1998; Zhu, 2000; Falck, Suykens, Schoukens et al., 2010). The latter class is often restricted to SISO or SIMO systems. Furthermore, noise models are often not explicitly accounted for. More crucially, perhaps, the majority of the existing methods cannot deal with closed-loop data in a consistent manner.

The choice of a parameterisation for the nonlinear static function remains a challenging topic. Often, this parameterisation consists in choosing an expansion in terms of basis functions, requiring the tuning of the parameters of these functions, or imposes severe

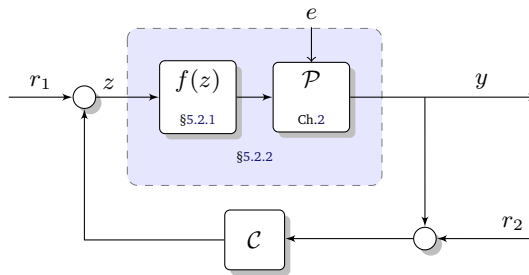


**Figure 5.1** – The closed-loop Hammerstein configuration with references to relevant paragraphs.

restrictions on the nonlinearity. A more recent class of methods introduces techniques from the machine learning community in the form of support vector machines. These methods may be used to model a wide class of nonlinearities, by mapping the nonlinear features to an infinite-dimensional feature space (Goethals, Pelckmans, Suykens et al., 2005; van Wingerden and Verhaegen, 2009a). Still, the choice of kernel functions is challenging and, furthermore, computational aspects limit the length of data sets used for identification. Hence, these techniques seem to have potential when little knowledge is available about the characteristics of the nonlinearity.

While the use of splines for modelling of functions is well-known and widespread (Lai and Schumaker, 2007), a recently developed linear regression framework (de Visser, Chu and Mulder, 2009) makes them particularly accessible to the engineering community. In this chapter we exploit this framework to model the static nonlinear function using a set of simplex splines. These simplex splines have attractive properties, e.g., they allow *a priori* specification of continuity conditions and form a partition of unity (Lai and Schumaker, 2007). In addition, the tuning of the spline basis is more intuitive and provides fewer degrees of freedom to the user than is the case for radial-basis-type functions. An important property of the identification scheme is that it allows the input signal to be correlated with the output signal, allowing for consistent closed-loop identification when the true system is within the given Hammerstein model class.

One application area of interest for Hammerstein models is the field of wind energy. In this chapter we will show, based on our previous work, that wind turbines admit a Hammerstein model structure (van der Veen, van Wingerden and Verhaegen, 2011, 2012), where the nonlinearities are introduced by the rotor torque and thrust which depend nonlinearly on the inputs. In this chapter we apply the presented identification technique to data obtained from a high-fidelity wind turbine simulation. It is important to note that, while a wind turbine also admits locally linear models for certain constant wind speeds, it is particularly hard in wind energy applications to maintain a reasonably constant wind speed throughout an identification experiment. In principle, the Hammerstein description of the turbine is globally valid, thereby removing the strict requirements on an experiment with regards to wind speed excursions.

The contributions of this chapter are threefold. First, we extend the closed-loop MOESP subspace identification scheme presented in Chapter 2 with a recent linear regression framework for multivariate splines (de Visser, Chu and Mulder, 2009), which results in a powerful method for closed-loop identification of multivariable systems with static input nonlinearities. First ideas for this approach and its application to wind turbine dynamics were presented in van der Veen, van Wingerden and Verhaegen (2011). Second, we introduce a separable least-squares (LS) regression framework to recover the low-rank structure which is lost in identification using the overparameterisation approach. Finally, we demonstrate the method on a high-fidelity model of a wind turbine under realistic turbulence conditions.

## 5.2 Identification of MIMO Hammerstein systems

In this section we describe a novel algorithm to identify multivariable Hammerstein systems. We consider the closed-loop configuration in Figure 5.1, where we will identify the part in the dashed rectangle, i.e., the nonlinearity and the linear dynamic subsystem. A controller  $\mathcal{C}$ , not necessarily linear, may be active. We assume that the feedback loop is well-posed. Note that if the signal  $f(z)$  entering the LTI subsystem  $\mathcal{P}$  is known, this subsystem can be identified using one of the closed-loop subspace identification techniques described in Chapter 2. Since in the cases to which we restrict our attention the intermediate signal  $f(z)$  is not known a few additional steps are necessary<sup>1</sup>. In Section 5.2.1, we describe a linear regression framework for the use of multivariate splines, which we will apply to describe the static nonlinear function. Then, in Section 5.2.2, we combine this spline framework with closed-loop subspace identification to obtain a single method for identification of the combined system.

### 5.2.1 Nonlinear static modelling using multivariate simplex splines

The static nonlinearity in the Hammerstein model will be approximated using a linear expansion in terms of basis functions. In this section we describe a recently introduced linear regression formulation of multivariate simplex splines (Lai and Schumaker, 2007; de Visser, Chu and Mulder, 2009). The power of simplex splines as opposed to the more common basis functions in this context (e.g., radial basis functions, sigmoid functions, thin-plate splines, hinge functions) lies in the fact that tuning of the basis is more directly related to *a priori* knowledge about the nonlinear function. First, one specifies a (data-based) triangulation on which the splines are defined. Subsequently, degrees of freedom for the user are the *spline order*, governing the degree of complexity that can be modelled and the *continuity order* of the spline function. This possibility to specify the continuity order is crucial when relying on well-behaved gradients or higher-order differentials of the function. The brief introduction presented here closely follows de Visser, Chu and Mulder (2009). The interested reader is referred to de Visser, Chu and Mulder (2009, 2011) for a detailed introduction.

#### Simplices and barycentric coordinates

Suppose a function  $f(x) : \mathbb{R}^n \rightarrow \mathbb{R}$  is to be approximated. In that case, the independent variables  $x$  form a subset of  $\mathbb{R}^n$ . The splines will be defined on a set of geometric elements, *simplices*, that together span this subset of  $\mathbb{R}^n$ . A simplex is defined as follows: given a set  $V_j$  of  $n + 1$  unique nondegenerate vertices  $V_j = \{v_1, \dots, v_{n+1}\} \in \mathbb{R}^n$ , the corresponding simplex  $t_j$  is defined as the convex hull of these points (i.e a line segment for  $n = 1$  and a triangle for  $n = 2$ , see Figure 5.2):

$$t_j \triangleq \text{Co}(V_j).$$

Each simplex has an associated local coordinate system in terms of its vertices, allowing every point  $x \in \mathbb{R}^n$  to be described as a linear combination of the vertices  $V_j$ . These so-called *barycentric coordinates*  $b(x) = (b_1, \dots, b_{n+1})^T$ , corresponding to  $x$ , are defined by:

$$x = \sum_{i=1}^{n+1} b_i v_i, \quad \sum_{i=1}^{n+1} b_i = 1.$$

Note that a point  $x$  is inside a simplex  $t_j$  if and only if its barycentric coordinates satisfy  $b_i \geq 0$ ,  $i = 1 \dots n + 1$ .

The subset of  $\mathbb{R}^n$  on which we wish the splines to be defined is partitioned into a union of simplices  $t_j$ ; the so-called triangulation (Figure 5.2). These simplices must

<sup>1</sup>Note that if the signal  $f(z)$  is known, we can treat the identification problem as two separate problems; one concerning estimation of the static nonlinearity and one concerning estimation of the LTI subsystem  $\mathcal{P}$ .

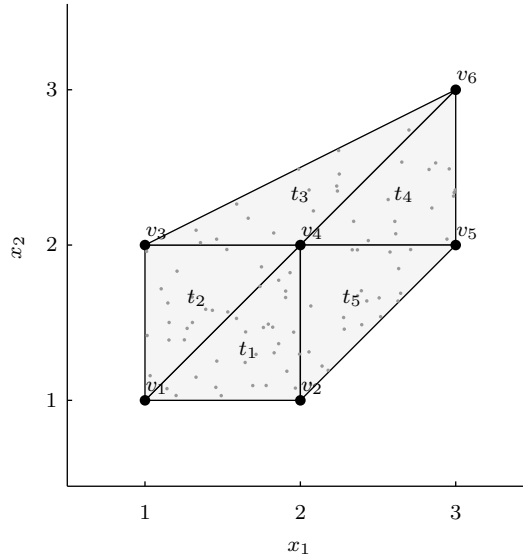


**Figure 5.2** – Example of a valid triangulation in  $\mathbb{R}^2$  based on 6 vertices and containing 5 simplices, where the vertices have been placed on the basis of scattered data points.

be non-overlapping (see de Visser, Chu and Mulder (2011) for further requirements on triangulations). The triangulation typically is such that it encloses all the  $n$ -variate data points available for regression.

The multivariate simplex spline in  $B$ -form

The simplex spline is typically expressed in the  $B$ -form, a terminology well-known in the literature on splines (de Boor, 1987). For our purposes it is sufficient to proceed directly to the expressions in terms of basis functions. We will define basis functions  $B_{\kappa}^d(b)$  evaluated in the point  $b \triangleq b(x)$ , where  $d$  denotes the degree of the spline function and the vector  $\kappa$  is a multi-index defined by:

$$\kappa = (\kappa_1, \dots, \kappa_{n+1})^T \in \mathbb{N}^{n+1},$$

subject to:

$$|\kappa| = \kappa_1 + \dots + \kappa_{n+1} = d. \quad (5.1)$$

The basis function  $B_{\kappa}^d(b)$  then admits the following rather simple representation:

$$B_{\kappa}^d(b) \triangleq \frac{d!}{\kappa!} b^{\kappa},$$

where it is important to note that the factorial operation on the multi-index  $\kappa$  is defined by:

$$\kappa! = \kappa_1! \kappa_2! \dots \kappa_{n+1}!,$$

and furthermore that  $b^{\kappa} \triangleq b_1^{\kappa_1} b_2^{\kappa_2} \dots b_{n+1}^{\kappa_{n+1}}$ . The elements of the multi-index are lexicographically sorted (Lai and Schumaker, 2007):

$$\kappa_{d,0,0,\dots,0} > \kappa_{d-1,1,0,\dots,0} > \kappa_{d-1,0,1,\dots,0} > \dots > \kappa_{0,\dots,0,1,d-1} > \kappa_{0,\dots,0,0,d},$$

which defines an ordering of all possible multi-indices under the constraint (5.1). In de Boor (1987) it was shown that a complete basis for the polynomials of degree  $d$  on a simplex is given by the set:

$$\{B_{\kappa}^d(b) \mid \kappa \in \mathbb{N}^{n+1}, |\kappa| = d\},$$

which is a set with cardinality  $\hat{d}$ . This follows from the fact that the constraint  $|\kappa| = d$  allows

$$\hat{d} = \frac{(d+n)!}{n!d!}$$

permutations that result in unique vectors  $\kappa$ . The basis functions allow any polynomial of degree  $d$  to be expressed in the convenient linear regression form:

$$p(b) = \sum_{|\kappa|=d} c_{\kappa} B_{\kappa}^d(b),$$

in which  $c_{\kappa}$  are called the  $B$ -coefficients. Gathering the basis functions on each simplex, the regression can be written in an equation of the form:

$$y_j = c^T \beta(x_j) + \epsilon_j,$$

where  $y_j$  is a scalar function value to be fitted,  $\beta(x_j)$  contains the basis functions evaluated in  $x_j$ ,  $c$  is the global coefficient vector and  $\epsilon_j$  is a Gaussian white noise element. Note that if a point  $x$  lies in simplex  $t_l$  (and thus not in any other simplex) only the basis functions corresponding to that simplex are non-zero (de Visser, Chu and Mulder, 2009), i.e., only the basis functions corresponding to simplex  $t_l$  are evaluated in  $\beta(x)$  leading to significant sparsity in the vectors  $\beta(x)$ .

Continuity between simplices

An important feature of splines is the intrinsic ability to constrain the solution to be  $C^r$ -continuous, where  $r$  is the desired continuity order. Splines are defined in a piecewise sense on individual simplices. Continuity conditions are prescribed for every edge shared by two neighbouring simplices. For invaluable insights regarding continuity constraints the interested reader is referred to de Visser, Chu and Mulder (2009); de Visser (2011); de Visser, Chu and Mulder (2011).

Here, it suffices to mention that the global set of constraints can be formulated as a single matrix equality constraint of the form  $Hc = 0$ , where  $H$  will be called the smoothness matrix.

The set of equations describing the global linear regression is then formulated as:

$$y_j = c^T \beta(x_j) + \epsilon_j, \quad j = 1, 2, \dots, N,$$

subject to:  $Hc = 0$ .

It is also possible to enforce *boundary* conditions in a similar manner to how continuity conditions are enforced (de Visser, Chu and Mulder, 2011). A very useful example would be to constrain the 2<sup>nd</sup> order directional derivatives at the global triangulation boundary to limit the typical divergence that polynomials exhibit outside the data domain.

A compact formulation

An important feature of the smoothness constraints is that the size of the polynomial basis can be reduced significantly *a priori*. The null space of  $H$  defines the space of all vectors  $c$  that satisfy the constraints. Thus, let  $\mathcal{N}_H = \ker(H)$  be a basis for the null space of  $H$ , then the global linear regression expression can be reformulated as:

$$y_j = \bar{c}^T \bar{\beta}(x_j) + \epsilon_j, \quad j = 1, 2, \dots, N, \quad (5.2)$$

with  $\bar{\beta}(x_j) \triangleq \mathcal{N}_H^T \beta(x_j)$ . If necessary, the original vector  $c$  can be retrieved from  $c = \mathcal{N}_H \bar{c}$ . The dimension of  $\bar{c}$  is always smaller than or equal to that of  $c$ , resulting in a smaller problem. This is of particular interest when we combine linear regression with LTI system identification in the next section.

## 5.2.2 Hammerstein identification

We consider an innovation Hammerstein model of the following form:

$$\mathcal{P} : \begin{cases} x_{k+1} = Ax_k + Bf(w_k) + Ke_k, \\ y_k = Cx_k + e_k. \end{cases} \quad (5.3a)$$

$$(5.3b)$$

The mapping  $f(w_k) : \mathbb{R}^q \rightarrow \mathbb{R}^m$  consists of  $m$  static nonlinear functions which need not be invertible. Based on the previous section we can express these nonlinearities as a set of  $m$  linear expansions:

$$f(w_k) = \begin{bmatrix} \bar{c}_1^T \bar{\beta}_1(w_k) \\ \vdots \\ \bar{c}_m^T \bar{\beta}_m(w_k) \end{bmatrix} \equiv \mathcal{C}\mathcal{B}(w_k) \in \mathbb{R}^m, \quad (5.4)$$

where  $\mathcal{C} = \text{diag}(\bar{c}_1^T, \dots, \bar{c}_m^T)$  contains the unknown but constant basis coefficients and  $\mathcal{B}(w_k)$  is the basis evaluated in  $w_k$ . Note that without loss of generality, linear inputs may be represented as elements in  $f(w_k)$  of the form  $f_i(w_k) = \bar{c}_i^T w_k$ .

We will use the well-known overparameterisation approach, first proposed by Chang and Luus (1971). This approach is popular due to its simplicity and intuitive appeal. If we define the low-rank matrix  $\check{B}$  according to:

$$\check{B} = \mathcal{B}\mathcal{C},$$

an equivalent system description is given by:

$$\mathcal{P} : \begin{cases} x_{k+1} = Ax_k + \check{B}\mathcal{B}(w_k) + Ke_k, \\ y_k = Cx_k + e_k. \end{cases} \quad (5.5a)$$

$$(5.5b)$$

The key result is that this system is an LTI system, where the  $m$ -dimensional unmeasurable input  $f(w_k)$  has been replaced by a higher-dimensional input  $\mathcal{B}(w_k)$ , which is fully determined by evaluating the basis functions at the measured points  $w_k$ . As a consequence of this, one of the closed-loop subspace identification schemes discussed in Chapter 2 can be applied without modification. The terminology ‘‘overparameterisation’’ stems from the fact that the full matrix  $\check{B}$  is estimated in the identification procedure, while it is actually a low-rank product  $\mathcal{B}\mathcal{C}$ . This implies a redundancy in the number of parameters. Finally, we note that since we estimate the product  $\check{B}$ , we can only retrieve the separate terms up to a nonsingular  $m$ -by- $m$  matrix.

## 5.3 Recovering the low-rank structure of the overparameterised model

In principle, one may directly use the overparameterised model as it correctly describes the system’s input-output behaviour. Furthermore, identifying the model up to this stage is a convex problem. In several cases, however, it may be desired to recover the low-rank structure, for instance to obtain a more compact description, or if there is a need to recover the signals between the nonlinearity and LTI system. In Goethals, Pelckmans, Suykens et al. (2005) this is referred to as projection onto the model class.

### 5.3.1 SVD truncation

Traditionally, one approach of recovering the low-rank structure of  $\check{B}$  has been to perform an SVD of this matrix and truncate it to the desired rank. It is immediately clear that under model mismatch and using noisy and finite data sequences it cannot be expected that  $\check{B}$  is of low rank and a truncated SVD decomposition will result in a loss of model fidelity, in the sense that since  $\check{B}$  minimises the least-squares criterion (2.27) any approximation of this matrix will increase the least-squares objective function. Ideally, one would solve the least-squares problem (2.27) subject to a rank-constraint on  $\check{B}_{\text{nl}}$ . Since such formulations are NP-hard to solve (Fazel, Hindi and Boyd, 2004), recent efforts in convex optimisation have been directed towards efficient methods to solve a convex relaxation of the rank constraint (Liu and Vandenberghe, 2009). This relaxation comes in the form of the nuclear norm  $\|\cdot\|_*$ , which equals the sum of the singular values of a matrix:

$$\|A\|_* = \sum_{i=1}^{\min(m,n)} \sigma_i(A).$$

By adding a penalty term of the form:

$$\lambda \|\check{B}\|_*$$

to the LS criterion (2.27) a “low rank” solution can be favoured over a least-squares optimum by properly selecting  $\lambda$ . By incorporating a heuristic for a low-rank solution in the least-squares problem, we can reduce the loss of model quality due to SVD truncation (Falck, Suykens, Schoukens et al., 2010). Tuning  $\lambda$  is an iterative process in which the least-squares error is increased in favor of a smaller nuclear norm until a desired trade-off is reached. It should be noted that some loss of model quality is inevitable, since the nuclear norm penalised regression will not achieve a truly rank-constrained solution. Further we note that in practice we have observed that it is typically difficult to achieve a solution with a numerical rank that approaches the desired rank if that desired rank is larger than 1 (Gebraad, van Wingerden, van der Veen et al., 2011).

### 5.3.2 Separable least-squares regression

Some improvement may be achievable over the solution obtained in the previous section by performing a nonlinear optimisation. Referring to the least-squares (LS) problem governing the estimation of  $B$ ,  $D$  and  $K$  (equation 2.27 in Section 2.3.4), we seek a  $\check{B}$ -matrix that is of rank  $m$ . In this section we describe how this LS problem can be modified to incorporate a rank constraint. In that case, the least-squares formulation becomes:

$$\min_{x_0, \check{B}, K} \left\| Y - \Phi \begin{bmatrix} x_0 \\ \text{vec}(\check{B}) \\ \text{vec}(K) \end{bmatrix} \right\|_2^2, \quad (5.6)$$

where  $\Phi$  depends on the already estimated matrices  $A$  and  $C$ , input and innovation data and  $Y$  contains output samples. For simplicity, but without loss of generality, we do not consider the estimation of  $D$ . The rank- $m$  matrix  $\check{B}$  can be parameterised as:

$$\check{B} = U(\vartheta)V, \quad (5.7)$$

where  $U(\vartheta) \in \mathbb{R}^{n \times m}$  and  $V \in \mathbb{R}^{m \times n_u}$  is fully parameterised. Although we could parameterise  $U(\vartheta)$  in terms of all its elements, without loss of generality we choose to parameterise it as an orthogonal matrix. The further derivations do not depend on the choice of parameterisation, thus we refer to appendix A for details on this parameterisation. Inserting the parameterisation (5.7) into the LS formulation (5.6) and exploiting the property of the Kronecker product  $\text{vec}(XYZ) = (Z^T \otimes X) \text{vec}(Y)$  (Brewer, 1978), we

obtain:

$$\min_{\Theta, \vartheta} \left\| Y - \Phi \underbrace{\begin{bmatrix} I_n & & \\ & I_{n_u} \otimes U(\vartheta) & \\ & & I_{n n_y} \end{bmatrix}}_{\Psi(\vartheta)} \underbrace{\begin{bmatrix} x_0 \\ \text{vec}(V) \\ \text{vec}(K) \end{bmatrix}}_{\Theta} \right\|_2^2 = \min_{\Theta, \vartheta} \|Y - \Psi(\vartheta)\Theta\|_2^2. \quad (5.8)$$

This LS problem is nonlinear, since the data matrix depends on  $\vartheta$ , but it has the form of a separable LS problem (Golub and Pereyra, 1973). Following the solution strategy of the separable LS problem (Golub and Pereyra, 1973; Ruhe and Wedin, 1980), we can solve this LS problem if we momentarily assume  $\vartheta$  fixed, in which case (5.8) becomes a standard linear LS problem. For brevity we shall denote the solution to this least-squares problem in terms of the left-inverse of  $\Psi(\vartheta)$ :

$$\hat{\Theta} = \Psi(\vartheta)^+ Y,$$

where  $\Psi(\vartheta)^+ \triangleq (\Psi(\vartheta)^T \Psi(\vartheta))^{-1} \Psi(\vartheta)^T$ . Substituting this solution into the LS problem (5.8) we obtain:

$$\min_{\vartheta} \left\| \underbrace{(I - \Psi(\vartheta)\Psi(\vartheta)^+)}_{\Pi_{\Psi}^{\perp}(\vartheta)} Y \right\|_2^2 = \min_{\vartheta} \left\| \Pi_{\Psi}^{\perp}(\vartheta) Y \right\|_2^2. \quad (5.9)$$

Since the matrix  $\Pi_{\Psi}^{\perp}(\vartheta)$  is an orthogonal projection matrix that depends on  $\vartheta$ , the particular LS residual encountered here is often referred to as the variable projection functional  $f(\vartheta)$ :

$$f(\vartheta) = \Pi_{\Psi}^{\perp}(\vartheta) Y.$$

The LS problem can be solved using any gradient-based optimisation algorithm. Note that the dimension of the nonlinear optimisation is only determined by the size of  $\vartheta$ ; the other parameters (i.e.,  $\Theta$  in (5.8)) have been eliminated from the problem by rewriting it in this form – this reduction in the number of parameters is the key advantage of separable LS regression. We proceed by evaluating the Jacobian of the objective in (5.9) for a Gauss-Newton solution. First, we perform a rank-revealing QR factorisation of the matrix  $\Psi(\vartheta)$ :

$$\Psi(\vartheta)\Pi = [Q_1 \quad Q_2] \begin{bmatrix} R_{11} & R_{12} \\ 0 & 0 \end{bmatrix},$$

where  $\Pi$  is a permutation matrix. Using this decomposition, the functional can be rewritten as:

$$f(\vartheta) = \Pi_{\Psi}^{\perp}(\vartheta) Y = Q_2 Q_2^T Y.$$

The Jacobian of the residual is obtained by taking the partial derivative with respect to each of the parameters  $\vartheta_j$ :

$$\begin{aligned} \frac{\partial f(\vartheta)}{\partial \vartheta_j} &= - (I - \Psi(\vartheta)\Psi^+(\vartheta)) \frac{\partial \Psi(\vartheta)}{\partial \vartheta_j} \Psi^+(\vartheta) Y \\ &\quad - (\Psi^+(\vartheta))^T \frac{\partial \Psi^T(\vartheta)}{\partial \vartheta_j} (I - \Psi(\vartheta)\Psi^+(\vartheta)) Y. \end{aligned}$$

In view of the computational complexity involved in calculating the second term and the fact that it is usually small in comparison to the first term the second term is usually dropped (this modification is due to Kaufman (1975)). Evaluation of the first term can proceed efficiently using the same  $QR$  decomposition obtained earlier. We first compute:

$$\Psi^+(\vartheta) Y = \Pi^T \begin{bmatrix} R_{11}^{-1} Q_1^T Y \\ 0 \end{bmatrix}_{\bar{m}-r}.$$

Here,  $r$  denotes the numerical rank of  $\Psi(\vartheta)$  and  $\bar{m}$  is the column dimension of  $\Psi(\vartheta)^2$ . Then the evaluation of the partial derivative results in:

$$\frac{\partial f(\vartheta)}{\partial \vartheta_j} = -Q_2 Q_2^T \frac{\partial \Psi(\vartheta)}{\partial \vartheta_j} \Pi \begin{bmatrix} R_{11}^{-1} Q_1^T Y \\ 0 \end{bmatrix}.$$

The partial derivative  $\frac{\partial \Psi(\vartheta)}{\partial \vartheta_j}$  is straightforward to calculate from its definition in (5.6). The complete Jacobian is built up as follows:

$$J(\vartheta) = \begin{bmatrix} \frac{\partial f(\vartheta)}{\partial \vartheta_1} & \frac{\partial f(\vartheta)}{\partial \vartheta_2} & \dots & \frac{\partial f(\vartheta)}{\partial \vartheta_{n_\vartheta}} \end{bmatrix}.$$

Finally, we solve the optimisation problem using the `lsqnonlin` solver in MATLAB and supplying it the Jacobian as derived above. We can use the linear LS solution (2.27) with a truncated SVD of the estimated  $\check{B}$ -matrix as an initial condition for the solver. For reasons of computational efficiency the algorithm above was implemented by calling LAPACK routines (Anderson, Bai, Bischof et al., 1999), in which the (possibly large) square matrix  $Q$  is stored in terms of its Householder reflectors and not explicitly.

### 5.3.3 Obtaining local linear models

Besides the ability to describe nonlinear systems that possess a Hammerstein structure, an additional advantage of the identification scheme presented here is that local linear models can be obtained even when the operating conditions do not allow the system to operate steadily in a single operating point. This is typically a requirement when obtaining a dataset for LTI model identification.

Based on description (5.5) we can obtain a linearised model defined around an operating equilibrium given by  $(x_k, y_k, w_k) = (x_{ss}, y_{ss}, w_{ss})$ . If we define the substitutions  $x_k \leftarrow x_k - x_{ss}$ ,  $y_k \leftarrow y_k - y_{ss}$  and  $w_k \leftarrow w_k - w_{ss}$ , the linearised system can be shown to be:

$$x_{k+1} = Ax_k + \check{B} \left. \frac{\partial \mathcal{B}(w)}{\partial w} \right|_{w=w_{ss}} w_k + Ke_k.$$

The matrix  $\frac{\partial \mathcal{B}(w)}{\partial w}$  containing partial derivatives of the polynomial basis functions (5.4) can be evaluated analytically (de Visser, Chu and Mulder, 2011).

## 5.4 Examples

In this section we demonstrate the algorithm on two examples. The first is a theoretical example chosen to show the potential of the algorithm to estimate 2D nonlinearities. In the second example we apply the method to data obtained from a detailed wind turbine simulation. This example exploits the capability to estimate MIMO systems with multiple input nonlinearities.

### 5.4.1 A theoretical example

To verify the method and the fixed-rank regression approach, we simulate the following discrete-time ( $\Delta t = 0.1$  s) system with two resonances:

$$\begin{aligned} y_k &= G(z)u_k + H(z)e_k, \\ u_k &= f(z_k), \end{aligned}$$

---

<sup>2</sup>Note that strictly-speaking the equality only holds if  $\Psi(\vartheta)$  is full-rank. Otherwise, the right-hand-side will give a basic solution to (5.6) (Golub and Van Loan, 1996).

**Table 5.1** – Mean and standard deviations of VAF on validation data for three methods on the basis of 100 experiments.

	Overparameterised	Truncated SVD	Fixed-rank regression
mean VAF (%)	60	20	82
std.dev. VAF (%)	12	20	6.8

where  $G(z)$  and  $H(z)$  are given by:

$$G(z) = \frac{0.2571z^3 - 0.2034z^2 - 0.1975z + 0.2474}{z^4 - 3.421z^3 + 4.838z^2 - 3.297z + 0.932},$$

$$H(z) = \frac{0.3454z + 0.2846}{z^2 - 0.9381z + 0.5681}.$$

We further have that:

$$e_k \sim \mathcal{N}(0, 0.5),$$

$$z_k \sim \mathcal{U}\left(\begin{bmatrix} 0 \\ 0 \end{bmatrix}, \begin{bmatrix} 1 \\ 1 \end{bmatrix}\right),$$

i.e.,  $e_k$  is Gaussian zero-mean white noise with standard deviation 0.5 and  $z_k$  is uniformly distributed on the unit interval. The input nonlinearity  $f(z_k)$  is Franke's test function (Franke, 1979) (Figure 5.3, (a)), a weighted sum of four exponentials:

$$u_k = \frac{3}{4}e^{-\frac{(9z_k(1)-2)^2 + (9z_k(2)-2)^2}{4}} + \frac{3}{4}e^{-\frac{(9z_k(1)+1)^2}{49} - \frac{(9z_k(2)-2)^2}{10}}$$

$$+ \frac{1}{2}e^{-\frac{(9z_k(1)-7)^2 + (9z_k(2)-3)^2}{4}} + \frac{1}{5}e^{-(9z_k(1)-4)^2 - (9z_k(2)-7)^2}$$

The system is simulated for  $N = 2000$  samples and this simulation is repeated 100 times with independent realisations of the input and noise sequences. The typical signal-to-noise ratio is approximately 8 dB. After each simulation, we identify the 6th order system and simulate it with a fresh dataset. The triangulation consists of two simplices spanning the  $z$ -plane as shown in Figure 5.3. The splines are 6th degree splines with  $C^1$ -continuity. This results in a basis with 42 functions. The gradient-search for fixed-rank regression typically converged within 5 iterations. We estimate the model quality on the basis of the variance-accounted-for (cf. (2.38) on page 36). Three cases are compared: the first is the overparameterised model (5.5), the second is the truncated SVD solution (§5.3.1), the third is the solution obtained after fixed-rank regression (§5.3.2). The results are summarised in Table 5.1. From the results in this table we see that under noisy conditions the truncated SVD solution typically results in a loss of model quality. Performing a fixed-rank regression however, the quality can be improved, even with respect to the overparameterised solution. In addition, the fixed-rank solution displays less variability between experiments.

Figure 5.3 shows the estimated nonlinear functions. The nonlinearity can only be recovered if we estimate the rank-one representation. Hence, for the overparameterised model representation we cannot estimate the nonlinearity and we only show it for the truncated SVD and fixed-rank solutions. The example shows that the nonlinearity is more reliably estimated with fixed-rank regression in this particular example.

## 5.4.2 Global identification of a wind turbine

In this section we apply the method described in the previous sections to data obtained from a detailed wind turbine simulation. This application exploits the capability to estimate MIMO systems with multiple input nonlinearities.

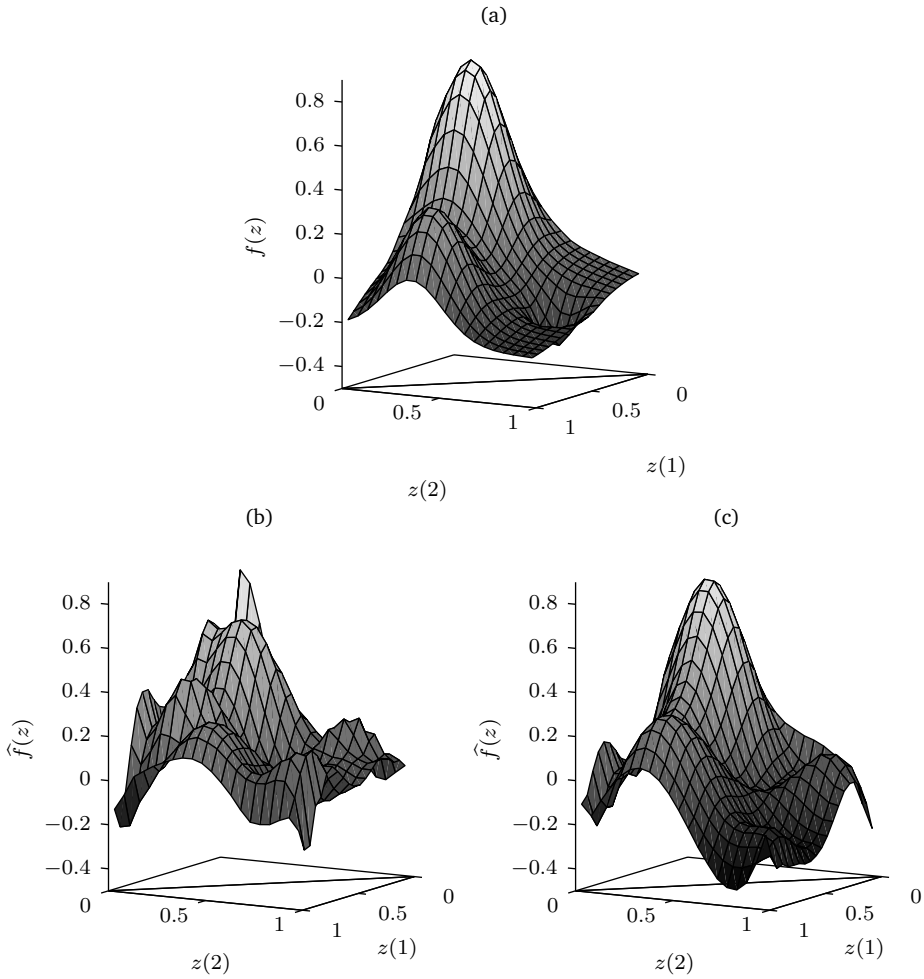


**Figure 5.3** – Franke’s test function  $f(z)$  (a), the function recovered and scaled from the truncated SVD solution (b), the function recovered and scaled from the fixed-rank regression solution (c).

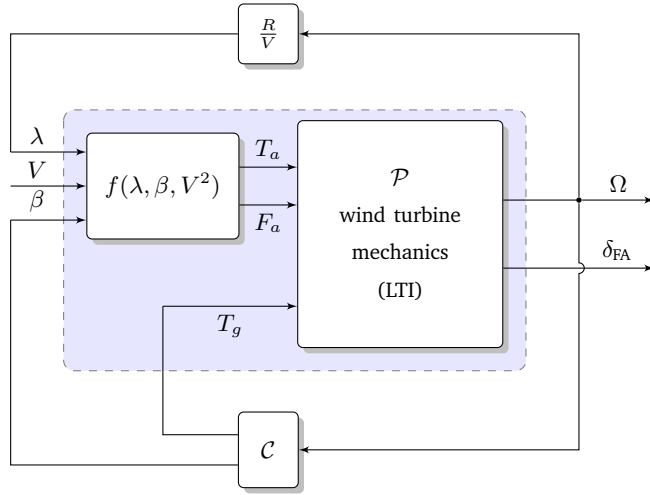


**Figure 5.4** – The closed-loop Hammerstein configuration found in wind turbine dynamics. The dashed part constitutes the Hammerstein representation of the turbine.

As pointed out in the introduction, wind turbines operate in a wind field where the mean wind speed may change significantly over time. This, in turn causes the operating point to vary continuously, in particular in above-rated conditions as the blades pitch further into the wind. The advantage of the present method is that it does not rely on measurement data which is restricted to an operating point and minor deviations from it, which, in addition implies that longer data sequences can be employed.

It was recently shown in van der Veen, van Wingerden and Verhaegen (2011) that the core dynamics of a wind turbine can be approximated by a Hammerstein model structure. In this structure, depicted in Figure 5.4, the static nonlinear mapping  $f(\lambda, \beta, V^2)$  determines the aerodynamic torque  $T_a$  and thrust  $F_a$  according to (Bianchi, De Battista and Mantz, 2007):

$$T_a = \frac{1}{2} \rho \pi R^3 C_Q(\lambda, \beta) V^2 \quad (5.10a)$$

$$F_a = \frac{1}{2} \rho \pi R^2 C_T(\lambda, \beta) V^2, \quad (5.10b)$$

where  $C_Q(\lambda, \beta)$  is the *torque coefficient* and  $C_T(\lambda, \beta)$  is the *thrust coefficient*.  $\beta$  is the blade pitch angle,  $\lambda = \Omega R/V$  is the tip speed ratio,  $V$  the wind speed,  $R$  the rotor radius and  $\rho$  the air density. Usually, the tip speed ratio  $\lambda$  is fairly tightly controlled (which is a consequence of regulating power production to an optimal or maximal value), so that we can assume  $\lambda = \lambda(\beta)$ , causing the coefficients to depend merely on  $\beta$ . Typical coefficients encountered during operation are shown in Figure 5.5.

*Remark 5.1.* Theoretically, it would also be possible to directly identify the full 3D surfaces  $C_Q$  and  $C_T$ , but since this introduces many additional degrees of freedom the resulting estimate was very unreliable on data obtained under turbulent conditions. Also, it is generally difficult or too intrusive on a real turbine to explore a wide range of tip speed ratios  $\lambda$  for each setting of the pitch angle  $\beta$ . This would be necessary to obtain data which uniformly covers a significant portion of the  $(\lambda, \beta)$ -plane.

The torque relation (5.10a) governs the aerodynamic torque entering the low-speed shaft of the turbine. At the end of the high-speed shaft, the generator torque  $T_g$  is active. The torque balance, further influenced by the drive train dynamics and rotatory inertias of the rotor and generator, will determine the rotor speed  $\Omega$ . The thrust relation (5.10b) governs the force exerted at the tower top and thus the fore-aft tower displacement  $\delta_{FA}$ .

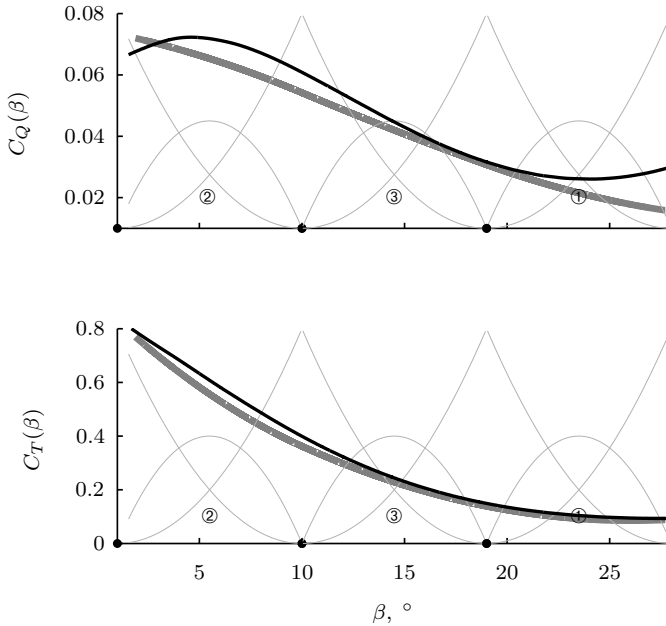


**Figure 5.5** – Coefficients for a typical pitch and speed regulated turbine; true (black) and estimated (gray) curves. The figure also shows the simplices ( $\beta$ -axis partitions) 1 to 3 and the 3 scaled spline basis functions defined on each simplex.

We tested the identification procedure on an aeroelastic simulation of the NREL Controls Advanced Research Turbine (CART 3) in the Bladed (*Bladed 2011*) environment. First, simulations were performed at a set of constant wind speeds to identify linear models for comparison. These linear models were verified against numerical linearisations and found to correspond well. Next, a realistic 2000 s simulation was performed under full 3D turbulence conditions (IEC Class II, mean wind speed  $17 \text{ m/s}$ , with turbulence intensity of 16%) causing the mean wind speed to vary between 9 and  $25 \text{ m/s}$  with a significant amount of stochastic excitation (Figure 5.6). The pitch reference signal was perturbed with a  $\pm 1^\circ$  random binary signal and the generator torque reference with a similar signal of  $\pm 100 \text{ Nm}$ . Data was captured at 12.5 Hz while operating under closed-loop control. Based on the SVD order indication obtained from the subspace method, a 24th order model was identified.

Examination of the governing turbine loads showed that during an identification experiment the fore-aft tower force, the side-side tower force and the blade flap-wise bending moments increase by 82%, 56% and 8%, respectively in terms of their RMS values. Since an identification experiment is only rarely performed and spans an infinitesimal fraction of its service life, we have not considered the impact of these increased loads on the fatigue life of the turbine. Furthermore, these load increases can be reduced significantly by filtering the perturbations to reduce frequency content near lightly damped turbine structural modes.

Figure 5.5 shows the true and the estimated nonlinearities, which we could recover in this case since we had access to the internal signals. The general trend of the nonlinearities is captured well. Figure 5.7(a) shows the linearised Hammerstein model. The figure shows that the Hammerstein model fairly accurately describes the varying gain of the system in the low-frequency region (0.2 – 2.0 Hz). Results at lower frequencies are inaccurate due to the presence of a controller with integral action which eliminates any low-frequency and steady-state speed errors. Furthermore, we observe some inaccuracy in the amplitudes of

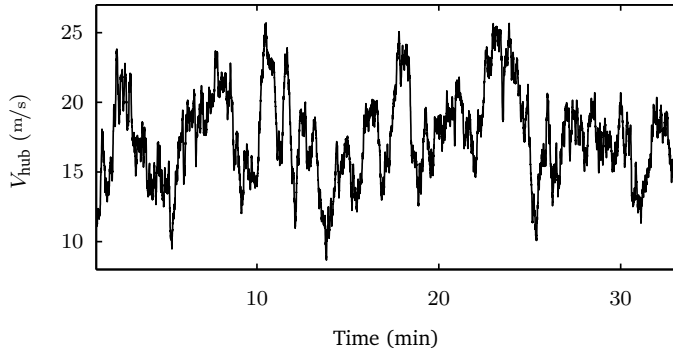


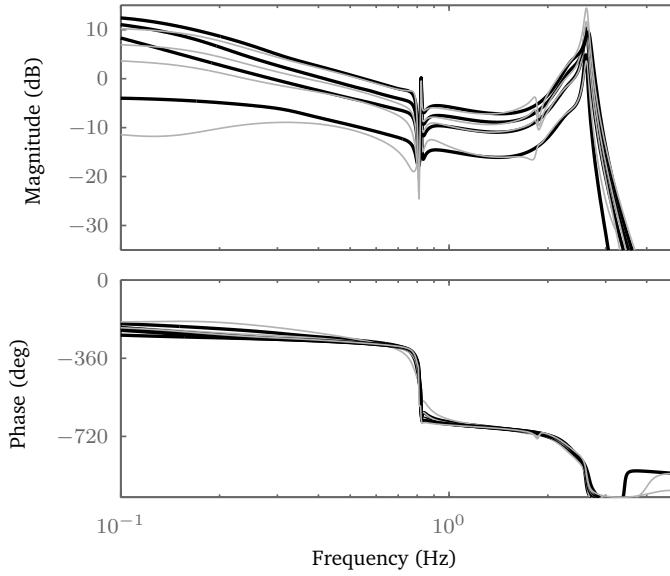
Figure 5.6 – Wind speed experienced by the turbine at hub height.

the resonant peaks. A limitation of a Hammerstein model is that local models can only vary between operating points by a matrix-valued gain, which results here in a trade-off between modelling of the magnitudes in the low frequency regime and at the resonant peak.

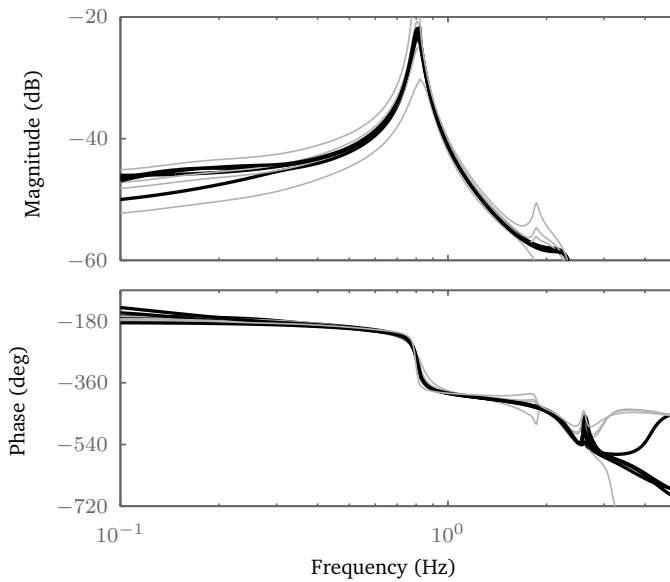
Figure 5.7(a) also shows that the models may vary in gain by as much as 15 dB and confirm the requirement for gain-scheduled control (Bossanyi, 2000). Clearly, an LTI model identified from this dataset would result in an “average” LTI model which does not convey this effect.

## 5.5 Discussion

In this chapter we have presented a framework for the identification of MIMO Hammerstein systems. We have used a recent framework for linear regression using multivariate splines, which allow for *a priori* specification of continuity conditions. We also introduced a method to recover the low-rank structure lost in the overparameterisation step by applying separable least-squares regression. The method has been demonstrated on both a theoretical example with a 2D nonlinearity and a realistic multivariable simulation of a wind turbine with two input nonlinearities. In both cases the approach was reasonably successful in identifying the underlying system. A challenge remains dealing with the number of basis functions, which rapidly grows for higher dimensions, higher spline orders and finer triangulations required to describe complicated nonlinear functions.



(a) pitch to generator speed



(b) pitch to tower fore-aft displacement

**Figure 5.7** – Linearised Bladed model (black) compared with linearised identified Hammerstein model (gray) for a range of wind speeds;  $V = \{12, 16, 20, 24\}$  m/s.



# Nonlinear data-driven modelling of wind turbines

In the previous chapter we developed a method to estimate both the static nonlinearity and the LTI subsystem in Hammerstein systems. This chapter presents a practical approach to identify a global model of a wind turbine from operational data, while it operates in a turbulent wind field with a varying mean wind speed and under closed-loop control. The approach is based on the realisation that the nonlinearities are dominated by the aerodynamics of the rotor which change with the operating condition. The dynamics of a wind turbine can be decomposed into a nonlinear static part, governed by the torque and thrust characteristics of the rotor, and a linear time invariant dynamic part. While the previous chapter assumed very little about the nonlinearity, it turns out that in the practice of identifying wind turbines it is necessary to assume that these nonlinearities are known. As will be shown in this chapter this poses no major limitations to properly estimating the dynamic behaviour and the practical applicability of the algorithm is demonstrated by applying it to experimental data obtained from the 600 kW NREL CART 3 research turbine.

## 6.1 Introduction

As was described in the introduction to this thesis in Section 1.3, most control design approaches require detailed models of a wind turbine. Even if that were not the case, models are crucial to understand the dynamic behaviour of the system. This fact is reflected by the current interest in operational modal analysis of wind turbines (Osgood, Bir, Mutha et al., 2011; Özbek and Rixen, 2012). In this chapter we present a solution to obtain such models for control design. Referring to the challenges we set out to solve in the introduction chapter (see Section 1.4), we present a solution to obtain models of wind turbines in a one-step procedure, i.e., on the basis of a single batch of input-output data, while the turbine is operating under closed-loop control in a three-dimensional time-varying wind field. Furthermore, this proposed method takes into account the nonlinearity of the wind turbine aerodynamics.

Considering the dynamics of wind turbines, reasonably accurate predictions can be made on the basis of first-principles aeroservoelastic modelling and such models are obviously the only ones available in the design stage of a turbine. Nevertheless, many factors contribute to uncertainty or errors in the prediction of dynamic modes and time constants. Among those are: differences between expected and actual material properties; differences in manufacturing; differences in local soil or foundation characteristics; modelling assumptions and simplifications and unmodelled sensor characteristics. System identification may aid in understanding the true underlying dynamics and as such may allow improvements to the design of controllers for power production and load reduction. In the control engineering community, system identification has proved to be a powerful tool for the analysis of dynamic systems. The capability to derive models from operational data allows engineers to gain insight into the dynamics of systems which have been modelled with certain coarse or restrictive assumptions or systems of which only simplified models are available. An additional motivation for system identification is that it automatically delivers a model that describes the phenomena which manifest themselves in



**Figure 6.1** – The CART 3 wind turbine at the National Wind Technology Center, Golden, CO, USA.

the data. In physical first-principles modelling, the model complexity is primarily a choice made by the user, who may opt for over-modelling to ensure that any possibly relevant dynamics are incorporated.

Often, well-established identification techniques for linear time invariant (LTI) dynamics are applied in practice. This is justified by the fact that many systems, among which wind turbines, permit a locally linear description of their dynamics around some constant operating point (Ljung, 1999; Verhaegen and Verdult, 2007). This justification is also valid for wind turbines and indeed first results on LTI identification of wind turbines were seen in the early 1990s and since then, several scientific articles have appeared on this topic (van Baars, Mosterd and Bongers, 1993; James III, Carne and Lauffer, 1993; van Baars and Bongers, 1994; Knudsen, Andersen and Toffner-Clausen, 1997; Marrant and van Holten, 2004; Hansen, Thomsen, Fuglsang et al., 2006; Iribas-Latour and Landau, 2009; Houtzager, Kulcsár, van Wingerden et al., 2010; van der Veen, van Wingerden and Verhaegen, 2010c; Iribas-Latour and Landau, 2012).

Almost all variable pitch wind turbines are controlled using gain-scheduled pitch control, due to the significantly varying gains at different wind speeds (Bossanyi, 2000), emphasizing the fact that wind turbines are nonlinear systems and the nonlinearity must be accounted for in the control design. One approach could be to identify models at several mean wind speeds (Jelavic, Peric and Petrovic, 2006; Iribas-Latour and Landau, 2012). However, since wind turbines operate in a continuously changing wind field it can be particularly difficult to maintain a reasonably steady operating point. This makes it hard, if not impossible, to obtain suitable data records for LTI identification, since large wind speed variations cause the linearity assumptions to be violated. If one could explicitly model the dominant nonlinear effects, one could use an arbitrary sequence of data obtained from the turbine in which the wind speed varies. As will be shown further on, the key benefit of the method presented in this chapter is that such data sets in which the wind speed varies arbitrarily can be used directly. This also implies that the amount of costly measurement time required to obtain identification data can potentially be smaller.

While identification techniques for general nonlinear systems are an area of active research, we have already argued in the introduction (Section 1.3) that these methods still present significant challenges in terms of reliability, computational complexity and the need for expert knowledge, making their application to real data troublesome.

Recently, identification techniques for linear parameter-varying systems have seen many improvements, but applying these techniques is still hampered by computational and technical issues (van Wingerden and Verhaegen, 2009b). In Chapter 5 we have explored the possibility of decoupling the dynamics of a wind turbine into a series connection of static nonlinear functions, governed by the torque and thrust coefficients, and a linear time invariant dynamic system (van der Veen, van Wingerden and Verhaegen, 2011). It was shown that a model could be identified on the basis of simulation data. In this chapter some of those ideas are revisited and tailored to be applied to real turbine data, where the turbine is operating under full turbulence and throughout a significant portion of its operating envelope. A turbine always operates in a 3D turbulent wind field with typical turbulence intensities of 10-20%. In the conditions experienced during the experiments performed for this paper, the turbulence intensity was as high as 23%. Since a turbine operates in turbulent wind and the mean wind speed can be estimated reliably, the system identification methods need to deal with significant stochastic content introduced by more rapid wind speed fluctuations. In other words, the signal-to-noise ratios seen in actual practice may provide a challenging task for system identification.

The identification method starts by parameterising the known or measured torque and thrust coefficient surfaces with splines, using the recently developed linear regression framework (de Visser, Chu and Mulder, 2009) that was earlier described in Section 5.2.1. As was discussed there, these simplex splines have attractive numerical properties. Knowledge of the thrust and torque coefficients allows us to estimate the thrust and torque of the rotor. Once these have been obtained, they are used together with the other measured input and output signals for identification of the dynamics of the wind turbine. It is assumed that these dynamics can be considered to be linear time invariant. An important property of the identification scheme is that it allows the input signal to be correlated with the output signal, allowing for consistent identification under closed-loop conditions. Wind turbines must necessarily operate under feedback control and hence it is advantageous to apply such identification techniques.

In some parts of the control engineering community, system identification has been adopted to complement first-principles modelling in the control design stage. The approach is typically to design a baseline controller on the basis of the first-principles model. This controller is then implemented on the real system. The system is then identified to obtain more refined models, in particular near the crossover frequency. The control design can subsequently be adjusted and made less conservative until the result is satisfactory. While some effort is usually made to calibrate and update first-principles models of wind turbines, the wind energy industry has only just started to adopt such an approach for control design. It should be noted that direct validation of aeroelastic models on the basis of measured data (e.g., calibrating loads in response to turbulent wind) is of limited use for control design (Bongers, 1994), since control design relies on models which accurately describe the gain and phase behaviour between inputs and outputs. For this purpose it is more interesting to directly model the relation between the actuators and the sensors on the basis of the gain and phase information that these signals contain.

This chapter presents two main contributions. First, an approach is presented to identify dynamic models of wind turbines based on operating data under realistic and time-varying wind conditions, by exploiting some physical knowledge about the wind turbine dynamics. This leads to a practically applicable and efficient algorithm. Second, experimental results are presented on the basis of real wind turbine data obtained from the three-bladed Controls Advanced Research Turbine (CART 3) (Figure 6.1) and the validity and value of the obtained results is demonstrated.

To the best of our knowledge, this chapter and the accompanying published work present the first (non-proprietary) results on the identification of multi-input-multi-output (MIMO) wind turbine dynamics (pitch and torque to rotor speed and tower motion) on the basis of real operational wind turbine data and over a wide operating range. Previous work was limited to identification of modal parameters, the use of simulation data or the identification of single-input-single-output models (van Baars, Mosterd and Bongers, 1993; James III, Carne and Lauffer, 1993; van Baars and Bongers, 1994; Knudsen, Andersen and Toffner-Clausen, 1997; Marrant and van Holten, 2004; Hansen, Thomsen, Fuglsang et al.,

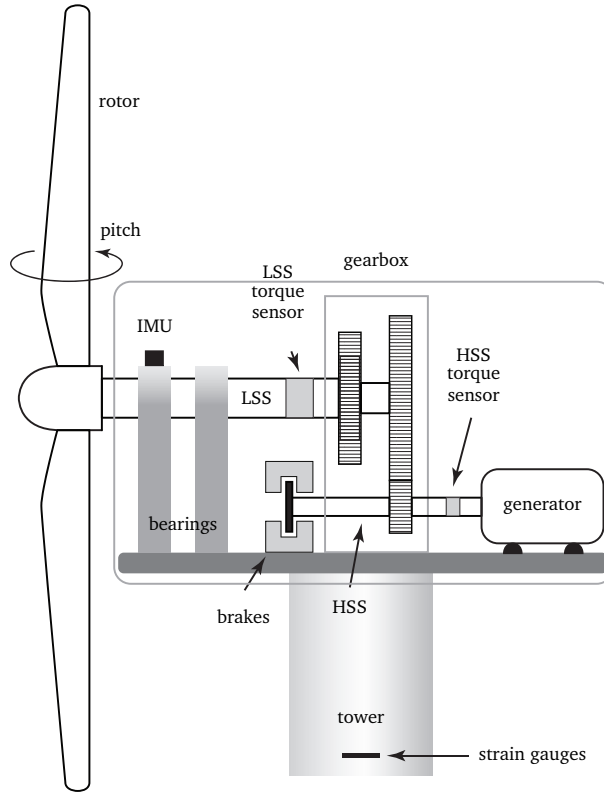


**Figure 6.2** – Schematic overview of the main components of the CART 3 turbine. Also shown are some locations of relevant sensors: the HSS and LSS torque sensors, the inertial measurement unit (IMU) and tower strain gauges.

2006; Iribas-Latour and Landau, 2009; Houtzager, Kulcsár, van Wingerden et al., 2010; van der Veen, van Wingerden and Verhaegen, 2010c; Iribas-Latour and Landau, 2012).

The organisation of this chapter is as follows. Section 6.2 provides a brief introduction into the most important aspects of wind turbine dynamics. Then, Section 6.3 presents our approach for system identification of wind turbines and how structural knowledge is exploited to arrive at this approach. Subsequently, Section 6.4 demonstrates the application of the presented identification scheme to experimental data obtained from the Controls Advanced Research Turbine, CART 3. The chapter concludes with a brief discussion.

## 6.2 Basic wind turbine mechanics

In this section some of the aspects governing the dynamics of a wind turbine are briefly described. The reader is referred to Burton, Sharpe, Jenkins et al. (2001); Manwell, McGowan and Rogers (2002) for far more extensive introductions. Identification of the CART 3 turbine (Figure 6.1) is considered, which is a typical horizontal axis, variable speed, variable pitch wind turbine. The CART 3 is a re-engineered 600 kW Westinghouse turbine, which has been converted from a 2-bladed to a 3-bladed configuration to result in a test bed for control research on the widespread 3-bladed configuration (Fleming, Wright, Fingersh et al., 2011). Figure 6.2 presents a schematic of the turbine.

### 6.2.1 Rotor

The rotor is the main component involved in converting wind energy into a torque  $T_a$  and a thrust  $F_a$ . The rotor is immersed in a wind field with mean (undisturbed) wind speed  $V_\infty$ , rotates with a rotational speed  $\Omega$  and has three blades of length  $R$ . The aerodynamic efficiency of the rotor is typically expressed in terms of a dimensionless tip speed ratio, defined by:

$$\lambda = \frac{\Omega R}{V_\infty}.$$

In steady-state conditions the thrust and torque are governed by well-known static relations (Bianchi, De Battista and Mantz, 2007):

$$T_a = \frac{1}{2} \rho \pi R^3 C_Q(\lambda, \beta) V_\infty^2, \quad (6.1a)$$

$$F_a = \frac{1}{2} \rho \pi R^2 C_T(\lambda, \beta) V_\infty^2, \quad (6.1b)$$

where  $C_Q(\lambda, \beta)$  is the *torque coefficient*,  $C_T(\lambda, \beta)$  is the *thrust coefficient*,  $\rho$  is the air density and  $\beta$  is the collective pitch angle of the blades. From these relations it follows that the thrust and torque change with wind speed, pitch angle and rotor speed. Typical torque and thrust coefficient surfaces are shown in Figure 6.3.

From the thrust and torque relations (6.1) it is evident that an incremental change in pitch is accompanied by changes in the rotor thrust and torque which depend on the local gradients of the thrust and torque coefficients in Figure 6.3. This is the main cause for the nonlinear behaviour of wind turbines and the requirement for gain-scheduled pitch control. It should be noted that changes in rotor thrust and torque do not occur immediately after a blade pitch change due to dynamic inflow and dynamic wake effects (Snel and Schepers, 1995; Henriksen, Hansen and Poulsen, 2012). Inclusion of these dynamics is crucial for subsequent control design.

Since the rotor consists of three flexible blades, any change in rotational speed involves the flexible modes of these blades and the modes of the rotor. As a consequence these modes may manifest themselves in the overall dynamics of the turbine.

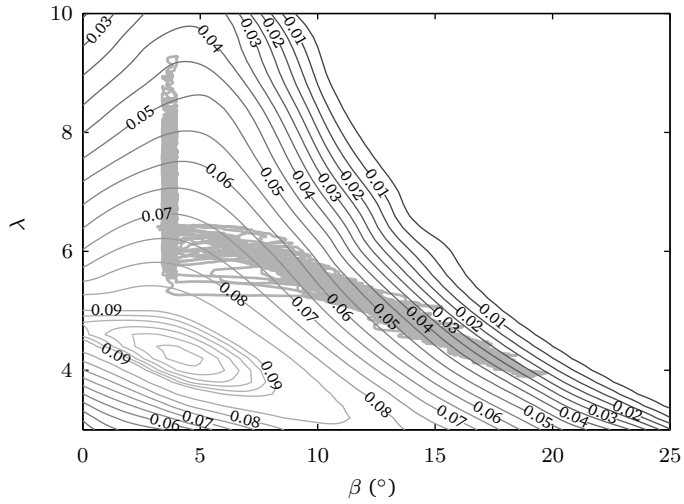
### 6.2.2 drive train

The torque equation (6.1a) governs the aerodynamic torque  $T_a$  entering the low-speed shaft (LSS) of the turbine. In many turbines, a compact high-speed generator is employed, which requires that a gearbox be used to convert the rotational speed and torque to a suitable range. At the end of the high-speed shaft, the generator torque  $T_g$  is active, with a rotational speed  $\omega$ . The gearbox typically consists of one or more (planetary) gear stages. The rotatory inertia of the rotor on the one hand and the generator on the other hand, combined with flexibilities of the shafts introduce drive train dynamics. These typically manifest themselves as highly resonant torsional modes with little intrinsic damping.

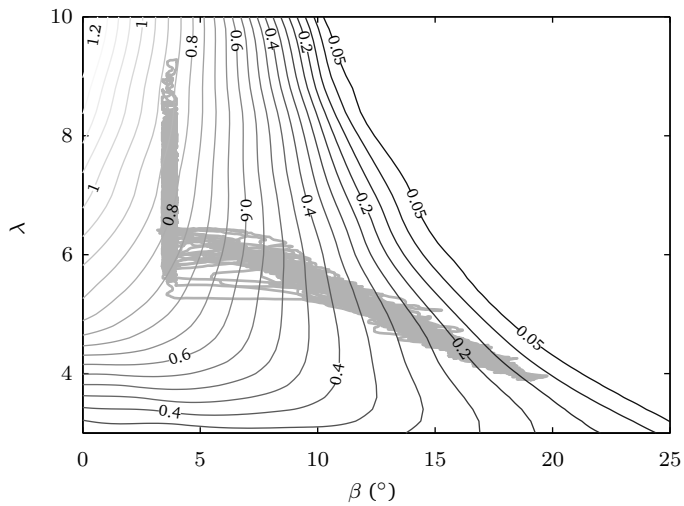
The dynamic torque balance will determine the rotor speed  $\Omega$  and generator speed  $\omega$ . Typically, the generator torque  $T_g$  and the pitch angle  $\beta$  can be used to regulate the rotor speed and wind turbine power output.

### 6.2.3 Tower

The rotor is mounted on the low-speed shaft of the drive train which is contained in the nacelle on top of a flexible tower. The thrust equation (6.1b) governs the thrust  $F_a$  acting on the thrust bearing of the turbine, causing a tower top motion and corresponding bending moment  $M_{\text{twt,FA}}$ . The drive train and generator dynamics are coupled with the tower motion, predominantly due to the reaction torque of the generator, and this coupling results in a side-side motion and corresponding bending moment  $M_{\text{twt,SS}}$  of the tower.



(a) The torque coefficient  $C_Q(\lambda, \beta)$  versus tip speed ratio  $\lambda$  and pitch angle  $\beta$ .



(b) The thrust coefficient  $C_T(\lambda, \beta)$  versus tip speed ratio  $\lambda$  and pitch angle  $\beta$ .

**Figure 6.3** – The torque and thrust curves of the CART 3 turbine and typical values of  $(\lambda, \beta)$  seen during operation.

## 6.2.4 Controls

Figure 6.4 depicts the layout of the CART 3 control system. In below-rated conditions, the aim of the control system is to maximise the power production efficiency of the turbine. This is achieved by keeping the pitch angle fixed at  $3.7^\circ$  and running the turbine at its optimal tip speed ratio  $\lambda$  (resulting in the highest power coefficient), given the current wind speed. This tip speed ratio is maintained by controlling the rotor rotational speed using the generator torque  $T_g$ . Then, as rated generator torque and rated rotor speed are reached, the turbine enters the so-called above-rated regime. In this regime the pitch angle

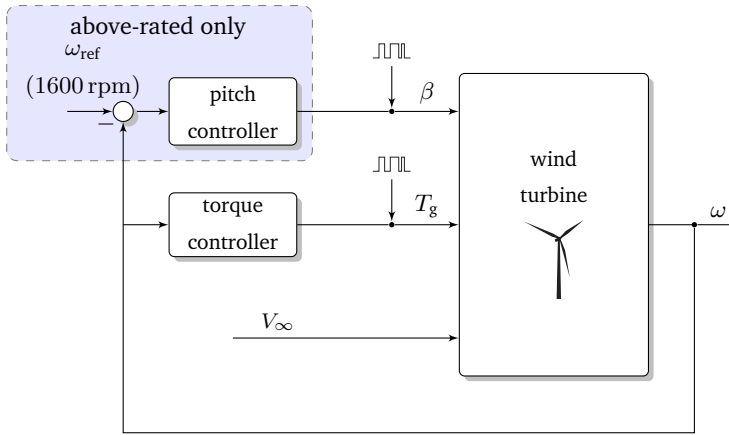


**Figure 6.4** – Schematic representation of the CART 3 control system. The diagram also indicates where perturbation signals are injected for system identification.

is used to maintain rated power. This is achieved by gradually pitching the blades into the wind (pitch-to-feather) so as to reduce the torque coefficient  $C_Q(\lambda, \beta)$ . Typically the torque and pitch are regulated using independent single-input-single-output PI controllers. Since the response to a change in pitch varies significantly with the current operating condition, gain scheduling of the pitch controller is necessary. A good review of typical wind turbine control system aspects can be found in Bossanyi (2000).

In the last decade wind turbine manufactures have increasingly considered the potential of advanced MIMO control strategies in an effort to balance multiple control objectives, such as optimal power production and load mitigation, in a more refined and systematic way. Such designs typically require a detailed description of the multivariable input-output behaviour.

### 6.3 Global system identification of wind turbines

In this section a novel and practical approach to identify a wind turbine from data captured under non-stationary wind conditions is described. Previous sections already discussed that wind turbines are nonlinear systems and that there is a demand for accurate MIMO models to support the future design of advanced multi-objective and multivariable controllers. It is first shown how the structure of the problem can be exploited to split the dynamics into a static nonlinearity and a linear time invariant (LTI) dynamic subsystem. Having done so, it is shown how the LTI part can be identified using a recent closed-loop subspace identification technique.

#### 6.3.1 Structure of the problem

In the previous chapter we have shown that the dynamics governing the rotor speed of a wind turbine can be approximated by a series connection of a static nonlinear mapping and an LTI subsystem (van der Veen, van Wingerden and Verhaegen, 2011). This situation is depicted in Figure 6.5. In this work four output signals are considered: the rotor speed  $\Omega$ , the generator speed  $\omega$  and the tower-base bending moments in the fore-aft and side-side directions,  $M_{\text{twr,FA}}$  and  $M_{\text{twr,SS}}$  respectively. The mechanical part of the turbine, consisting of the dynamics of the drive train, the tower, the generator and the rotor structure and their interactions, is assumed to be linear and time invariant. The aerodynamics of the rotor interact with this dynamic system through a rotor thrust and torque, which are governed by the relations in (6.1).

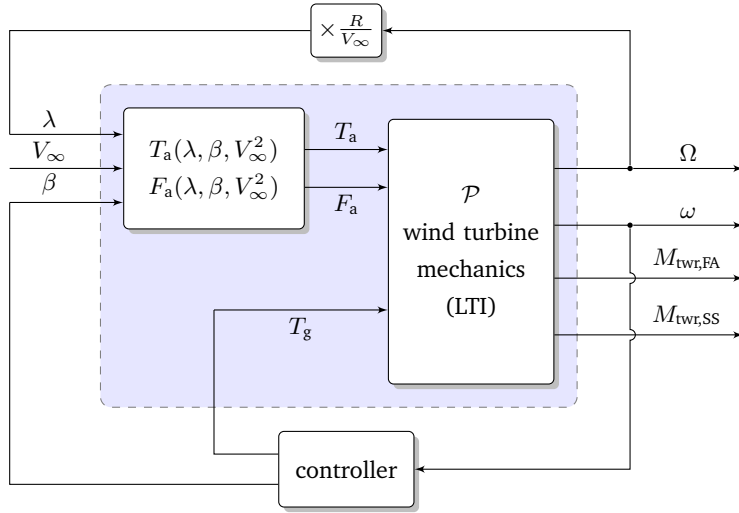


**Figure 6.5** – Schematic representation of the structure recognised in wind turbine dynamics. The dashed part constitutes the Hammerstein representation of the turbine.

It is important to note that since these relations are static, they would imply that a change in wind speed or pitch would result in an instantaneous change of rotor torque and thrust. In reality, however, the aerodynamic response is governed by several time constants related to dynamic inflow and wake dynamics (Snel and Schepers, 1995; Henriksen, Hansen and Poulsen, 2012). It will be assumed that these time lags are incorporated in the time invariant dynamics of the model.

In the literature on system identification, a configuration as depicted in Figure 6.5, consisting of a static nonlinearity followed by an LTI system, is known as a Hammerstein system. In Hammerstein system identification, as it was applied in van der Veen, van Wingerden and Verhaegen (2011), the goal is to estimate both subsystems simultaneously. It turned out that when data from a real turbine under full turbulence conditions is used, it is practically impossible to estimate both the torque and thrust coefficients and the dynamic behaviour, when it is assumed that the thrust and torque signals are not measurable. The estimated models were found to be extremely sensitive to variations in the data. For this reason it was necessary to resort to a two-step procedure in which it is assumed that the thrust and torque coefficients are known, either from aerodynamic modelling or from previous measurements. In the wind energy community significant efforts have traditionally been directed towards prediction of (static) wind turbine performance characteristics and hence static thrust, torque and power characteristics are known with good confidence. There is limited literature on the estimation of performance characteristics (i.e., torque, thrust and power coefficients) of wind turbines on the basis of field data and it is still an area of active research, demonstrating that determining these coefficients empirically is challenging (Gottschall and Peinke, 2008). Obviously, the situation would improve if measurements of aerodynamic torque and thrust could be obtained, but this is not often the case and if torque and thrust sensors are available these measurements can only be obtained indirectly after further processing<sup>1</sup>. While static performance characteristics may be well-known from first-principles calculations, prediction of the dynamic behaviour is still challenging and in this work system identification is applied to accurately model this dynamic behaviour on the basis of measurement data.

It is important to outline the validity of the assumptions under which the dynamics can be assumed to be time invariant. First, aerodynamic time constants are typically related to

<sup>1</sup>E.g., a measured torque on the low-speed shaft would incorporate not only the aerodynamic torque, but also components due to drive train dynamics and rotor acceleration.

local inflow velocities at the blade leading edges. As a consequence, these time constants vary with the operating condition of the wind turbine. Second, the pitch angle may see variations over a typical range of 35 degrees. These changes influence the dynamic modes of the rotor and therefore may cause shifts in natural frequencies. These shifts however, were found to be small.

On a final note it is worth mentioning that wind turbines are inherently linear time-varying systems and indeed are often considered as such (Skjoldan and Hansen, 2012). Since we only consider collective pitch and measure outputs in the fixed (hub, tower) frame of reference we do not need to resort to transformations such as the frequently-used Coleman transformation.

### 6.3.2 Modelling the aerodynamic coefficients using splines

In the previous chapter we have developed an approach to identify the static nonlinear functions  $C_Q$  and  $C_T$  and the linear time invariant dynamics simultaneously using a so-called Hammerstein identification method (van der Veen, van Wingerden and Verhaegen, 2011, 2012). The disadvantage of these methods is that, depending on the character and input dimension the nonlinearities, many more parameters need to be estimated (e.g., the full surfaces  $C_Q$  and  $C_T$  need to be parameterised) compared to LTI identification and hence these methods may be more sensitive to noise and turbulence. In this chapter it is assumed that reasonable estimates of these performance coefficients are available. At the time of writing (2012), initiatives were being discussed to estimate those coefficients from a tailored measurement campaign on the CART 3 turbine, possibly with the aid of LIDAR data.

Typically, a blade element momentum code (Manwell, McGowan and Rogers, 2002) is used to obtain tabulated estimates of  $C_Q$  and  $C_T$  versus  $\lambda$  and  $\beta$ . For the CART 3 turbine the WT\_Perf tool (Buhl, 2012) was used to estimate the performance coefficients. For the purpose of system identification a recent linear regression framework for multivariate splines (de Visser, Chu and Mulder, 2009) is applied to fit spline interpolants to these tabulated data. The advantage of doing so is that  $C_Q$  and  $C_T$  are subsequently defined as functions and, as such, function and gradient evaluation can proceed analytically. Furthermore, the interpolants can be prescribed to be, in our case,  $C^1$ -continuous, implying that the gradients are well-defined everywhere within the interpolated domain.

The ability to obtain gradients of the coefficients  $C_Q$  and  $C_T$  is crucial for model linearisation (cf. Section 6.3.4) and gain-scheduling (Bossanyi, 2000; Bianchi, De Battista and Mantz, 2007). The interested reader is referred to de Visser, Chu and Mulder (2009, 2011) for a detailed introduction into the spline regression framework.

### 6.3.3 Identification of a wind turbine

Using the knowledge of the wind speed, rotor speed and the pitch angle the aerodynamic thrust and torque can be computed at each time instant  $k$  using the torque and thrust relations, which are repeated here:

$$\begin{aligned} T_a(k) &= \frac{1}{2} \rho \pi R^3 C_Q(\lambda(k), \beta(k)) V_\infty^2(k), \\ F_a(k) &= \frac{1}{2} \rho \pi R^2 C_T(\lambda(k), \beta(k)) V_\infty^2(k). \end{aligned}$$

These signals enter the mechanical subsystem which is assumed to be LTI. The mechanical subsystem is modelled as an innovation state-space system which represents a generic LTI system with measurement and process noise (see Chapter 2), of the form (2.3), in which:

$$y_k = \begin{bmatrix} \Omega(k) \\ \omega(k) \\ M_{\text{twt,FA}}(k) \\ M_{\text{twt,SS}}(k) \end{bmatrix}, \quad u_k = \begin{bmatrix} T_a(k) \\ F_a(k) \\ T_g(k) \end{bmatrix}.$$

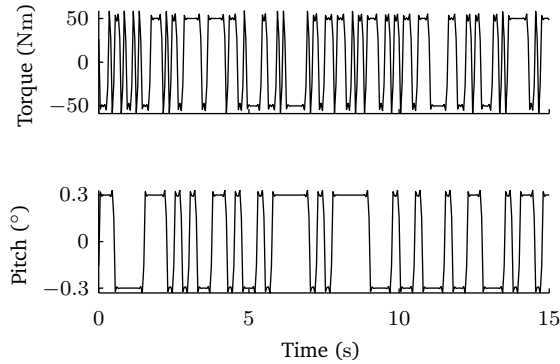


**Figure 6.6** – Example time traces of perturbations applied to the pitch and torque reference signals.

Note that  $V_\infty$  is the free-stream wind speed ahead of the turbine. Usually, this is not available and hard to measure. In Section 6.3.4 it is described how this wind speed signal can be estimated.

Now that the inputs and outputs of the LTI subsystem have been defined, we can estimate the system matrices of the innovation model using any closed-loop subspace identification technique described in Chapter 2. In this chapter we have chosen to use the closed-loop MOESP method.

### 6.3.4 Further aspects related to system identification

In this subsection several important aspects related to system identification and its application in engineering practice are described. These aspects are related to the design of an identification experiment, wind speed estimation, how to deal with periodic disturbances and how to validate identified models.

#### Experiment design

To be able to identify a system in closed-loop it is necessary to inject perturbations into the controller reference signals. This is necessary to be able to correlate the actuator inputs to the turbine's dynamic responses measured by the sensors. In the case considered here, the inputs to the turbine are the collective pitch angle demand  $\beta$  and the demanded generator torque  $T_g$ . The pitch angle is perturbed by an additive random binary pitch perturbation of  $\pm 0.3^\circ$ . The demanded generator torque is perturbed by a similar signal with amplitude  $\pm 50$  Nm. The torque perturbation is a pseudorandom binary sequence, generated by sampling the sign of a Gaussian random number generator at a rate of 10 Hz. This implies that the perturbations have spectra that are more-or-less flat up to 4 Hz. The pitch is perturbed by a similar signal, sampled at 4 Hz, resulting in a spectrum that is flat up to about 1 Hz. Figure 6.6 shows examples of these perturbation signals, which have further been filtered and rate limited according to the hardware constraints. See Section 3.4.2 for more notes on experiment design.

While a fairly reliable estimate of the wind speed can be obtained for low frequencies of up to 0.3 Hz (essentially governed by the drive train frequencies, cf. Section 6.3.4), the faster variations of wind speed introduce significant stochastic perturbations on the rotor torque and thrust, with which the identification method must cope.

Signals are sampled at a high rate of 400 Hz, which is governed by the control system. These signals are filtered and resampled to 20 Hz before identification. A measurement sequence of 1490 s ( $\sim 25$  min) is used for identification.

### Estimating the rotor effective wind speed

A common difficulty in wind energy engineering is to reliably estimate the undisturbed mean wind speed upwind of the rotor, i.e., that wind speed resulting in the correct aerodynamic torque as predicted by (6.1a). The nacelle anemometer is affected by induction of the rotor and periodic effects due to the three rotor blades. A potential solution is to use Light Detection and Ranging (LIDAR) measurements (Smith, Harris, Coffey et al., 2006; Simley, Pao, Kelley et al., 2012). A LIDAR is capable of measuring the wind speed at several locations upwind of the rotor in a non-intrusive manner. One method would be to average a number of spatially separated measurements upwind of the rotor to estimate the mean wind speed. Still, evolution of turbulent structures would cause the wind speed estimate to be reliable only at low frequencies. At present, LIDAR data was not available on the CART 3 and therefore a method is presented that is based on torque measurements on the low-speed shaft. Similar procedures were used in van der Hooft and van Engelen (2004); Johnson, Fingersh, Balas et al. (2004). It is important to note that these methods and the method presented here can only be expected to yield accurate estimates at low frequencies, as a consequence of neglecting drive train dynamics and other dynamics propagating into the drive train system (for instance the side-side motion, or the fore-aft motion).

The rotor acceleration is governed by:

$$J\dot{\Omega} = T_a - T_{LSS},$$

where  $T_{LSS}$  is the measured LSS torque and  $J$  is the rotor inertia. Since the LSS torque can only be measured accurately at low frequencies, all signals have been filtered with a zero-phase low-pass filter with a cutoff frequency of 0.3 Hz. This eliminates any components due to drive train dynamics ( $\sim 2.6$  Hz), fore-aft-motion-induced wind speed changes ( $\sim 0.85$  Hz) and related dynamics, of which it is assumed no knowledge is available. The aerodynamic torque can now be estimated as:

$$\hat{T}_a \approx J\hat{\Omega} + \hat{T}_{LSS},$$

where the hats denote the filtered signals. By invoking the torque relation (6.1a) and using the knowledge of the pitch angle  $\beta$  and rotor speed  $\Omega$  together with the estimated torque  $\hat{T}_a$ , the wind speed  $V_\infty$  can be estimated using a root-finding technique.

Although the LSS torque is not commonly measured on commercial turbines, the generator torque together with the gearbox ratio can be used instead, owing to the fact that at low frequencies these signals are equivalent.

A final remark is in order regarding the position of CART 3 in relation to utility-scale wind turbines. On multi-MegaWatt commercial wind turbines drive train and tower frequencies may well be an order of magnitude lower, causing them to become more relevant. One solution is to then choose a smaller filter bandwidth than the current 0.3 Hz. On the other hand one could apply more sophisticated filtering techniques as proposed in Østergaard, Brath and Stoustrup (2007); Knudsen, Bak and Soltani (2011). However, these techniques require a significant amount of additional (prior) information on the dynamics of the turbine.

### Dealing with periodic disturbances

As was described in some detail in Section 3.2, wind turbines experience significant periodic loads which need to be accounted for in the identification procedure. In this work we have used the techniques presented in that Section (3.2) to properly model the periodic disturbances and avoid modelling errors.

### Disturbances due to yaw motion

During data analysis and identification it was found that the side-side motion of the tower contained significant frequency content that was unaccounted for by the input signals and

the periodic effects described in the previous section. After further investigation it was found that this content could be linked to yawing of the turbine. The yaw system only periodically aligns the turbine with the wind. When this happens, the nacelle is set in a sudden motion by the yaw drive, which causes a significant excitation of the lightly damped side-side motion of the tower. To account for these effects, the current yaw angle  $\psi(k)$  of the nacelle was added as an additional input and was found to account for these effects in a very satisfactory way.

Based on the discussions in Section 3.2 on compensating for periodic disturbances and this section on compensating for yaw motion the input signal defined in Section 6.3.3 is extended accordingly, so that the input signal becomes:

$$u_k = [ T_a(k) \quad F_a(k) \quad T_g(k) \mid \psi(k) \mid \varphi_1(k) \quad \cdots \quad \varphi_p(k) ]^T.$$

#### Validation methods

It is especially relevant for real systems, of which no “true” model is known, to be able to validate identified models. For this purpose several techniques are used. The first is to compare the outputs of the identified model with the measured outputs. This is done both on the data set used for identification and on an independent dataset, as a means of cross-validation. As quality measure the variance-accounted-for (Verhaegen and Verdult, 2007) (VAF) is used, see (2.38) on page 36.

In this work we use an additional means of simulating the identified system. Since the wind turbine is a marginally stable system, errors accumulate and simulated trajectories cannot be compared to the measured ones. For this reason the identified models are simulated in closed-loop with the actual controllers on CART 3. This not only causes the trajectories to match better, since the controllers attempt to meet the reference signals, but also serves as a verification of the model in the sense that it shows whether the closed-loop is stable as is the case for the true system.

Besides the ability to describe the nonlinear dynamics of the wind turbine, an additional advantage of the identification scheme presented here is that local linear models can be obtained even when the operating conditions do not allow the system to operate steadily in a single operating point. Hence, as a second means of validation the identified model is linearised at several wind speeds and compared to linearised models obtained from a model of the CART 3 turbine in the FAST simulation environment (Jonkman, 2012).

Considering an operating point of the turbine defined by the triple  $(\bar{V}_\infty, \bar{\beta}, \bar{\Omega})$ , a linearised description around this operating point can be obtained. To do so, the torque and thrust inputs (6.1a) are linearised around this operating point:

$$\delta T_a = \frac{1}{2} \rho \pi R^3 \left[ \frac{\partial(C_Q V_\infty^2)}{\partial V_\infty} \quad \frac{\partial(C_Q V_\infty^2)}{\partial \beta} \quad \frac{\partial(C_Q V_\infty^2)}{\partial \Omega} \right] \Bigg|_{(V_\infty, \beta, \Omega) = (\bar{V}_\infty, \bar{\beta}, \bar{\Omega})} \begin{pmatrix} \delta V_\infty \\ \delta \beta \\ \delta \Omega \end{pmatrix},$$

$$\delta F_a = \frac{1}{2} \rho \pi R^2 \left[ \frac{\partial(C_T V_\infty^2)}{\partial V_\infty} \quad \frac{\partial(C_T V_\infty^2)}{\partial \beta} \quad \frac{\partial(C_T V_\infty^2)}{\partial \Omega} \right] \Bigg|_{(V_\infty, \beta, \Omega) = (\bar{V}_\infty, \bar{\beta}, \bar{\Omega})} \begin{pmatrix} \delta V_\infty \\ \delta \beta \\ \delta \Omega \end{pmatrix},$$

where  $\delta T_a$  and  $\delta F_a$  are the variations about the steady-state values. The directional derivatives of the torque and thrust coefficients are readily evaluated analytically on the basis of their spline representations (de Visser, 2011). These derivatives are guaranteed to be finite and well-behaved, by virtue of the fact that the spline functions were prescribed to be  $C^1$ -continuous. The LTI component of the model remains invariant under changes in the operating point.

## 6.4 Experimental results

To validate the presented approach for identification of wind turbines and demonstrate its practical value, identification experiments were performed on the CART 3 research

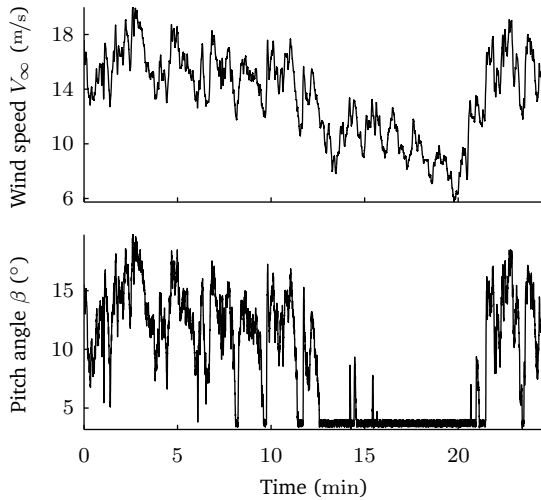


**Figure 6.7** – Wind speed experienced by the turbine and corresponding collective blade pitch angle.

turbine. During suitable wind conditions, i.e., with significant wind speed variations, the perturbation signals were applied and data acquisition was started.

Figure 6.7 shows an example of the wind speeds and pitch angles experienced during such an experiment. The wind speed varies considerably, and the effective turbulence intensity  $I$ , defined as the ratio of the standard deviation of the wind speed to the mean wind speed is equal to  $I = 23\%$ . This is a very significant turbulence level and is far higher than the commonly used wind turbine class A, which corresponds to  $I = 16\%$  (*Wind turbines – Design requirements 2005*). This indicates that one needs to deal with a significant amount of stochastic excitation. Furthermore, the wind speed varies throughout a significant part of the operational regime of the turbine since the cut-in wind speed is near  $6 \text{ m/s}$  and the cut-out wind speed is near  $24 \text{ m/s}$ . Since the full operational regime is experienced, the full nonlinear behaviour of the turbine is captured. This is, for instance, reflected in the collective pitch angle which reaches high values and varies through a wide range of almost  $20^\circ$ , as the turbine control system attempts to maintain rated power at above-rated wind speeds. It can also be seen that there is a period of below-rated operation, between 13 and 21 minutes from the start, where the turbine operates in *fine pitch* and the pitch angle is kept fixed at  $3.7^\circ$  (aside from the additive perturbation).

A model of the turbine was identified on the basis of the dataset corresponding to Figure 6.7. For the identification algorithm window sizes of  $p = 180$  and  $f = 140$  were chosen (see Chapter 2, Section 2.3 for details). Periodic signals, as discussed in Section 3.2, were added to model 1P, 2P and 3P disturbances. The order detection mechanism of the MOESP algorithm (2.24) indicated a number of possible system orders and for each of those orders a model was identified and the fit on the identification data was evaluated in terms of the VAF. Based on this evaluation, a model order of  $n = 23$  turned out to give good VAF values (upwards of 90%) and these values showed little improvement for higher model orders.

As described in Section 6.3.4 several methods can be applied to validate identified models. The following subsections describe two validation approaches.

#### 6.4.1 Time-domain validation in closed-loop

Figure 6.8 shows the distributions of the wind speeds present in the data sets used for identification and validation respectively. These distributions may indicate that the

emphasis of the identified model will be on a wind speed near 15 m/s, since that wind speed is most abundant. The validation data set contains more data at lower wind speeds.

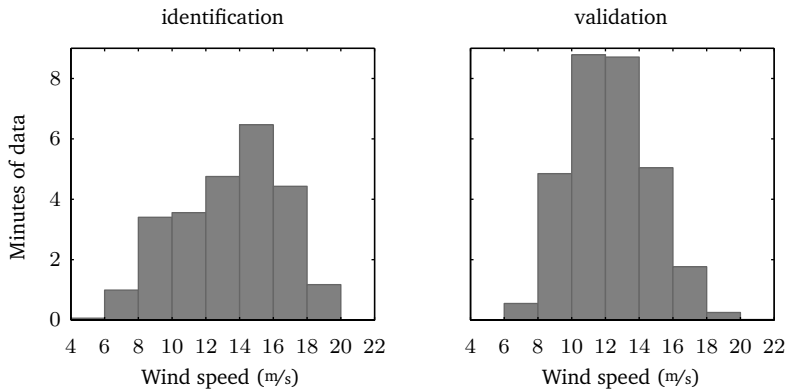


**Figure 6.8** – Histograms displaying the distributions of wind speeds in the identification and validation data sets.

A primary step in validating identified models is typically to study the model's prediction capability on a dataset. The first check is to pass the input data that was used for identification through the model and observe the outputs. These results are shown in the first column of Table 6.1 in terms of the variance-accounted-for (cf. Section 6.3.4) for each channel. This column verifies that the model delivers good prediction capability on the identification dataset. The side-side motion is not as accurately modelled.

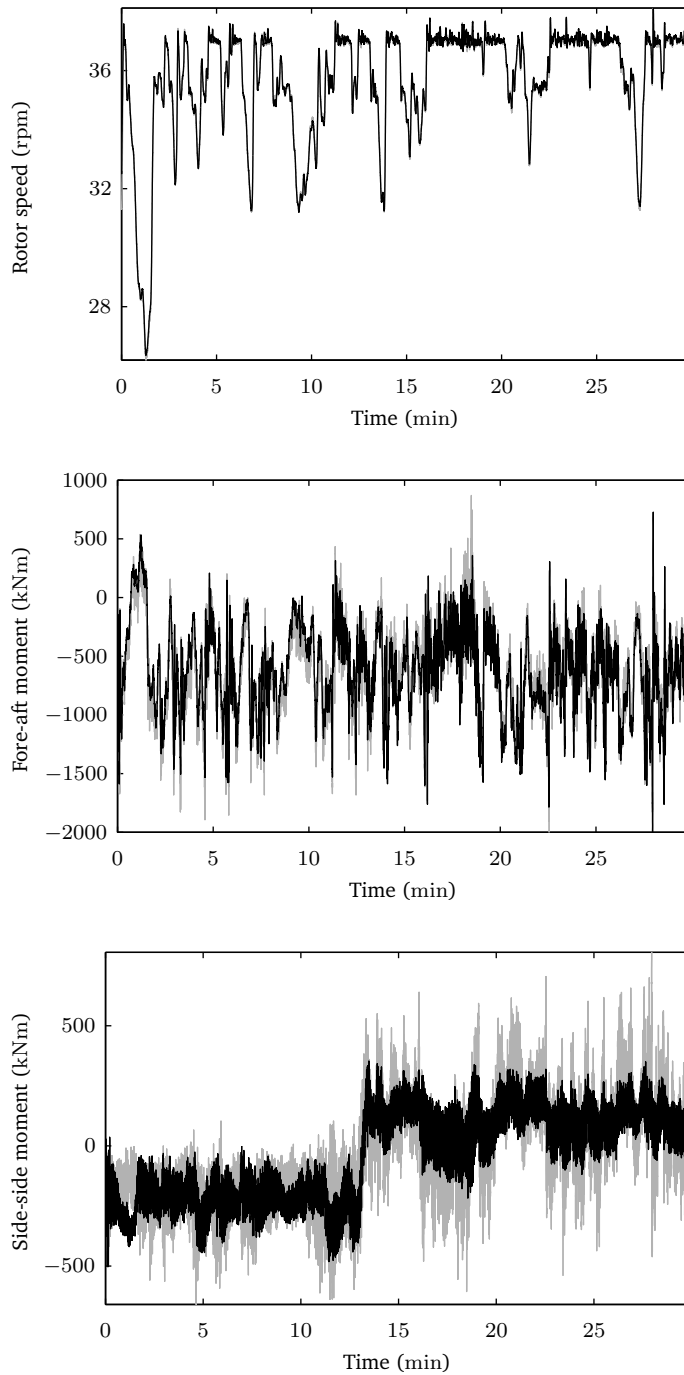
In a second validation step the model was subjected to inputs from an independent dataset. The problem with the open-loop dynamics of the wind turbine is that it contains an integrator (the rigid body mode of the drive train) and therefore is unstable. For this reason, the validation was performed in closed-loop. That is, the configuration depicted in Figure 6.4 was simulated, where the identified model took the place of the real wind turbine. The second column in Table 6.1 shows the results for this simulation. Time traces of these results are also shown in Figure 6.9. The results are overall very encouraging. One reason that the tower side-side motion shows differences, mainly in the high frequency content, could be that during these tests a drive train damper was intermittently active, which was not active in the simulations. Furthermore, motion could result from gyroscopic coupling of the rotor to the tower during yaw motions. Note also that it was essential to include the yaw position of the nacelle as an input to account for a significant part of the tower side-side motion.

Figure 6.10 compares the true and simulated outputs in terms of power spectra in the frequency domain. Note that the low-frequency content is accurately accounted for. The differences in high-frequency content could be due to the fact that turbulence above the 0.3 Hz bandwidth mentioned in Section 6.3.4 is active on the real turbine which is not a known input to the simulation model. In addition, the power levels of the high frequency content are much lower (upwards of 10 dB) causing this content to play a very limited role in the fit of the identified model to the data.

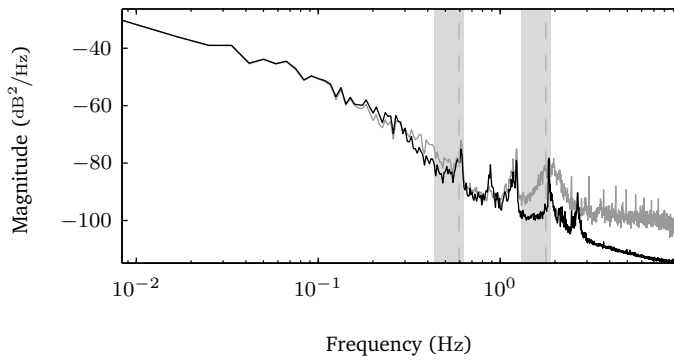
Finally, in these plots we also show the bands in which the periodic 1P, 2P and 3P disturbances are active. These periodic loads have been incorporated in the identification procedure by means of the azimuth position (cf. Section 3.2), to account for the special character of these disturbances and to be able to consistently identify models. It is not necessarily the case, though, that this results in accurate models describing the transfer from the periodic signals to the outputs. This is mainly due to the fact that the rotor speed varies and its distribution varies between data sets. This effect can be a reason for the mismatch between the spectra in Figure 6.10 within the gray frequency bands.

**Table 6.1** – The variance-accounted-for for the four output signals on the identification and validation data set.

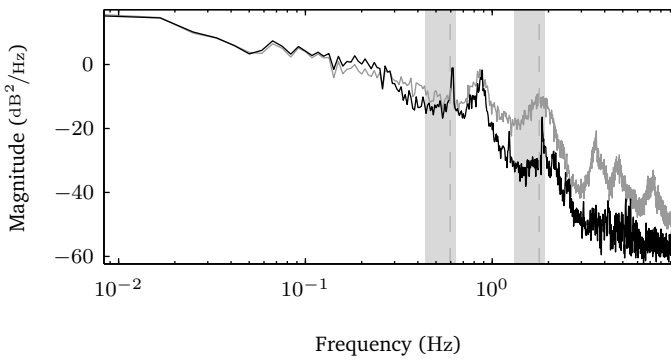
output	open-loop		closed-loop	
	identification data	validation data	identification data	validation data
$\Omega$	97.0%	70.4%	99.7%	99.7%
$\omega$	97.0%	70.4%	99.7%	99.7%
$M_{\text{twr,FA}}$	93.5%	90.4%	64.5%	82.3%
$M_{\text{twr,SS}}$	77.2%	66.8%	69.7%	65.9%



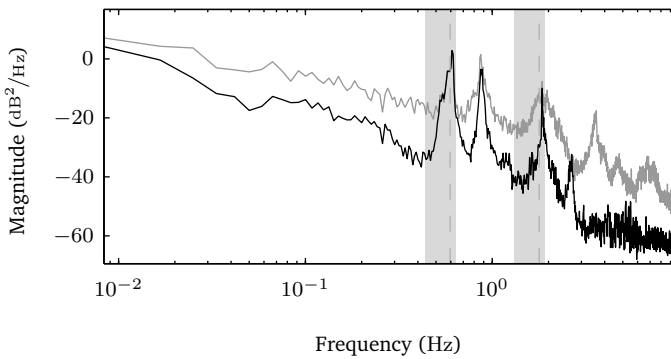
**Figure 6.9** – Validation results using an independent dataset. True CART 3 measurements (gray) compared to identified model outputs (black) under closed-loop control.



(a) rotor speed



(b) fore-aft bending moment



(c) side-side bending moment

**Figure 6.10** – Comparison of power spectra of measurement signals. True CART 3 measurements (gray) compared to identified model outputs (black) under closed-loop control. Also shown are the bands in which the 1P and 3P periodic loads are present along with their mean values (dashed).

## 6.4.2 Comparison of local linear models

In the next two subsections we examine the local behaviour of the identified models. First, we consider time domain simulations of local linear models obtained from the FAST aeroservoelastic model and the identified Hammerstein model. Next, we consider the frequency domain behaviour of these linear models.

### Time domain results

To compare the behaviour of the linearised FAST models and the linearised Hammerstein models with real data, short segments of validation data were extracted from a large measurement data set. The wind speed signal was binned into  $2 \text{ m/s}$  intervals centred around wind speeds of  $8 \text{ m/s}$  to  $17 \text{ m/s}$  with steps of  $1 \text{ m/s}$ . To establish the validity of such an approach, data was generated using the linear models at a certain wind speed (the “central” model) using random inputs. The same inputs were then used to simulate models in the vicinity of these central models. If the models are not too different, this should be reflected in the outputs being very similar and hence the VAFs between the outputs of the central models and surrounding models should be close to 100%. The results are shown in Figure 6.11. This figure shows that in all cases (except near  $13 \text{ m/s}$  for the FAST model) VAF values within the bands of  $V \pm 1 \text{ m/s}$  are quite high, being 95% or more. This should convince us that data within  $\pm 1 \text{ m/s}$  from the wind speed at which a model was linearised should be usable to compare two modelling methods (first principles vs. system identification) to each other.

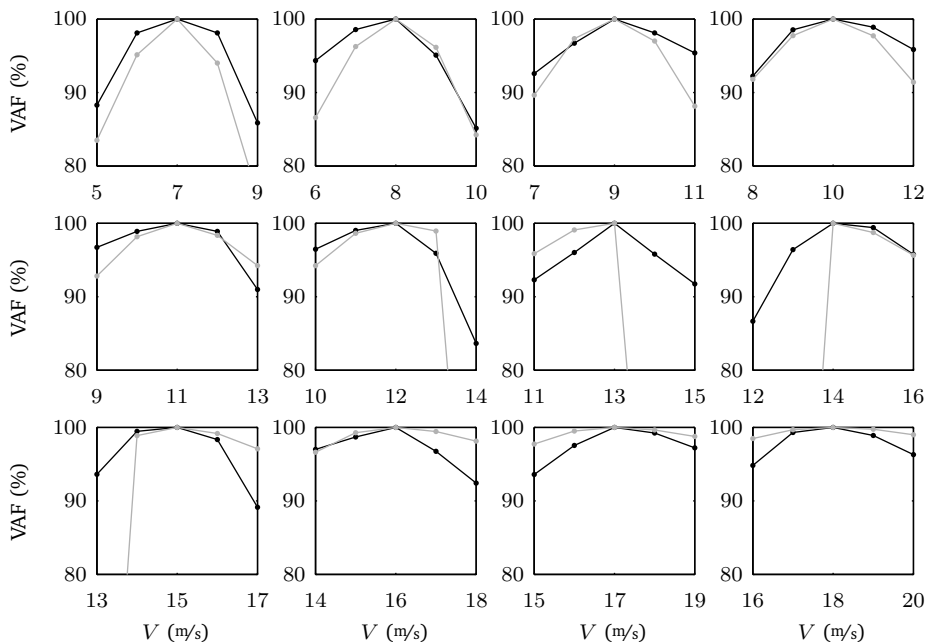


**Figure 6.11** – VAF values showing to what extent the outputs of neighbouring linear models are similar to the outputs of a central linear model; FAST linear models (gray) and linearised Hammerstein models (black). In all cases (except near  $13 \text{ m/s}$  for the FAST model) VAF values within the bands of  $V \pm 1 \text{ m/s}$  are quite high, being 95% or more.

All consecutive sequences longer than 20 seconds were considered, resulting in one

or more data sets for each wind speed bin. Figure 6.12 shows the results of one such

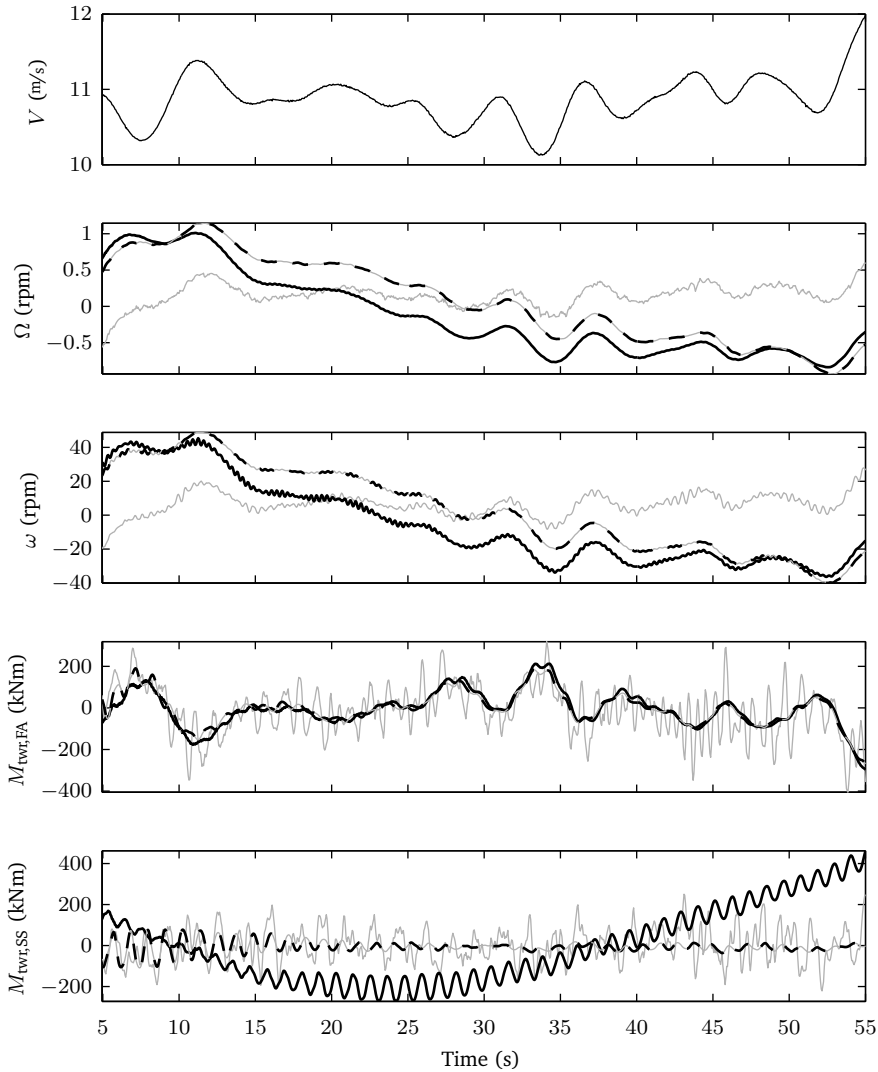


**Figure 6.12** – Results of a simulation of models linearised at  $V = 11$  m/s. The gray line is the measured signal, the black line is the linearised FAST model and the dashed line is the linearised Hammerstein model. Note that due to the integrator associated with the drive train the simulation results soon drift from the measured values.

simulation using a segment of data near 11 m/s. The rotor and generator speed signals clearly show the effect of the integrator associated with the rigid body mode of the drive train. These signals soon drift away from the measured signals, both due to accumulation of small errors and due to difficulties in estimating the integrator. The rigid-body dynamics are associated with DC and very low frequencies. In closed-loop operation these frequencies

are very tightly controlled by the (practically) infinite gain of the PI speed controller at these frequencies. Hence the very low frequencies are hard to identify in closed loop. On the other hand, if the model is to be used as a basis for controller design, the exact rigid body behaviour at these low frequencies is not important for the same reason and these models are still suitable.

The results in Figure 6.12 also demonstrate that, apart from the drift, the dynamics are captured well. Because of the drift, the quality of the models as judged by a VAF computed on the basis of these signals will turn out to be very poor. As a remedy, we have zero-phase filtered all signals with a 2<sup>nd</sup> order Butterworth high-pass filter with a pass-band starting at 0.05 Hz to eliminate low-frequency drifts. This procedure results in the signals shown in Figure 6.13. It can be seen that comparison is now much easier. Furthermore, VAFs computed on the basis of these results will improve and reflect whether the relevant dynamics are captured well or not. Table 6.2 shows the VAF values for all data sets, along with the mean VAF values found for each wind speed bin. The highlighted cells correspond to the simulation shown in Figure 6.12.

On the basis of the values in Table 6.2 it can be concluded that in many cases the Hammerstein model outperforms the FAST model, in particular at higher wind speeds. This is remarkable, since the Hammerstein model structure can only allow overall gain variations and not local (frequency-specific) variations in the dynamics. These figures also reflect the overall difficulty in fitting the side-side tower bending moment, an issue we have already seen in the previous section. As it turns out, these difficulties also hold for the FAST models. Finally, it is interesting to see that while most samples in the identification data set are associated with wind speeds between 13 m/s and 17 m/s, the VAF values are also high outside this range. At lower windspeeds, however, the FAST model performs as well as the identified model, while at the higher wind speeds the identified model clearly performs better.

#### Frequency domain results

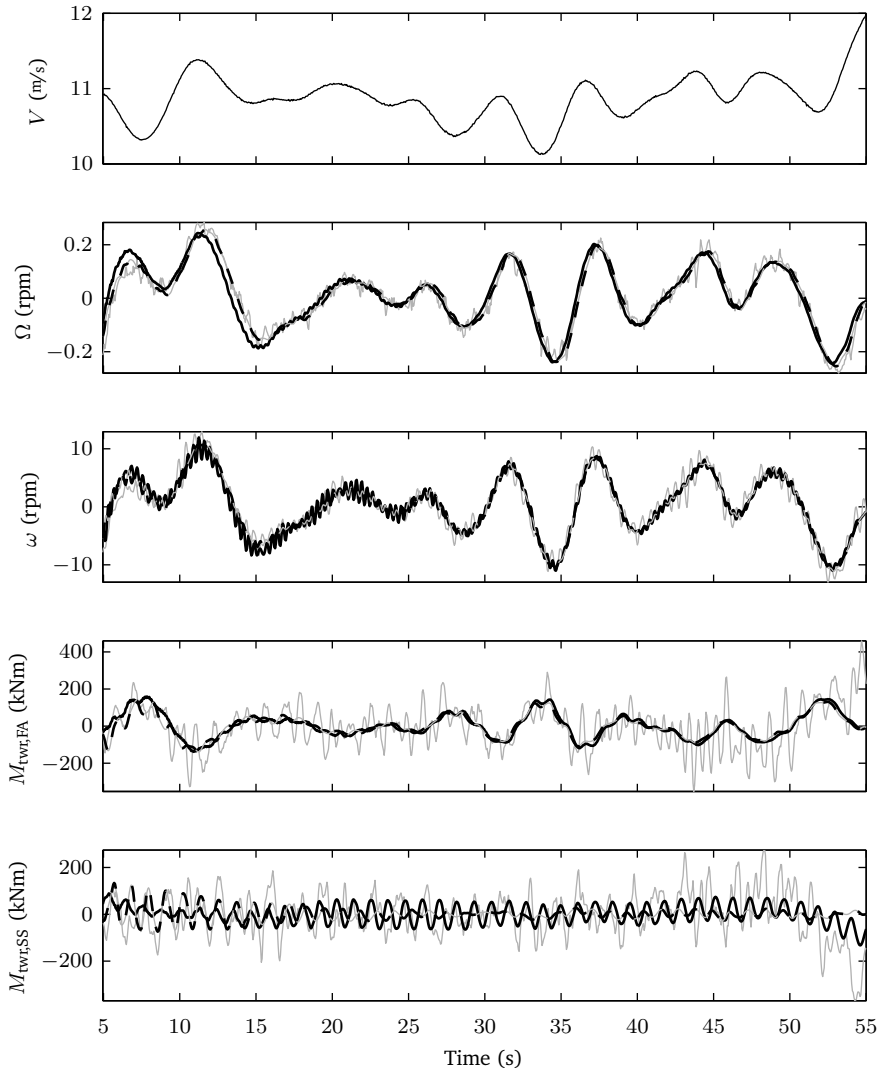
Figures 6.14 and 6.15, respectively, show the linearised models from pitch to generator speed and from pitch to fore-aft bending moment at two wind speeds. Figure 6.16 shows the linear models from generator torque demand to generator speed and side-side bending moment. The comparisons in the figures display good agreement, in particular in terms of the overall trend. It is important to realise that, while the FAST simulation model has to some extent been empirically tuned to match the true CART 3 dynamics, it by no means provides a 100% accurate reference model. For instance, in Figure 6.15 it seems that the FAST linear model underestimates the damping of the tower fore-aft mode. This is supported by the spectral estimate, which shows strong agreement with the identified model in terms of the damping of the tower mode. In this context it is interesting to note that in previous research, an attempt was made to design an active fore-aft tower damper for the CART 3 turbine on the basis of an aeroelastic model (Bossanyi, Fleming and Wright, 2012). In field tests, however, it was found that the tower damping was much higher than predicted (as just pointed out) thereby removing the load reduction benefits of having an active tower damping controller. This underlines the usefulness of system identification in obtaining accurate models for control design as well as for pointing out differences between a first-principles model and the true system it is meant to describe.

Figure 6.16(a) shows that the low-frequency and static behaviour is captured very accurately. The identified responses in Figure 6.16(b) also reveal a mode at 1.87 Hz, which is not predicted by the FAST model. The existence of this mode is confirmed by the spectral analysis. Also note that the estimate in Figure 6.16(b) is unreliable outside the resonance bands, since there the sensor signals are dominated by noise. This is reflected in the noisy character of the spectral estimate. The transfer functions from torque demand to tower fore-aft bending moment and from pitch angle to tower side-side bending moment have not been shown. These frequency responses are rather small in magnitude due to little coupling between those input-output pairs.

Finally, in table 6.3 some of the identified modal parameters are shown which follow from the eigenvalues of the identified system matrix. The identified values are compared

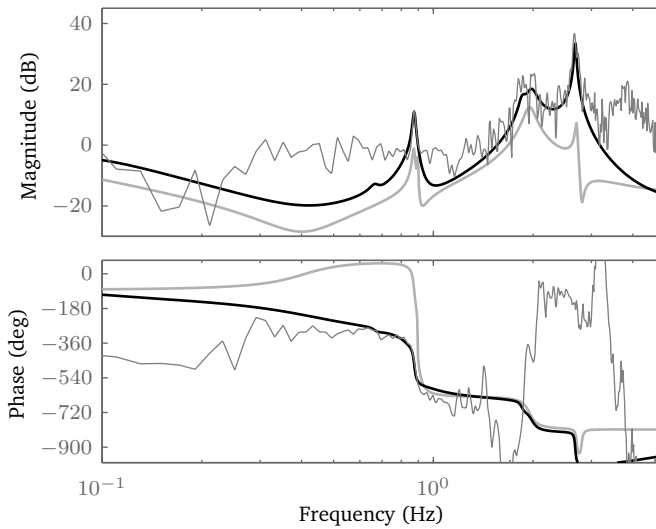
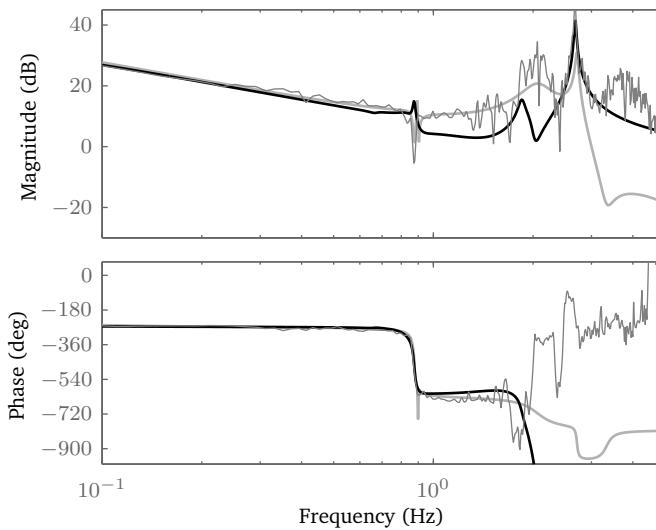
Wind speed	Output	mean VAF (%)		VAF individual data sets (%)										
		FAST	ID	FAST	ID	FAST	ID	FAST	ID	FAST	ID	FAST	ID	
8 m/s (7–9 m/s) 02:04	$\Omega$	<b>91.9</b>	<b>90.4</b>	91.9	90.4									
	$\omega$	<b>89.0</b>	<b>91.0</b>	89.0	91.0									
	$M_{\text{twr,FA}}$	<b>25.4</b>	<b>24.2</b>	25.4	24.2									
	$M_{\text{twr,SS}}$	<b>6.3</b>	<b>11.4</b>	6.3	11.4									
9 m/s (8–10 m/s) 03:24	$\Omega$	<b>91.0</b>	<b>88.1</b>	97.5	95.0	86.0	81.9	94.5	92.1	85.9	83.3			
	$\omega$	<b>87.8</b>	<b>87.3</b>	94.9	95.3	82.4	84.4	93.5	90.9	80.4	78.6			
	$M_{\text{twr,FA}}$	<b>35.8</b>	<b>33.1</b>	44.1	43.7	20.5	20.4	74.0	68.4	4.4	0.0			
	$M_{\text{twr,SS}}$	<b>23.4</b>	<b>26.5</b>	0.0	0.0	20.9	3.8	48.8	69.8	23.8	32.6			
10 m/s (9–11 m/s) 03:22	$\Omega$	<b>91.2</b>	<b>86.1</b>	88.6	79.2	88.4	85.5	92.6	92.1	89.1	80.0	97.6	93.6	
	$\omega$	<b>86.0</b>	<b>85.4</b>	79.9	79.8	87.5	85.9	88.3	89.3	83.1	81.1	91.3	90.8	
	$M_{\text{twr,FA}}$	<b>25.1</b>	<b>24.3</b>	3.7	6.1	36.3	25.8	34.2	35.7	0.2	0.0	51.4	53.9	
	$M_{\text{twr,SS}}$	<b>0.0</b>	<b>21.2</b>	0.0	23.3	0.0	58.3	0.0	0.0	0.0	14.1	0.0	10.4	
11 m/s (10–12 m/s) 03:33	$\Omega$	<b>88.3</b>	<b>93.2</b>	89.9	94.7	78.1	83.6	88.5	96.3	96.6	98.3			
	$\omega$	<b>86.2</b>	<b>91.0</b>	88.0	91.5	76.3	85.1	88.4	94.2	91.9	93.1			
	$M_{\text{twr,FA}}$	<b>30.3</b>	<b>37.5</b>	33.1	33.6	21.5	27.8	31.1	51.8	35.5	36.8			
	$M_{\text{twr,SS}}$	<b>12.5</b>	<b>19.2</b>	7.8	3.3	0.0	4.6	0.0	12.6	42.3	56.4			
12 m/s (11–13 m/s) 04:20	$\Omega$	<b>65.0</b>	<b>83.5</b>	60.3	77.2	97.7	97.2	0.0	63.6	84.6	89.0	82.3	90.7	
	$\omega$	<b>67.9</b>	<b>82.3</b>	48.8	74.8	97.2	96.9	39.5	68.4	76.9	85.5	77.0	85.9	
	$M_{\text{twr,FA}}$	<b>38.7</b>	<b>54.5</b>	87.4	91.2	32.9	37.8	47.7	62.8	6.9	16.9	18.4	63.8	
	$M_{\text{twr,SS}}$	<b>12.5</b>	<b>18.4</b>	42.8	19.5	0.0	15.2	19.5	33.7	0.0	9.1	0.0	14.5	
13 m/s (12–14 m/s) 04:45	$\Omega$	<b>0.0</b>	<b>35.9</b>	0.0	76.6	0.0	56.3	0.0	10.8	0.0	0.0			
	$\omega$	<b>0.0</b>	<b>42.0</b>	0.0	78.3	0.0	55.9	0.0	34.0	0.0	0.0			
	$M_{\text{twr,FA}}$	<b>63.0</b>	<b>78.8</b>	62.3	82.2	80.9	86.8	63.3	76.3	45.6	69.8			
	$M_{\text{twr,SS}}$	<b>0.0</b>	<b>13.7</b>	0.0	23.5	0.0	0.0	0.0	22.2	0.0	9.2			
14 m/s (13–15 m/s) 05:21	$\Omega$	<b>57.6</b>	<b>81.3</b>	59.7	83.7	54.6	82.1	75.3	87.9	50.5	69.0	48.0	83.7	
	$\omega$	<b>60.4</b>	<b>64.6</b>	67.2	74.2	70.2	72.2	49.8	49.6	38.6	42.7	76.5	84.4	
	$M_{\text{twr,FA}}$	<b>62.8</b>	<b>70.9</b>	65.4	72.6	59.4	73.2	65.2	67.7	45.7	61.1	78.3	79.9	
	$M_{\text{twr,SS}}$	<b>7.5</b>	<b>15.4</b>	4.3	1.9	17.7	40.5	8.7	14.6	0.0	7.8	6.7	12.0	
15 m/s (14–16 m/s) 06:28	$\Omega$	<b>49.6</b>	<b>82.7</b>	59.7	86.3	54.9	84.7	34.3	77.1					
	$\omega$	<b>52.9</b>	<b>54.1</b>	55.4	57.7	59.5	66.0	43.7	38.5					
	$M_{\text{twr,FA}}$	<b>50.8</b>	<b>61.9</b>	58.6	57.9	50.1	54.2	43.8	73.7					
	$M_{\text{twr,SS}}$	<b>1.2</b>	<b>10.0</b>	3.7	0.0	0.0	20.0	0.0	10.0					
16 m/s (15–17 m/s) 06:39	$\Omega$	<b>35.0</b>	<b>86.8</b>	35.0	86.8									
	$\omega$	<b>67.6</b>	<b>67.9</b>	67.6	67.9									
	$M_{\text{twr,FA}}$	<b>70.1</b>	<b>66.9</b>	70.1	66.9									
	$M_{\text{twr,SS}}$	<b>31.5</b>	<b>13.2</b>	31.5	13.2									
17 m/s (16–18 m/s) 04:26	$\Omega$	<b>61.2</b>	<b>80.6</b>	61.2	80.6									
	$\omega$	<b>44.3</b>	<b>51.6</b>	44.3	51.6									
	$M_{\text{twr,FA}}$	<b>36.1</b>	<b>36.5</b>	36.1	36.5									
	$M_{\text{twr,SS}}$	<b>11.7</b>	<b>23.8</b>	11.7	23.8									

**Table 6.2** – Table comparing VAF values for simulations using short segments of data near certain mean wind speeds (first column). VAF values are compared for the linearised FAST models versus the linearised identified Hammerstein model. The first column also indicates how much data (min:sec) was available for identification in each wind speed range.



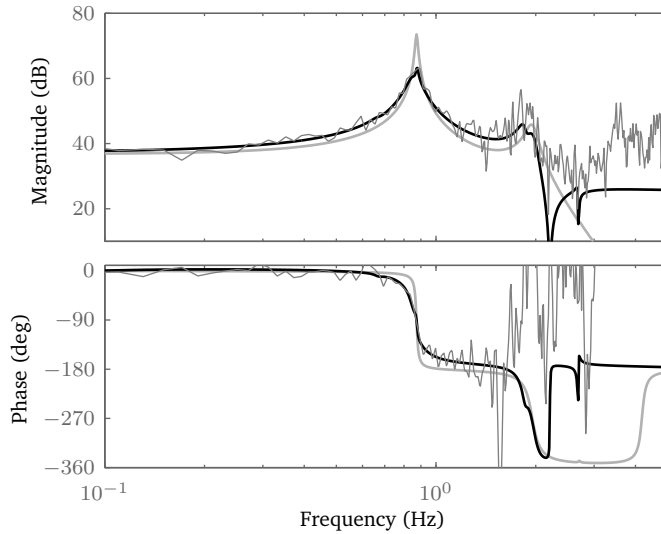
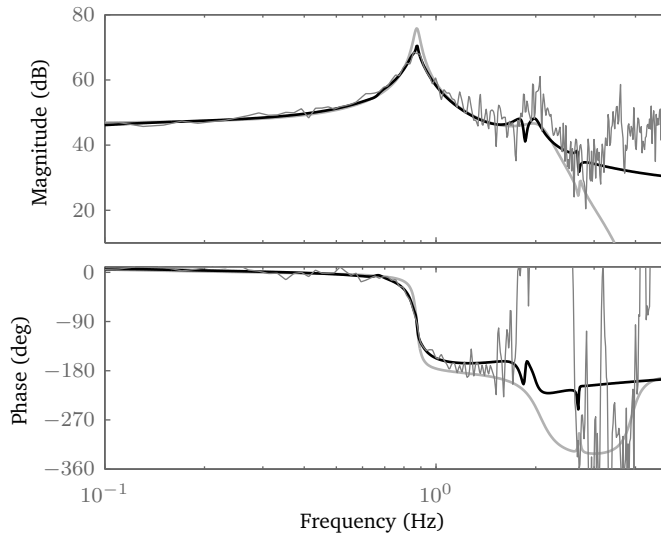
**Figure 6.13** – Results of a simulation of models linearised at  $V = 11$  m/s. The gray line is the measured signal, the black line is the linearised FAST model and the dashed line is the linearised Hammerstein model. The highlighted cells in Table 6.2 contain the VAF values for the data shown in this figure. Note, compared to Figure 6.12, that in this case the simulated signals have been high-pass filtered and hence the signals do not drift away from the measured signals.

with the values predicted by the FAST model. Note that there is a good agreement of the drive train damping predicted by FAST and the identified value. This is due to the fact that the damping in the FAST model was tuned on the basis of earlier results on the

(a) from pitch angle to generator speed ( $8 \text{ m/s}$ )(b) from pitch angle to generator speed ( $16 \text{ m/s}$ )

**Figure 6.14** – Comparison of linearised models obtained at  $V = 8 \text{ m/s}$  and  $V = 16 \text{ m/s}$  using linearisation (gray line) and identification (black line). Also shown is the spectral transfer function estimate (thin gray line).

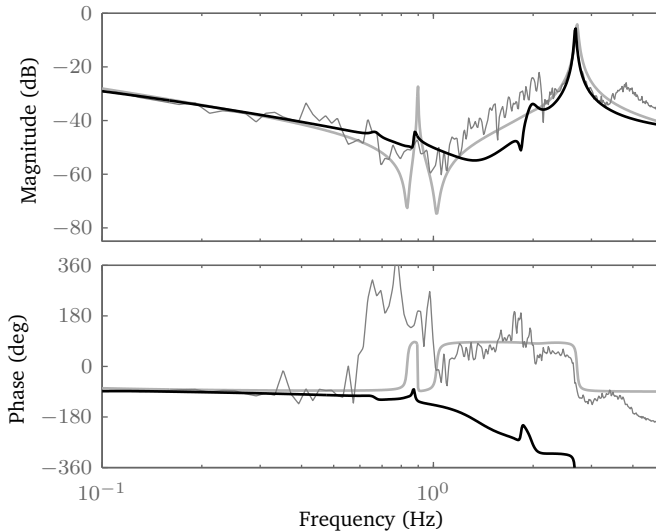
identification of the drive train dynamics.

(a) from pitch angle to tower fore-aft bending moment ( $8 \text{ m/s}$ )(b) from pitch angle to tower fore-aft bending moment ( $16 \text{ m/s}$ )

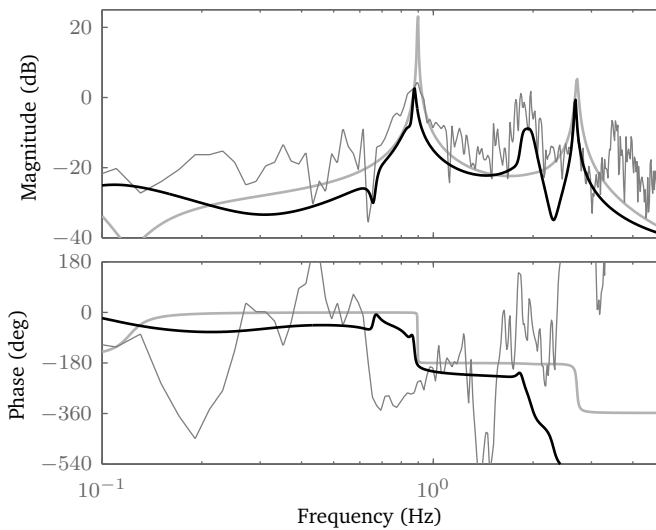
**Figure 6.15** – Comparison of linearised models obtained at  $V = 8 \text{ m/s}$  and  $V = 16 \text{ m/s}$  using linearisation (gray line) and identification (black line). Also shown is the spectral transfer function estimate (thin gray line).

## 6.5 Concluding remarks

In this chapter a practical method was presented to identify models of wind turbines based on measurement data. It was shown how standard identification tools can be tailored for



(a) from torque demand to generator speed



(b) from torque demand to tower side-side bending moment

**Figure 6.16** – Comparison of LTI models obtained using linearisation (gray line) and identification (black line). Also shown is the spectral transfer function estimate (thin gray line).

the application to wind turbines. The advantage of the method is that it can deal with data captured over a broad operating range while the turbine is under closed-loop control. Results of experiments of the CART 3 turbine show that the method gives promising results, both in terms of time-domain and frequency-domain validation. These results establish the

**Table 6.3** – Predicted and estimated modal parameters of the CART 3 turbine.

mode	predicted		estimated	
	frequency (Hz)	damping (–)	frequency (Hz)	damping (–)
1 <sup>st</sup> drive train	2.75	0.008	2.68	0.006
1 <sup>st</sup> tower fore-aft	0.87	0.010	0.79	0.528
1 <sup>st</sup> tower side-side	0.90	0.001	0.88	0.009

value of system identification in conjunction with first-principles modelling and as a basis for control design.

One assumption in the method presented here is that knowledge of the performance coefficients of the turbine is available, which is typically the case in practice. Efforts directed towards estimating those coefficients, for instance from LIDAR data, are therefore valuable in conjunction with the approach presented in this chapter.

# Conclusions and recommendations

In the introduction we argued that advanced control methods can lead to reductions in the cost of energy. We also discussed that accurate models of wind turbines are of fundamental importance to be able to design such advanced controllers for simultaneous power and load regulation. System identification was proposed as a powerful tool to obtain such models. We anticipated a number of challenges associated with applying system identification to wind turbines, to which we have sought solutions that are described in the different chapters of this thesis.

Starting with closed-loop identification of linear time invariant systems in Chapter 2, we have gradually tailored these methods to result in techniques to identify nonlinear wind turbine models in Chapter 6. Finally, in Chapter 4 we have demonstrated how the same identification framework can play a role in an adaptive predictive control setting. At several points along the way we have demonstrated the potential and added value of these identification methods on the basis of experimental data. In this chapter we will draw our conclusions and discuss some opportunities for future research in this area.

## 7.1 Conclusions

The main conclusion of this thesis is that accurate and data-driven modelling of wind turbines is indeed possible making use of a Hammerstein nonlinear modelling framework. In this framework all available measurement data can be used in an efficient and effective way since the model describes the turbine in all its operating conditions. Furthermore, we have shown that it is important to incorporate well-known system information, such as the static power curve, in the identification procedure to obtain accurate and reliable models.

The presented framework addresses most of the challenges listed in the introduction. The first challenge is that wind turbines and many other aeroelastic systems must operate in closed-loop. This can be addressed using the recent closed-loop subspace identification methods which have been presented in Chapter 2 using a common underlying framework. Among those methods is the closed-loop MOESP algorithm developed as part of this thesis. Based on a number of theoretical and experimental examples we have established the reliability and consistency of each of the methods. It turns out that the predictor-based subspace identification method (PBSID<sub>opt</sub>) and the closed-loop MOESP (CLMOESP) method perform very well in practical cases. An advantage of the CLMOESP method is that the order indication is crisper. This means that the user can more readily select possible state space system orders and evaluate the performance. The closed-loop identification framework in Chapter 2 forms the basis for all methods in subsequent chapters and readily extends to identification of Hammerstein models.

Besides the challenge arising from operating in closed-loop, wind turbines experience dominant periodic loads which further complicate reliable identification of linear time invariant models. In Chapter 3 we have extended the methods from Chapter 2 to deal with the periodic disturbances that are prevalent in wind turbine systems in a straightforward way. Doing so, allowed us to consistently identify the dynamics of such a system which would otherwise be very hard.

Another challenge mentioned in the introduction is the poor signal-to-noise ratio experienced when measuring in noisy conditions, for instance due to turbulent wind. Also, performing identification experiments is expensive and hence optimal use must be made of available time. The examples in Chapter 3 have largely been devoted to these aspects. We have demonstrated the potential of system identification on the basis of several realistic examples, giving further evidence for the reliability and performance of the methods in Chapter 2. First, we have performed “one-shot” controller design for an aeroelastic flutter control problem. Second, we have shown that system identification can support controller design, not just by providing a tool to deliver models of the system, but to examine the closed-loop performance. In the process of controller evaluation on the CART 3 turbine, the closed-loop characteristics could be determined to a large extent on the basis of 10 minute experiments. This example shows that performance can be judged reliably on the basis of short experiments, despite measuring under severe turbulence conditions. In all examples domain knowledge helped to understand by which mechanisms periodic disturbances are generated, how to design perturbation signals, how to designate relevant bandwidths in view of stochastic disturbances, how to choose input and output signal configurations and when to expect certain behaviour in identified models (e.g., nonminimum phase behaviour).

The linear identification framework of Chapter 2 can be combined with a predictive control law, to result in a combined framework for identification and control. This subspace predictive control (SPC) framework may be seen as a first step in bringing the fields of identification and control closer together. While the SPC framework was developed before in the literature, we have shown the results of applying it to two realistic experimental setups. In the process of developing a real-time feasible implementation we have developed a square root covariance filter with directional forgetting of past information. Such a scheme offers a safe way to discount old information compared to widespread recursive least-squares algorithms with exponential forgetting, by ensuring boundedness of the covariance matrix and retaining adaptivity. Two experimental cases demonstrate the capabilities of SPC. In the first example it was shown that without any prior model information, damping could be achieved on a flexible structure which switched between two radically different dynamic behaviours. In the second example it was shown that speed regulation of a scale wind turbine could be achieved, both in terms of tracking a reference as well as in terms of rejecting disturbances due to wind speed variations.

The identification methods presented thus far work for systems which operate steadily around a fixed operating point. This was valid for the CART 3 drive train dynamics in Chapter 3 since those dynamics can be considered to be almost LTI. If we consider the full dynamics of a wind turbine, however, the nonlinearity appears continuously due to the time-varying nature of the wind. Our main conclusion above is that this challenge can be addressed by extending the framework of Chapter 2 to Hammerstein nonlinear systems, which we have done in an intuitive way in Chapter 5. We also concluded that prior knowledge should be incorporated and have devoted Chapter 6 to making the approach of Chapter 5 practically feasible and to demonstrate this feasibility. To achieve this we have assumed that a good characterisation of the static performance of the turbine is available in order to make the algorithms more robust to poor signal-to-noise ratios.

Using experimental data from the CART 3 turbine extensive validation has been performed by comparing identified models to models from an aeroelastic code and by evaluating identified models on the basis of input-output data. The validation showed that the Hammerstein model structure could accurately describe the most important dynamics for overall regulation of the turbine and load control. In the case of the CART 3 turbine the identified models indicated that certain modes were not correctly modelled by the aeroelastic code in terms of frequency and damping. This is key information in establishing fundamental control system limitations in the form of unstable modes and nonminimum phase zeros. Open-loop time-domain simulations at various wind speeds showed that the identified models outperformed the first principles models in the majority of the cases.

By presenting the value of system identification and providing practical tools, we have bridged part of the gap between scientific theory and industrial practice. Over the past few years, wind turbine manufacturers have shown an increasing interest in applying

system identification in their control design approaches. While there will always be further challenges, as discussed in the next section, it is hoped that these tools can complement physical modelling in industrial practice.

## 7.2 Recommendations

While this thesis has addressed a number of challenges mentioned in the introduction, there are opportunities for further research.

In Chapter 6 we have successfully exploited the idea of representing a wind turbine system as a Hammerstein structure. Important follow-up steps would be to investigate application to data from a full-scale (possibly floating) wind turbine. This may imply that certain time varying modes related to the rotor become relevant. In such cases the extension of the LTI subsystem to a simple LPV structure could perhaps be helpful. While the focus in this thesis has been on models of the dynamics governing production and load control, the methods could be extended to simultaneously perform modal analysis. This would lead to a combination of the results in this thesis with the results of operational modal analysis, with the added feature of knowing relations between the input signals and the modes of the turbine.

In Chapter 2 we have organised many closed-loop subspace methods found in recent literature. These methods were presented in their basic forms. Recent years have seen a large interest in regularisation techniques. Some of these aim at imposing certain properties (stability, positive realness, polytopic constraints on pole locations) on identified models, while others aim at making the estimation process more reliable in the presence of noise. At some instances we have employed these techniques, but frequently have not found them to be very useful or necessary. An up-to-date categorisation of the literature on these ideas including an experimental justification could be valuable to be able to judiciously select a method for the problem at hand.

For control design purposes the positions of zeros in identified models are just as important as the positions of the poles. These zeros define fundamental limits on the control system performance, in particular taking into consideration that actuator inputs are always constrained. Accuracy of the identification of zeros is frequently disregarded, however, and efforts could be directed towards more accurate and reliable identification of zeros. A particular challenge is that, contrary to resonances, zeros block the transfer between inputs and outputs and hence the measured outputs at the frequencies of these zeros are dominated by noise. Appropriate perturbation signal design or incorporation of prior knowledge could be ways to solve this challenge.

Robust control methods require uncertainties to be specified in some way in order to design controllers with robust performance and stability. Uncertainty descriptions are hard to obtain for subspace methods, in particular due to the SVD model reduction step. While one could derive first order variance results for subspace methods, just as is typically done for the prediction error methods, it is unlikely that results will be reliable. Even in the case of prediction error methods, variance results strongly rely on the smoothness of the prediction error criterion and are only well-known to be reliable for linear least-squares formulations. It seems that development of tailored Monte Carlo methods and bootstrapping techniques could be much more useful, such that based on a limited number of independent identification experiments a good characterisation of uncertainties can be found.

In Chapter 4 we have made some efforts to show the potential of direct data-driven control in the form of SPC. While these results are interesting, it is very hard to establish the reliability of SPC. In its current state, it can only be considered for non-safety-critical applications, in condition monitoring applications, or as a supervisory system, for instance to generate optimal trajectories. Furthermore, the framework is limited to systems that are essentially linear and, at most, slowly time varying. Extensions to certain nonlinear systems, such as have been made for Hammerstein and LPV systems, and a further fusion between obtaining a model and designing a controller are of interest to broaden the scope of these methods.



# Parameterizing an orthogonal matrix

Parameterizing a matrix  $Q(\vartheta) \in \mathbb{R}^{m \times n}$  with  $m > n$  as a matrix with orthonormal columns has the advantages that the matrix always has condition number one, its pseudoinverse is given by its transpose, it requires fewer parameters than a full parameterisation and all parameters  $\vartheta$  can be restricted to the interval  $[0, 2\pi)$ .

Considering the QR factorisation of a tall matrix  $A \in \mathbb{R}^{m \times n}$  into an orthogonal matrix  $\tilde{Q} \in \mathbb{R}^{m \times m}$  and an upper-triangular factor  $\tilde{R} \in \mathbb{R}^{m \times n}$ :

$$A = \tilde{Q}\tilde{R},$$

we can find a sequence of  $mn - \frac{1}{2}(n+1)n$  elementary Givens rotations that achieves this factorisation (Golub and Van Loan, 1996, Section 5.2.3):

$$\tilde{Q}^T = \prod_{l=1}^n \prod_{k=m}^{l+1} G_{kl}, \quad \text{such that } \tilde{Q}^T A = \tilde{R},$$

where  $G_{kl}$  is an elementary Givens rotation of the form

$$G_{kl} = I_{k-2} \oplus \begin{bmatrix} \cos(\vartheta_i) & \sin(\vartheta_i) \\ -\sin(\vartheta_i) & \cos(\vartheta_i) \end{bmatrix} \oplus I_{m-k},$$

where  $\oplus$  denotes the direct sum of matrices (i.e., diagonal concatenation). The representation thus found for the  $m$ -by- $n$  matrix  $\tilde{Q} = \tilde{Q}(\vartheta)$  is defined in terms of the  $mn - \frac{1}{2}(n+1)n$  parameters in  $\vartheta$ . The derivative of  $\tilde{Q}(\vartheta)$  with respect to one of the elements of  $\vartheta$  is easily found by replacing the elementary rotation corresponding to that element,  $\vartheta_i$ , by its partial derivative, given by:

$$\frac{\partial G_{kl}}{\partial \vartheta_i} = I_{k-2} \oplus \begin{bmatrix} -\sin(\vartheta_i) & \cos(\vartheta_i) \\ -\cos(\vartheta_i) & -\sin(\vartheta_i) \end{bmatrix} \oplus I_{m-k}.$$

We only need to consider the “thin” QR factorisation of  $A$ :

$$A = QR,$$

with  $\tilde{Q} \in \mathbb{R}^{m \times n}$  and  $\tilde{R} \in \mathbb{R}^{n \times n}$ . This is achieved by retaining only the first  $n$  columns of  $\tilde{Q}(\vartheta)$ .



# Floating wind turbines and fundamental limitations<sup>1</sup>

Wind energy is a clean, renewable and extremely fast growing form of electricity generation and the potential to install turbines deep offshore is only just being realised. The vast majority of commercial offshore turbines have foundations on the seabed thereby restricting the depths at which offshore farms can be installed. In an attempt to facilitate access to a potential multi-TeraWatt resource, a number of floating concept wind turbines have emerged. In this reproduction of a recent tutorial paper we review the control challenges associated with the design of floating turbines and summarise recent developments in the area. Of particular interest is a fore-aft oscillation induced by attempting to regulate the generator speed to its rated value. We conclude with a discussion of how the control problems presented are likely to change with increasing turbine size and structural flexibility.

## B.1 Introduction

Recent years have seen an increasing interest in development of concepts for offshore wind turbines. Typically, the most powerful, sustained and low-turbulent winds can be found at sea. Furthermore, offshore sites suffer less from complicated political, societal and environmental issues related to visual impact, noise emission and acquiring the required real estate (surface area).

To fully access the multi-TeraWatt offshore resource (Roddier and Weinstein, 2010), wind turbine deployment needs to be viable in deep waters and at sites with loose seabeds. In the former, monopiled solutions are not cost effective (Roddier, Cermelli, Aubault et al., 2010); and in the latter, they are not possible – a realisation that has motivated the development of a number of floating wind turbine concepts, see for example (Nielsen, Hanson and Skaare, 2006; Roddier, Cermelli, Aubault et al., 2010). Despite skepticism from some quarters, the transition to floating offshore structures is a natural one, and has been made previously by the oil and gas industry with considerable success (Roddier and Weinstein, 2010). The installation and maintenance of platform-based floating turbines carries the considerable advantage over both monopile and spar-buoy type concepts that both processes can be performed onshore circumventing the need for extraordinarily expensive access vessels (Roddier, Cermelli, Aubault et al., 2010).

The designers of floating wind turbines are faced with some formidable challenges, most notably the considerable structural vibrations induced by wind and wave loads (Lackner, 2009). To sustain these high loads, offshore turbines tend to be heavier, and therefore more expensive, than their onshore counterparts. With capital expenditure dominating wind power plant costs (Fingersh, Hand and Laxson, 2006), any efforts to reduce these material weights leads directly to a reduction in the cost of energy, thereby motivating the search for load reduction via advanced control. Aside from the necessary safety systems, the control objectives can classically be stated as achieving optimal power production whilst

---

<sup>1</sup>This appendix is a reprint of an article published elsewhere: G. J. van der Veen, I. A. Couchman and R. O. Bowyer (2012). 'Control of floating wind turbines'. In: *Proceedings of the 2012 American Control Conference, Montreal, QC, Canada*

keeping the forces and moments that the components experience to a minimum (Bianchi, De Battista and Mantz, 2010). In this section we focus on the additional challenges faced when designing a controller for power production of a floating wind turbine.

In Section B.2 simplified wind turbine dynamics are presented to facilitate the demonstration of the control issues. The operational regions are described in Section B.3 along with a detailed discussion of the control design problems associated with regulating generator speed to the rated value, whilst producing nameplate power. Section B.4 compares and contrasts the published solutions to such problems, whilst Section B.5 gives a discussion of how the problems will scale to tomorrow's larger, more aerodynamically efficient turbine designs.

## B.2 Dynamics

The combined torque  $T_a$  (Nm) generated by three blades of length  $R$  (m), pitched at  $\beta$  ( $^\circ$ ), rotating at  $\Omega$  (rad/s) in an apparent wind of speed  $V$  (m/s) is defined:

$$T_a(\Omega, V, \beta) := \frac{1}{2}\pi R^3 \rho C_Q(\Omega, V, \beta) V^2,$$

where  $C_Q : \mathbb{R}_+ \times \mathbb{R}_+ \times \mathbb{R} \rightarrow \mathbb{R}_+$  is the torque coefficient defined by the blade profile<sup>2</sup>,  $\mathbb{R}, \mathbb{R}_+$  the sets of real and non-negative real numbers respectively and  $\rho$  (kg/m<sup>3</sup>) is the air density (Burton, Sharpe, Jenkins et al., 2001, p. 6).

The aerodynamic torque is transferred to the electrical generator through the gearbox. For simplicity we consider an ideal gearbox with gear ratio  $R_g$ , and hence the power transfer is lossless and the high speed shaft rotates at  $R_g \Omega$  (rad/s).

The stator side of the generator provides a torque against the motion of  $T_g$  (Nm) and hence the power generated by the system  $P$  is defined  $P := T_g R_g \Omega$ . If the (scaled) electrical and aerodynamic torques are not equal, the rotor will accelerate or decelerate:

$$J \frac{d\Omega}{dt} = T_a(\Omega, V, \beta) - R_g T_g - \alpha \Omega,$$

where  $\alpha$  is the viscous friction and  $J$  the mass moment of inertia of the rotating parts (Soltani, Wisniewski, Brath et al., 2011).

A side effect of extracting power from the wind is the thrust force  $F_a$  (N) on the turbine defined:

$$F_a(\Omega, V, \beta) := \frac{1}{2}\pi R^2 \rho C_T(\Omega, V, \beta) V^2,$$

where  $C_T : \mathbb{R}_+ \times \mathbb{R}_+ \times \mathbb{R} \rightarrow \mathbb{R}_+$  is the thrust coefficient, again inferred from the blade profile (Burton, Sharpe, Jenkins et al., 2001, p. 35). The thrust force results in a motion of the rotor from both the platform movement and flexibility of the tower. The dynamics of nacelle fore-aft position  $z$  (m) is represented as the superposition of a tower bending mode and a platform tilting mode, each of which can be expressed as a second order system with associated natural frequency and damping ratio:

$$\begin{aligned} \ddot{z}_1(t) + 4\pi\zeta_1 f_1 \dot{z}_1(t) + 4\pi^2 f_1^2 z_1(t) &= F_a(\Omega(t), V(t), \beta(t)), \\ \ddot{z}_2(t) + 4\pi\zeta_2 f_2 \dot{z}_2(t) + 4\pi^2 f_2^2 z_2(t) &= F_a(\Omega(t), V(t), \beta(t)), \\ z(t) &= a_1 z_1(t) + a_2 z_2(t), \end{aligned}$$

where the parameters  $\zeta_1, \zeta_2, f_1, f_2$  denote the damping and natural frequency (Hz) of the platform (subscript 1) and tower (subscript 2) respectively, and  $a_1, a_2$  represent the contribution of the two modes to the nacelle motion, see Figure B.1.

<sup>2</sup>The torque coefficient  $C_Q$  is written as a function of rotor speed and wind speed as opposed to the more commonly used tip speed ratio  $\lambda := \frac{\Omega R}{V}$  for notational ease when considering linearisations in Sections III and V.

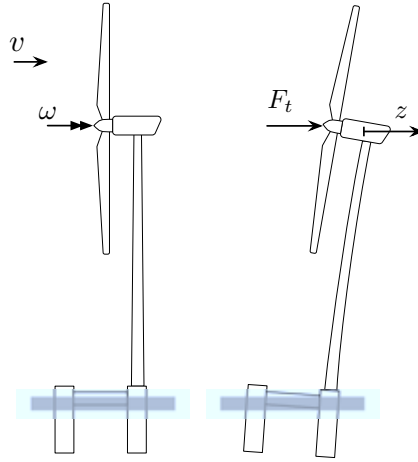


**Figure B.1** – Floating wind turbine configuration. The nacelle displacement is caused by platform tilt and tower bending.

A motion of the nacelle forwards increases the apparent rotor wind speed, thereby affecting both the driving torque and thrust force:

$$\ddot{z}_1 + 4\pi\zeta_1 f_1 \dot{z}_1 + 4\pi^2 f_1^2 z_1 = F_a(\Omega, \bar{V} - \dot{z}, \beta), \quad (\text{B.1a})$$

$$\ddot{z}_2 + 4\pi\zeta_2 f_2 \dot{z}_2 + 4\pi^2 f_2^2 z_2 = F_a(\Omega, \bar{V} - \dot{z}, \beta), \quad (\text{B.1b})$$

$$z = a_1 z_1 + a_2 z_2, \quad (\text{B.1c})$$

$$J \frac{d\Omega}{dt} + R_g T_g + \alpha \Omega = T_a(\Omega, \bar{V} - \dot{z}, \beta), \quad (\text{B.1d})$$

where  $\bar{V}$  is the mean wind speed and  $\dot{z}$  is the component resulting from the motion of the nacelle.

## B.3 Control objectives

### B.3.1 Regions of operation

The aim of a wind turbine is to maximise the power produced subject to constraints on generator speed and power. As a result, the operation of the wind turbine can be divided into three regions (Pao and Johnson, 2009). In low wind speeds, prior to either the generator speed or the power reaching their limits, the aim is to maximize power. In order to do this, the pitch angle and electrical torque are controlled to operate the blades at their most aerodynamically efficient. In high winds, with both generator speed and power at their respective limits, the goal is to adjust the pitch to maintain these values. The produced power can be written

$$P = \frac{1}{2} \pi R^3 \rho \Omega C_Q(\Omega, V, \beta) V^2 = \frac{1}{2} \pi R^2 \rho C_P(\lambda, \beta) V^3,$$

where  $\lambda := \Omega R / V$  is the tip-speed ratio and  $C_P(\lambda, \beta) := \lambda C_Q(\lambda V / R, V, \beta)$ , see (Burton, Sharpe, Jenkins et al., 2001, p. 6). Figure B.2 shows how in full load the pitch can be changed to reduce aerodynamic efficiency and maintain power at its rated value. A number of transition strategies have been proposed for the interval between these regions, for an exposition see (Bianchi, De Battista and Mantz, 2010).

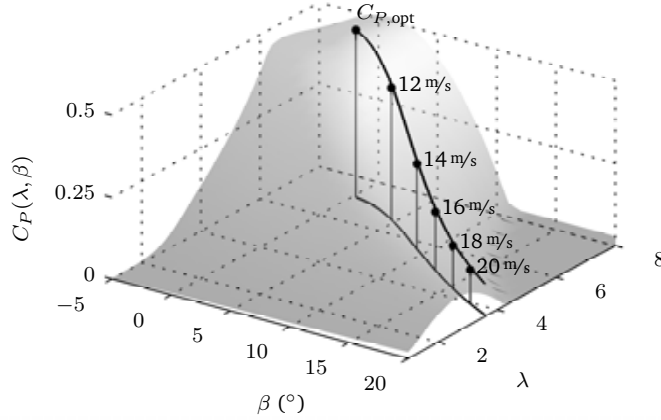


**Figure B.2** – The power coefficient curve and a representation of the above-rated operating strategy required to maintain  $P = P_{\text{rated}}$ . These data have been scaled for intellectual property reasons but are typical for most utility-scale wind turbines.

### B.3.2 Control in above rated conditions

The main problem associated with the control of floating wind turbines concerns the tilt stability in full load (Larsen and Hanson, 2007). To understand this problem, we must first consider the effect of changing wind speed on the steady state thrust. The steady state thrust curve, an example of which is shown in Figure B.3, is defined, in the above rated region, as the thrust required at a given wind speed to produce rated power at constant rated generator speed. The steady state pitch varies along the operating curve to achieve constant power production:

$$\begin{aligned} dP &:= \Omega_{\text{rated}} \left( \frac{\partial T_a}{\partial V} \delta V + \frac{\partial T_a}{\partial \beta} \delta \beta \right) = 0, \\ \implies \delta \beta &= -\frac{\partial T_a}{\partial V} \left( \frac{\partial T_a}{\partial \beta} \right)^{-1} \delta V, \end{aligned}$$

where  $dP$  denotes the total derivative of  $P$ , see (Polyanin and Zaitsev, 2003), and the partial derivatives are evaluated along the equilibrium trajectory. The variation of pitch to maintain rated power yields a thrust curve with the gradient  $\frac{dF_a}{dV}$  derived as:

$$\begin{aligned} dF_a &:= \frac{\partial F_a}{\partial V} \delta V + \frac{\partial F_a}{\partial \beta} \delta \beta, \\ &= \left( \frac{\partial F_a}{\partial V} - \frac{\partial F_a}{\partial \beta} \frac{\partial T_a}{\partial V} \left( \frac{\partial T_a}{\partial \beta} \right)^{-1} \right) \delta V, \\ \implies \frac{dF_a}{dV} &= \frac{\partial F_a}{\partial V} - \frac{\partial F_a}{\partial \beta} \frac{\partial T_a}{\partial V} \left( \frac{\partial T_a}{\partial \beta} \right)^{-1}. \end{aligned} \quad (\text{B.2})$$

It is clear from Figure B.3 that  $\frac{dF_a}{dV} < 0$  for all  $V$  above rated, a condition that is necessarily true for all conventional pitch-to-feather wind turbines (Burton, Sharpe, Jenkins et al., 2001).

In normal operation at above rated wind speed, the turbine nacelle will move forwards and backwards. When the turbine is moving forwards, the rotor sees a slightly higher relative wind speed and, if the generator speed controller is faster than the motion, the

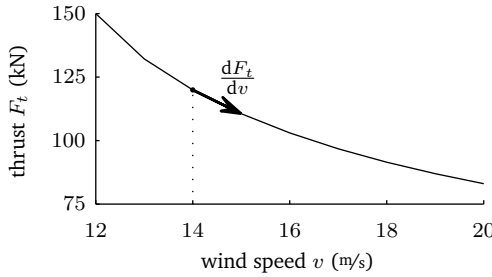


**Figure B.3** – Steady-state values of rotor thrust  $F_a$  as a function of wind speed  $V$ , indicating the gradient of the steady-state curve.

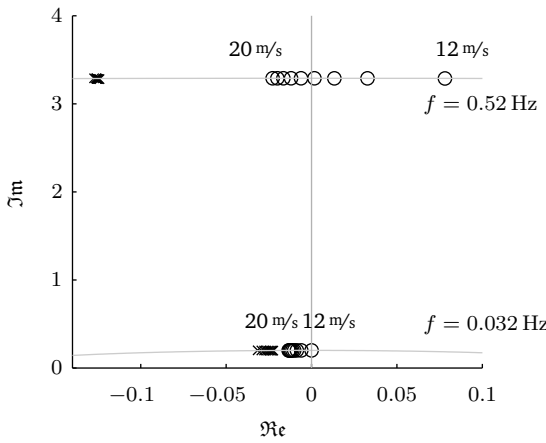


**Figure B.4** – Poles and zeros in the dynamics from pitch to generator speed as a function of wind speed due to the tower bending mode (top) and the platform tilt mode (bottom). Only the upper half of the complex plane is shown.

blades are pitched to prevent the generator speed from growing. As  $\frac{dF_a}{dV} < 0$ , this reduces the rotor thrust, thereby causing the nacelle to move further forwards. The converse is true when the nacelle is moving backwards. This problem is known in control circles within the wind turbine community as the ‘*negative damping problem*’ (Larsen and Hanson, 2007).

The problem can be viewed analytically by considering a linearised model of (B.1), with an example pole-zero map shown in Figure B.4. For commercial reasons, the parameters are not specific to a given turbine or floating foundation, rather certain quantities such as natural frequencies are selected to be in the vicinity of existing published works (Lackner and Rotea, 2011; Namik and Stol, 2011) and efficiency tables from Jonkman, Butterfield, Musial et al. (2009). It is well-known in control theory that the closed-loop poles of a system migrate towards the open-loop zeros as the feedback gain is increased. On the basis of the pole-zero configuration in Figure B.4 it becomes clear that as the feedback gain is increased the nacelle fore-aft oscillation becomes less damped, whilst the generator speed tracking improves. In the case where the zeros are in the right half plane, which for the model visualised in Figure B.4 is true only for the tower zeros, the frequencies provide bandwidth limits on the pitch to generator speed loop (Åström, 2000). In this example the control system bandwidth must be smaller than the frequency of the tower to avoid instability.

The phenomenon of negative damping is in no way unique to floating turbines. However, in turbines with fixed foundations, it is less of a problem because the lowest frequency eigenmode is that of the first tower fore-aft mode. The generator speed controller can be designed to have a low gain at or above this frequency with a higher gain for lower frequencies. This implies that the generator speed can not reject disturbances at or above the lowest fore-aft mode. Proportional-integral (PI) controllers are commonplace with a variety of gain-scheduling schemes proposed to address the parameter varying system nature (Bianchi, De Battista and Mantz, 2010). In other words, the speed controller is designed to ensure tracking of signals lower than the tower fore-aft natural frequency. This results in a generator speed response with a maximum over-shoot of less than the generator speed limit in most operational cases (Burton, Sharpe, Jenkins et al., 2001, p. 213). With floating turbines, the lowest natural frequency is that of the platform tilt resonance and this is typically an order of magnitude lower than that of the tower (Nielsen, Hanson and Skaare, 2006). If one were to simply detune the generator speed controller such that the generator speed only tracks signals lower than the platform natural frequency, the generator would regularly exceed its over-speed limit in normal operation. This is illustrated in Figure B.5 for the example turbine in this paper. A more advanced solution is therefore necessary.

## B.4 Control of tilt oscillations

### B.4.1 Passive solutions

Typically in structural design, one way to reduce an oscillation is to include a tuned mass damper and indeed these have been considered and are implemented in some onshore wind turbines (Leithead and Dominguez, 2006). However, tuned resonators are at their most effective for sharp peaks whilst the fore-aft resonant peak is broad and so they are shown to have only limited benefit (Leithead and Dominguez, 2006). It may also be an option to add hydrodynamic damping to the motion of the platform in the water although this may represent a significant cost.

### B.4.2 Active solutions

Having briefly detailed passive solutions, we now turn our attention to active alternatives using blade pitch actuators as the control input. We constrain our review to collective blade pitch strategies as the problem concerns the thrust on the turbine as opposed to its out of plane moments. Benefits from individual blade pitch algorithms are typically seen in side-side tower motions and blade loads and are similar for onshore and offshore turbines. The interested reader can discover more in Lackner (2009).

As discussed in Section B.3.2, poor generator speed tracking results in frequent shutdowns resulting from the generator speed reaching its limit. One way to circumvent this problem is to detune the existing PI controller on generator speed such that the bandwidth is lower than the natural frequency of the platform; and also reduce the rated generator speed, see (Jonkman, 2008). This means that larger deviations of generator speed can be tolerated without shutdown, although a reduction in the power produced and an increase in its standard deviation is implied and therefore this solution is neither economically viable nor appreciated by the electricity generating company.

A number of proposed solutions exploit information about the tower fore-aft motion. In the simplest form, this purely involves appending the pitch demand from the generator speed controller with a gain multiplied by the nacelle fore-aft velocity, an approach sometimes referred to as '*parallel compensation*', (Leithead and Dominguez, 2006) see Figure B.6. To analyse this strategy, consider the inner transfer function, labeled  $G(s)$  on Figure B.6, and how it evolves with increasing velocity feedback gain,  $k_t$ , see Figure B.7.

From Figure B.7 it is clear that an increasing gain moves the platform and nacelle poles away from their respective zeros. This leads to poorer generator speed tracking in the frequency region of the fore-aft motions, but an increased damping of nacelle oscillation.

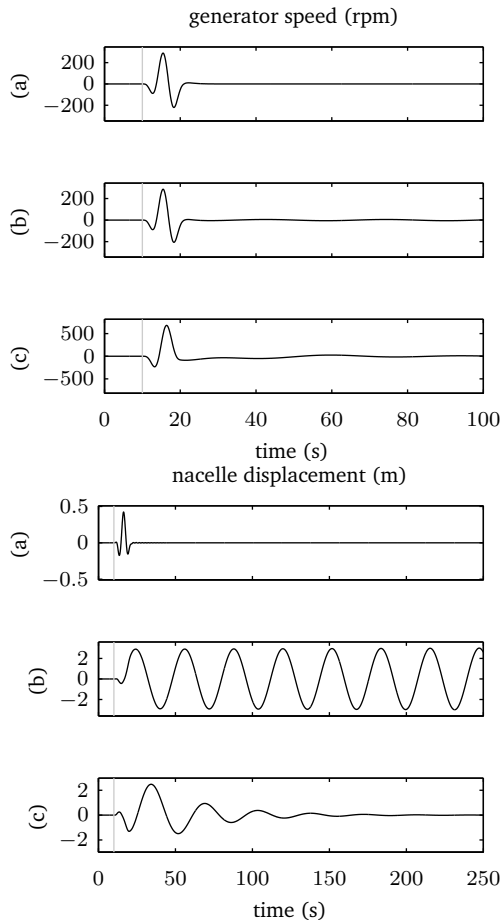


**Figure B.5** – Generator speed (left) and nacelle displacement (right) in response to an IEC class III extreme operating gust initiated at  $t = 10$  s ( $\bar{V} = 12$  m/s). Cases: **(a)** on-shore turbine, conventional controller, **(b)** floating turbine, conventional controller. **(c)** floating turbine, reduced bandwidth controller. Note the different scales. The bandwidth of the conventional controller is  $f_{bw} = 0.22$  Hz whilst that of the reduced bandwidth controller is  $f_{bw} = 0.02$  Hz.

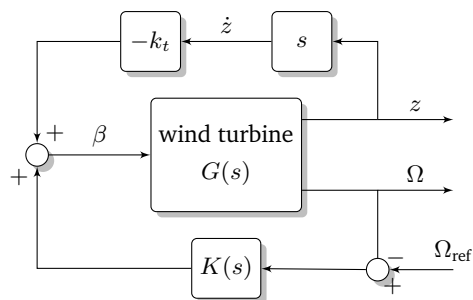


**Figure B.6** – Parallel modification to generator speed controller

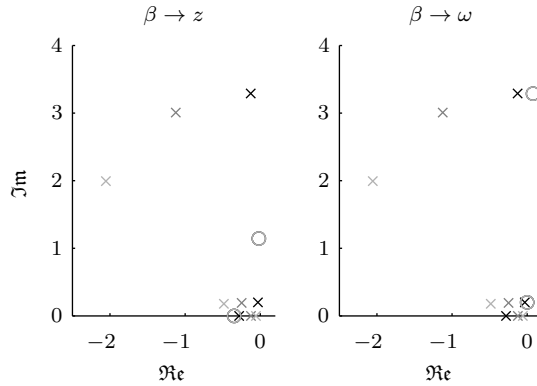


**Figure B.7** – Pole zero maps showing the effect of velocity feedback on the open-loop system ( $k_t = 0$  (black),  $k_t = 5$  (gray),  $k_t = 10$  (light gray)). Left figure: pitch to nacelle displacement. Right figure: pitch to generator speed.

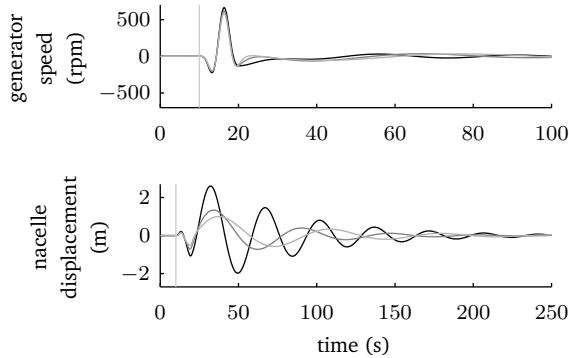


**Figure B.8** – Generator speed (top) and nacelle displacement (bottom) in response to an IEC class III extreme operating gust initiated at  $t = 10$  s ( $\bar{V} = 12$  m/s). Velocity feedback with  $k_t = 0$  (black),  $k_t = 5$  (gray) and  $k_t = 10$  (light gray).

Specific versions of this solution are discussed in a number of sources under a variety of guises. In Larsen and Hanson (2007), the gain  $k_t$  is chosen such that the generator speed loop does not respond at all to deviations resulting from motion of the nacelle, whilst Jonkman (2008) discusses the option to have both a higher and lower gain to change the priority of generator speed tracking and nacelle velocity damping.

Another way to design such a controller would be to consider the single input two output system mapping collective blade pitch angle to generator speed and nacelle velocity. Clearly, a single control input cannot independently control two outputs. Using a squaring down approach (Goodwin, Graebe and Salgado, 2001), the control objective can be made to design a controller to minimise the output  $\tilde{y} := c_1\Omega + c_2\dot{z}$  where  $c_1, c_2 \in \mathbb{R}$  are weighting constants. Notice that  $\{c_1, c_2\}$  can now be selected such that the loop  $\beta \mapsto \tilde{y}$  has zeros far into the left half plane (i.e., minimum-phase), this does not imply that the performance constraints on generator speed tracking can be circumvented. The loop  $\beta \mapsto \Omega$  still has the same zeros, and these still define the restrictions on the closed loop (Goodwin, Graebe and Salgado, 2001).

Published solutions taking the parallel compensation form vary with regards to how the

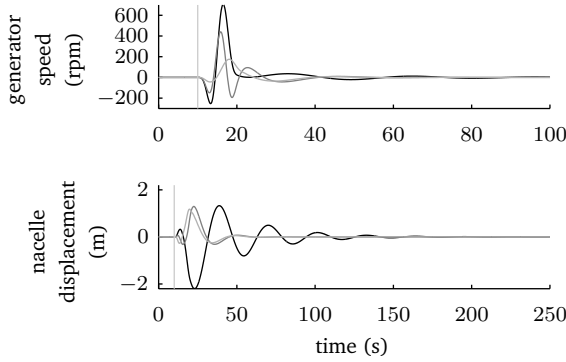


**Figure B.9** – Generator speed (top) and nacelle displacement (bottom) in response to an IEC class III extreme operating gust initiated at  $t = 10$  s ( $\bar{V} = 12$  m/s). LQR with control weights:  $R = 10^{12}$  (black),  $R = 10^3$  (gray) and  $R = 10^0$  (light gray).

nacelle velocity is obtained. In Jonkman (2008) an accelerometer is fitted to the nacelle and the signal integrated whilst in Lackner and Rotea (2011) the velocity is inferred from information about the platform tilt angle. A range of filters for dealing with these real sensors have been proposed, see for example (Larsen and Hanson, 2007).

In order to give an indication of the performance restrictions implied by the sensors, we consider a full state feedback solution in the form of a linear quadratic regulator with integral action. The cost matrices  $Q$  and  $R$  were selected to reflect both the scale of the signals and the relative importance of a lack of deviations in their respective values. Notice that we now have a tall transfer function, and that we cannot hope to control each of the measured outputs independently at all times (Goodwin, Graebe and Salgado, 2001, pp. 796–800). The LQR design essentially results in a form of soft-sharing control (Goodwin, Graebe and Salgado, 2001, pp. 796–800). An interesting observation is that the MIMO system does not have any transmission zeros, but that this does not imply an absence of performance limitations. Non-minimum phase zeros still lie between the pitch and generator speed, thus irrespective of information from extra sensors, the performance limitations due to that zero still remain (Åström, 2000; Goodwin, Graebe and Salgado, 2001). That is not to say that extra information cannot give improved performance, it simply says that the bandwidth of the generator speed response is still limited by the frequency of the right half plane zeros. The closed-loop responses of the LQR solution are shown in Figure B.9, with the conclusion being that increased measurement will only lead to a marginal increase in performance. This suggests that an additional control degree of freedom may be required, in the form of an additional actuator.

## B.5 Future turbines

From the analysis of the linearised dynamics in Section B.3.2, it is clear that the position of the platform zeros defines the difficulty of the problem and the limit of the efficacy of the solution. In order to consider quantitatively what affects the position of these zeros, and thereby examine how the control problem is likely to evolve, we consider a simplified model linearised about  $\Omega = \Omega_{\text{rated}}$ ,  $\dot{z} = 0$ ,  $z = \bar{z}$ ,  $\beta = \bar{\beta}$ , where  $\bar{\cdot}$  denotes the equilibrium value, assuming a stiff tower for brevity:

$$\begin{aligned} \ddot{\delta z}_1 + 4\pi\zeta_1 f_1 \dot{\delta z}_1 + 4\pi^2 f_1^2 \delta z_1 &= \frac{\partial F_a}{\partial \Omega} \delta \Omega - \frac{\partial F_a}{\partial V} a_1 \delta z_1 + \frac{\partial F_a}{\partial \beta} \delta \beta, \\ J \delta \dot{\Omega} + \alpha \delta \Omega &= \frac{\partial T_a}{\partial \Omega} \delta \Omega + \frac{\partial T_a}{\partial V} a_1 \delta z_1 + \frac{\partial T_a}{\partial \beta} \delta \beta, \end{aligned}$$

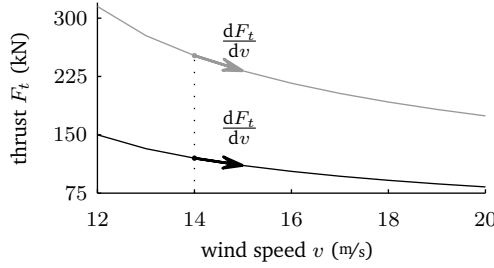


**Figure B.10** – Figure showing the effect on the thrust curve of increasing rotor size and power to maintain a constant rated wind speed. Light gray is the larger turbine with the greater nameplate power.

where  $\delta z_1, \delta\Omega, \delta\beta$  represent the deviation of  $z_1, \Omega, \beta$  from their equilibrium values, respectively. By taking Laplace transforms, substituting for  $\delta z_1$  and using (B.2), the following transfer function from pitch to generator speed can be obtained:

$$\frac{\Omega(s)}{B(s)} = \frac{\frac{\partial \tau}{\partial \beta} s^2 + \frac{\partial T_a}{\partial \beta} \left( 4\pi\zeta_1 f_1 + a_1 \frac{dF_a}{dV} \right) s + 4\pi^2 f_1^2 \frac{\partial T_a}{\partial \beta}}{\left( s^2 + \left( 4\pi\zeta_1 f_1 + a_1 \frac{\partial F_t}{\partial V} \right) s + 4\pi^2 f_1^2 \right) \left( Js + \alpha - \frac{\partial T_a}{\partial \Omega} \right) - s \frac{\partial T_a}{\partial V} \frac{\partial F_a}{\partial \Omega}},$$

where  $\Omega$  and  $B$  denote the Laplace transforms of  $\delta\Omega$  and  $\delta\beta$  respectively.

Typically, it is fair to assume that:

$$16\pi^2 f_1^2 \gg \left( 4\pi\zeta_1 f_1 + a_1 \frac{dF_a}{dV} \right)^2, \quad (\text{B.3})$$

and this is reflected by the complex nature of the platform zeros and the fact that their frequency is almost exactly the platform natural frequency, see Figure B.4. In this case, the zeros of the transfer function can be well approximated by

$$z \approx -\frac{1}{2} \left( 4\pi\zeta_1 f_1 + a_1 \frac{dF_a}{dV} \right) \pm j2\pi f_1.$$

Should these zeros be in the right half plane, they provide hard limits on the bandwidth of the full load controller. Even in the left half plane, their position determines the amount of fore-aft oscillation that must be tolerated in order to achieve a given performance level of generator speed tracking. Clearly, increasing the damping  $\zeta_1$  lessens the problem whilst increasing the gradient of the steady state thrust curve makes it worse.

From Figure B.3, it can be seen that the curve is less steep at higher wind speeds and therefore the problem is typically most pronounced in just above rated conditions. We now consider how the problem will evolve for the next generation of wind turbines, by considering a simplified relationship between  $C_Q$  and  $C_T$  via the axial induction factor (Burton, Sharpe, Jenkins et al., 2001). Figure B.10 shows the effect on the thrust curve of increasing rotor size and power to maintain a constant rated wind speed.

- Increased rotor size. Larger rotors typically lead to a better investment because they can extract more power for the same tower height (Leithead, 2007), but this will make the problem more severe because the magnitude of the gradient  $\frac{dF_a}{dV}$  increases, see Figure B.10, thereby increasing the real part of the platform zeros.
- Taller towers. Taller towers tend to give the turbine access to less turbulent air and a smoother resource due to the shape of the boundary layer (Leithead, 2007).

However, these taller towers are likely to lead to lower natural frequencies of both tower and platform. This creates a more restrictive problem because it is these natural frequencies that define the bandwidth limitations on the generator speed controller.

## B.6 Conclusions

In this appendix, we have described some of the control issues associated with designing a floating wind turbine. Solutions from the literature have been discussed and their relative efficacy demonstrated on a simple numerical example. These solutions all relate to using the collective blade pitch angle as the control input. Additional control inputs may prove advantageous, a promising option being active mass dampers. Currently, they are not considered due to their cost and need for infeasible mechanical travel (Lackner and Rotea, 2011).

Further improvements could be made by controlling also the electrical torque  $T_g$  in full load as in Lackner (2009). This is typically reserved for damping oscillations in the drive-train (Bossanyi, 2003b), although this happens considerably faster than the fore-aft motion of interest. Another promising avenue for research is the use of active mass dampers. Currently, they are not considered due to their cost and need for infeasible mechanical travel (Lackner and Rotea, 2011). In the final section of this appendix some insight was given into how the problem is likely to scale to the next generation of larger, taller and more efficient wind turbine.



# Bibliography

- Akaike, H. (1967). 'Some problems in the application of the cross-spectral method'. In: *Spectral Analysis of Time Series*. Ed. by B. Harris. Wiley, pp. 81–107.
- Alenany, A., H. Shang, M. Soliman and I. Ziedan (Aug. 2011). 'Brief paper - improved subspace identification with prior information using constrained least squares'. In: *Control Theory Applications, IET* 5.13, pp. 1568–1576.
- Anderson, E., Z. Bai, C. Bischof, S. Blackford, J. Demmel, J. Dongarra, J. Du Croz, A. Greenbaum, S. Hammarling, A. McKenney and D. Sorensen (1999). *LAPACK Users' Guide*. Third. Philadelphia, PA: Society for Industrial and Applied Mathematics.
- Åström, K. J. and B. Wittenmark (1994). *Adaptive Control*. 2<sup>nd</sup> edition. Prentice Hall.
- Åström, K. J. (2000). 'Limitations on control system performance'. In: *European Journal of Control* 6:1, pp. 2–20.
- Aviation Investigation Report – Loss of Rudder in Flight* (2005). Report Number A05F0047. Transportation Safety Board of Canada. URL: <http://publications.gc.ca/site/eng/318053/publication.html>.
- Baars, G. E. van and P. M. M. Bongers (Dec. 1994). 'Closed loop system identification of an industrial wind turbine system: experiment design and first validation results'. In: *Proceedings of the 33rd IEEE Conference on Decision and Control, 1994*. Vol. 1, 625–630 vol.1.
- Baars, G. E. van, H. Mosterd and P. M. M. Bongers (Dec. 1993). 'Extension to standard system identification of detailed dynamics of a flexible wind turbine system'. In: *Proceedings of the 32nd IEEE Conference on Decision and Control, 1993*. 3514–3519 vol.4.
- Bai, E.-W. (1998). 'An optimal two-stage identification algorithm for Hammerstein-Wiener nonlinear systems'. In: *Automatica* 34.3, pp. 333–338.
- Barlas, T. K. and G. A. M. van Kuik (2007). 'State of the art and perspectives of smart rotor control for wind turbines'. In: *Journal of Physics, Conference series: The Science of Making Torque from Wind* 75.012080.
- Barlas, T. K. and G. A. M. van Kuik (2010). 'Review of state of the art in smart rotor control research for wind turbines'. In: *Progress in Aerospace sciences* 46.1, pp. 1–27.
- Barlas, T. K., G. J. van der Veen and G. A. M. van Kuik (2012). 'Model predictive control for wind turbines with distributed active flaps: incorporating inflow signals and actuator constraints'. In: *Wind Energy* 15.5, pp. 757–771.
- Basualdo, S. (2005). 'Load alleviation on wind turbine blades using variable airfoil geometry'. In: *Wind Engineering* 29.2, pp. 169–182.
- Bauer, D. and M. Jansson (2000). 'Analysis of the asymptotic properties of the MOESP type of subspace algorithms'. In: *Automatica* 36.4, pp. 497–509.
- Bauer, D. and L. Ljung (2002). 'Some facts about the choice of the weighting matrices in Larimore type of subspace algorithms'. In: *Automatica* 38.5, pp. 763–773.
- Bazanella, A., M. Gevers and L. Mišković (2009). 'Closed-loop identification of MIMO systems: a new look at identifiability and experiment design'. In: *European Journal of Control* 16/3, pp. 228–239.
- Moheimani, S. O. R. and A. J. Fleming (2006). *Piezoelectric Transducers for Vibration Control and Damping*. Springer.
- Bemporad, A. and M. Morari (1999). 'Robust Model Predictive Control: A Survey'. In: *Robustness in Identification and Control* 245, pp. 207–226.

- Bergamasco, M. and M. Lovera (2010a). 'Continuous-time subspace identification in closed-loop'. In: *19th International Symposium on Mathematical Theory of Networks and Systems, Budapest, Hungary*.
- Bergamasco, M. and M. Lovera (2010b). 'Continuous-time subspace identification in closed-loop using Laguerre filters'. In: *Proc. of the 49<sup>th</sup> IEEE Control Conference on Decision and Control*. Atlanta.
- Bergamasco, M. and M. Lovera (2011a). 'Continuous-time predictor-based subspace identification for helicopter dynamics'. In: *37<sup>th</sup> European Rotorcraft Forum, Gallarate, Italy*.
- Bergamasco, M. and M. Lovera (May 2011b). 'Continuous-time predictor-based subspace identification using Laguerre filters'. In: *Control Theory Applications, IET 5.7*, pp. 856–867.
- Bernhammer, L. O., R. De Breuker, M. Karpel and G. J. van der Veen (2012). 'Aeroelastic control using distributed floating flaps activated by piezoelectric tabs'. In: *AIAA Journal of Aircraft*. in press.
- Bernhammer, L. O., S. P. W. Teeuwen, R. D. Breuker, G. J. van der Veen and E. van Solingen (2012). 'Performance optimization and gust load alleviation of a UAV wing using variable camber'. In: *ICAST2012: 23<sup>rd</sup> International Conference on Adaptive Structures and Technologies, Nanjing, China*.
- Bianchi, F. D., H. De Battista and R. J. Mantz (2007). *Wind Turbine Control Systems; Principles, modelling and gain scheduling design*. Springer-Verlag London.
- Bianchi, F. D., H. De Battista and R. J. Mantz (2010). 'Robust multivariable gain-scheduled control of wind turbines for variable power production'. In: *International Journal of Systems and Control* Vol. 1-2010/Iss.3, pp. 103–112.
- Bianchi, F. D., R. J. Mantz and C. F. Christiansen (2004). 'Control of variable-speed wind turbines by LPV gain scheduling'. In: *Wind Energy* 7.1, pp. 1–8.
- Bianchi, F. D., R. J. Mantz and C. F. Christiansen (2005). 'Gain scheduling control of variable-speed wind energy conversion systems using quasi-LPV models'. In: *Control Engineering Practice* 13.2, pp. 247–255.
- Bir, G. (2008). *Multiblade Coordinate Transformation and Its Application to Wind Turbine Analysis*. Tech. rep. NREL.
- Bisplinghoff, R. L., H. Ashley and R. L. Halfman (1996). *Aeroelasticity*. Dover books on physics. Dover Publ.
- Bittanti, S., P. Bolzern and M. Campi (1990). 'Convergence and exponential convergence of identification algorithms with directional forgetting factor'. In: *Automatica* 26.5, pp. 929–932.
- Bladed (2011). Accessed: Dec 15, 2011. GL Garrad Hassan Ltd. URL: <http://www.gl-garradhassan.com>.
- Bombois, X. J. A., G. Scorletti, M. Gevers, P. M. J. Van den Hof and R. Hildebrand (2006). 'Least costly identification experiment for control'. In: *Automatica* 42.10, pp. 1651–1662.
- Bongers, P. M. M. (1994). 'Modeling and identification of flexible wind turbines and a factorizational approach to robust control'. PhD thesis. Delft University of Technology.
- Boor, C. de (1987). 'B-form basics'. In: *Geometric Modeling: Algorithms and New Trends*, pp. 131–148.
- Bossanyi, E. A. (2000). 'The design of closed loop controllers for wind turbines'. In: *Wind Energy* 3.3, pp. 149–163.
- Bossanyi, E. A. (2003a). 'Individual blade pitch control for load reduction'. In: *Wind Energy* 6.2, pp. 119–128.
- Bossanyi, E. A. (2003b). 'Wind turbine control for load reduction'. In: *Wind Energy* 6.3, pp. 229–244.
- Bossanyi, E. A. (2005). 'Further load reductions with individual pitch control'. In: *Wind Energy* 8.4, pp. 481–485.
- Bossanyi, E. A. (Oct. 2012). 'Wind turbine control applications of turbine-mounted lidar'. In: *The science of making torque from wind*. Oldenburg, Germany.
- Bossanyi, E. A., P. A. Fleming and A. D. Wright (2012). 'Field test results with individual pitch control on the NREL CART3 wind turbine'. In: *50<sup>th</sup> AIAA Aerospace Sciences Meeting including the New Horizons Forum and Aerospace Exposition, Nashville, Tennessee*.
- Brewer, J. W. (1978). 'Kronecker products and matrix calculus in system theory'. In: *IEEE Transactions on circuits and systems* 25.9, pp. 772–781.

- Buhl, M. L. (2012). *NWTC Design Codes (WT\_Perf)*. Last accessed 16-May-2012. URL: <http://wind.nrel.gov/designcodes/simulators/fast/>.
- Buhl, T., D. C. Bak, M. Gaunaa and P. B. Andersen (2007). 'Load alleviation through adaptive trailing edge control surfaces: adapwing overview'. In: *Proceedings of the European Wind Energy Conference and Exhibition*, pp. 20–23.
- Burton, T., D. Sharpe, N. Jenkins and E. Bossanyi (2001). *Wind Energy Handbook*. John Wiley & Sons.
- Cao, L. and H. Schwartz (2000). 'A directional forgetting algorithm based on the decomposition of the information matrix'. In: *Automatica* 36.11, pp. 1725–1731.
- Chang, F. and R. Luus (Oct. 1971). 'A noniterative method for identification using Hammerstein model'. In: *Automatic Control, IEEE Transactions on* 16.5, pp. 464–468.
- Chiuso, A. (2006a). 'Asymptotic equivalence of certain closed loop subspace identification methods'. In: *Proceedings of the 14<sup>th</sup> IFAC Symposium on System Identification*.
- Chiuso, A. (Aug. 2006b). 'Asymptotic variance of closed-loop subspace identification methods'. In: *IEEE Transactions on Automatic Control* 51.8, pp. 1299–1314.
- Chiuso, A. (2007a). 'On the relation between CCA and predictor based subspace identification'. In: *IEEE Transactions on Automatic Control* 52.10, pp. 1795–1812.
- Chiuso, A. (2007b). 'The role of vector autoregressive modeling in predictor-based subspace identification'. In: *Automatica* 43.6, pp. 1034–1048.
- Chiuso, A. (Mar. 2010). 'On the asymptotic properties of closed-loop CCA-type subspace algorithms: equivalence results and role of the future horizon'. In: *IEEE Transactions on Automatic Control* 55.3, pp. 634–649.
- Chiuso, A., R. Muradore and E. Marchetti (2010). 'Dynamic calibration of adaptive optics systems: a system identification approach'. In: *IEEE Transactions on Control Systems Technology* 8.3, pp. 705–713.
- Chiuso, A. and G. Picci (2003a). 'Constructing the state of random processes with feedback'. In: *Proceedings of the 13<sup>th</sup> IFAC Symposium on System Identification*. Rotterdam, The Netherlands.
- Chiuso, A. and G. Picci (2003b). 'Geometry of oblique splitting subspaces, minimality and Hankel operators'. English. In: *Directions in Mathematical Systems Theory and Optimization*. Ed. by A. Rantzer and C. Byrnes. Vol. 286. Lecture Notes in Control and Information Sciences. Springer Berlin Heidelberg, pp. 85–126.
- Chiuso, A. and G. Picci (2005). 'Consistency analysis of some closed-loop subspace identification methods'. In: *Automatica* 41.3. Data-Based Modelling and System Identification, pp. 377–391.
- Chiuso, A., G. Pillonetto and G. De Nicolao (Dec. 2008). 'Subspace identification using predictor estimation via Gaussian regression'. In: *Proceedings of the 47<sup>th</sup> IEEE Conference on Decision and Control*, pp. 3299–3304.
- Chou, C. T. and M. Verhaegen (1997). 'Subspace algorithms for the identification of multivariable dynamic errors-in-variables models'. In: *Automatica* 33.10, pp. 1857–1869.
- Deistler, M., K. Peterzell and W. Scherrer (1995). 'Consistency and relative efficiency of subspace methods'. In: *Automatica* 31.12, pp. 1865–1875.
- Di Ruscio, D. (2003). 'Subspace System Identification of the Kalman Filter'. In: *Modeling, Identification and Control* 24.3, pp. 125–157.
- Di Ruscio, D. (2004). *Subspace System Identification of the Kalman Filter*. Tech. rep. Porsgrunn, Norway: Telemark University College.
- Di Ruscio, D. (2009a). 'A Bootstrap Subspace Identification Method: Comparing Methods for Closed Loop Subspace Identification by Monte Carlo Simulations'. In: *Modeling, Identification and Control* 30.4, pp. 203–222.
- Di Ruscio, D. (2009b). 'Closed and Open Loop Subspace System Identification of the Kalman Filter'. In: *Modeling, Identification and Control* 30.2, pp. 71–86.
- Dong, J. (2009). 'Data driven fault tolerant control: a subspace approach'. PhD thesis. Delft University of Technology.
- Dong, J., M. Verhaegen and E. Holweg (2008). 'Closed-loop subspace predictive control for fault tolerant MPC design'. In: *Proceedings of the 17<sup>th</sup> IFAC World Congress*. Vol. 17.
- Dong, J. and M. Verhaegen (2009). 'Cautious H<sub>2</sub> optimal control using uncertain Markov parameters identified in closed loop'. In: *Systems & Control Letters*, pp. 378–388.

- Engelen, T. van (2006). 'Design model and load reduction assessment for multi-rotational mode individual pitch control'. In: *Proceedings of the European Wind Energy Conference (EWEC)*. Athens, Greece.
- Enqvist, M. (2012). 'Invertible time series and system identification in a nonlinear closed-loop setting'. In: *European Research Network on System Identification (ERNSI workshop)*. Maastricht, Netherlands.
- EURELECTRIC (2011). *Power Statistics and Facts 2011*. Union of the Electricity Industry - EURELECTRIC. URL: <http://www.eurelectric.org>.
- Evans, M., M. Cannon and B. Kouvaritakis (2012). 'Robust and stochastic linear MPC for systems subject to multiplicative uncertainty'. In: *Preprints of 4<sup>th</sup> IFAC Nonlinear Model Predictive Control Conference*.
- Falck, T., J. A. K. Suykens, J. Schoukens and B. De Moor (Dec. 2010). 'Nuclear norm regularization for overparametrized Hammerstein systems'. In: *Proc. of the 49<sup>th</sup> IEEE Control Conference on Decision and Control*. Atlanta, pp. 7202–7207.
- Favoreel, W., B. De Moor, P. Van Overschee and M. Gevers (1999). 'Model-free subspace-based LQG-design'. In: *Proc. of the American Control Conference*. Vol. 5, pp. 3372–3376.
- Favoreel, W. and B. De Moor (1998). 'SPC: Subspace Predictive Control'. In: *Proc. IFAC World Congress, Beijing*, pp. 235–240.
- Fazel, M., H. Hindi and S. Boyd (July 2004). 'Rank minimization and applications in system theory'. In: *Proc. of the American Control Conference*. Vol. 4, pp. 3273–3278.
- Ferreau et al., H. (2012). *qpOASES User's Manual*. Catholic University of Leuven. URL: <http://homes.esat.kuleuven.be/~optec/software/qpOASES/>.
- Fingersh, L., M. Hand and A. Laxson (2006). *Wind turbine design cost and scaling model*. Tech. rep. NREL.
- Fleming, P. A., J. W. van Wingerden, A. K. Scholbrock, G. J. van der Veen and A. D. Wright (2013). 'Field testing of a wind turbine drivetrain/tower damper using advanced design and validation techniques'. In: *Accepted for the American Control Conference, Washington, DC*.
- Fleming, P. A., A. D. Wright, L. J. Fingersh and J. W. van Wingerden (2011). 'Resonant vibrations resulting from the re-engineering of a constant-speed 2-bladed turbine to a variable-speed 3-bladed turbine'. In: *49<sup>th</sup> AIAA Aerospace Sciences Meeting*.
- Franke, R. (1979). *A Critical Comparison of Some Methods for Interpolation of Scattered Data*. Tech. rep. Naval Postgraduate School.
- Franklin, G., J. Powell and A. Emani-Naeini (1994). *Feedback control of dynamic systems*. Addison Wesley.
- Frost, S. A., M. J. Balas and A. D. Wright (2009). 'Direct adaptive control of a utility-scale wind turbine for speed regulation'. In: *International Journal of Robust and Nonlinear Control* 19.1, pp. 59–71.
- Garnier, H. and L. Wang, eds. (2008). *Identification of continuous-time models from sampled data*. Springer.
- Gebraad, P. M. O., J. W. van Wingerden, G. J. van der Veen and M. Verhaegen (July 2011). 'LPV subspace identification using a novel nuclear norm regularization method'. In: *Proc. of the American Control Conference*, pp. 165–170.
- Gevers, M. (2005). 'Identification for control: from the early achievements to the revival of experiment design'. In: *European Journal of Control* 11.4-5, pp. 335–352.
- Gevers, M., A. S. Bazanella, X. J. A. Bombois and L. Mišković (Dec. 2009). 'Identification and the information matrix: how to get just sufficiently rich?' In: *IEEE Transactions on Automatic Control* 54.12, pp. 2828–2840.
- Gill, P. E., G. H. Golub, W. Murray and M. A. Saunders (1974). 'Methods for modifying matrix factorizations'. English. In: *Mathematics of Computation* 28.126, pages.
- Gilson, M., H. Garnier, P. Young and P. Van den Hof (2011). 'Optimal instrumental variable method for closed-loop identification'. In: *Control Theory Applications, IET* 5.10, pp. 1147–1154.
- Gilson, M. and G. Mercère (2006). 'Subspace based optimal IV method for closed loop system identification'. In: *IFAC Symposium on System Identification*.
- Goethals, I., K. Pelckmans, J. A. K. Suykens and B. De Moor (2005). 'Identification of MIMO Hammerstein models using least squares support vector machines'. In: *Automatica* 41.7, pp. 1263–1272.

- Goethals, I., T. Van Gestel, J. A. K. Suykens, P. Van Dooren and B. De Moor (Oct. 2003). 'Identification of positive real models in subspace identification by using regularization'. In: *IEEE Transactions on Automatic Control* 48.10, pp. 1843–1847.
- Golub, G. H. and V. Pereyra (1973). 'The differentiation of pseudo-inverses and nonlinear least squares problems whose variables separate'. In: *SIAM Journal on Numerical Analysis* 10.2, pp. 413–432.
- Golub, G. H. and C. F. Van Loan (1996). *Matrix Computations*. 3rd. The Johns Hopkins University Press.
- Goodwin, G. C., S. F. Graebe and M. E. Salgado (2001). *Control system design*. Prentice Hall, Inc.
- Gottschall, J. and J. Peinke (2008). 'How to improve the estimation of power curves for wind turbines'. In: *Environmental Research Letters* 3.1.
- Guennebaud, G., B. Jacob et al. (2010). *Eigen v3*. <http://eigen.tuxfamily.org>.
- Hägglund, T. (1983). 'The problem of forgetting old data in recursive estimation'. In: *Proc. of the IFAC Workshop Adaptive Systems in Control and Signal Processing, San Francisco*.
- Hägglund, T. (1985). 'Recursive estimation of slowly time-varying parameters'. In: *Proc. of the IFAC Symposium on Identification and System Parameter Estimation, York*.
- Hallouzi, R. (2008). 'Multiple-Model Based Diagnosis for Adaptive Fault-Tolerant control'. PhD thesis. Delft University of Technology.
- Hansen, M. H. (2003). 'Improved modal dynamics of wind turbines to avoid stall-induced vibrations'. In: *Wind Energy* 6.2, pp. 179–195.
- Hansen, M. H. (2007). 'Aeroelastic instability problems for wind turbines'. In: *Wind Energy* 10.6, pp. 551–577.
- Hansen, M. H., K. Thomsen, P. Fuglsang and T. Knudsen (2006). 'Two methods for estimating aeroelastic damping of operational wind turbine modes from experiments'. In: *Wind Energy* 9.1-2, pp. 179–191.
- Hansson, A., Z. Liu and L. Vandenbergh (2012). 'Subspace system identification via weighted nuclear norm optimization'. In: *CoRR abs/1207.0023*.
- Haverkamp, L. R. J. (2001). 'State space identification: Theory and practice'. PhD thesis. Delft University of Technology.
- Hayman, G. (2012). *NWTC Design Codes (MCrunch)*. Last accessed 16-May-2012. URL: <http://wind.nrel.gov/designcodes/postprocessors/mcrunch/>.
- Heinze, S. and M. Karpel (2006). 'Analysis and wind tunnel testing of a piezoelectric tab for aeroelastic control applications'. In: *AIAA Journal of Aircraft* 43.6, pp. 1799–1804.
- Henriksen, L. C. (2008). 'Model predictive control of a wind turbine with constraints'. In: *Proceedings of the European Wind Energy Conference (EWEC)*. Brussels, Belgium.
- Henriksen, L., M. Hansen and N. Poulsen (2012). 'A simplified dynamic inflow model and its effect on the performance of free mean wind speed estimation'. In: *Wind Energy*, n/a–n/a.
- Ho, B. L. and R. E. Kalman (1966). 'Effective construction of linear state-variables models from input/output functions'. In: *Regelungstechnik* 14, pp. 545–548.
- Hooft, E. L. van der and T. G. van Engelen (2003). *Feed forward control of estimated wind speed*. Technical report ECN-C-03-137. Energy research Center of the Netherlands.
- Hooft, E. L. van der and T. G. van Engelen (2004). 'Estimated wind speed feed forward control for wind turbine operation optimisation'. In: *Proceedings of the European Wind Energy Conference, London*.
- Hooft, E. L. van der, P. Schaak and T. G. van Engelen (2003). *Wind turbine control algorithms*. Tech. rep. DOWEC-F1W1-EH-030094/0. ECN.
- Houtzager, I., B. Kulcsár, J. W. van Wingerden and M. Verhaegen (2010). 'System identification for the control of wind turbine systems'. In: *Proc. of the 3<sup>rd</sup> conference, The Science of Making Torque from Wind, Heraklion, Crete, Greece*.
- Houtzager, I., J. W. v. Wingerden and M. Verhaegen (2010). *Predictor-based Subspace Identification Toolbox Version 0.4*. URL: <http://www.dsc.tudelft.nl/~datadriven/pbsid/>.
- Houtzager, I., J. W. van Wingerden and M. Verhaegen (2009a). 'Fast-array recursive closed-loop subspace model identification'. In: *15th IFAC Symposium on System Identification, Saint Malo, France*.
- Houtzager, I., J. W. van Wingerden and M. Verhaegen (2009b). 'VARMAX-based closed-loop subspace model identification'. In: *Proceedings of the 48<sup>th</sup> IEEE Conference on Decision and Control*, pp. 3370–3375.

- Wind turbines – Design requirements* (2005). International Electrotechnical Commission. Standard.
- Inman, D. J. (2001). *Engineering Vibration*. 2<sup>nd</sup> ed. Prentice-Hall, Inc.
- Iribas-Latour, M. and I.-D. Landau (2009). 'Identification of wind turbines in closed-loop operation in the presence of three-dimensional turbulence wind speed: torque demand to measured generator speed loop'. In: *Wind Energy* 12.7, pp. 660–675.
- Iribas-Latour, M. and I.-D. Landau (2012). 'Identification in closed-loop operation of models for collective pitch robust controller design'. In: *Wind Energy (Online pre-print)* N/A.
- James III, G. H., T. G. Carne and J. P. Lauffer (1993). *The natural excitation technique (NExT) for modal parameter extraction from operating wind turbines*. Tech. rep. Sandia.
- Jansson, M. (2003). 'Subspace identification and ARX modeling'. In: *Proceedings of the 13<sup>th</sup> IFAC symposium on system identification*. Rotterdam, Netherlands, pp. 1625–1630.
- Jansson, M. and B. Wahlberg (1998). 'On consistency of subspace methods for system identification'. In: *Automatica* 34.12, pp. 1507–1519.
- Jelavic, M., N. Peric and I. Petrovic (Sept. 2006). 'Identification of wind turbine model for controller design'. In: *Power Electronics and Motion Control Conference, 2006. EPE-PEMC 2006. 12th International*, pp. 1608–1613.
- Johnson, K. E., L. J. Fingersh, M. J. Balas and L. Y. Pao (2004). 'Methods for increasing region 2 power capture on a variable speed HAWT'. In: *42nd AIAA Aerospace Sciences Meeting and Exhibit, Reno, Nevada*.
- Johnson, K. E., L. Y. Pao, M. J. Balas and L. J. Fingersh (June 2006). 'Control of variable-speed wind turbines: standard and adaptive techniques for maximizing energy capture'. In: *Control Systems, IEEE* 26.3, pp. 70–81.
- Johnson, K. E. and L. J. Fingersh (2008). 'Adaptive pitch control of variable-speed wind turbines'. In: *Journal of Solar Energy Engineering* 130.3, 031012, p. 031012.
- Johnson, W. (1994). *Helicopter theory*. Dover Publications.
- Johnstone, R. M., C. R. Johnson Jr., R. R. Bitmead and B. D. O. Anderson (1982). 'Exponential convergence of recursive least squares with exponential forgetting factor'. In: *Systems & Control Letters* 2.2, pp. 77–82.
- Jonkman, J. (2007). *Dynamics Modeling and Loads Analysis of an Offshore Floating Wind Turbine*. Tech. rep. NREL/TP-500-41958. NREL.
- Jonkman, J. (2008). 'Influence of control on the pitch damping of a floating wind turbine'. In: *46th AIAA Aerospace Science Meeting, Reno, US*.
- Jonkman, J. (2012). *NWTC Design Codes (FAST)*. Last accessed 16-May-2012. URL: <http://wind.nrel.gov/designcodes/simulators/fast/>.
- Jonkman, J., S. Butterfield, W. Musial and G. Scott (2009). *Definition of a 5-MW Reference turbine for offshore system development*. Tech. rep. NREL.
- Juang, J. N. and R. S. Pappa (1985). 'An eigensystem realization algorithm (ERA) for modal parameter identification and model reduction'. In: *AIAA Journal of Guidance, Control and Dynamics* 8.5, pp. 620–627.
- Kadali, R., B. Huang and A. Rossiter (2003). 'A data driven subspace approach to predictive controller design'. In: *Control Engineering Practice* 11.3, pp. 261–278.
- Katayama, T. (2005). *Subspace Methods for System Identification*. Springer.
- Katayama, T., H. Kawauchi and G. Picci (2005). 'Subspace identification of closed loop systems by the orthogonal decomposition method'. In: *Automatica* 41.5, pp. 863–872.
- Katayama, T. and H. Tanaka (2007). 'An approach to closed-loop subspace identification by orthogonal decomposition'. In: *Automatica* 43.9, pp. 1623–1630.
- Kaufman, L. (1975). 'A variable projection method for solving separable nonlinear least squares problems'. In: *BIT Numerical Mathematics* 15 (1), pp. 49–57.
- Khalil, H. (2002). *Nonlinear Systems*. Prentice Hall.
- Klein, V. and E. A. Morelli (2006). *Aircraft System Identification: Theory And Practice*. AIAA.
- Knudsen, T. (2001). 'Consistency analysis of subspace identification methods based on a linear regression approach'. In: *Automatica* 37.1, pp. 81–89.
- Knudsen, T., P. Andersen and S. Toffner-Clausen (1997). 'Comparing PI and robust pitch controller on a 400 kW wind turbine by full scale tests'. In: *Proceedings of the European Wind Energy Conference (EWEC)*. Dublin, Ireland.
- Knudsen, T., T. Bak and M. Soltani (2011). 'Prediction models for wind speed at turbine locations in a wind farm'. In: *Wind Energy* 14.7, pp. 877–894.

- Korte, R. B. C. de (Jan. 2009). 'Subspace-Based Identification Techniques for a 'Smart' Wind Turbine Rotor Blade: A Study Towards Adaptive Data-Driven Control'. MA thesis. Delft University of Technology.
- Kuersteiner, G. M. (Jan. 2005). 'Automatic inference for infinite order vector autoregressions'. In: *Econometric Theory* 21 (01), pp. 85–115.
- Kulcsár, B. and M. Verhaegen (Dec. 2010). 'Robust cautious data driven control with guaranteed mean square stability'. In: *Proceedings of the 49<sup>th</sup> IEEE Control Conference on Decision and Control*. Atlanta, pp. 2276–2281.
- Kulhavý, R. and M. Kárný (1984). 'Tracking of slowly varying parameters by directional forgetting'. In: *Preprints of the 9<sup>th</sup> IFAC Congress*. Vol. 10, pp. 178–183.
- Kulhavý, R. (1987). 'Restricted exponential forgetting in real-time identification'. In: *Automatica* 23.5, pp. 589–600.
- Kumar, A. and K. Stol (Jan. 2009). 'Scheduled model predictive control of a wind turbine'. In: *Aerospace Sciences Meetings*. American Institute of Aeronautics and Astronautics, pages.
- Kung, S. K. (1978). 'A new low-order approximation algorithm via singular value decomposition'. In: *29th Asilomar Conference on Circuits, Systems and Computers*, pp. 705–714.
- Lackner, M. A. (Dec. 2009). 'Controlling platform motions and reducing blade loads for floating wind turbines'. In: *Wind Engineering* 33.6, pp. 541–554.
- Lackner, M. A. and M. A. Rotea (2011). 'Structural control of floating wind turbines'. In: *Mechatronics* 21.4, pp. 704–719.
- Lai, M.-J. and L. L. Schumaker (2007). *Spline functions on triangulations*. Cambridge University Press.
- Larsen, T. J. and T. D. Hanson (2007). 'A method to avoid negative damped low frequent tower vibrations for a floating, pitch controlled wind turbine'. In: *Journal of Physics: Conference Series* 75.1.
- Larsen, T., H. A. Madsen and K. Thomsen (2005). 'Active load reduction using individual pitch, based on local blade flow measurements'. In: *Wind Energy* 8.1, pp. 67–80.
- Lee, L. H. and K. Poolla (1999). 'Identification of linear parameter-varying systems using non-linear programming'. In: *Journal of Dynamic Systems, Measurements and control* 121.1, pp. 71–78.
- Leith, D. J. and W. E. Leithead (1996). 'Appropriate realization of gain-scheduled controller with application to wind turbine regulation'. In: *International Journal of Control* 65.2, pp. 223–248.
- Leithead, W. E. (2007). 'Wind energy'. In: *Philosophical Transactions of the Royal Society A: Mathematical, Physical and Engineering Sciences* 365.1853, pp. 957–970.
- Leithead, W. E. and S. Dominguez (2006). 'Coordinated control design for wind turbine control systems'. In: *EWEC Athens, Greece*.
- Lescher, F., J. Y. Zhao and A. Martinez (2006). 'Multiobjective  $H_2/H_\infty$  control of a pitch regulated wind turbine for mechanical load reduction'. In: *Proceedings of the European Wind Energy Conference (EWEC)*. Athens, Greece.
- Liu, Z. and L. Vandenberghe (2009). 'Interior-point method for nuclear norm approximation with application to system identification'. In: *SIAM Journal on Matrix Analysis and Applications* 31.3, pp. 1235–1256.
- Ljung, L. (29th Dec. 1999). *System Identification: Theory for the User*. 2nd ed. Prentice Hall PTR.
- Ljung, L. and T. McKelvey (1996). 'Subspace identification from closed loop data'. In: *Signal Processing* 52.2, pp. 209–215.
- Lyzell, C., M. Enqvist and L. Ljung (2009). 'Handling certain structure information in subspace identification'. In: *Proceedings of the 15<sup>th</sup> IFAC Symposium on System Identification*.
- Manwell, J., J. McGowan and A. Rogers (2002). *Wind energy explained: Theory, design and application*. Chichester: John Wiley and Sons, Ltd.
- Marrant, B. A. H. and Th. van Holten (2004). 'System identification for the analysis of aeroelastic stability of wind turbine blades'. In: *Proceedings of the European Wind Energy Conference (EWEC)*. London, England.
- Marrant, B. A. H. and Th. van Holten (2006). 'Comparison of smart rotor blade concepts for large offshore wind turbines'. In: *Offshore Wind Energy and other Renewable Energies in Mediterranean and European Seas*. Civitavecchia, Italy.

- Mercère, G., S. Lecœuche and M. Lovera (2004). 'Recursive subspace identification based on instrumental variable unconstrained quadratic optimization'. In: *International Journal of Adaptive Control and Signal Processing* 18, pp. 771–797.
- Miller, D. N. and R. A. de Callafon (2013). 'Subspace identification with eigenvalue constraints'. In: *Automatica*. In press.
- Mohd-Moktar, R. and L. Wang (2008). 'Continuous-time state space model identification using closed-loop data'. In: *Second Asia International Conference on Modelling & Simulation, Kuala Lumpur, Malaysia*.
- Molenaar, D-P. (2003). 'Cost effective design and operation of variable-speed wind turbines'. PhD thesis. Delft University of Technology.
- Namik, H. and K. Stol (2011). 'Performance analysis of individual blade pitch control of offshore wind turbines on two floating platforms'. In: *Mechatronics* 21.4, pp. 691–703.
- Narendra, K. S. and P. G. Gallman (1966). 'An iterative method for the identification of nonlinear systems using a Hammerstein model'. In: *IEEE Transactions on Automatic Control* 11, pp. 546–550.
- Ng, T. S., G. C. Goodwin and B. D. O. Anderson (1977). 'Identifiability of mimo linear dynamic systems operating in closed loop'. In: *Automatica* 13.5, pp. 477–485.
- Niederberger, D., A. Fleming, S. O. R. Moheimani and M. Morari (2004). 'Adaptive multi-mode resonant piezoelectric shunt damping'. In: *Smart Materials and Structures* 13.5, p. 1025.
- Nielsen, F. G., T. D. Hanson and B. Skaare (2006). 'Integrated dynamic analysis of floating offshore wind turbines'. In: *ASME Conference Proceedings* 2006.47462, pp. 671–679.
- Nijssen, R. P. L. (2006). 'Fatigue life prediction and strength degradation of wind turbine rotor blade composites'. PhD thesis. Delft University of Technology.
- Nilsen, G. W. (2005). 'Topics in open and closed Loop Subspace System Identification: finite data based methods'. PhD thesis. Norwegian University of Science and Technology.
- Ogata, K. (1997). *Modern Control Engineering*. Prentice Hall.
- Ohta, Y. and T. Kawai (2004). 'Continuous-time subspace system identification using generalized orthonormal basis functions'. In: *16th International Symposium on Mathematical Theory of Networks and Systems, Leuven, Belgium*.
- Ohtsubo, K. and H. Kajiwara (2004). 'LPV technique for rotational speed control of wind turbines using measured wind speed'. In: *OCEANS '04. MTT/IEEE TECHNO-OCEAN '04* 4, pp. 1847–1853.
- Oku, H. and T. Fujii (Dec. 2004). 'Direct subspace model identification of LTI systems operating in closed-loop'. In: *Proceedings of the 43<sup>rd</sup> IEEE Conference on Decision and Control*. Vol. 2, 2219–2224 Vol.2.
- Osgood, R., G. Bir, H. Mutha, B. Peeters, M. Luczak and G. Sablon (2011). 'Full-scale modal wind turbine tests: comparing shaker excitation with wind excitation'. In: *Structural Dynamics and Renewable Energy, Volume 1*. Ed. by T. Proulx. Vol. 10. Conference Proceedings of the Society for Experimental Mechanics Series. Springer New York, pp. 113–124.
- Østergaard, K. Z. (2008). 'Robust, Gain-Scheduled Control of Wind Turbines'. PhD thesis. Aalborg University.
- Østergaard, K. Z., P. Brath and J. Stoustrup (2007). 'Estimation of effective wind speed'. In: *Journal of Physics, Conference series: The Science of Making Torque from Wind* 75.012082.
- Østergaard, K. Z., J. Stoustrup and P. Brath (2008). 'Rate bounded linear parameter varying control of a wind turbine in full load operation'. In: *Proceedings of the 17<sup>th</sup> IFAC world congress*. Seoul, South-Korea.
- Østergaard, K. Z., J. Stoustrup and P. Brath (2009). 'Linear parameter varying control of wind turbines covering both partial and full load conditions'. In: *International Journal of Robust and Nonlinear Control*, special issue on Wind turbines: New challenges and advanced control solutions 19.-, pages.
- Özbek, M. and D. J. Rixen (2012). 'Operational modal analysis of a 2.5MW wind turbine using optical measurement techniques and strain gauges'. In: *Wind Energy*.
- Pan, C.-T. and R. J. Plemmons (1989). 'Least squares modifications with inverse factorizations: parallel implications'. In: *Journal of Computational and Applied Mathematics* 27.1-2. Special Issue on Parallel Algorithms for Numerical Linear Algebra, pp. 109–127.
- Pao, L. Y. and K. E. Johnson (June 2009). 'A tutorial on the dynamics and control of wind turbines and wind farms'. In: *Proc. of the American Control Conference*, pp. 2076–2089.

- Peternell, K., W. Scherrer and M. Deistler (1996). 'Statistical analysis of novel subspace identification methods'. In: *Signal Processing* 52.2. Subspace Methods, Part II: System Identification, pp. 161–177.
- Phan, M., L. G. Horta, J.-N. Juang and R. W. Longman (1993). 'Linear system identification via an asymptotically stable observer'. In: *Journal of Optimization Theory and Applications* 79 (1). 10.1007/BF00941887, pp. 59–86.
- Phan, M., L. G. Horta, J.-N. Juang and R. W. Longman (1995). 'Improvement of observer/Kalman filter identification (OKID) by residual whitening'. In: *Journal of Vibration and Acoustics* 117.2, pp. 232–239.
- Pintelon, R. and J. Schoukens (May 2012). *System Identification: A Frequency Domain Approach*. John Wiley & Sons-IEEE Press.
- Pintelon, R., J. Schoukens, G. Vandersteen and K. Barbé (2010). 'Estimation of nonparametric noise and FRF models for multivariable systems – Part I: Theory'. In: *Mechanical Systems and Signal Processing* 24.3, pp. 573–595.
- Polyanin, A. D. and V. F. Zaitsev (2003). *Handbook of Exact Solutions for Ordinary Differential Equations (2nd edition)*. Chapman & Hall/CRC Press, Boca Raton.
- Preumont, A. and K. Seto (2008). *Active Control of Structures*. Wiley.
- Qin, S. J., W. Lin and L. Ljung (2005). 'A novel subspace identification approach with enforced causal models'. In: *Automatica* 41.12, pp. 2043–2053.
- Qin, S. J. and L. Ljung (Dec. 2003a). *Closed-loop Subspace Identification with Innovation Estimation*. Tech. rep. LiTH-ISY-R-2559. SE-581 83 Linköping, Sweden: Department of Electrical Engineering, Linköping University.
- Qin, S. J. and L. Ljung (2003b). 'Closed-loop subspace identification with innovation estimation'. In: *IFAC Symposium on System Identification, Rotterdam*.
- Ruhe, A. and P. Å. Wedin (1980). 'Algorithms for separable nonlinear least squares problems'. In: *SIAM Review* 22, pp. 318–337.
- Red Eléctrica de España (2012). *Power demand tracking in real time*. Red Eléctrica de España, S.A. URL: <https://demanda.ree.es/>.
- Renewable Energy Focus (June 2009). *Floating offshore wind turbine installed by Siemens and StatoilHydro*. <http://www.renewableenergyfocus.com>.
- Roddier, D. and J. Weinstein (2010). 'Floating wind turbines'. In: *Focus on Offshore Technologies, Mechanical Engineering*, pp. 2–6.
- Roddier, D., C. Cermelli, A. Aubault and A. Weinstein (2010). 'Windfloat: a floating foundation for offshore wind turbines'. In: *Journal of Renewable and Sustainable Energy* 2.3, 033104, p. 033104.
- Sayed, A. (2003). *Fundamentals of Adaptive Filtering*. New York: Wiley.
- Schlipf, D., D. J. Schlipf and M. Kühn (2012). 'Nonlinear model predictive control of wind turbines using lidar'. In: *Wind Energy*. URL: <http://dx.doi.org/10.1002/we.1533>.
- Schlipf, D., D. Trabucchi, O. Bischoff, M. Hofsäss, J. Mann, T. Mikkelsen, A. Rettenmeier, J. Trujillo and M. Kühn (2010). 'Testing of frozen turbulence hypothesis for wind turbine applications with a scanning lidar system'. In: *ISARS*. Paris, France.
- Seeger, M. (2004). *Low Rank Updates for the Cholesky Decomposition*. Tech. rep. Department of EECS, University of California at Berkeley. URL: <http://upseeger.epfl.ch/software/in dex.shtml#chollrup>.
- Selvam, K., S. Kanev, J. W. van Wingerden, T. van Engelen and M. Verhaegen (2009). 'Feedback-feedforward individual pitch control for wind turbine load reduction'. In: *International Journal of Robust and Nonlinear Control, special issue on Wind turbines: New challenges and advanced control solutions* 19.1, pp. 72–91.
- Simley, E., L. Y. Pao, N. Kelley, B. Jonkman and R. Frehlich (2012). 'LIDAR Wind Speed Measurements of Evolving Wind Fields'. In: *50th AIAA Aerospace Sciences Meeting*.
- Skjoldan, P. F. and M. H. Hansen (2012). 'Implicit floquet analysis of wind turbines using tangent matrices of a non-linear aeroelastic code'. In: *Wind Energy* 15.2, pp. 275–287. URL: <http://dx.doi.org/10.1002/we.467>.
- Skjoldan, P. and M. Hansen (2009). 'On the similarity of the coleman and lyapunov-floquet transformations for modal analysis of bladed rotor structures'. In: *Journal of Sound and Vibration* 327.3 - 5, pp. 424–439.
- Skogestad, S. and I. Postlethwaite (1996). *Multivariable feedback control, analysis and design*. John Wiley and sons.

- Smith, D. A., M. Harris, A. S. Coffey, T. Mikkelsen, H. E. Jørgensen, J. Mann and R. Danielian (2006). 'Wind lidar evaluation at the Danish wind test site in Høvsøre'. In: *Wind Energy* 9.1-2, pp. 87–93.
- Snel, H. and J. Schepers (1995). *Joint investigation of dynamic inflow effects and implementation of an engineering method*. Tech. rep. Energy Research Centre of the Netherlands.
- Soliman, M., O. P. Malik and D. Westwick (2012). 'Fault tolerant control of variable-speed variable-pitch wind turbines: a subspace predictive control approach'. In: *Proceedings of the 16<sup>th</sup> IFAC symposium on system identification*. Brussels.
- Soliman, M., O. P. Malik and D. T. Westwick (July 2011). 'Multiple model predictive control for wind turbines with doubly fed induction generators'. In: *Sustainable Energy, IEEE Transactions on* 2.3, pp. 215–225.
- Soltani, M., R. Wisniewski, P. Brath and S. Boyd (Sept. 2011). 'Load reduction of wind turbines using receding horizon control'. In: *Control Applications (CCA), 2011 IEEE International Conference on*, pp. 852–857.
- Stotsky, A. and B. Egardt (2012). 'Proactive control of wind turbine with blade load constraints'. In: *Proceedings of the Institution of Mechanical Engineers, Part I: Journal of Systems and Control Engineering* 226.7, pp. 985–993.
- Sutherland, H. J., P. S. Veers and T. D. Ashwill (1993). 'Fatigue life prediction for wind turbines: A case study on loading spectra and parameter sensitivity'. In: *The 5th ASTM Symposium on Composite Materials: Fatigue and Fracture, Atlanta, GA*.
- Tischler, M. and R. Rempfle (2006). *Aircraft And Rotorcraft System Identification: Engineering Methods With Flight-test Examples*. AIAA.
- Tóth, R. (2010). *Modeling and Identification of Linear Parameter-Varying Systems*. Springer Germany.
- Trnka, P. and V. Havlena (2009). 'Subspace like identification incorporating prior information'. In: *Automatica* 45.4, pp. 1086–1091.
- UPWIND (2012). *UpWind project website*. Last visited 20 August 2012. URL: <http://www.upwind.eu/>.
- Van den Hof, P. M. J. (1998). 'Closed-loop issues in system identification'. In: *Annual Reviews in Control* 22, pp. 173–186.
- Van den Hof, P. M. J. and R. A. de Callafon (Dec. 1996). 'Multivariable closed-loop identification: from indirect identification to dual-youla parametrization'. In: *Proceedings of the 35th IEEE Conference on Decision and Control*. Vol. 2, pp. 1397–1402.
- Van den Hof, P. M. J. and R. J. P. Schrama (1995). 'Identification and control—closed-loop issues'. In: *Automatica* 31.12, pp. 1751–1770.
- Van Gestel, T., J. A. K. Suykens, P. Van Dooren and B. De Moor (Sept. 2001). 'Identification of stable models in subspace identification by using regularization'. In: *IEEE Transactions on Automatic Control* 46.9, pp. 1416–1420.
- Van Overschee, P. and B. De Moor (Dec. 1997). 'Closed loop subspace system identification'. In: *Proceedings of the 36<sup>th</sup> IEEE Conference on Decision and Control*. Vol. 2, 1848–1853 vol.2.
- Van Overschee, P. and B. L. R. De Moor (1996). *Subspace identification for linear systems: theory, implementation, applications*. Dordrecht, The Netherlands: Kluwer Academic Publishers Group.
- Vandersteen, G., Y. Rolain and J. Schoukens (1997). 'Non-parametric estimation of the frequency-response functions of the linear blocks of a Wiener-Hammerstein model'. In: *Automatica* 33.7, pp. 1351–1355.
- Veen, G. J. van der, I. A. Couchman and R. O. Bowyer (2012). 'Control of floating wind turbines'. In: *Proceedings of the 2012 American Control Conference, Montreal, QC, Canada*.
- Veen, G. J. van der, J. W. van Wingerden, M. Bergamasco, M. Lovera and M. Verhaegen (2012). 'Closed-loop subspace identification methods: an overview'. In: *IET Control Theory and Applications (submitted)* —, pages.
- Veen, G. J. van der, J. W. van Wingerden and M. Verhaegen (Dec. 2010a). 'Closed-loop MOESP subspace model identification with parametrisable disturbances'. In: *Proc. of the 49<sup>th</sup> IEEE Control Conference on Decision and Control*. Atlanta.
- Veen, G. J. van der, J. W. van Wingerden and M. Verhaegen (2010b). *Closed-loop MOESP subspace model identification with parametrisable disturbances*. Technical report 10-015. Delft Center for Systems and Control, Delft University of Technology.

- Veen, G. J. van der, J. W. van Wingerden and M. Verhaegen (2010c). 'Closed-loop system identification of wind turbines in the presence of periodic effects'. In: *Proc. of the 3<sup>rd</sup> conference, The Science of Making Torque from Wind, Heraklion, Crete, Greece*.
- Veen, G. J. van der, J. W. van Wingerden and M. Verhaegen (July 2011). 'Data-driven modelling of wind turbines'. In: *Proc. of the American Control Conference (ACC), 2011*. San Francisco, pp. 72–77.
- Veen, G. J. van der, J. W. van Wingerden and M. Verhaegen (2012). 'Global identification of wind turbines using a Hammerstein identification method'. In: *IEEE Transactions on Control Systems Technology*.
- Veen, G. van der, J. van Wingerden, P. Fleming, A. Scholbrock and M. Verhaegen (2013). 'Global data-driven modeling of wind turbines in the presence of turbulence'. In: *Control Engineering Practice* 21.4, pp. 441–454.
- Verdult, V. (2002). 'Nonlinear system identification; A state-space approach'. Ph.D. Thesis. University of Twente.
- Verdult, V., N. Bergboer and M. Verhaegen (2003). 'Identification of fully parameterized linear and nonlinear state-space systems by projected gradient search.' In: *Proceedings of the IFAC symposium on system identification (SYSID)*. Rotterdam, The Netherlands.
- Verhaegen, M. (1989). 'Round-off error propagation in four generally-applicable, recursive, least-squares estimation schemes'. In: *Automatica* 25.3, pp. 437–444.
- Verhaegen, M. (1993a). 'Application of a subspace model identification technique to identify LTI systems operating in closed-loop'. In: *Automatica* 29, pp. 1027–1040.
- Verhaegen, M. (1993b). 'Subspace model identification part 3. analysis of the ordinary output-error state-space model identification algorithm'. In: *International Journal of Control* 58.3, pp. 555–586.
- Verhaegen, M. and A. Varga (1994). *Some Experience with the MOESP Class of Subspace Model Identification Methods in Identifying the BO105 Helicopter*. Tech. rep. DLR Oberpfaffenhofen.
- Verhaegen, M. and V. Verdult (2007). *Filtering and System Identification; A Least Squares Approach*. 1st, Cambridge, UK: Cambridge University Press.
- Verhaegen, M. and D. Westwick (1996). 'Identifying MIMO Hammerstein systems in the context of subspace model identification methods'. In: *International Journal of Control* 63.2, pp. 331–349.
- Visser, C. C. de (2011). 'Global Nonlinear Model Identification with Multivariate Splines'. PhD thesis. Delft University of Technology.
- Visser, C. C. de, Q. P. Chu and J. A. Mulder (2009). 'A new approach to linear regression with multivariate splines.' In: *Automatica*, pp. 2903–2909.
- Visser, C. C. de, Q. P. Chu and J. A. Mulder (2011). 'Differential constraints for bounded recursive identification with multivariate splines'. In: *Automatica* 47.9, pp. 2059–2066.
- Wang, N., K. Johnson and A. Wright (Sept. 2012). 'Fx-rls-based feedforward control for lidar-enabled wind turbine load mitigation'. In: *IEEE Transactions on Control Systems Technology* 20.5, pp. 1212–1222.
- Wills, A., D. Bates, A. Fleming, B. Ninness and S. Moheimani (Jan. 2008). 'Model predictive control applied to constraint handling in active noise and vibration control'. In: *Control Systems Technology, IEEE Transactions on* 16.1, pp. 3–12.
- Wind Energy Factsheets* (2010). European Wind Energy Association.
- Wingerden, J. W. van (2008). 'Control of Wind Turbines with 'Smart' Rotors: Proof of Concept & LPV Subspace Identification'. PhD thesis. Delft University of Technology.
- Wingerden, J. W. van (2012). 'The asymptotic variance of the PBSIDopt algorithm'. In: *Proceedings of the 16<sup>th</sup> IFAC symposium on system identification*. Brussels.
- Wingerden, J. W. van, A. W. Hulskamp, T. Barlas, I. Houtzager, H. Bersee, G. A. M. van Kuik and M. Verhaegen (Mar. 2011). 'Two-degree-of-freedom active vibration control of a prototyped "smart" rotor'. In: *Control Systems Technology, IEEE Transactions on* 19.2, pp. 284–296.
- Wingerden, J. W. van, A. W. Hulskamp, T. Barlas, B. Marrant, G. A. M. van Kuik, D.-P. Molenaar and M. Verhaegen (2008). 'On the proof of concept of a "smart" wind turbine rotor blade for load alleviation'. In: *Wind Energy* 11.3, pp. 265–280.
- Wingerden, J. W. van and M. Verhaegen (2009a). 'Closed loop identification of MIMO Hammerstein models using LS-SVM'. In: *15<sup>th</sup> IFAC Symposium on System Identification*.

- Wingerden, J. W. van and M. Verhaegen (2009b). 'Subspace identification of bilinear and LPV systems for open- and closed-loop data'. In: *Automatica* 45.2, pp. 372–381.
- Woodley, B. R. (2001). 'Model Free Subspace Based  $H_\infty$  Control'. PhD thesis. Stanford University.
- Zervos, A. and C. Kjaer (2008). *Pure Power – Wind Energy Scenarios up to 2030*. European Wind Energy Association.
- Zhu, Y. (2000). 'Identification of Hammerstein models for control using ASYM'. In: *International Journal of Control* 73.18, pp. 1692–1702.

# List of abbreviations

1P	once-per-revolution
2D	two-dimensional
2P	twice-per-revolution
3D	three-dimensional
3P	three-times-per-revolution
ARMAX	autoregressive moving average with external inputs
ARX	autoregressive with external inputs
CART	controls advanced research turbine
CLMOESP	closed-loop MOESP
ERA	eigensystem realization algorithm
GBN	generalized binary noise
LPV	linear parameter-varying
LS	least squares
LTI	linear time invariant
LTV	linear time-varying
MFC	macro fiber composite
MIMO	multiple-input and multiple-output
MOESP	multivariable output-error state space
MPC	model predictive control
N4SID	numerical algorithm for subspace state space identification
OKID	observer/Kalman filter identification
PBSID	predictor-based subspace identification
PEM	prediction error method
PRBN	pseudorandom binary noise
PSD	power spectral density
PWM	pulse width modulation
RLS	recursive least squares
RMS	root-mean-square
RPM	revolutions per minute
SISO	single-input and single-output
SNR	signal-to-noise ratio
SPC	subspace predictive control
SVD	singular value decomposition
VAF	variance-accounted-for
VARX	vector autoregressive with external inputs



# Summary

## Identification of wind energy systems

Gijs van der Veen

In the next decades wind energy is expected to secure a firm share of the total energy production capacity in many countries. To increase competitiveness of wind power with other power sources it is essential to lower the cost of wind energy. Given the design of a turbine, this objective can be attained in several ways: by increasing the energy production of a wind turbine, by lowering loads on the wind turbine in order to reduce maintenance costs and by mass production. Research performed in recent years has shown that *advanced control* plays an important role in the first two aspects. Refined control design can increase power production, for instance by using feedforward information about the wind field provided by modern (distributed) sensors. At the same time, control can reduce wear of the turbine by mitigating fatigue and extreme loads, also using feedforward and feedback information from multiple sensors in combination with novel actuator concepts. For the design process of new and advanced control concepts which meet these objectives, detailed models are essential. Data-driven modelling provide such models and help to understand differences between the behaviour of theoretical models and the real wind turbine.

A number of challenges hamper the application of standard black-box identification techniques to data from real wind turbines. The aim of this thesis is to address these challenges in an effort to bring theoretical results and industrial practice closer together, and to provide evidence for the potential of system identification. The end result is a set of tools that can be applied by engineers.

The first challenge is given by the fact that wind turbines and many other aeroelastic systems must operate in closed-loop. This is an obstacle for the traditional subspace methods which rely on the input signal and stochastic excitations to be uncorrelated; an assumption which is necessarily violated in closed-loop. In this thesis we present an overview of recent methods for closed-loop subspace identification, thereby establishing a number of tools to solve the identification problem for linear time invariant systems which may be operating in closed-loop. Among these tools is the closed-loop MOESP method developed as part of this thesis. We present a common underlying framework for these methods, allowing us to show that the large variety of closed-loop subspace methods found in the recent literature in fact consists of a few variants with many similarities.

The second challenge is that wind turbines experience dominant periodic loads which complicate reliable identification of linear time invariant models. In this thesis we address this challenge by extending closed-loop subspace identification methods to deal with these periodic disturbances. Doing so allows us to consistently identify the dynamics of such a system which would otherwise be hard. Evidence for the reliability and performance of these methods is given by applying them to realistic examples.

A third challenge is the poor signal-to-noise ratio experienced when measuring in the presence of significant stochastic excitations, for instance due to turbulent wind. Besides, a fourth challenge is that performing identification experiments is expensive and hence optimal use must be made of available time. Parts of this thesis are devoted to these two challenges. First, we perform “one-shot” controller design for an aeroelastic flutter control problem, where the flutter point may be shifted to a significantly higher wind speed

and dynamic loads may be actively reduced. We also show that system identification can support controller design, not just by providing a tool to deliver models of the system, but to examine the closed-loop performance. In the process of controller evaluation on the CART 3 turbine, the closed-loop characteristics were determined on the basis of a 10 minute experiment for each of the tested controllers. In all examples domain knowledge helped to achieve reliable and accurate models.

The fifth and perhaps most important challenge is that wind turbines are nonlinear systems. Hence, identification techniques for linear time invariant systems are of limited value. As the main result of this thesis we show that for the purpose of control design a wind turbine may be described adequately with the Hammerstein model structure. This structure allows the turbine to be modelled globally and allows long measurement sequences to be used effectively and efficiently. Low signal-to-noise ratios require that we incorporate prior information to obtain reliable models. We develop a practical identification approach and show its feasibility on real data. Using experimental data from the CART 3 turbine extensive validation was performed. The validation showed that the Hammerstein model structure could accurately describe the important dynamics for power and speed regulation of the turbine and for load control. In the case of the CART 3 turbine the identified models indicated that certain modes were not correctly modelled by the aeroelastic code in terms of frequency and damping. This is essential information for establishing fundamental control system limitations in the related to unstable modes and nonminimum phase zeros. Open-loop time-domain simulations at various wind speeds show that the identified models outperform the first principles models in the majority of the investigated cases.

In the traditional control design paradigm there are the disjoint steps of dynamic modelling on the one hand and control design on the other hand. Ideally these two steps should be combined in a new control paradigm, such that input-output data directly leads to the controller. This is an ambitious view, but as a first step in bringing the fields of identification and control together, the subspace predictive control (SPC) framework is an interesting development. In this framework system parameters are estimated adaptively using a recursive least squares scheme with forgetting to result in an adaptive and fault-tolerant control system. In this thesis we show the results of applying SPC to two realistic experimental setups. In the process of developing a real-time feasible implementation we developed a square root covariance filter with directional forgetting of past information. Such a scheme offers a safe way to discount old information compared to widespread recursive least-squares algorithms with exponential forgetting by ensuring boundedness of the covariance matrix and retaining adaptivity. This is an important issue when an estimation scheme must deal with slowly time-varying dynamics. Two examples are studied to demonstrate the capabilities of the SPC adaptive control law. In the first example we show that without any prior model information, damping may be achieved on a flexible structure which switches between two radically different dynamic behaviours. In the second example we show that speed regulation of a scaled wind turbine may be achieved, in terms of tracking a reference as well as in terms of rejecting disturbances due to wind speed variations.

# Samenvatting

## Identificatie van windenergiesystemen

Gijs van der Veen

Vandaag de dag levert windenergie een aanzienlijke bijdrage aan de energieproductie in veel landen en het ligt in de verwachting dat deze bijdrage in de komende decennia zal toenemen. Om de concurrentiepositie van windenergie ten opzichte van andere energiebronnen te vergroten is het van groot belang de prijs van windenergie te verlagen. Voor een gegeven windmolen kan deze doelstelling op drie manieren bereikt worden: door de energieopbrengst te verhogen, door belastingen op de windmolen te verlagen om onderhoudskosten te verlagen en door massaproductie. Onderzoek in de afgelopen jaren heeft aangetoond dat geavanceerde regelconcepten in de eerste twee aspecten een belangrijke rol kunnen spelen. Een verfijnd regelaarontwerp kan leiden tot een hogere energieopbrengst, bijvoorbeeld door voorwaartskoppeling van informatie over het aanstromende windveld, verkregen uit moderne (gedistribueerde) sensoren. Tegelijkertijd kan een dergelijke regeling de levensduur verlengen door vermoeiingsbelastingen en piekbelastingen te verkleinen, gebruik makend van voorwaartskoppeling en terugkoppeling van informatie uit meerdere sensoren in combinatie met nieuwe actuatorconcepten. Voor het ontwerpproces van nieuwe en geavanceerde regelaarconcepten die tegemoet komen aan deze wensen is de beschikbaarheid van gedetailleerde modellen essentieel. Systeemidentificatie op basis van meetgegevens kan een belangrijke rol vervullen in het verkrijgen van dergelijke modellen en kan het inzicht in de verschillen tussen het gedrag van theoretische modellen en de echte windmolen vergroten.

Een aantal uitdagingen staat het toepassen van standaard systeemidentificatiemethodes in de weg wanneer deze toegepast worden op data van een echte windmolen. In dit proefschrift worden deze uitdagingen aan de orde gesteld, met als doel theoretische resultaten en de industriële praktijk nader tot elkaar te brengen en om de potentie van systeemidentificatie te belichten. Het eindresultaat is een reeks methodes die gebruikt kan worden door ingenieurs.

Een eerste uitdaging bestaat uit het feit dat windmolens en vele andere aeroelastische systemen noodzakelijkerwijs in een gesloten regellus moeten functioneren. Dit belemmert de toepassing van traditionele *subspace* algoritmes die aannemen dat het ingangssignaal en de stochastische verstoringen ongecorrleerd zijn; een aanname die in gesloten lus niet geldt. In dit proefschrift geven we een overzicht van recente methodes voor *subspace* identificatie in gesloten lus. Hiermee hebben we een aantal methodes verschaft om lineaire tijdsinvariante systemen te identificeren die mogelijkerwijs in gesloten lus functioneren. Een van deze methodes is de gesloten lus MOESP methode die ontwikkeld is voor dit proefschrift. We hebben dit overzicht van methodes gepresenteerd aan de hand van een gemeenschappelijk onderliggend raamwerk, waardoor aangetoond kan worden dat de vele methodes in de literatuur feitelijk bestaan uit een beperkt aantal varianten met veel overeenkomsten.

Een tweede uitdaging is dat windmolens aan zeer dominante periodieke belastingen onderhevig zijn die betrouwbare identificatie in de weg staan. In dit proefschrift hebben we dit probleem opgelost door gesloten lus *subspace* identificatiemethodes uit te breiden zodat deze om kunnen gaan met deze periodieke signalen. Hierdoor zijn we in staat de dynamica van dergelijke systemen consistent te schatten terwijl dit normaal gesproken moeilijk zou

zijn. De betrouwbaarheid en prestaties van deze methodes zijn aangetoond door toepassing op realistische praktijkvoorbeelden.

Een derde uitdaging is de beperkte signaal-ruisverhouding die optreedt wanneer gemeten wordt in de aanwezigheid van significante stochastische verstoringen, bijvoorbeeld door turbulentie. Een vierde uitdaging vormt het feit dat het uitvoeren van identificatie-experimenten kostbaar is. Daarom moet de beschikbare tijd optimaal benut worden. Delen van dit proefschrift zijn gewijd aan deze aspecten. Allereerst hebben we in één iteratie succesvol een regelaarontwerp gemaakt voor een aeroelastisch *flutter*probleem, waarbij we in staat waren de *flutter*grens aanzienlijk te verhogen en dynamische belastingen te onderdrukken. Daarnaast hebben we laten zien dat systeemidentificatie regelaarontwerp kan ondersteunen, niet alleen als middel om modellen van het systeem te verkrijgen, maar ook om de gesloten lus prestaties van een regelsysteem te evalueren. Gedurende de evaluatie van verschillende regelaars op de CART 3 turbine konden de gesloten lus eigenschappen bepaald worden op basis van metingen die slechts 10 minuten besloegen. In alle voorbeelden was relevante domeinkennis essentieel om betrouwbare en nauwkeurige modellen te kunnen schatten.

De vijfde en wellicht belangrijkste uitdaging is dat windmolens niet-lineaire systemen zijn. Daarom zijn identificatietechnieken voor lineaire, tijdsinvariante systemen van beperkte waarde. Een belangrijk resultaat in dit proefschrift is dat we hebben aangetoond dat een windmolen voor regelaarontwerptoeepassingen adequaat beschreven kan worden met de Hammerstein modelstructuur. Dit staat een globale modelbeschrijving van de molen toe, waarbij lange meetseries effectief en efficiënt benut kunnen worden. De lage signaal-ruisverhouding vereist dat we voorkennis gebruiken om betrouwbare identificatiemethodes te verkrijgen. We hebben een praktisch uitvoerbare identificatiebenadering ontwikkeld en deze uitvoerbaarheid aangetoond op basis van echte meetdata. Gebruik makend van meetgegevens van de CART 3 turbine hebben we de geïdentificeerde modellen uitvoerig gevalideerd. Deze validatie heeft uitgewezen dat de Hammerstein modelstructuur de relevante dynamica voor vermogens- en snelheidsregeling van de windmolen en belastingsonderdrukking adequaat kan beschrijven. In het voorbeeld van de CART 3 turbine wezen de geïdentificeerde modellen erop dat de frequentie en demping van bepaalde eigenbewegingen onjuist gemodelleerd werden door de beschikbare aeroelastische modellen. Dit levert tevens essentiële informatie op voor het bepalen van fundamentele beperkingen op het regelsysteem, opgelegd door onstabiele eigenbewegingen en niet-minimum-fase nulpunten. Door middel van simulaties van het ongeregelde geïdentificeerde model bij verschillende windsnelheden is aangetoond dat de geïdentificeerde modellen in verreweg het merendeel van de onderzochte gevallen beter presteerden dan het gelineariseerde aeroelastische model.

Het traditionele model van het regelaarontwerpproces bestaat uit twee stappen: modelvorming (bv. door middel van systeemidentificatie) en regelaarontwerp. Idealiter zouden deze twee stappen gecombineerd worden op zodanige wijze dat gemeten ingangs- en uitgangsdata direct de gewenste regelaar oplevert. Hoewel dit een utopisch beeld is, is het *subspace predictive control* (SPC) raamwerk een eerste stap in het bijeen brengen van systeemidentificatie en regelaarontwerp. In dit raamwerk worden de systeemparameters adaptief geschat, resulterend in een adaptieve en fouttolerante regeling. In dit proefschrift laten we de resultaten zien van de toepassing van SPC op twee realistische opstellingen. Als nevenproduct van het ontwikkelen van een *realtime* uitvoerbare implementatie hebben we een *square root* covariantiefilter ontwikkeld met richtingsgevoelige afwaardering van verouderde informatie. Een dergelijk schema biedt een veilige manier om oude informatie te vergeten, vergeleken met beschikbare recursieve algoritmes, door begrenzing van de covariantiematrix te garanderen en door adaptiviteit te handhaven. Dit is een belangrijk aspect wanneer een schatter langzaam variërende parameters moet schatten. Door middel van experimentele voorbeelden hebben we de kwaliteiten van de SPC regelstrategie laten zien. In het eerste voorbeeld hebben we gedemonstreerd dat demping van een flexibele constructie bewerkstelligd kon worden zonder enige voorkennis van het systeem, terwijl deze constructie omschakelde tussen twee zeer verschillende dynamische gedragingen. In het tweede voorbeeld kon de snelheid van een schaalmodel van een windmolen geregeld worden. Zowel het volgen van een snelheidsreferentiesignaal als het onderdrukken van rotorsnelheidsvariëaties ten gevolge van windsnelheidsveranderingen waren succesvol.

# Acknowledgements

A PhD research project is largely about learning how to exploit academic freedom. While the prospect of freedom is very attractive, it can be intimidating and discouraging at times. I would certainly not have persevered without the help and encouragement of many people and I would like to thank my promotors in particular. I thank Michel Verhaegen for giving me immense freedom to define my research and teaching me how to use that freedom. I thank Jan-Willem van Wingerden for always being enthusiastic about my research ideas and encouraging me. I am grateful to my committee members for reading my thesis, providing valuable feedback and participating in the defense. I thank Gijs van Kuik for always providing a bird's eye view of my work and showing its value to me.

I would like to thank Ian Couchman and Dick Veldkamp of Vestas for their interest in my work and for many hours of cooperation on interesting topics mixed with leisurely talk. This is also the place to thank Vestas Wind Systems, Denmark, for funding this research and giving me the freedom to define it. I am grateful to Paul Fleming, Andy Scholbrock and Florian Haizmann for their hospitality and help during my visit to NREL.

Thanks to all of my DCSC colleagues for sharing the daily life of a PhD student. In particular Pieter, Edwin, Ivo H., Ivo G., Patricio, Jacopo, Mernout, Sachin, Hans and Noortje. Supporting M.Sc. students working on their thesis has been a very rewarding experience: thanks to Pieter, Sachin, Nick and Sandra for being great people to work with. Thanks to Lars for providing great opportunities for collaboration. Thanks to Coen for sharing his ideas with me during his brief visit to DCSC. The technical support of Kees Slinkman and Nico van Beek has been essential for successful execution of the lab and wind tunnel sessions; working with them was a pleasure.

Finally, I thank my parents, my sister, family and friends for their support and encouragement during these four years and before.



# Curriculum Vitae

Gijs van der Veen was born on the 15<sup>th</sup> of April, 1984 in Vianen, The Netherlands.

He attended grammar school from 1996 to 2002 at the Herbert Vissers College in Nieuw-Vennep. In 2002 he started studying Aerospace Engineering at Delft University of Technology, where he obtained his Master of Science degree (cum laude) in 2008. During his education he served an internship at the Nonlinear Systems Laboratory at Virginia Polytechnic Institute and State University in 2007. His graduation project was performed jointly between the groups of Control and Simulation and Aerospace Structures and was entitled: "Design of a smart truss: an experimental study of damping enhancement techniques".

In March 2009 he started his Ph.D. project "Identification of wind energy systems" at the Delft Center for Systems and Control (DCSC) under the supervision of Michel Verhaegen and Jan-Willem van Wingerden. This Ph.D. project was funded by and carried out together with Vestas Wind Systems A/S, Denmark. The focus of this research was on development of system identification techniques and their validation in practical contexts. During his Ph.D. research he supervised several Master students, participated in international conferences and received his DISC certificate from the Dutch Institute for Systems and Control.